Cranfield University

K. M. Khalifa

Two-phase Slug Flow Measurement using Ultrasonic Techniques in Combination with T-Y Junctions

School of Engineering

PhD

Cranfield University

School of Engineering

PhD thesis

2010

K. M. Khalifa

Two-phase Slug Flow Measurement using Ultrasonic Techniques in Combination with T-Y Junctions

Supervisor: Prof. M. L. Sanderson

Academic Year 2010 to 2011

This thesis is submitted in partial fulfilment of the requirements for the degree of PhD

ABSTRACT

The accurate measurement of multiphase flows of oil/water/gas is a critical element of oil exploration and production. Thus, over the last three decades; the development and deployment of in-line multiphase flow metering systems has been a major focus worldwide. Accurate measurement of multiphase flow in the oil and gas industry is difficult because there is a wide range of flow regimes and multiphase meters do not generally perform well under the intermittent slug flow conditions which commonly occur in oil production.

This thesis investigates the use of Doppler and cross-correlation ultrasonic measurements made in different high gas void fraction flow, partially separated liquid and gas flows, and homogeneous flow and raw slug flow, to assess the accuracy of measurement in these regimes.

This approach has been tested on water/air flows in a 50mm diameter pipe facility. The system employs a partial gas/liquid separation and homogenisation using a T-Y junction configuration. A combination of ultrasonic measurement techniques was used to measure flow velocities and conductivity rings to measure the gas fraction. In the partially separated regime, ultrasonic cross-correlation and conductivity rings are used to measure the liquid flow-rate. In the homogeneous flow, a clamp-on ultrasonic Doppler meter is used to measure the homogeneous velocity and combined with conductivity ring measurements to provide measurement of the liquid and gas flow-rates. The slug flow regime measurements employ the raw Doppler shift data from the ultrasonic Doppler flowmeter, together with the slug flow closure equation and combined with gas fraction obtained by conductivity rings, to determine the liquid and gas flow-rates.

Measurements were made with liquid velocities from 1.0m/s to 2.0m/s with gas void fractions up to 60%. Using these techniques the accuracies of the liquid flow-rate measurement in the partially separated, homogeneous and slug regimes were $\pm 10\%$, $\pm 10\%$ and $\pm 15\%$ respectively. The accuracy of the gas flow-rate in both the homogeneous and raw slug regimes was $\pm 10\%$. The method offers the possibility of further improvement in the accuracy by combining measurement from different regimes.

(Keywords: T-Y junction, ultrasonic cross-correlation, ultrasonic Doppler flowmeter, multiphase flow, conductivity ring, signal analysis)

ACKNOWLEDGEMENTS

The completion of this research work has only been made possible through the valuable contributions of a number of people over the past years. The following list is by no means exhaustive.

I would like to thank my supervisor Prof. M. L. Sanderson who has been a constant source of guidance and experience, support and ideas throughout the duration of this work. I really appreciate all his concern, help and effort.

I would also like to express my sincere gratitude to Dr. Hoi Yeung the Head of the Group for his unflinching support, unquestioning assistance and unreserved cooperation which made the project execution phase move quickly.

A big thank you to all those in and out of the PSE group with a special mention to Dr Salem Al–lababidi, Dr. Wang Meihong and Dr. Firoz Khan for their valuable support, Mr. Flemming Nielsen, Mr. David Whittingham and Mr. Clive Wood for their technical support and assistance, and to the 'department treasure' Mrs Sam Skears for her patience and assistance.

To my father Mohamed, my mother Aisha, my patient wife and all my brothers and sisters, thank you so much for continually rooting for me, supporting me and helping me out even in your discomfort. I know words may seem cheap, but I will still say a big and sincere thank you to all of you.

Finally, I would like to thank my sponsor (Libyan Government) for granting me a scholarship to do my PhD programme, and all my friends for their endless encouragement and support, without which the research journey would not have been possible.

TABLE OF CONTENTS

TABLE OF FIGURES

TABLE OF TABLES

NOMENCLATURE

Symbol	Denotes	Unites
A	Pipe cross section area	m^2
A_b	Signal with scatterers	m^2
A_g	Area where gas presents	m^2
A_i	Area of venturi inlet	m^2
A_l	Area where liquid presents	m^2
A_o	Signal without scatterers	m^2
A_t	Area of venturi throat	m^2
B_s	Signal bandwidth	bits
C	Constant	--
C_c	Acoustic velocity in coupling material	m/s
C_D	Venturi discharge coefficient	--
C_i	Constant	--
C_k	Duckler and Hubbar constant	--
C_l	Acoustic velocity in water	m/s
C_o	Constant	--
C_w	Acoustic velocity in the transducer wedge	m/s
C_W	Channel size	mm
d	Pipe diameter	m
D	Bubble diameter	mm
df	Difference frequency of repetition rates	Hz
f_{df}	Film region frequency	Hz
f_{ds}	Slug frequency	Hz
f_g	The monopole resonant frequency	Hz
f_r	Received frequency	Hz
Fr	Froude number	--
f_s	Sampling frequency	s
f_t	Transmitted frequency	Hz
G*	dimensionless conductivity reading	--
$h_{L(u)}$	Height of liquid	mm
i	Sigmoidal transfer function in NN	--
I_m	Gamma measured count-rate	--
I_o	Gamma count-rate when oil presents	--
I_v	Gamma count-rate when the pipe is empty	--
I_w	Gamma count-rate when water presents	--
k	constant	--
k_r	Wave number	--
L	length	m

L_d	Transmitted signal length	m
L_E	Slug unit length	m
L_f	Film region length	m
L_s	Slug liquid body length	m
L_u	Received signal path length	m
M	Total mass flow-rate	kg/s
m_g	Gas mass flow-rate	kg/s
m_o	Oil mass flow-rate	kg/s
M_o	Raw number value	--
m_w	Water mass flow-rate	kg/s
n	Columns	--
N	Number of points in operations	--
N_o	Column numbers	--
P	Pressure	Pa
Q	Volumetric flow-rate	m^3/s
Q_g	Gas volumetric flow-rate	m^3/s
Q_l	Liquid volumetric flow-rate	m^3/s
Q_o	Oil volumetric flowrate	m^3/s
Q_w	Water volumetric flowrate	m^3/s
R/r	Refer to dimensionless of the vertical axis	--
R_B	Average scatterer radius	mm
Re	Logarithm of the count-rate	--
Re_s	Slug Reynolds number	--
Rm	Logarithm of the count-rate for mixture flow	--
Ro	Logarithm of the count-rate for oil	--
R_u	Transducer radius	mm
Rw	Logarithm of the count-rate for water flow	--
s	Slip ratio	--
S	Scattering cross section	Micro m
T	Time	s
t_f	Time of passing film	s
t_{PE}	Piezoelectric thickness	mm
t_s	Time of passage slug body	s
v	Voltage	V
V	Velocity	m/s
V_C	Correlated translational velocity	m/s
V_d	Drift velocity	m/s
$V_{Doppler}$	Velocity measured by Doppler	m/s
V_f	Film velocity	m/s

V_g	Gas mean velocity	m/s
V_i	Fluid velocity	m/s
V_l	Liquid mean velocity	m/s
V_m	Superficial mixture velocity	m/s
V_o	Oil phase velocity	m/s
V_{PE}	Ultrasonic velocity generated by the piezoelectric	m/s
V_s	Slug velocity	m/s
V_{sg}	Superficial gas velocity	m/s
V_{sl}	Superficial liquid velocity	m/s
V_{ST}	Slug velocity corrected by V_T	m/s
V_T	Translational velocity	m/s
v_u	Normalised value for the voltage value	V
$V_{X.Corre}$	Cross-correlation velocity	m/s
$w(t)$	Length of window function	s
WC	Water-cut	--
w_i	Weight factor	--
w_s	Slug frequency	Hz
x_i	Input raw factor	--
$X\ (\tau, w)$	STFT represents by time frequency atoms	--
$x(t)$	Input signal	--
y	NNs outputs	--
α_l	Liquid fraction	--
α_g	Gas fraction	--
α_s	Liquid hold-up in the slug body	--
α_f	Liquid hold-up in the film region	--
α	Transducers angle in the Doppler case	degree
β	Water-cut	--
μ_i	The linear attenuation coefficient for two phase flow.	--
μ_l, μ_g, μ_m	Liquid phase and gas phase viscosity Mixture viscosity	N/m^2
θ	Ultrasonic path angle to the flow direction	--
ρ_l, ρ_g, ρ_m	Liquid and gas phase and mixture density	kg/m^3
$\tau\ , \tau_m$	Time delay and Maximum time delay	s
Δf	Frequency change	Hz
ΔP	Differential pressure	Pa
γ	Isentropic index	--

Term	Denotes
ADC	Analogue to digital converter
CA, CB, CC, CD	Conductivity ring A, B, C, D
CW	Continue wavelet
D.P	Deferential pressure
DAS	Data Acquisition System
DFT	Discrete Fourier Transform
DOPPLER	Ultrasonic Doppler
e.m.f	Electromotive force
ECT	Electrical Capacitance Tomography
ERT	Electrical Resistance Tomography
FFT	Fast Fourier Transform
F_gH	High Pressure Gas Flowmeter
F_gL	Low Pressure Gas Flowmeter
FW	Water Flowmeter
GVF	Gas Void Fraction
LVF	Liquid Volume Fraction
MLP	Multilayer Perceptron
MPF	Multi-Phase Flow
MPFM	Multi-Phase Flowmeter
MPI	Multi-Channel Pressure Indicator
NMR	Nuclear Magnetic Resonance
NN	Neural Network
PD	Positive Displacement
PDF	Probability Density Function
PET	Position Emission Tomography
P_gH	High Gas Flow Pressure
P_gL	Low Gas Flow Pressure
PVC	Polyvinyl chloride
PZT	Piezoelectric
R_X	Receiver
STFT	Short Time Fourier Transform
TDX	Multi wave transducer
T_gH	High Gas Flow Temperature
T_gL	Low Gas flow Temperature
T_X	Transmitter
USA	Ultrasonic Transducer A
USB	Ultrasonic Transducer B
WT	Wavelet Transform

Chapter 1

INTRODUCTION

1.1 BACKGROUND

It is quite common in oil production for more than one company to transport their products through the same common pipeline. However, each oil production company needs to know how much it is injecting into this pipeline. Therefore they need an MPFM, which has the ability to work under various flow regimes especially slug flow for allocation metering.

More than one phase flowing in a conduit is a very common phenomenon in the chemical and petroleum industries. However, online measurement of each phase with a high accuracy can be a real challenge for these industrial engineers. These flows (Liquid/Gas) can be configured in different flow patterns or regimes such as stratified, wavy, annular, bubble, slug, and dispersed flow in horizontal pipelines. Slug flow occurs commonly in oil and gas production pipelines and because it is an intermittent flow, it is difficult to control and accurately measure online.

When fiscal (for taxation or revenue generating purposes) monitoring is the purpose of the measurement, the full separation method is currently the most accurate measurement method for fiscal metering application. A high accuracy two-phase flow measurement (MPFM) is required in the oil industry, especially in the case of fiscal metering, since any error implies incorrect financial transfers. (Money may be gained or lost in the process).

The problem of how to measure two-phase (oil-water-gas) slug or mixture flow with high accuracy has been considered by many researchers in order to fulfil the requirements of the oil and gas industry. The conventional method of measuring two-phase flow is to separate the flow of each phase and then use well known single-phase flowmeters. However, when the purpose of separating oil-water-gas is to control and monitor the oil production, or to monitor and test each well of an oil

production field, the separation method would be time consuming, very expensive, interrupt production when implementing, as well as requiring a large space for bulky equipment. Thorn et al. (1997). As a result the requirement of online measurement using accurate multiphase flowmeters has emerged.

A number of multiphase flowmeters employing a variety of technologies have been developed to eliminate the need for two-phase full separation deployment. These techniques offer substantial operating advantages over separation procedures. In-line multiphase flow measurement is usually carried out by methods which require the multiphase flow to be pre-conditioned (partial separation or homogenisation). In addition there are several computational methods which can be employed such as neural networks and closure methods. In general, multiphase flow metering has been developed to give online measurement for liquid and gas flowing in a pipeline. However, the accuracy of these flowmeters is still not meeting the oil and gas companies' expectations. They remain expensive.

1.2 THE THESIS SCOPE

This research work experimentally investigates a potential measurement of two-phase slug flow in a 50 mm diameter horizontal pipe using different ultrasonic techniques; ultrasonic Doppler (500 kHz) and cross-correlation flowmeters, in combination with T and Y junctions to provide pre-conditioning and pure slug flow closure measurement. Two-phase slug flow measurement requiring pre-conditioning (partially separated and homogeneous) is investigated and followed by two-phase slug flow measurement requiring no conditioning (slug flow closure method). The proposed approach produces three independent measuring sections providing liquid flow-rate measurement in a partially separated (liquid dominated) section, liquid and gas flow-rate measurements in a homogeneous section, and liquid and gas flow-rate measurement based on slug flow closure measurement in a fully developed slug flow.

T and Y junctions were used to partially separate the two-phase slug flow and to provide a homogeneous flow, respectively. The ultrasonic Doppler flowmeter was deployed to measure the flow velocity in homogeneous and slug flow regime

sections, whereas an ultrasonic cross-correlation flowmeter was used to measure the bubbly flow velocity in a partially liquid separated section, assuming there is no slip between the two phases. Flush-mounted conductivity rings were used in all mentioned sections to measure the phase fraction.

These techniques were successfully implemented to obtain the following measurements:

- Liquid flow-rate measurement in the partially separated liquid section.
- Liquid and gas flow-rate measurements in the homogeneous section.
- Liquid and gas flow-rates using slug closure in the raw slug flow section.

Clamp-ons ultrasonic flowmeters (Doppler and cross-correlation) are promising techniques to facilitate non-intrusive and non-invasive two-phase flow metering as they do not require breaking into the pipeline for installation. Hence, a metering system could be refitted without having to stop the production process.

Ultrasonic Doppler flowmeter have generally been used in the measurement of a single-phase liquid with a small (GVF) flow (less than 3%) in different pipe sizes and orientations. The work in this thesis is to extend use of ultrasonic Doppler measurements to higher GVF in two-phase flow in horizontal pipeline. This reveals the potential of this flowmeter to be used in wider ranges of GVF and flow velocities with a competing accuracy.

1.3 OBJECTIVES, TASKS, OVERVIEW AND STRUCTURE OF THE WORK

1.3.1 Objectives

This thesis experimentally investigates two-phase high GVF (partial separation, homogeneous and raw slug) flow measurement using different ultrasonic techniques. These measurements are based on preconditioning and no-conditioning of two-phase flow.

The work proposed a measurement technique based on primary partial separation of the two phase air/liquid slug flow using a vertical 150 mm diameter pipe T-junction and then homogenising it using a 50mm diameter pipe Y-junction and a static mixer. In the partial liquid separated section an ultrasonic cross-correlation technique to measure the bubbly flow velocity. A Doppler flowmeter is used clamped on to a meter downstream of the Y-junction to measure the velocity of the two-phase homogeneous flow. The same Doppler meter is also used in the horizontal raw slug flow section for slug flow measurement. A flush-mounted conductivity ring is used to measure the fraction of the two-phase flow at all the above positions.

1.3.2 Thesis tasks

The tasks involved in this thesis are as follows:

- To build simple T and Y junctions to partially separate and homogenise the two-phase flows, respectively.
- To conduct a literature review of two-phase flow metering involving clamp-on ultrasonic techniques and assess their limitations under flow pre-conditioning (homogeneous) and no flow conditioning sections (raw slug).
- To deploy ultrasonic cross-correlation technique as a flow velocity measurement technique in partially separated liquid dominated flow.
- To experimentally investigate the performance of a clamp-on ultrasonic Doppler flowmeter under a homogeneous flow regime over a wide range of GVF on a horizontal 50mm pipeline and assess its limitation.
- To undertake experimental data for various liquid flow-rates on a horizontal pipeline with a wide range of GVF in raw slug without flow preconditioning.
- To draw conclusions about the overall performance of such a system and make recommendations for future work.

1.3.3 Project overview

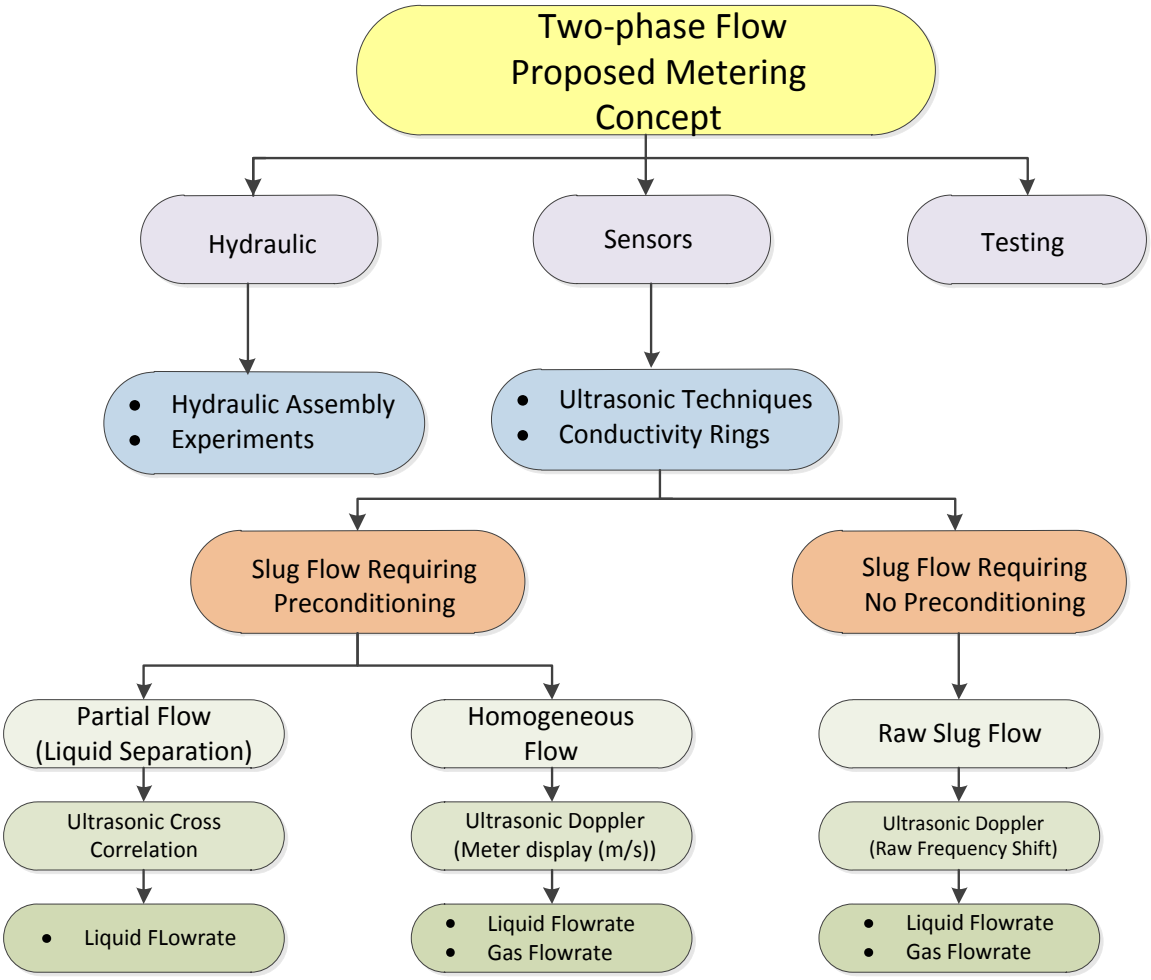

Figure 1-1, The proposed concept of the two-phase flow measurements

Figure 1-1 displays the proposed two-phase slug flow metering system using different ultrasonic techniques and conductivity rings. The work has been divided into several tasks and subtasks, beginning with the hydraulic design and experiments where the test rig is built to modify two-phase slug flow into liquid and gas partial separations and homogenised flow. In the sensor section, in order to obtain the two-phase flow measurements, the flow is categorised into three main measuring areas: first is liquid partial separation flow-rate measurement where ultrasonic cross-correlation is used to measure the velocity of the mixture; the second is homogeneous flow where an ultrasonic Doppler flowmeter is deployed to measure the mixture velocity; and, the third is the raw slug flow closure measurement. The ultrasonic Doppler meter is deployed to measure the slug and film velocity and liquid

flow measurements, also conductivity rings are deployed in all measuring areas to measure GVF.

1.4.1 Thesis structure

Figure 1-2 illustrates the main concepts and links in the research work carried out to fulfil the theses objectives.

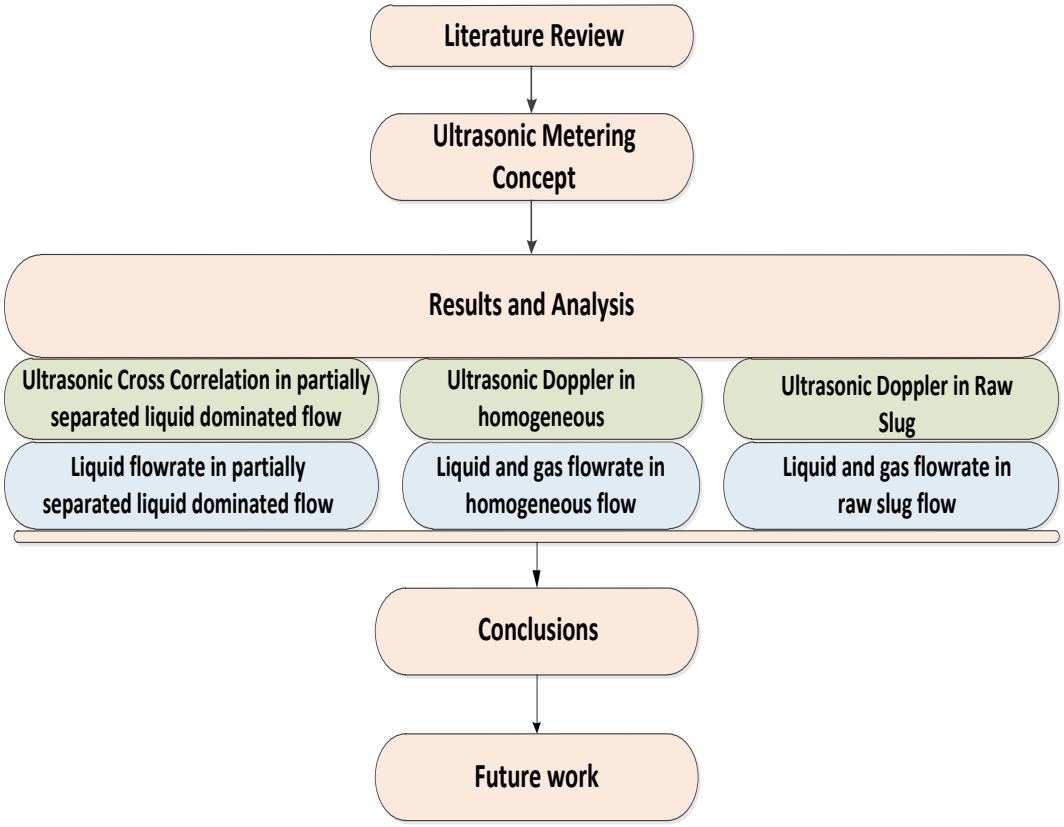

Figure 1-2, Thesis Roadmap

This thesis is divided into 7 chapters including the introduction, and the remainder are presented as the following:

Chapter 2, Literature Review of Multiphase Flow

This chapter critically reviews the literature relating to multiphase flow (MPF) starting with current state of understanding of MPF, slug flow-types and their problems, slug regime parameters and correlations. Flow regime identification techniques have been focused on in term of flow regimes map two-phase flow behaviour; correlations of liquid hold-up, two-phase gas void fraction (GVF)

concentrations and velocity profile. This chapter has also reviewed measurement techniques in MPF, commercial two-phase flowmeters classifications, different ultrasonic techniques in terms of their performance and applications. Finally, signal processing technique is widely reviewed, such as First Fourier Transform (FFT), Short Time Fourier Transform (STFT), and wavelet analyses.

Chapter 3, Overall Metering Concept

This is concerned in general with the T-Y-junctions metering concept overview and the ultrasonic techniques. It is divided into several main parts: the general PASE laboratory Two Phase Test Rig facilities and how the required liquid and gas are supplied; reference measurements techniques; T-Y junctions general description. Here, descriptions are given of the ultrasonic measurement techniques used at each measuring section, the ultrasonic cross-correlation methods in partially separated liquid dominated flow, Doppler in the homogeneous section and in the slug flow section.

Chapter 4, Liquid Dominated Flow Measurement Section (Partial Separation)

This summarises the specific experimental set up and data acquisition used in liquid flow rate measurement in partial separated liquid dominated flow. Ultrasonic cross correlation, its installation and its signal processing are illustrated in details. Finally, the result of the liquid flowrate measurement using cross correlation technique has been clearly addressed.

Chapter 5, Homogeneous Flow Measurement Section

This chapter is primarily focused on the specific experimental set up and data acquisition used in homogeneous flowrate measurement. This measurement includes the hydraulic description of the homogeneous section, Y-junction and ultrasonic Doppler installation, ultrasonic Doppler signalling processing. The ultrasonic Doppler technique was assessed downstream of the reference meters in a controlled flow. A correction factor for flowrate was obtained. Lastly, liquid and gas flowrate measurement using ultrasonic Doppler in homogeneous flow are clearly illustrated.

Chapter 6, Raw Slug Flow Measurement Section

This chapter discusses the experimental set up for the ultrasonic Doppler transducer in raw slug flow; this includes its installation in different pipe position (3 and 6 o'clock positions). This chapter also considers ultrasonic Doppler frequency shift signal gathering and analysis using different software. Slug and film velocity measurement using Doppler are clearly illustrated. Finally, liquid and gas flowrate in the slug flow using Doppler is addressed.

Chapter 7, Conclusions and Future Work

Chapter 7 summarises the most significant findings of this work and recommends future work. It concludes the performance assessment of the proposed metering results. Future work is clearly proposed in term of gas flowrate measurement in partial separated gas flow and signal processing in raw slug flow using STFT.

Chapter 2

LITERATURE REVIEW OF MULTIPHASE FLOW

2.1 INTRODUCTION

This literature review chapter examines various aspects of multiphase flows in pipelines and measurement techniques. The initial part of this chapter focuses on the flow regimes that can occur in a horizontal pipe for different gas and liquid superficial velocities.

A selective background and the detailed principles and techniques used to measure multiphase flows in pipelines are discussed. Slug flow parameter and correlations have been explained. The chapter reviews current commercially available multiphase flow metering systems in terms of their capabilities, limitations, accuracies, applications and flow regimes conditions.

Ultrasonic multiphase flowmeters that are currently commercially available are described and explained in terms of installations, application and performance. Finally, data signal processing such as Fourier Transform, Short Time Fourier Transform and Wavelet Analysis are presented.

2.2 MULTIPHASE FLOWS

The flow of multiphase mixtures is a well known flow in industrial plants such as chemical reactors, power generation units, oil wells and pipelines (Fossa and Guglielmini, 1998).

As mentioned earlier, multiphase flow is when more than one phase or component exists; this can be (liquid/liquid) such as water/oil, or (liquid/gas) such as oil, gas, water or (solid/liquid) such as sand/oil/water or all the phases together in a pipeline, such as gas/oil/water/sand, Kavosh (2005). However, the main problem encountered in measuring multiphase flow (Gas/Liquid) is how accurately in the pipeline it can be measured and this problem has received a great deal of attention from the petroleum industry.

A considerable amount of work has been done to highlight various technologies employed in most of the multiphase flowmeters. These flowmeter concepts are discussed in this section. The measurement approaches are classified into three main categories – complete separation, partial separation and homogenisation; additionally pattern recognition and image processing, which offer multiphase flow measurement based on data processing, are also included as multiphase measurement methods.

2.2.1 Horizontal Gas-Liquid Flow Regimes

In fully developing single-phase flow, the flow velocity distribution is determined solely by the pipe roughness and the Reynolds number. In multiphase flow, the phases can be differently disposed in various ways within the pipe cross section. This leads to the concept of the flow being deferred by the flow regimes.

In the horizontal pipe, six flow regimes have been identified:

Stratified (Smooth) Flow

This occurs as a consequence of gravitational separation. The liquid flows along the bottom of the pipe as gas flows on the top of the surface filling the gap above the liquid. This flow regime is associated with low gas velocities; the liquid hold-up in this regime can be large.

Stratified (Wavy) Flow

With higher gas velocity the stratified wavy flow occurs. Waves on the liquid surface can be produced by the gas velocity. Large waves may emerge and some droplets are very likely to be created as a result.

Annular Mist Flow

This occurs at high gas velocities. As a result a thin liquid film exists around the internal wall of the pipe. Typically most of the liquid is entrain in the form of droplets in the gas. Small droplets appear on the bottom of the pipe as a result of gravity.

Slug Flow

On increasing the liquid velocities of the wavy flow regime, the slug flow regime takes shape. Basically, large frothy waves of liquid form a slug that can fill the whole pipe cross section following with a gas blockage. A surge wave can also be a form of slug which exists upon a thick film of liquid on the bottom of the pipe.

Elongated bubble Flow

At the top of the pipe wall elongated bubble flow consists of a mostly liquid flow with elongated bubbles present. In this flow regime, collisions between the individual bubbles occur more frequently with increasing gas flow rate and they coalesce into elongated “plugs”. This flow is often called plug flow.

Dispersed Flow

In this flow pattern, the gas phase is distributed as distinct bubbles within a pipe filled with liquid. The gas appears in the form of small bubbles which have a tendency to present in the top region of the pipe as gravity holds the liquid in the bottom.

The flow regimes above occur in a horizontal pipe; these regimes change from one to another as gas and liquid velocity increase and decrease. Figure 2-1 shows the flow regimes in a horizontal pipe line.

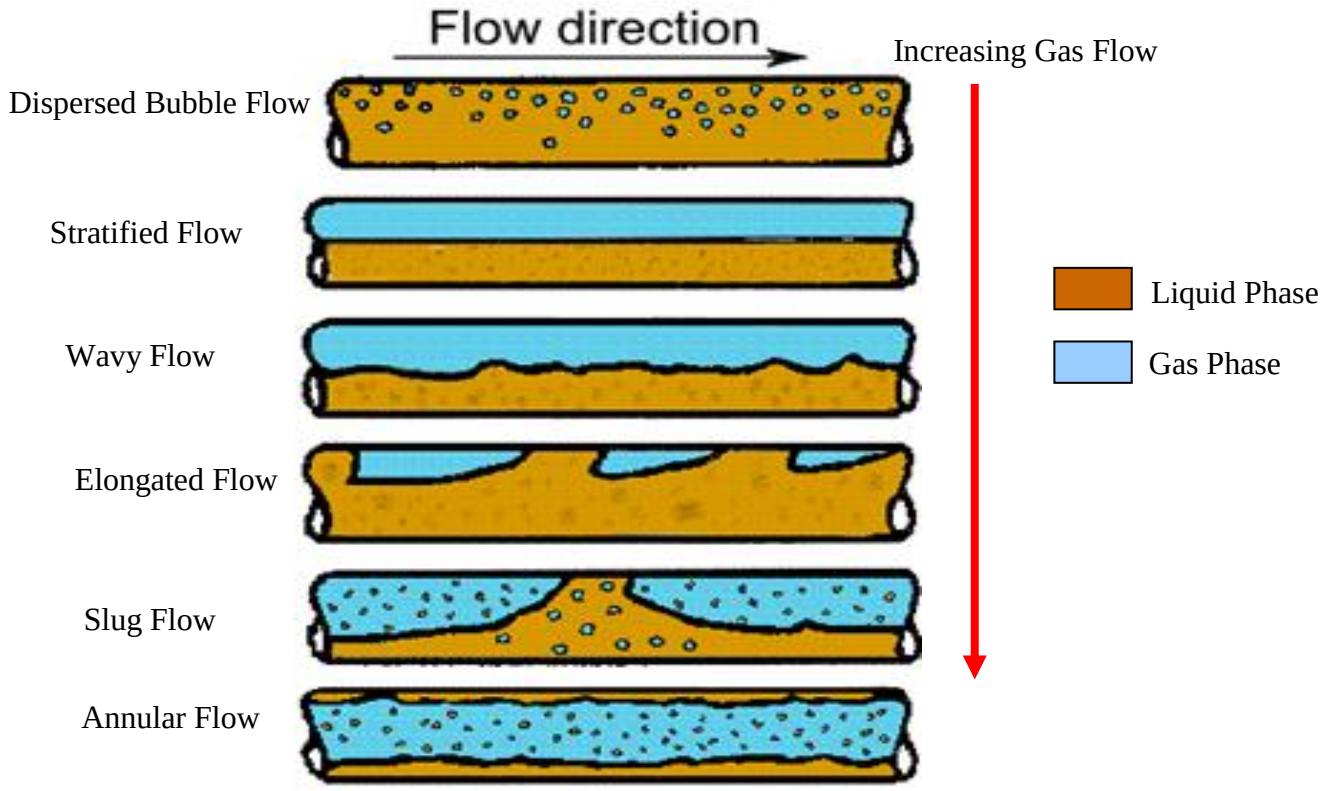

Figure 2-1, Flow regimes in horizontal pipe

2.2.2 Flow regime identification

There is no specific method to identify two phase flow regimes in a pipeline. However, several methods have been used to gather accurate information that can reflect the true flow regimes. Dong et al. (2001). These methods are as follows:

- Direct methods: These methods are based on directly identifying the flow regime; they use visual inspection. High speed photography system can be used.
- Indirect methods: These are based on statistical analyses of measurement fluctuating signals (for example from pressure transducers), which can reflect the fluctuating characteristics of two phase flows, and flow regimes are identified as a result.

2.2.3 Multiphase Flow Parameters

In order to be able to quantify the occurrence of the flow regimes, it is necessary to specify the parameters of the multiphase flow, they are as follows:

Superficial Phase Velocity

The term superficial phase velocity refers to the phase velocity that would present in the stream but neglecting any other phase that exists with it in the same stream.

The superficial velocity for both phases is identified as the individual volumetric flow-rate divided by the area cross section of the internal pipe diameter.

$$V_{sl} = \frac{Q_l}{A} \quad \textbf{(2. 1)}$$

$$V_{sg} = \frac{Q_g}{A} \quad \textbf{(2. 2)}$$

The mixture velocity (V_m) is calculated by the sum of the gas and liquid superficial velocities.

$$V_m = V_{sl} + V_{sg} \quad \textbf{(2. 3)}$$

Gas and Liquid Volume Fraction

The gas volume fraction (GVF) is the ratio of the volumetric flow of gas to the total volumetric flowrate.

$$GVF = \frac{Q_g}{Q_g + Q_l} \quad \textbf{(2. 4)}$$

The liquid volume fraction (LVF) is the ratio of the volumetric flow of liquid to the total volumetric flowrate. Both liquid and gas volume fraction are calculated as no slip assumption.

$$LVF = \frac{Q_l}{Q_l + Q_g} \quad \textbf{(2. 5)}$$

Gas Void Fraction and Liquid Hold-up

The void fraction of gas or liquid is the fraction of the pipe area at a given cross section which is occupied by the gas phase or liquid phase respectively.

Gas void fraction,

$$\alpha_g = \frac{A_g}{A} \quad \textbf{(2. 6)}$$

Liquid Hold-up,

$$\alpha_l = \frac{A_l}{A} \quad \textbf{(2. 7)}$$

And

$$A = A_g + A_l \quad \textbf{(2. 8)}$$

$$\alpha_g + \alpha_l = 1 \quad \textbf{(2. 9)}$$

The average (in situ) velocity for each phase is as follows:

$$V_l = \frac{Q_l}{A_l} = \frac{V_{sl}}{LVF} \quad \textbf{(2. 10)}$$

$$V_g = \frac{Q_g}{A_g} = \frac{V_{sl}}{GVF} \quad \textbf{(2. 11)}$$

Slip effects

In no-slip conditions is the gas void fraction equal to the gas volume fraction, and the Liquid Hold-up is equal to the Liquid Volume Fraction.

In the majority of flow regimes the Liquid Hold-up will be larger than the Liquid Volume Fraction and the gas void fraction will be smaller than the gas volume fraction

The liquid or gas fraction of the pipe cross sectional area, as measured under two-phase flow conditions, are known as liquid hold-up and gas void fraction, respectively. As a result of slip, the liquid hold-up can be larger than the liquid volume fraction. Liquid hold-up is equal to the liquid volume fraction only under conditions of no slip, when the flow is homogeneous and the two phases travel at equal velocities. (Handbook of Multiphase Flow Metering, 2005).

2.2.4 *Gas-Liquid Flow Regimes Map in Horizontal Flow*

In two-phase flow, the behaviour of the gas and liquid flowing in a pipe reveals various flow characteristics, and these depend on the gas pressure, gas and liquid velocity, as well as geometry and orientation of the piping (i.e. horizontal, near horizontal or vertical).

These flow characteristics can be identified as shown in Figure 2-2, which is a flow regime map for horizontal flow. However, a flow regime map is rig specific and cannot be used as a generalisation for every test rig. The flow regime strongly depends upon the pipe geometry, gas and liquid velocities, the distance of mixing point, roughness of the pipe, and the fittings and valves used within the line. All the previous elements can alter the point where flow is developed. Since flow development can vary at different distances from the mixing points, it is preferable to draw a flow regime map for each test rig at the measuring section.

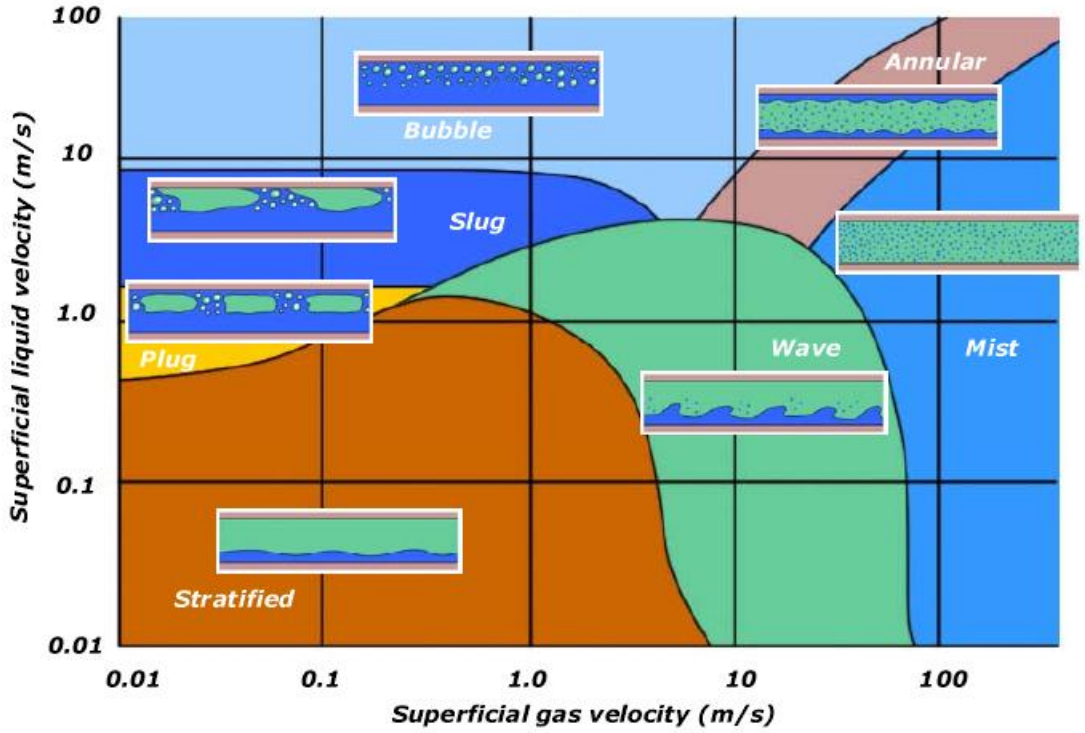

Figure 2-2, Flow regimes map in horizontal pipe, taken from Handbook of Multiphase Flow Metering (2005)

2.3 CURRENT STATUS IN MULTIPHASE FLOW MEASUREMENTS

Multiphase metering methods can be classified into two major groups. The first group is the conditioning methods where the condition of the phases in the pipe is changed (complete separations, partial separations or mixed) upstream of the metering point. The second group is the direct method, where the phase parameter measurements are achieved without a pre-conditioning process.

2.3.1 Complete separation

Multiphase flow measurement can be obtained using a full separation method, as shown in Figure 2-3, where the mixture flow is injected into a suitably large vessel to allow the settlement of gas and liquid (oil and water) to occur as a result of the different densities of the fluids. As a result, the separated oil/water/gas can be measured individually using single-phase metering techniques.

This multiphase flowmeter technique offers the best measurement accuracy and has therefore been used as a fiscal measurement technique.

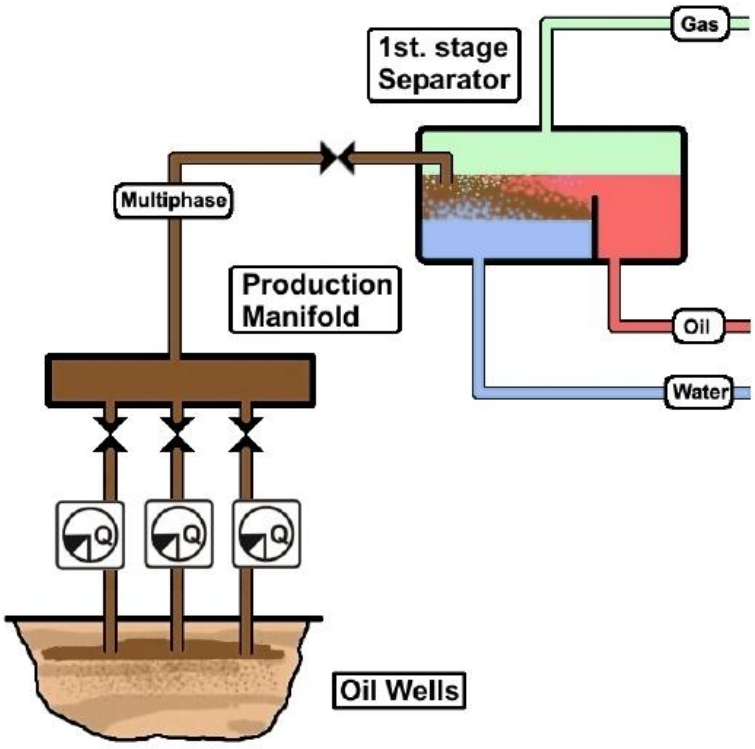

Figure 2-3, Multiphase flow measurement based on full separation

The main disadvantage of this technique is that it occupies a large footprint in an off-shore platform as a result of the bulky equipment required. It is also a time consuming procedure to allow the mixture to settle down. Operation and maintenance costs can be high since there are many valves and flowmeters involved.

2.3.2 Partial separation

In the partial separation based system, shown in Figure 2-4, the flows have to be conditioned via special pipe configuration in order to modify the multiphase flow to suit the installed measurement techniques. The multiphase flow is divided into two main sections – liquid dominated flow and gas dominated flow sections; each flow line then only requires to be measured over a restricted range of phase fractions. A number of multiphase measurement techniques have been employed to partially separate flows which contain gravity separation systems and T junctions.

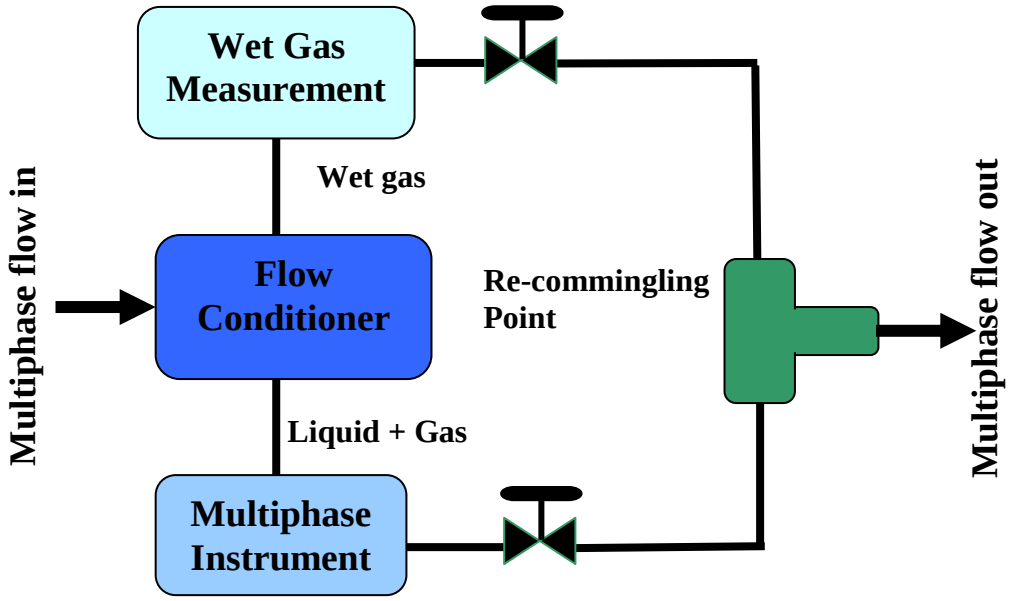

Figure 2-4, Multiphase flow measurement partial separation system

As a result of gas carry-under and liquid carry-over in the partially separated liquid and gas, these measurements involve velocity and fraction measurement techniques, which are essential to measure the flow-rates of liquid and gas.

Once the separated phases have been measured using multiphase flowmeters, the separated phases are brought together into one single line after the configuration

system in the re-commingling point, and the multiphase flow is released to flow into the same pipe upstream of the measuring sections.

2.3.3 Homogeneous based system

In the homogeneous based system, the multiphase flow is conditioned using a special configuration to ensure the multiphase flow is in its homogeneous state. As the phases are flowing as one, component velocity and the density is the same around the cross section, the velocity and phase fraction are measured. Finally, the individual phase flow-rate is obtained. The flow then continues to travel in the pipeline via the multiphase flowmeter output.

The advantage of this system is the multiphase flow is dealt with as a mixture flow where only one velocity measurement technique is needed.

2.4 MEASUREMENT STRATEGIES - INFERENTIAL APPROACH

There are some measurement techniques that need to be implemented to measure mass flow-rate of oil and gas components in the multiphase flow.

In order to calculate individual and total mass flow-rate (M), it is essential to know both the instantaneous velocity of each phase and their cross sectional fractions as well as the density for each phase at the measurement temperature. Figure 2-5 illustrates the principle of multiphase flow measurement. Thorn et al. (1997).

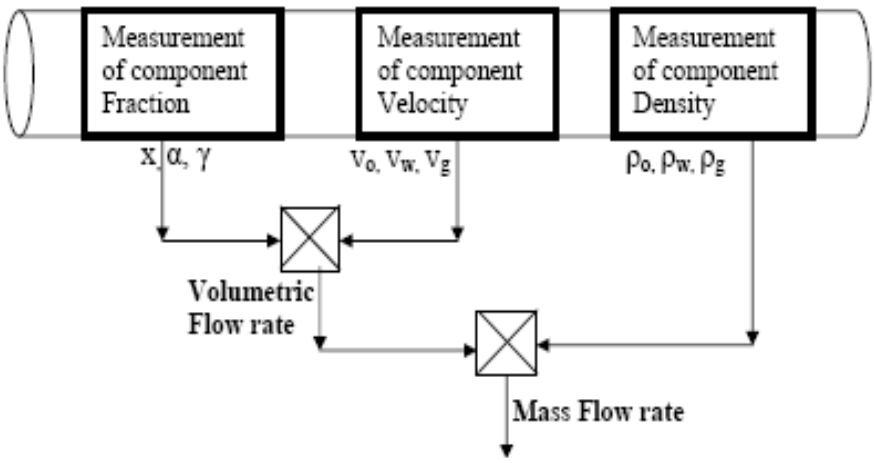

Figure 2-5, Principle of multiphase flow measurement

An important requirement for obtaining multiphase flow measurement is to measure the velocity (V_g, V_o and V_w) and two fractions which are normally the gas void fraction α_g and water-cut β.

$$M = (\alpha_l V_g \rho_g + \beta V_L \rho_w + [1-(\alpha_g + \beta)]V_l \rho_O)A \quad \textbf{(2. 12)}$$

The flow-rate equation can be illustrated as the following:

$$m_g = \alpha_g A V_g \rho_g, \qquad m_g = Q_g \rho_g \quad \textbf{(2. 13)}$$

$$m_W = \beta A V_l \rho_W, \qquad m_W = Q_W \rho_W \quad \textbf{(2. 14)}$$

$$m_O = (1-(\alpha_g + \beta))AV_L \rho_O, \qquad m_O = Q_O \rho_O \quad \textbf{(2. 15)}$$

$$M = m_g + m_W + m_O \quad \textbf{(2. 16)}$$

2.4.1 Flow conditions and measurement requirements

Table 2-1 describes the measurement strategy for various flow conditions Table 2-1.

Flow condition	Flow measurement methods	Need for fraction measurement	Volumetric flow-rates equations in use
Full separation of multiphase flow	Single-phase measurement techniques for gas and liquid	No fraction measurement technique required	Oil, gas, water flow-rates are measured separately using a single-phase flowmeter: $Q_o = V_o A_o,\ m_o = Q_o \rho_o$ $Q_g = V_g A_g,\ m_g = Q_g \rho_g$ $Q_w = V_w A_w,\ m_w = Q_w \rho_w$
Partial separation of multiphase flow	Multiphase flow measurement metering.	Fraction measurement required in liquid dominated and gas dominated sections.	Partial separated liquid dominated: $Q_l = V_l \alpha_l A, m_l = Q_l \rho_l$ Partial separated gas dominated: $Q_g = V_g \alpha_g A,\ m_g = Q_g \rho_g$
Homogeneous flow	Multiphase flow measurement metering	Fraction measurement required	$Q_o = V_m \alpha_o A$ $Q_w = V_m \beta A$ $Q_g = V_m \alpha_g A$
ANNs (Pattern recognition)	Statistical information of the flow such as pressure, cross-correlation, fraction measurement.	Fraction measurement techniques can be useful to provide statistical information.	Q_o, Q_g and Q_w from previously trained data As a result: m_o, m_g and m_w, or it could be directly obtained.

Table 2-1, Measurement strategy according to flow conditions

2.5 SLUG FLOW REGIME IN HORIZONTAL PIPE

The main features of gas-liquid slug flow are intermittency and irregularity. (Barnea and Taitel, 1993).

A slug flow regime in two-phase flow is characterised by a series of liquid plugs separated by relatively large gas pockets. In the two-phase flow pattern, slug flow can be easily observed as a consequence of gas and liquid flowing simultaneously in a pipe, over certain ranges of flow-rates. Slug flows are commonly associated with many industrial applications such as the production of hydrocarbons in wells and their transport in lines, creation of steam and water in power generation, steaming and condensation in liquid-vapour systems of thermal power stations, emergency core cooling of nuclear reactors, and heat and mass transfer between gas and liquid in chemical reactors plants. (Fabre and Line, 1992).

Slug flows are considered to be the most severe flow regimes that need to be dealt with in a production stage. They can cause significant practical operating problems and severe damage for oil and gas production equipments as a result of hammering and vibrating behaviour. Figure 2-6 illustrates slug flow in a horizontal pipeline.

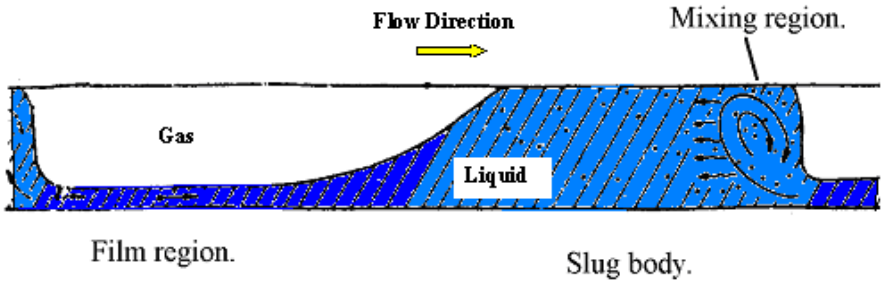

Figure 2-6, Slug flow in horizontal pipe, adapted from Fabre and Line (1992)

2.5.1 Slug flow initiation

Slug formation and its nature from stratified/wavy to slug flow transition in a horizontal pipe have been experimentally addressed by many multiphase researchers. Researchers have attempted to establish mathematical relationships of experimental data or models for the slug flow initiation and its frequencies within a "fully developed" flow.

Slug flow is initiated as a result of waves which start to appear on the surface of stratified liquid gas flows. These waves can continue to develop picking up liquid flowing in front of them, until they block the pipe cross section, thus developing slugs as shown in Figure 2-8. These slugs may grow if the slug heads move more rapidly than the tails; and eventually they would collapse. Steady slug flow is acquired if the slug head and tail move at the same velocity. In multiphase pipelines, all these events take place at different periods, hence some slugs grow, other slugs collapse; also slugs might move at different velocities. (Moissis and Griffith, 1962; Taitel and Barnea, 1990).

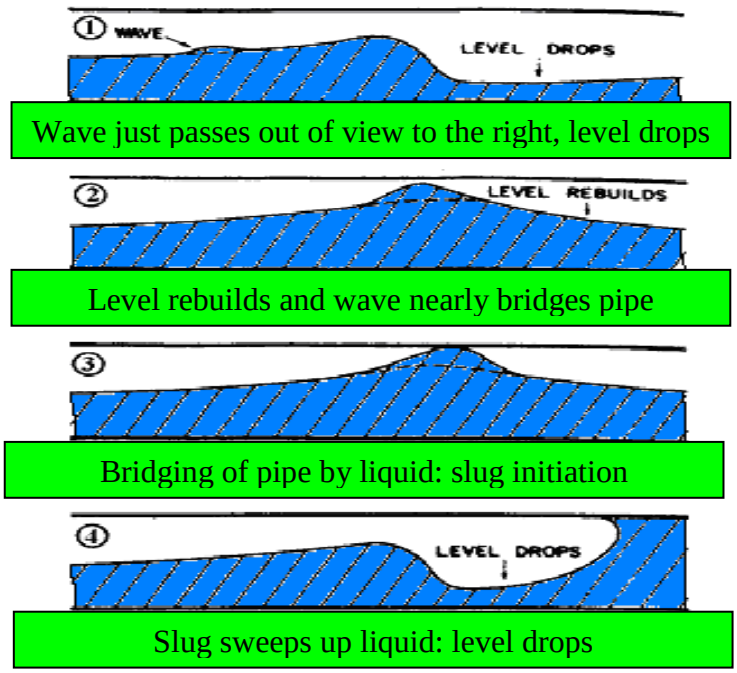

Figure 2-7, Slug flow formation

2.5.2 Slug flow types

2.5.2.1 Slug types

In general, slug flow belongs to a class of intermittent flows which has very significant features in terms of its unsteady phenomenon (Fabre and Line, 1992). Slug flow can be categorised into two main types: hydrodynamic and terrain slugging.

Terrain slugging is caused by liquid build-up in a local undulation of flow lines with variable topography. Hydrodynamic slugging is the normal slugging pattern encountered in straight flow pipelines. Hydrodynamic slugging occurs as a result of gas and liquid entering the line which is set up in a flow-rate to give a stratified/wavy flow, in which the gas flows above the liquid in parallel streams, and slugs originate from waves at the gas-liquid interface that grow to fill the pipe cross section (Ujang et al., 2006)

2.5.3 Slug parameters and correlations

Studying slug flow parameters and correlations in horizontal piping has received increased attention recently. Slug flow can occur in large and long oil pipelines. This plays a negative role in oil and gas productivity and this also affects oil and gas equipment.

Slug parameters of the liquid/gas flow can be divided into four general categories:

1. Slug and film velocity
2. Slug frequency
3. Slug and film hold-up
4. Slug and film lengths

Figure 2-8 illustrates slug and film flow parameters and their presentations in a pipeline.

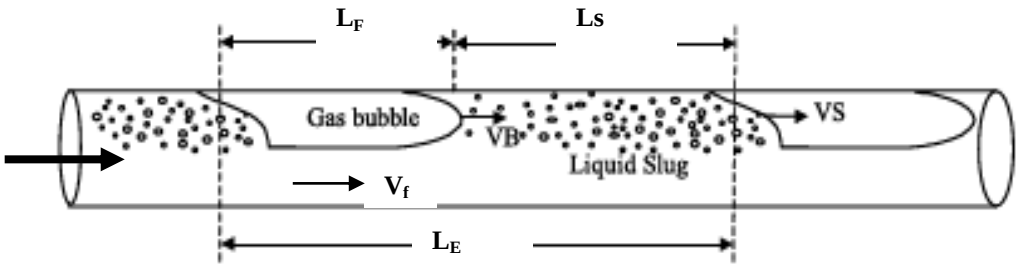

Figure 2-8, Simplified slug flow model construction

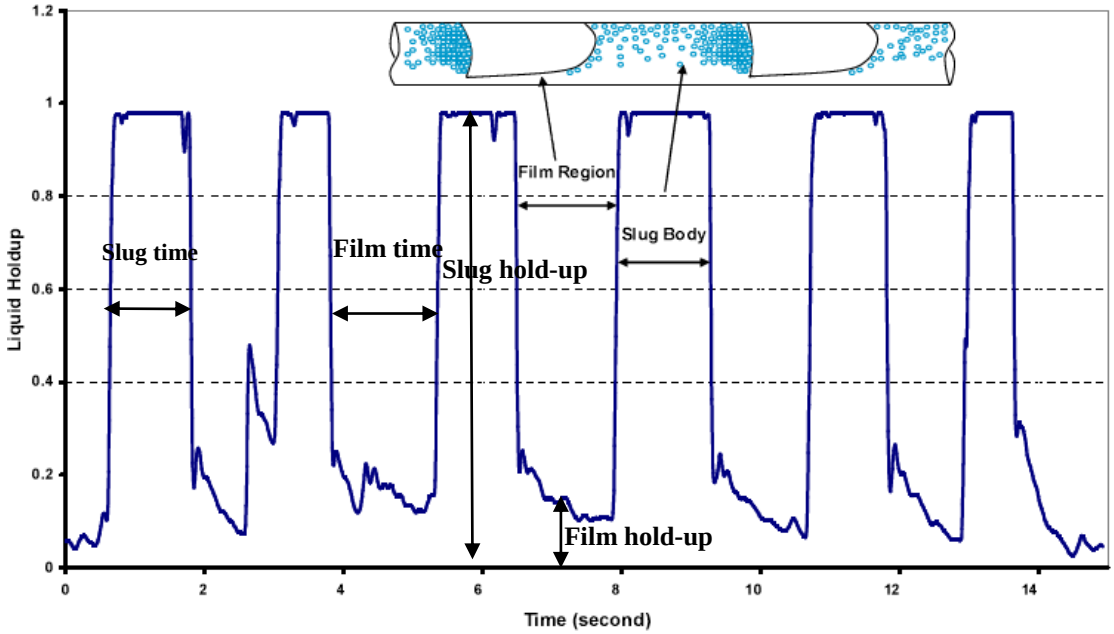

Figure 2- 9, Slug flow signal captured by a conductivity ring, adapted from ADDALI (2010)

Figure 2- 9 presents a conductivity ring volts outputs and time series for slug flow. Slug and film time, length and hold-up are illustrated in this figure.

2.5.3.1 Slug and film velocity

Slug and film velocity can be obtained using several equations which are mainly based on mixture velocity and other empirical constants.

$$V_m = V_{sl} + V_{sg} \qquad \textbf{(2. 17)}$$

where V_m is the superficial mixture velocity, and V_{sl} and V_{sg} are superficial liquid and gas velocities, respectively.

Duckler and Hubbard (1975) assume that there is no gas entrainment in the liquid film and no liquid droplet entrainment in the gas bubble.

As;

$$\rho_m = \rho_l \alpha_s + \rho_g \alpha_g \quad \textbf{(2. 18)}$$

$$\mu_m = \mu_l \alpha_s + \mu_g \alpha_g \quad \textbf{(2. 19)}$$

$$\alpha_g = (1 - \alpha_f) \quad \textbf{(2. 20)}$$

where, d is the pipe diameter, ρ_m and μ_m are mixture density and viscosity, ρ_l, ρ_g, μ_l, and μ_g are liquid and gas density, and liquid and gas viscosity, respectively.

The Reynolds number within the slug can be gained using the following equation:

$$\mathrm{Re}_s = \frac{V_m \rho_m d}{\mu_m} \quad \textbf{(2. 21)}$$

Slug and film velocity can be calculated from these two equations:

Slug velocity:

$$V_T = C_o V_m + V_d \quad \textbf{(2. 22)}$$

Based on mixture Froude number the V_d and C_o can be obtained for each group.

Group	Froude Number Values Range (F_r)
Group 1	F_r<2
Group 2	2< F_r <4
Group 3	F_r >4

where Froude number (F_r) is defined as the ratio of a characteristic velocity to a gravitational velocity:

$$F_r = \frac{V^2}{gd} \quad \textbf{(2.23)}$$

Group 1 : $V_T = 1.141 V_m + 0.2017$ **(2. 24)**

Group 2: $V_T = 1.1891 V_m + 0.0285$ **(2. 25)**

Group 3: $V_T = 1.20644 V_m$ **(2. 26)**

Film velocity by Duckler and Hubbard (1975):

$$V_f = V_m (1 - C \frac{\alpha_s - \alpha_f}{\alpha_f}) \alpha_f \quad \textbf{(2. 27)}$$

where the constant can be obtained using:

$$C = 0.021\ln(\mathrm{Re}_s) + 0.022 \quad \textbf{(2. 28)}$$

The constant C is used to calculate the film velocity by Duckler and Hubbard (1975).

2.5.3.2 Slug frequency and hold-up

Empirical correlations are usually required for slug frequency w_s and the liquid hold-up α_s in the slug body.

Gregory et al. (1977) provided correlations to calculate slug frequency as the following:

$$w_s = 0.0226\left[\frac{V_s}{gd}\left(\frac{19.75}{V_m} + V_m\right)\right]^{1.2} \quad \textbf{(2. 29)}$$

where, g is gravity acceleration 9.8 m/s^2, d is the pipe diameter, V_s is slug velocity.

Liquid hold-up with the slug was calculated by Gregory et al. (1977) and their proposed correlation was:

$$\alpha_s = \frac{1}{1 + (V_m / 8.66)^{1.39}} \quad \textbf{(2. 30)}$$

Liquid hold-up with the film as in the Duckler and Hubbard model is as follows:

$$C_k = 0.021\ln\left(\frac{V_m d\rho_l}{\mu_l}\right) \quad \textbf{(2. 31)}$$

$$\alpha_f = \frac{2C_k}{1 + C_k} \quad \textbf{(2. 32)}$$

2.5.3.3 Slug length

There are several methods to calculate the slug and film lengths. Both Duckler and Taitel (1976) developed a correlation to predict liquid slug length as below:

$$L_s = \frac{V_m}{(\alpha_s - \alpha_f)}\left[\frac{(1-\alpha_f)\rho_m}{\rho_l} + C_i(\alpha_s - \alpha_f)\right] \quad \textbf{(2. 33)}$$

2.6 TWO-PHASE GAS VOID FRACTION CONCENTRATION AND VELOCITY PROFILE

Ekambara et al. (2008) have studies on bubbly two-phase flow in a horizontal pipe using CFD simulation. The simulations were carried out to obtain results under fully developed bubble flow conditions in the 50mm internal diameter and 9m long horizontal pipe lines using CFX for air-water system. Liquid (V_l) and gas (V_g) superficial velocities varied from 3.8 to 5.1m/s and 0.2 to 1.0m/s, respectively, and average volume fractions varied in the range from 4 to 16%. They reported that the predicted volume fraction profile shows a peak in the top of the pipe, where gas bubbles tend to migrate toward the upper wall as shown in Figure 2-10.

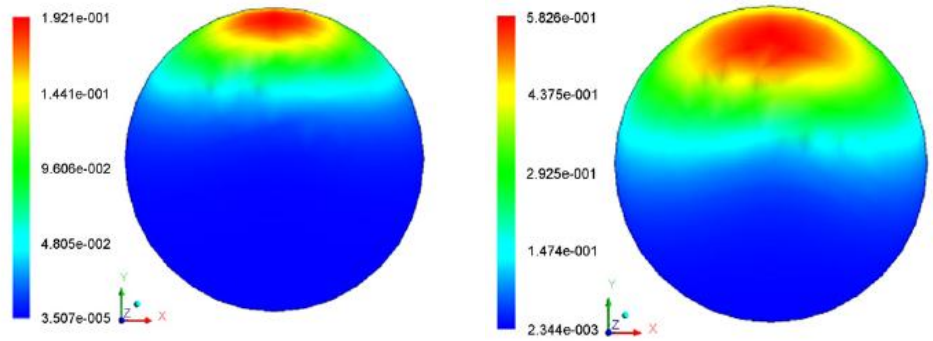

V_g = 0.25 m/s, V_l = 5.1 m/s,

V_g = 0.50 m/s, V_l = 5.1 m/s,

Figure 2-10, Gas void fraction profile in two-phase flow, taken from Ekambara et al. (2008)

These results show that the axial liquid velocity profile has a slight degree of asymmetry due to the presence of gas flow which concentrates on the top of the pipe. The degree of asymmetry decreases with increasing liquid flow or decreasing gas flow.

The slip velocity between liquid and gas would be greater, because of the big difference in densities between phases, which is an important feature of two-phase flow.

Ekambara et al. (2008) have shown it is manifest that the liquid phase occupies a dominant position in the pipe bottom section where the movement of the gas phase is controlled by the liquid phase with a small slip velocity between them, whereas at the top of the pipe a large slip velocity occurs. The reason for this large slip velocity is

that gas moves with less limitation by liquid and liquid velocity tends to decrease due to the boundary condition.

Iskandrani and Kojasoy (2000) investigated local void fraction distribution around a 0.05m diameter pipe and they observed that the void fraction distribution showed a sharp decrease towards the bottom of the pipe and that the liquid layer thickness decreased by increasing gas flow-rates at a given liquid flow. Bubbles seem to concentrate at the upper wall under the dominant influence of buoyancy force, and, as a result of coalescence of bubbles when the GVF increases, big bubbles appear.

The influence of gas flow on local gas void fraction in regard to the horizontal pipe bottom and upper part of the cross section is illustrated in Figure 2-11.

where, $r/R = -1$ identifies the bottom of the pipe, whereas, $r/R = 1$ refers to the top of the pipe.

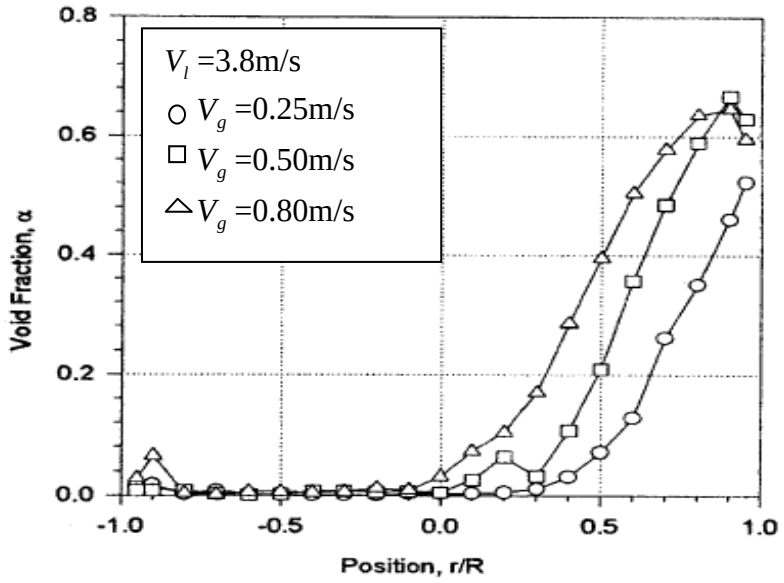

Figure 2-11, Influence of gas flow on local void fraction, taken from Iskandrani and Kojasoy (2000)

It is clear that at the upper part of the pipe, gas concentration is increased as the GVF increases, whereas liquid concentration seems to increase as a result of gravity force towards the lower part of the pipe (0.0 -1.0) where 0.0 and 1.0 are the bottom and the top of the pipe respectively.

A typical void fraction profile has been shown by Haoues et al. (2007). They reported that as a result of bubbles migration towards the upper part of the horizontal pipe, different profile structures can appear along a pipe section. In order to provide a well presented profile structure of two-phase liquid gas bubbly flow in a horizontal pipe, nine typical GVF profiles have been highlighted, as illustrated in Figure 2-12.

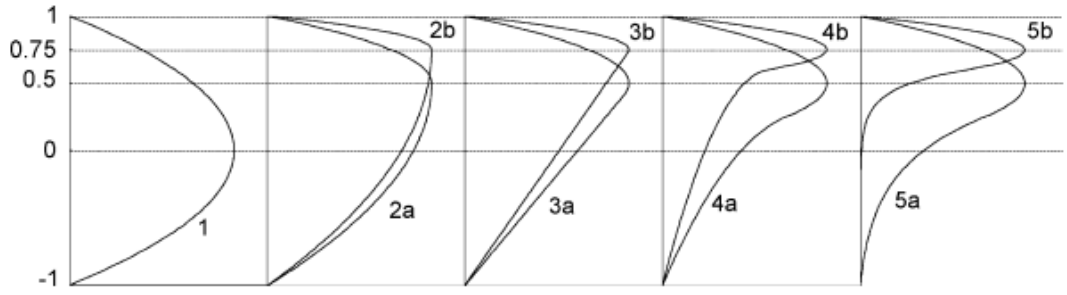

Figure 2-12, Typical void fraction profiles, taken from Haoues et al. (2007)

Haoues et al.'s (2007) study shows a non-symmetric void fraction profile with a maximum of its concentration near the top of the pipe wall. As the GVF is increased, different locations of GVF concentration occur.

Figure 2-13 shows some of these locations, starting from a single phase liquid flow as the gas flowrate increases.

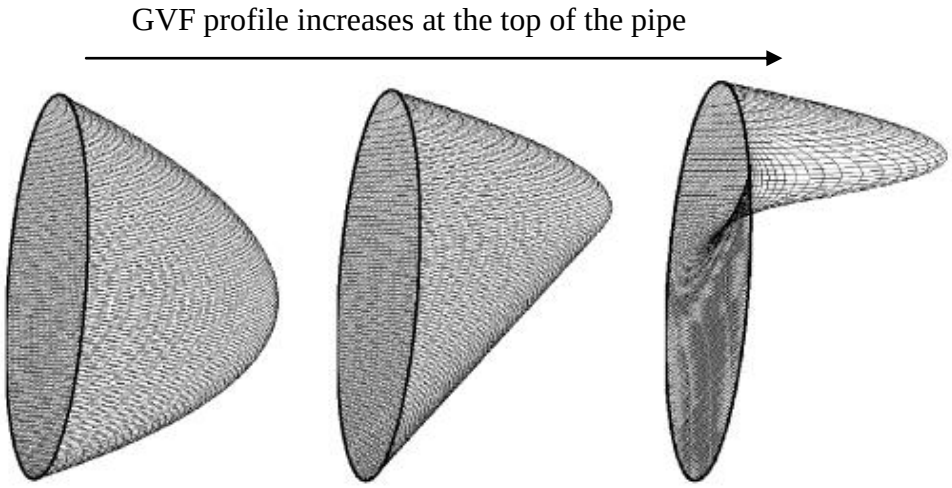

Figure 2-13, Void fraction profiles

2.6.1 Velocity profile of water/air mixture flow

Kocamustafaogullari et al. (1994) reported in their experimental investigations the internal structure of air-water flowing horizontally using a double-sensor resistivity probe technique for measurements of local interfacial parameters, including void fraction, and bubble interface velocity in 50mm pipe diameter, see Figure 2-14.

The experiments have been performed under bubbly flow conditions by deploying double-sensor resistivity probes. Liquid and gas superficial velocities ranged from 3.74 to 6.59m/s and 0.21 to 1.34m/s, respectively, and void fractions spanned from 3.73 to 21.5%. The temperature range was approximately 21-23°C, at atmospheric system pressure.

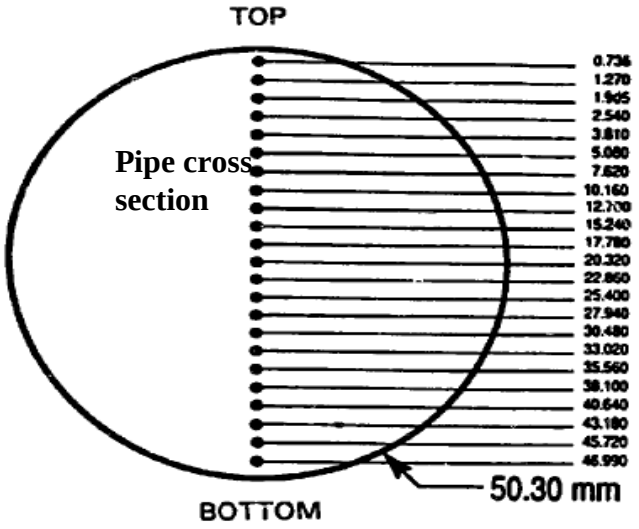

Figure 2-14, Probe positions along vertical axis of test section, taken from Kocamustafaogullari et al. (1994)

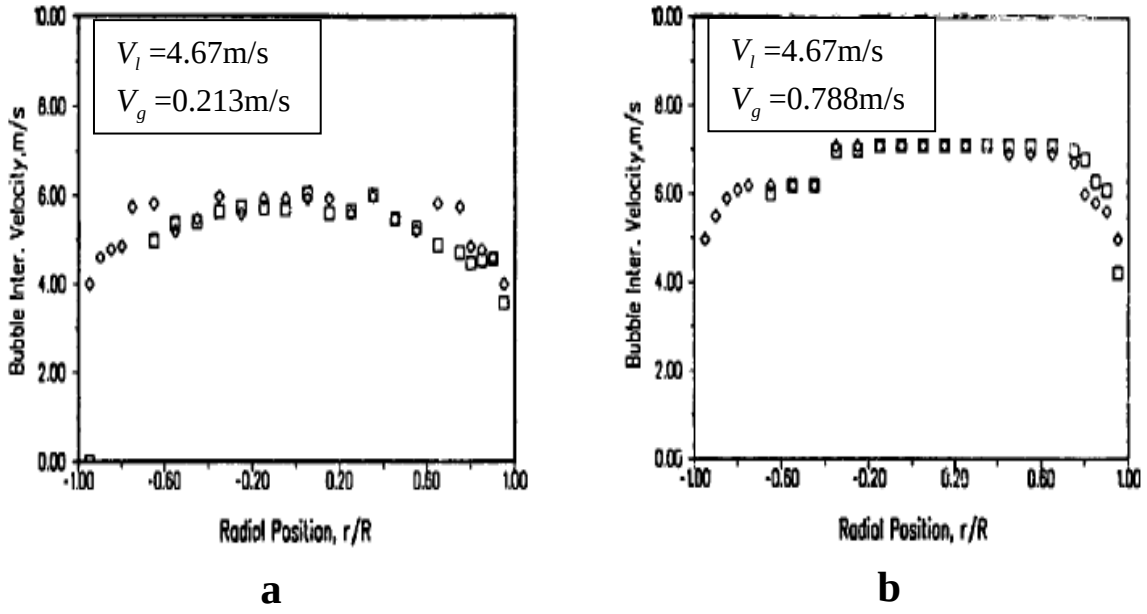

Figure 2- 15, Distribution of mean velocity in air/water taken from Kocamustafaogullari et al. (1994)

By observing the velocity profiles in Figure 2- 15 (a) at various radial positions at low superficial gas velocity, there is a fairly uniform distribution over a large portion of the flow area, except for the wall regions. At higher gas superficial velocity, the two-phase velocity profile shows mixture velocity increasing at the top of the pipe, as shown in Figure 2- 15 (b).

2.7 MEASUREMENTS TECHNIQUES IN MULTIPHASE FLOW

There are some requirements for multiphase measurement meters in order to measure the flow-rate of each phase. These requirements are briefly explained below. As mentioned earlier, the multiphase flowmeters have their own principles, which are illustrated in more details in the following section.

2.7.1 Velocity and volume flow measurements

2.7.1.1 Velocity measurement using venturi

A Venturi is often used to determine the velocity of the flow. In a Venturi meter the differential pressure (P_1-P_2) across the upstream section and the Venturi throat is measured and then related to the mass flow-rate, (Handbook of Multiphase Flow Metering, (2005)). For single-phase flows, the pressure drop across the restriction is a straightforward function of the velocity and density of the fluid. For multiphase

flows, the analysis is rather more complicated as the mixture density is changing. (Piwoda, 2003)

Obviously, this meter has no moving parts, and as a result it is considered to be easy to build. In terms of footprint, as this flowmeter does occupy a large footprint in an oil and gas platform. Figure 2-17 shows a Venturi flow meter.

Although Venturi flowmeters have generally been used for large water flow-rates measurement, they are also adapted to be used for slurry and multiphase flow measurements, (Baker, 2000).

The high energy recovery makes venturi even more attractive to be implemented in many applications such as measuring a wet gas in the AGAR flowmeter and measuring the mixture velocity in the ROXAR flowmeter. The downstream angle cone within this meter should be small, in order to make pressure recovery large and to minimise the friction losses (Jama and Sanderson, 2004).

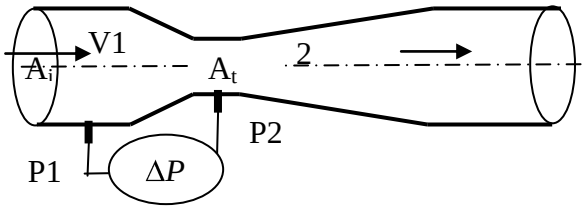

Figure 2-16, Venturi flowmeter diagram

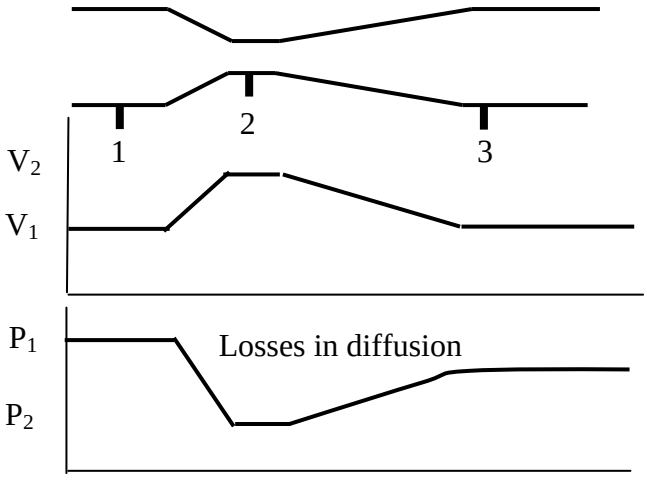

Figure 2-17, Venturi velocity and pressure changes, taken from Sanderson, (2009)

The mixture flow-rate through the Venturi is given as:

$$Q_m = \frac{C_D A_t}{\sqrt{1-\{\frac{A_t}{A_i}\}^2}} \sqrt{2\Delta P.\rho_m} \quad \textbf{(2. 34)}$$

where A_t and A_i are the areas at the throat and the inlet, C_D is the discharge coefficient, ρ_m is the mixture density, ΔP is the differential pressure, and Q_m is the mixture flow-rate through the Venturi.

The mixture density can be calculated using the following equation:

$$\rho_m = \alpha_g \rho_g + (1-\alpha_g)\rho_l \quad \textbf{(2. 35)}$$

2.7.1.1.1 The advantages and disadvantages of Venturi

There are some advantages to using Venturi over some other measurement techniques; there is low loss in flow pressure and it is less affected by upstream flow distortions. However, the drawbacks of using Venturi are that they have low differential pressure, are expensive to construct and have a longer axial length of meter. (Baker 2000).

2.7.1.2 Cross-correlation velocity measurement

This is based on using two similar measurements, each in a different axial location in the pipe. The velocity is determined by comparing the two measurements, for example, the time required for a bubble to travel between the two sensors leads to the velocity since the distance between the sensors is known. (Piwoda, 2003).

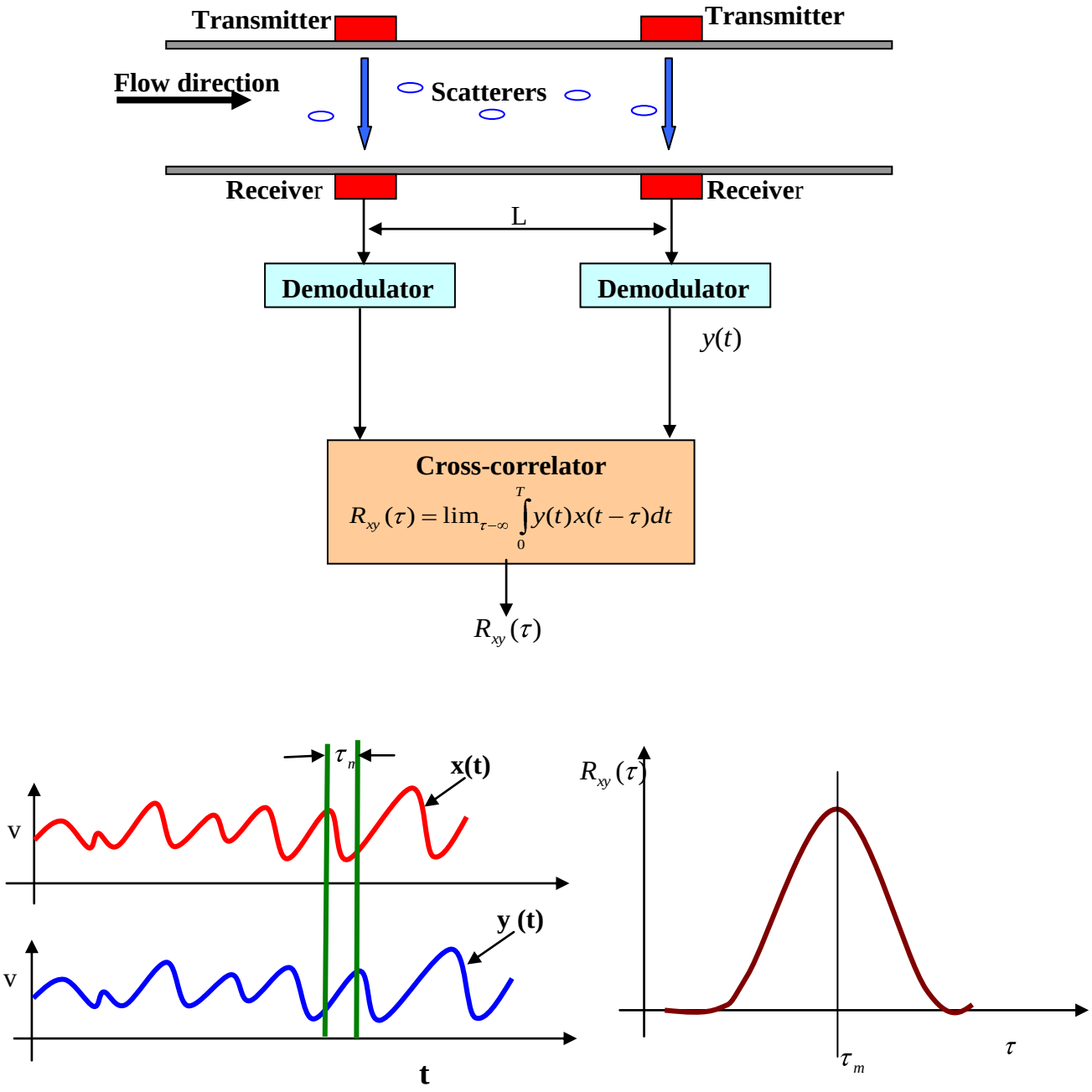

Figure 2-18, Cross-correlation meter, adopted from Xu et al. (1987)

Figure 2-18 illustrates the cross-correlation measurement method, identical sensors are installed with a known axial distance (L) apart. The maximum time delay (τ_m) taken by the bubbles travelling from the upstream transducer to the downstream transducer is obtained by cross correlating technique (Yan, 1996). The moving

bubble velocity (V) is then obtained from the transducers distance L and the maximum time delay τ_m:

$$Rxy(\tau) = \frac{1}{T}\int_0^T x(t)\,y(t-\tau)dt \qquad \textbf{(2. 36)}$$

The velocity of the flow V can be found from:

$$V = L/\tau_m \qquad \textbf{(2. 37)}$$

The method can be further referred as follows:
High and low frequencies occur as a result of large and small bubbles moving within the flow. Small bubble sizes relate to the velocity of the liquid, assuming that they flow at the same velocity of the liquid, whereas the large sized bubbles can refer to the gas velocity. Cross-correlation of different frequency components of the signal can be used to measure gas and liquid velocities.

The cross-correlation ultrasonic flowmeters are not generally used as a measuring method. However they are available for specific applications from some manufacturers (Sanderson and Yeung, 2002).

The greatest advantages of cross-correlation techniques are convenient for two-phase flows (e.g. liquid gas) and are inexpensive compared to transit time meters. However, the drawbacks of these techniques are that the correlation signal depends on the disturbance source and the source of correlation velocity could vary according to the velocity of the main fluid, which may result in further uncertainty in the sensed velocity (Baker, 2002).

2.7.1.3 Positive displacement meter

This is a method to measure the volumetric flow-rate of a liquid or gas; it is based on separating the flow stream into known volumes and counting the number of them over time, as shown in Figure 2-19. The fluid separation can be undertaken using vanes, gears, pistons or diaphragms.

When a positive displacement (PD) meter is involved in measuring multiphase flow, it is adapted to measure the total volumetric of multiphase flow-rate as a mixture (gas and liquid) flow (Jama, 2004). There is considered to be an approximately linear relationship between the rotating vanes and flow-rate for this kind of volumetric flowmeter. However, this relationship is valid within some uncertainty limits defined by upper and lower ranges (Baker, 2000).

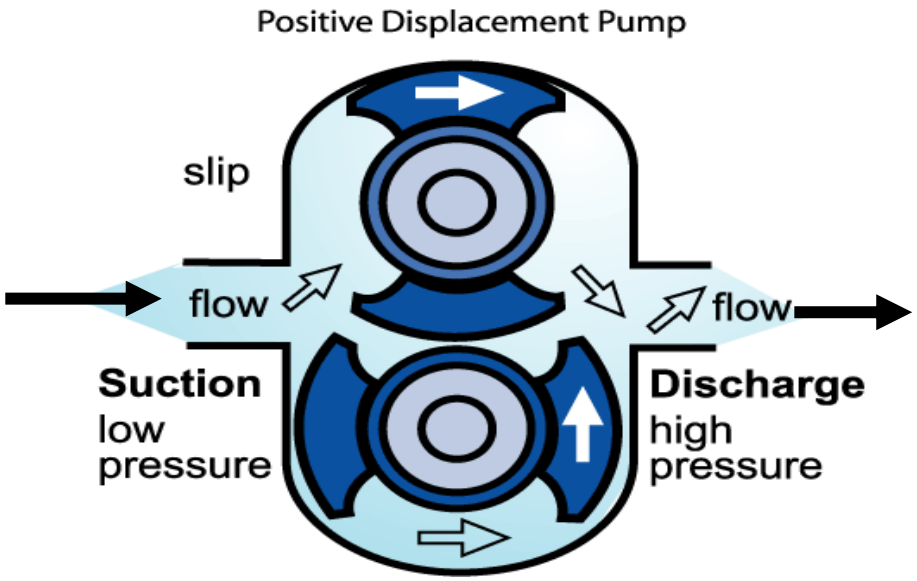

Figure 2-19, Positive Displacement meter

The rotary displacement or PD, besides its capability to measure single-phase flow, is also capable of metering mixture (gas/liquid) volumetric flow-rate.

The PD flowmeter has advantages such as it is high accuracy, large turndown, transfer standard use, and pulse output (mechanical or electrical) is proportional to the flow-rate. However, the disadvantages of using PD are that it can cause total line blockage, high accuracy version can be bulky, it can be damaged by sudden flow change, it may corrode in water, and it may create flow pulsation (Baker, 2000).

2.7.2 The advantages and disadvantages of various multiphase flow measurement techniques

Table 2-2 shows some widely used measurement methods for multiphase flow measurement and it shows their advantages and drawbacks in terms of the application used and the flow conditions. These measurement methods have been implemented in some of the multiphase flowmeters that have been illustrated earlier in this chapter.

No.	Measurement method	Advantages	Disadvantages
1	Positive displacement meter	Reliable and accurate for high viscosity	Performance degradation with increase in water cut
2	Momentum (Venturi meter)	Simple and inexpensive	Dependent on pressure drop correlation of MPF
3	Cross-correlation and momentum meter	Simple and inexpensive	Flow regime dependent
4	Cross-correlation and densitometer	Simple and inexpensive	Flow regime dependent and radioactivity
5	Mass (Coriolis) meter	Simple and accurate	Performance degradation with increase in gas content
6	Separation of phases	Simple and accurate	Not real time measurement

Table 2-2, Advantages and disadvantages of Multiphase flowmeters, taken from Babelli (2002)

2.7.2.1 Accuracy and fiscal metering in MPFMs

Accuracy in multiphase flowmeters is not constant as this accuracy depends upon many factors such as operational conditions, oil continuous, water-cuts and GVF.

The performance of a multiphase flowmeter does not meet that of a single-phase flowmeter because the latter do not have to deal with as many flow variables as the former. At present, multiphase flowmeters cannot be considered for fiscal metering purposes if traditional accuracies are required. The technology is still new and cannot yet offer the required accuracy.

2.7.2.2 Tomography methods

Tomography in general is a name for a collection of methods used for image reconstructions based on projections of objects.

This technique is based on the tomography process as a measurement technique which is used to determine the concentrations of each phase of the multiphase flow. As the computer capability increases, the tomography technique can be more efficient and reliable. The main advantage of using this technique is that it offers online multiphase flow measurement without flow disturbance.

Figure 2-20 demonstrates some main components associated with the tomography meter as a multiphase flow measurement.

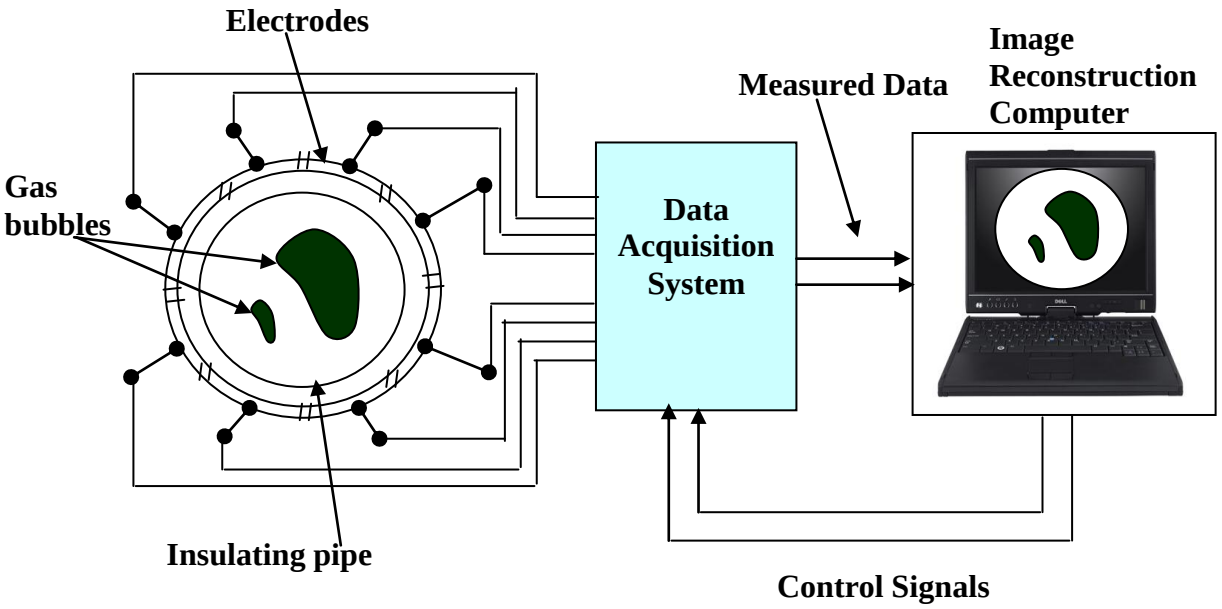

Figure 2-20, Multiphase flow imaging system, taken from Yan (1996)

Tomography is used to obtain multiphase flow measurement; it is based on dividing the pipe cross section into (N) parts of equivalent area (α_g).

The volumetric flow-rate of phase Q instantaneously can be given as:

$$Q = A\sum_{i=1}^{N} \alpha_g V_i \qquad \textbf{(2. 38)}$$

where: α_g and V_i are the void fraction of phase and fluid velocity, respectively, in the i part, and A is the area cross section.

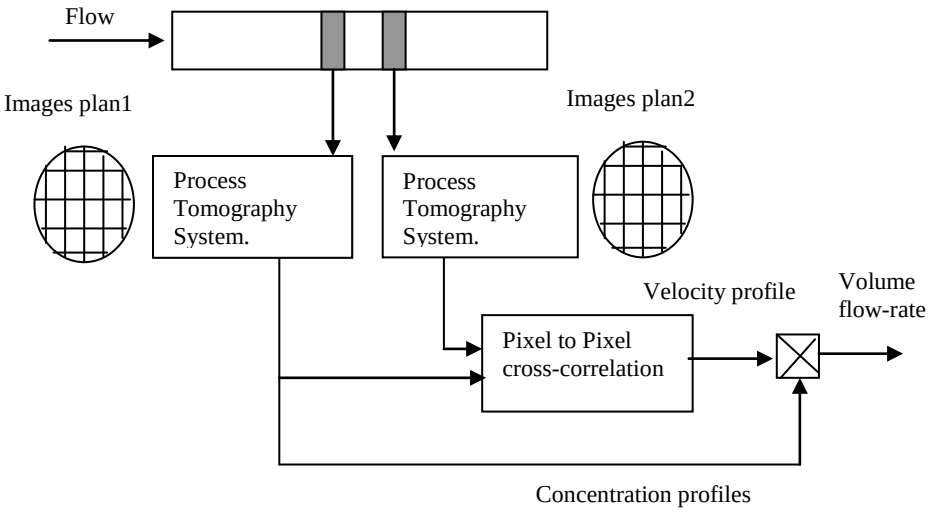

Figure 2-21, Tomography MPF Measurement, taken from Ismail et al. (2005)

The sensors, which detect the signals that are generated by the scatterers, can be based on different measurement techniques such as ultrasound, optical, capacitance, and impedance (Liu et al., 2005).

As can be seen from Figure 2-21, there are two image series of the flow simultaneously acquired in two continuous cross-sections of the pipe. Processing the two image series deploying cross-correlation methods can determine the flow velocity (V). Subsequently, the volume phase flow equation can be applied after the concentration distribution α is directly gained by the tomography image (Ismail et al., 2005).

Currently, there are several forms and shapes of tomography transducers or sensors, including ionising radiation (e.g., x-ray and γ-ray), nuclear magnetic resonance (NMR), optical, positron emission tomography (PET), microwave and ultrasound, electrical (i.e., capacitive, conductive and inductive). However, there are advantages and drawbacks for every one of these techniques. Therefore, the choice can be made according to the application which is under investigation, (Ismail et al., 2005).

These techniques are still very expensive and sensitive to use and there is much room for improvement before they can be implemented in the oil and gas industry reliably.

Qiu et al. (2007) developed a multi-model tomography system to fulfil the necessity for multiple tomography data where a single measurement technique or a single-modality such as Electrical Resistance Tomography (ERT) or Electrical Capacitance Tomography (ECT), was not able to provide the information sufficiently well on the process. They deployed ITS M3000 software based on a visual programming paradigm to control the operation and data process. This software offers the displaying of raw data and reconstructed images, interpretation strategies and control signal outputs. Figure 2-22 and Figure 2-23 illustrate a tomography system arrangement and multiphase flow detection using ITS M3000 software.

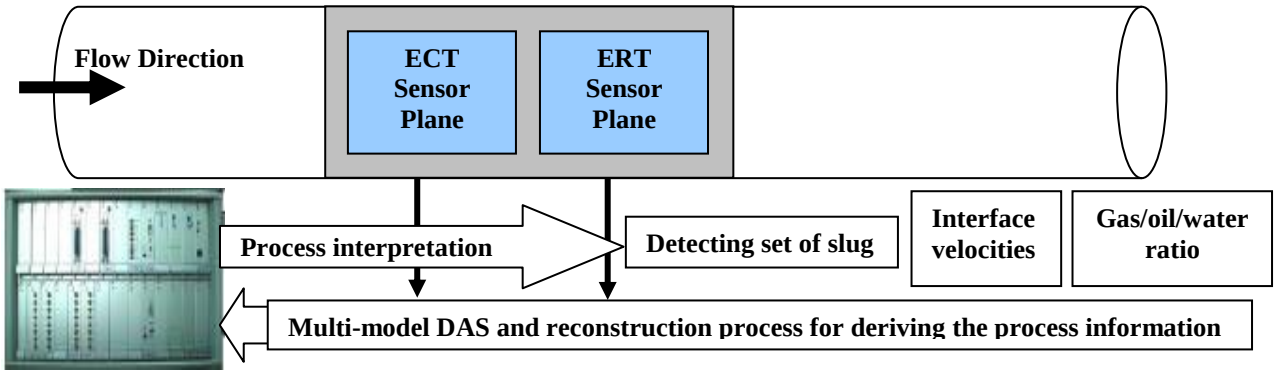

Figure 2-22, Tomography system arrangement in the industrial application, adapted from Qiu et al. (2007)

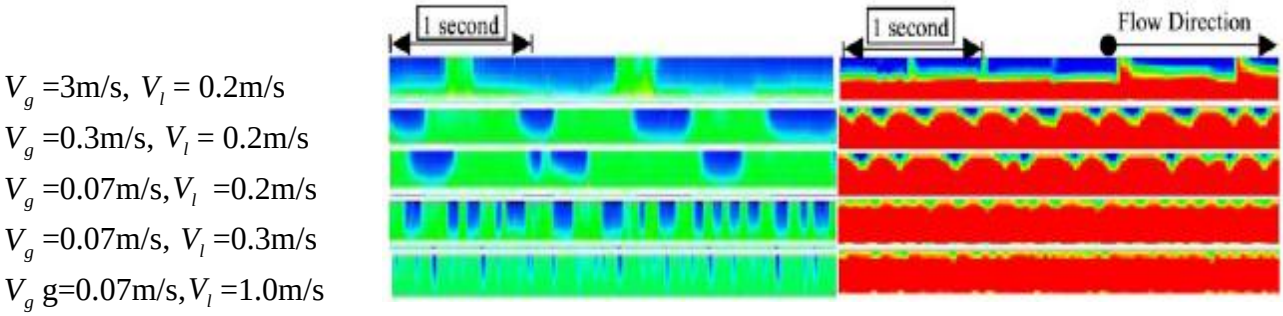

Figure 2-23, Detecting of air/oil/water multiphase flow with ITS M3000 multi-model system (a) gas/water, (b) gas/oil, taken from Qui et al. (2007)

2.7.3 Phase Fractions Measurement

There are a number of technologies used in multiphase flow measurements for the measurement of phase fractions; some of the most common are briefly illustrated below, as shown in Figure 2-24.

2.7.3.1 Gamma densitometer (single and dual beam)

There are a number of gamma ray methods that have been implemented in flow measurement; Figure 2-24 illustrates the gamma density meter main components. There are two commonly used gamma rays – single and dual energy gamma rays.

2.7.3.1.1 Single energy

This type of gamma densitometer is based on ray attenuation measurement and on the attenuation of a narrow beam of gamma. (Handbook of Multiphase Flow Metering, 2005). Single energy gamma rays can be used for two phase flows (liquid/liquid, gas/liquid).

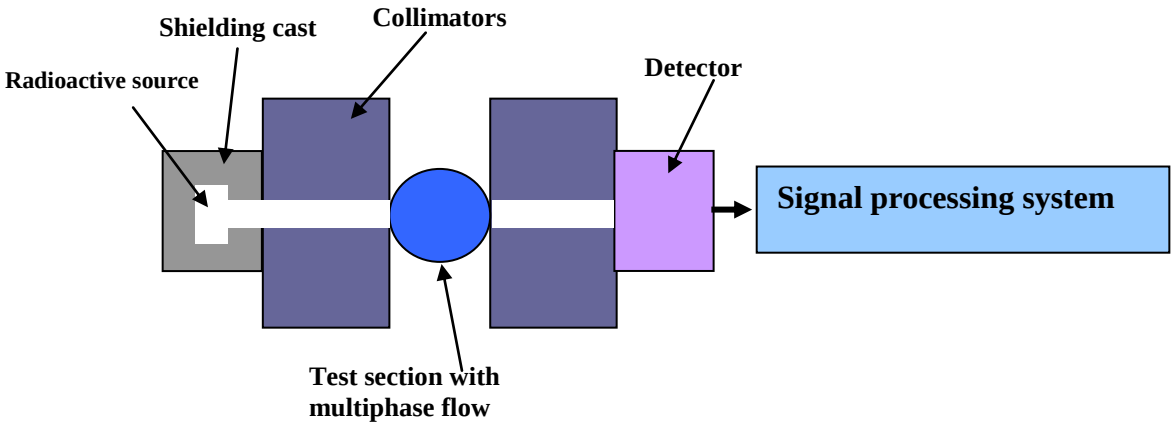

Figure 2-24, Gamma densitometer, taken from Jiang and Rezkallah (1993)

The density of the mixture is measured by gamma ray densitometer and related with the densities of the liquid and gas as illustrated in the following equation:

$$I_m(e) = I_v(e)\exp(-\sum_{i=1}^{2}\alpha_i\mu_i(e)d) \qquad \textbf{(2. 39)}$$

where, $I_m(e)$ is the measured count-rate, $I_v(e)$ is the count rate when the pipe is empty, μ_i is the linear attenuation coefficients for the two phase flow, and d the inner diameter of the meter piping.

Apart from the fraction of the phases α_i, the attenuation coefficients μ_i are also initially unknown. However, the term μ_i can be found by calibration where the meter is fully filled with individual phases.

The following equations can be used in present of full of water and then full of oil.

Water $$I_w = I_v \exp(-\alpha_w \mu_w d) \quad \textbf{(2. 40)}$$

Oil $$I_o = I_v \exp(-\alpha_o \mu_o d) \quad \textbf{(2. 41)}$$

However, as the sum of water cut and oil fraction is equal 1.

$$\alpha_o + \alpha_w = 1 \quad \textbf{(2. 42)}$$

The water fraction in two phase liquid/liquid mixture:

$$\alpha_w = \frac{\ln(I_w) - \ln(I_m)}{\ln(I_w) - \ln(I_o)} \quad \textbf{(2. 43)}$$

2.7.3.1.2 Dual energy gamma ray

Dual energy levels of gamma ray attenuation are basically used to determine the volumetric fraction of three phase flow (oil, water and gas). This is generally based on two main equations for each energy to be obtained when two beams of gamma rays that have different energies are applied. These two equations are as follows:

$$I_m(e) = I_v(e) \exp(-\sum_{i=1}^{2} \alpha_i \mu_i(e) d) \quad \textbf{(2. 44)}$$

where: $I_v(e)$ in the measured count-rate when the pipe is empty, μ_i is the linear attenuation coefficients for the three phase flow (μ_o, μ_w, μ_g), d is the inner diameter of the meter piping, ρ_o, ρ_w, ρ_g is the density of oil, water and gas, $\alpha_o, \alpha_w, \alpha_g$ is the volumetric fraction of oil, water and gas respectively (Sanderson, 2009).

$$\alpha_o + \alpha_w + \alpha_g = 1 \quad \textbf{(2. 45)}$$

A full set of linear equations is given below. R_o, R_e, R_w and R_m represent logarithms of the count rates for oil, gas, water and the mixture, respectively at energies e_1 and e_2.

$$\begin{bmatrix} R_w(e_1) & R_o(e_1) & R_g(e_1) \\ R_w(e_2) & R_o(e_2) & R_g(e_2) \\ 1 & 1 & 1 \end{bmatrix} \begin{bmatrix} \alpha_w \\ \alpha_o \\ \alpha_g \end{bmatrix} = \begin{bmatrix} R_m(e_1) \\ R_m(e_2) \\ 1 \end{bmatrix} \quad \textbf{(2. 46)}$$

The elements in the matrix are determined in a calibration process by filling the instrument with 100% water, 100% oil and 100% gas (air) or alternatively by calculations based on the fluid properties. Together with the measured count rates at the two energy levels from a multiphase mixture it is then possible to calculate the unknown phase fractions (Handbook of Multiphase Flow Metering, 2005).

Figure 2-25 presents the logarithm of the count rates of the two energy levels plotted along the axis. The corners of the triangle are the water, oil and gas calibrations, and any point inside this triangle represents a particular composition of water, oil and gas, e.g. a point half way on the water-gas line represents 50% water and 50% gas mixture.

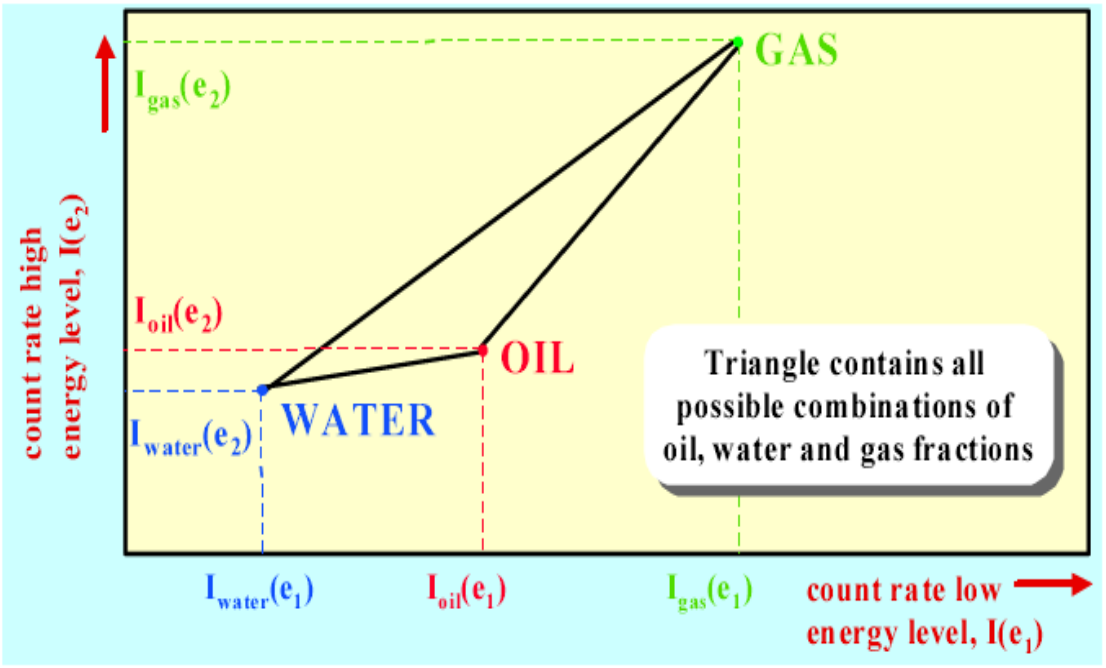

Figure 2-25, Dual energy gamma ray response triangle, taken from Handbook of MFM (2005)

2.7.3.2 Electrical impedance methods (capacitance and conductance)

The basic principle of impedance method for fraction measurement is to measure the electrical impedance across two opposed electrodes, which are in contact with the

flowing oil–water–gas as a mixture. The resistance and capacitance depend on the permittivity and conductivity of the flowing oil, water and gas components, the flow regime, the excitation frequency of the detection electronics, the void fraction and water fraction.

2.7.3.2.1 Electrical Capacitance

The main objective of the capacitance based measurement is to determine the dielectric constant of the mixture (liquid and gas); the principle of this technique is based on two electrodes installed on the internal walls of the pipe, opposite to each other and in constant contact with the flowing fluid (Sanderson, 2009). This technique is used for oil continuous flow since the fluid is not conductive.

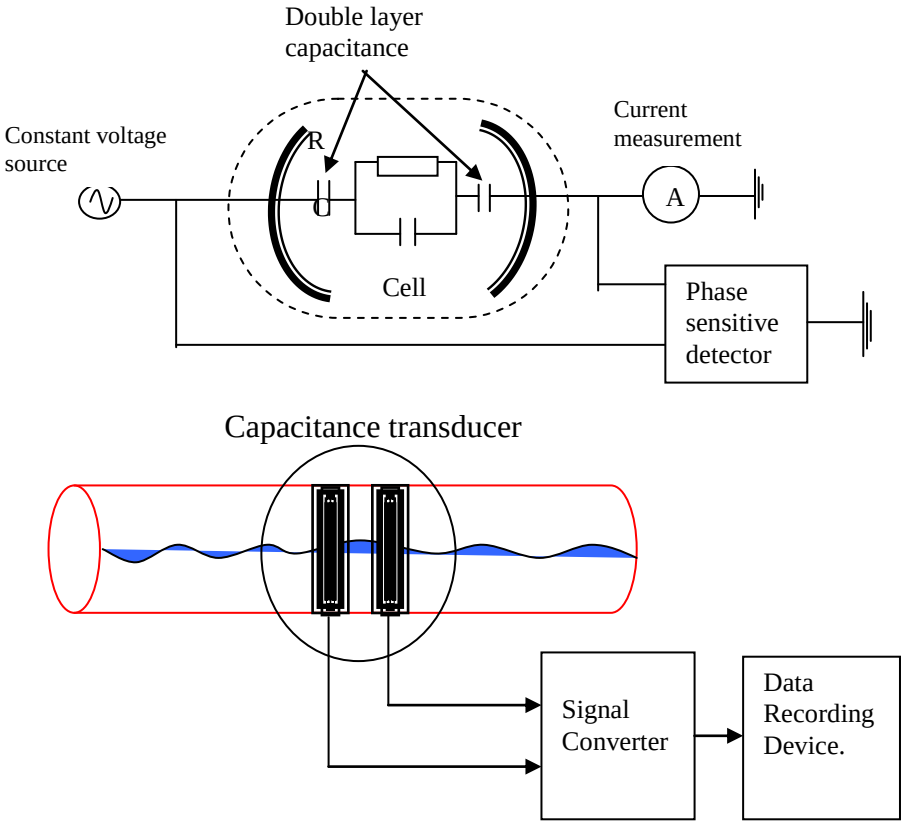

Figure 2-26, Electrical capacitance, taken from, (Sanderson, 2009)

2.7.3.2.2 Conductive measurement

The fluid conductivity can be measured by injecting a controlled electrical current into the flowing fluid; the voltage drop between two electrodes along an insulated section of the pipe can then eventually be determined. The injected current can be connected to the flowing fluids by being inserted electrodes in the flow or in a non-contacting mode by coils (inductive mode). Ohm's law is used to calculate the resistance or conductance from both the current and the voltage drop (Handbook of Multiphase Flow Metering, 2005).

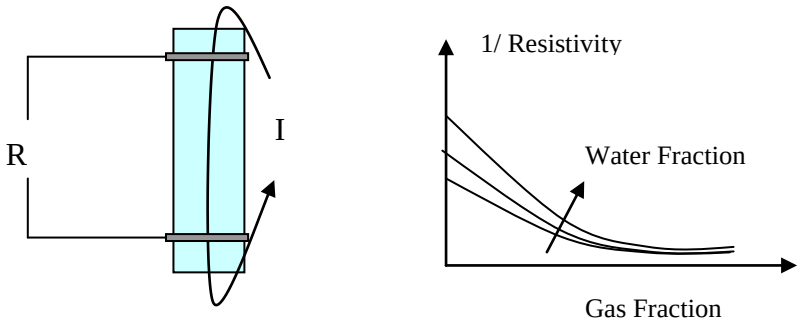

Figure 2-27, Typical conductance measurement principle, Taken from Handbook of Multiphase Flow Metering (2005).

2.8 PATTERN RECOGNITION (NEURAL NETWORK)

2.8.1 Neural network background

The neural network (NN) offers a convenient method for nonlinear modelling; it is also called pattern recognition, where a features collection is fed into the network, and the task is to assign the input to one or more class. NNs very much perform as biological networks within the brain, they are based on cause and effect relationships which are able to be trained and learned, and they have the ability to arrange large quantities of information into orderly patterns. Lang et al. (2003).

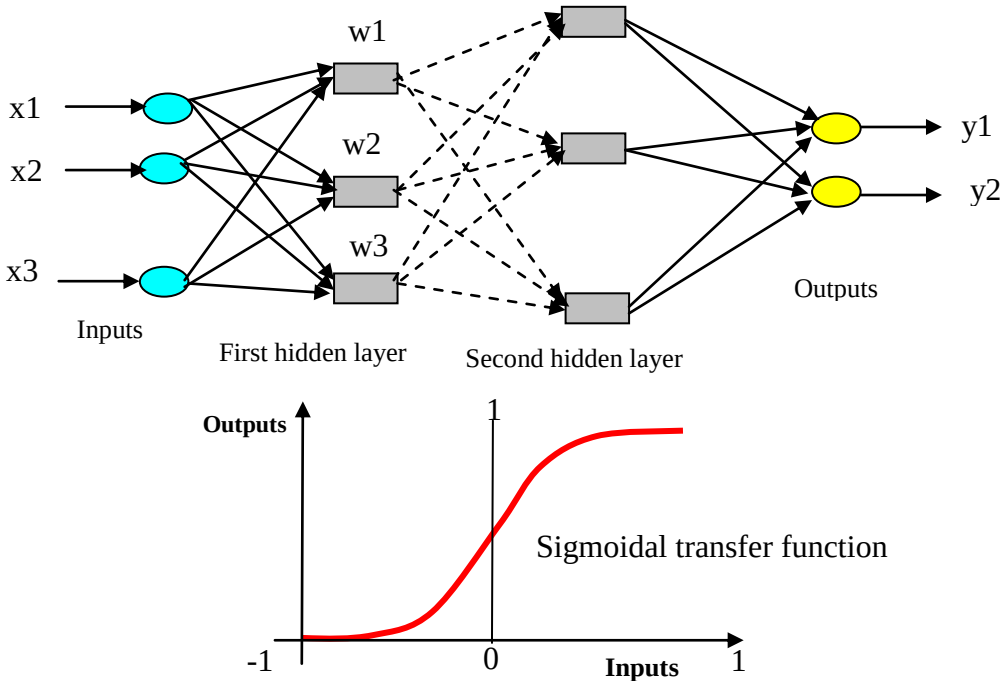

Figure 2-28, Neural networks Scheme

This nonlinear function is the most common type of the activations used to construct NNs. A sigmoidal transfer function can be written as the following:

$$i = \sum_{i=1}^{n} w_i x_i \qquad \textbf{(2. 47)}$$

$$y = \frac{1}{1+e^{-\alpha i}} \qquad \textbf{(2. 48)}$$

Where α is the shape parameter of the sigmoid function, the values w1, w2, w3 are weight factors associated with each node to determine the strength of input row vector x1, x2, and x3.

In order to find the relationship between the input and output layers, as shown in Figure 2-28, it is crucial that networks are trained to minimise the errors between the guessed inputs and the actual outputs Sanderson, (2009). They can offer the relationship between the input such as pressure, capacitance, conductance and gamma ray sensors, and output such as the mass flow-rates for each individual phase.

The NN has the ability to learn which can yield a new generation of algorithms, summarised into the following(Shaike and Al-Dahhan, 2003).:

- Based on past knowledge gained to expect future.
- Establish rules of reasoning in complicated environments.
- Offer solutions when explicit algorithms and models are unavailable or too bulky.

2.8.2 Advantages and disadvantages of NNs

2.8.2.1 Advantages of NNs

There are some essential advantages of using NNs. They are as the following:

1. NNs are adaptive, they have the ability to process data and learn from them, and as a result they offer solutions from the available data. They also decrease the processing time by learning underlying relationships even if they are difficult to find and demonstrate.
2. NNs can generalise; they can correctly process data that only largely resemble the given data on which they were trained originally.
3. NNs are nonlinear; they are capable of resolving a complex interaction among the input variables in a system.
4. NNs are highly parallel; their numerous matching, and independent operations can be performed simultaneously.

2.8.2.2 Disadvantages of NNs

The NN disadvantages are summarised as follows Aggarwal and Yonghua (1997):

1. They can be difficult in accounting for their outputs; they are like the human brain that performs and expresses opinions that it can not easily demonstrate.
2. Training methods are imperfectly understood; there is no classified way of finding the perfect results that rely greatly on the accuracy of the training data used.

3. NNs can consume large amounts of computer time; in the training stage, it is quite common for NNs training to consume massive amounts of time.
4. It is possible to over train neural networks.
5. No error boundary.

2.8.3 Some examples for neural networks with Multiphase flow

ANNs have been developed to be deployed in multiphase flow measurement based on pattern recognition methods. These offer online measurement of multiphase flow using a data processing paradigm that was inspired by the way the biological nervous system processes data. The advantages of using ANNs in multiphase flow measurement are their abilities to represent both linear and non-linear relationships.

This approach of ANNs to multiphase flow measurement requires no conditioning of the multiphase flow since they are able to measure the flow without inserting a probe in the system. As shown in Figure 2-29. There are more details addressed about ANN types and their multiphase flow applications.

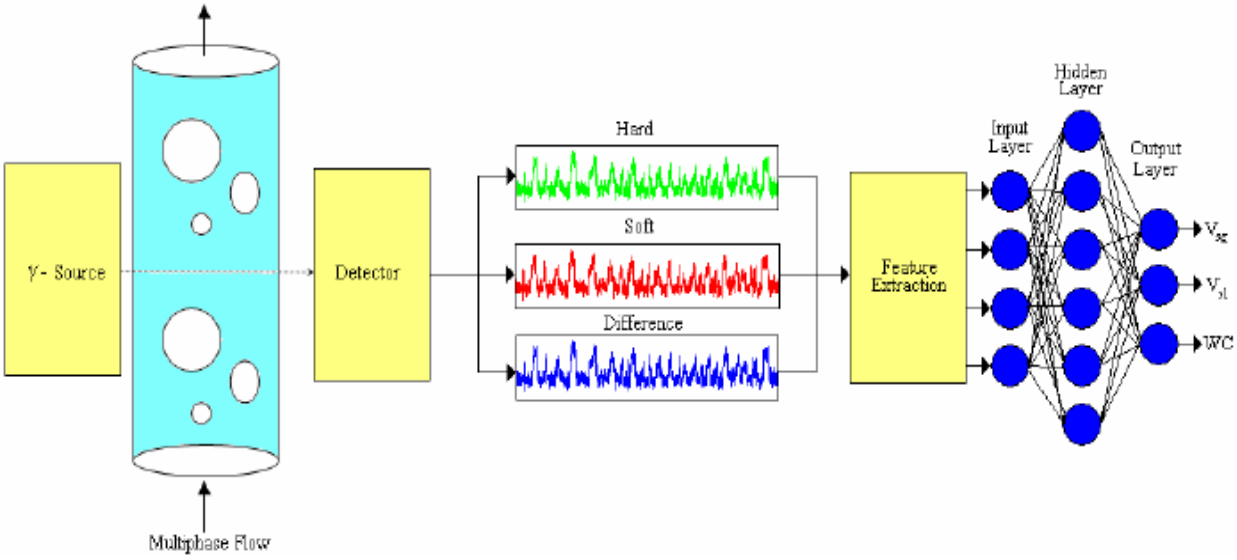

Figure 2-29, Three layer feed-forward artificial neural network

Jama (2004) presented a wet gas measuring technique involving the use of a standard Venturi meter together with the advanced pattern recognition method. He used a multilayer perceptron (MLP) NN to construct a non-linear mapping between different feature vectors and the corresponding gas and liquid flow-rates using a correctly labelled training data. The PR system developed by Jama relies on pressure sensors to extract relevant information in the form of features. A Bayesian MLP NN

is then used to relate these features to the gas and liquid superficial velocities, from which the volumetric flow-rates can be calculated. When the generalisation performance of different developed measurement scenarios was tested, the cross-sensor data fusion of the amplitude features achieved 100% of the test data to within $\pm 5\%$ error across the whole flow (Jama, 2004).

Blaney and Yeung (2007) have investigated the exploitation of a single clamp-on densitometer with pattern recognition data processing techniques. The aim of this investigation is to infer the superficial phase velocities and the liquid phase water cut, which leads to obtaining the individual component mass flow rates of the multiphase flow. They have assumed that the difference between the water and oil phase velocity were negligible and that their velocities could be represented by a common value for the total liquid phase.

They have clamped the gamma densitometry technique on the vertical section at the top of the catenary riser in Cranfield University Multiphase Flow Test Facility to exploit non-intrusive multiphase flow metering for 126 different multiphase fluid conditions. All signal processing and neural network simulations were performed using MATHWORKS Inc MATLAB version 7.1.0.246 (R14). Two neural network models were developed for comparison: a single multilayer perceptron and a multilayer hierarchical flow regime-dependent. Feature extraction from the time-varying gamma hard and soft (the direct and scattered gamma) count signals was employed to produce input parameters for the neural network models. Features were also extracted from a third synthesized 'difference' signal that recorded the absolute difference between the hard and soft counts.

Analysis of the signal characteristics have shown that reliable statistical representation of the multiphase flow can be attained with measurement periods of 20 min with no appreciable difference in the neural network classification accuracy. The single MLP neural network model classified 97% of all test point gas superficial velocities to within ±10% and 71% to 5%; however, the liquid parameter predictions were not of the same standard. The liquid sensitivity to feature correlations was also found to be flow regime dependent.

2.9 ULTRASONIC MEASURING TECHNIQUES

Ultrasonic sensors are used to transmit and receive acoustic waves higher than the audible. The received signal depends upon the property of the measured material. At the receiver, the ultrasonic signal carries the data about the parameters to be evaluated. Ultrasonic sensors cover a frequency range from 20 kHz to about 1 GHz (Hauptmann et al., 2002).

Currently, ultrasonic flowmeter techniques are the only interrogation techniques commonly and commercially available for clamp-on volumetric flow measurement (Sanderson, 1999).

2.9.1.1 Generating and detecting ultrasound

Ultrasound is commonly generated and detected by using piezoelectric crystals O'Sullivan and Wright (2002). An important requirement of piezoelectrics is to achieve certain characteristics such as damping, directionality, etc. There are some designs which allow the transducers to be installed on the outside of a pipe as clamp-on without breaking into the pipe. The dimensions and the material of the working pipe and the investigated flow are essential elements in choosing the right ultrasonic transducers.

There are several ultrasonic transducer techniques commercially available that offer different ultrasonic techniques within a variety of shapes and sizes. Figure 2-30 shows a simple piezoelectric transducer for generating ultrasound.

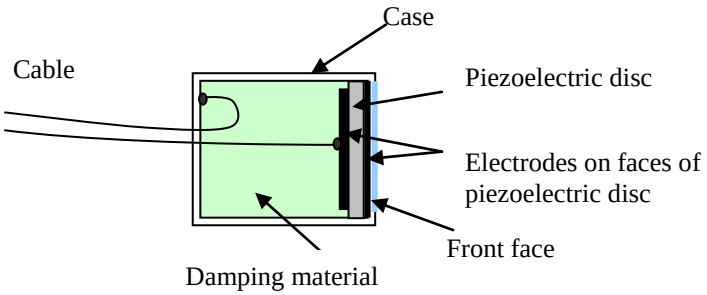

Figure 2-30, Piezoelectric transducer, taken from Asher (1997)

2.9.1.2 Principles of Piezoelectric

When mechanical stress is applied to a piezoelectric material, it yields an electromotive force (e.m.f.) and vice versa. A piezoelectric has the ability to function as a transmitter and receiver of ultrasound. When it is implemented as a transmitter, the voltage makes the contacting slice or element to behave as a piston radiator and generate a sound wave in the material in front of the front face of the transducer. Whereas functioning as a receiver, the sound waves impinging on the facing material face of the transducer generate strains in the piezoelectric element; the consequential e.m.f. is picked up by the electronic system.

The investigated material (fluid flow) and pipe geometries governs the thickness of the piezoelectric and the frequency used, for example for a typical PZT, a 1 MHz piezoelectric would have to be 2mm thick. The thickness can also be evaluated from the ultrasonic velocity (V_{PE}); hence thickness for a fundamental frequency corresponds to a half wavelength of sound in the piezoelectric material (Asher, 1997).

$$t_{PE} = \frac{V_{PE}}{2f} \qquad \textbf{(2. 49)}$$

Examples of transducer designs are the retro-fit (i.e. hot tap) and the clamp-on. The clamp-on transducer can offer measurement of the investigated material without breaking into the pipe, where the pipe geometries and materials are essential to be acknowledged to obtain an accurate measurement (Goudinakis et al., 1999).

2.9.2 Measurement Principles of Ultrasonic Techniques

2.9.2.1 Transit Time Techniques

The transit-time or time-of-flight method is the most commonly used in ultrasonic flow metering and the most accurate and it is available as a spool piece meter for liquids and gases or as clamp-on design. The principle of this technique is based on the small difference in time taken for an ultrasound wave to travel upstream and downstream under flow condition.

As it can be seen from the Figure 2- 31 that transit time means the difference between the time of flight of ultrasonic waves transmitted upstream and downstream in the investigated material.

The fluid velocity V along the ultrasonic path in a pipe of diameter d in meters at an angle θ to the flow direction is given as the following:

$$V = \frac{d\partial t}{2t_1 t_2 \sin\theta\cos\theta} \qquad \textbf{(2. 50)}$$

Where t_1 is the time of flight in seconds for upstream path Lu, t_2 is the time of flight in seconds for downstream path Ld, and $\partial\tau$ is the difference between t_1 and t_2, Sanderson (1999).

The shortest time that can be measured determines the accuracy of the instrument. Achieving 1% uncertainty, for a 100mm tube, time must be measured to within 1ns, Baker (2002).

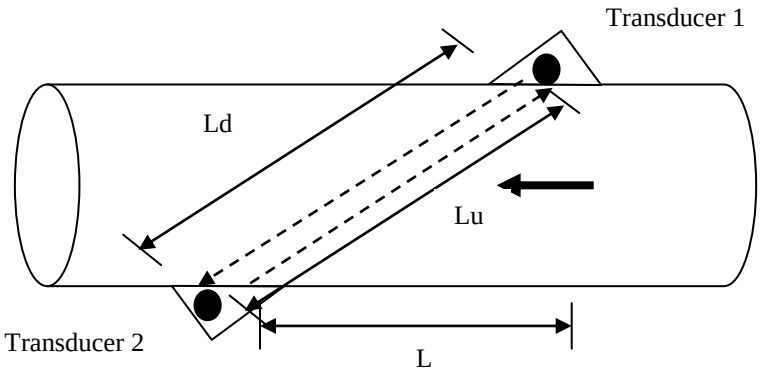

Figure 2- 31, Basic ultrasonic diagram.

There are three optional methods to obtain this transit time difference:

- Direct time measurement, or dt method.
- By measurement of the phase shift of two sinusoidal signals, or $d\phi$ method.
- By sing-around technique or df method.

Direct time measurement or dt method

In this method, the leading edge system is in function, and involves the measurement of the time interval between the leading edges of the two acoustic pulses transmitted across the flowing medium up-and downstream, Benard (1988). The transducers are installed opposite each other perform as transmitter and receiver.

The following equation is illustrated the speed of flow V:

$$\mathrm{V}=\frac{2Ldt}{\cos\theta(t_1+t_2)} \qquad \textbf{(2. 51)}$$

Where, L is the space between transducers, dT is the different between t_1-t_2, and θ is the angle between the beam and direction of flow, t_1 travel time of pulse upstream, and t_2 travel time of pulse downstream.

Phase shift or $d\theta$

In the phase shift principle of operating ultrasonic flow-meters each transducer sends out a burst of ultrasonic signals, and is then switched to function as a receiver. The phase of the two signals is modified by the flow and the phase difference is referring to the speed of flow.

Reflex type flow-meters are commercially available flow-meters which use this technique. This type of ultrasonic flow-meters increases the length of the flight path of the signals, which makes it convenient for smaller bore flow-meters Benard (1988).

$$V=\frac{d\theta C_l^{\,2}}{4fL} \qquad \textbf{(2. 52)}$$

Sing-around method

This ultrasonic technique, receives pulses trigger off another set of pulses and the pulse repetition rate is measured. The transducers functionality is then reversed and another repetition rate is measured. The difference in the sign-around repetition rates is a measure of the speed of the flow. The system can consist of one or two pairs of transducers and the general principle of measurement is similar in that the transit time of the acoustic pulse is the primary measurement. The velocity of the flow is derived by the following equation, Benard (1988):

$$V = \frac{dfL}{2\cos\theta} \qquad \textbf{(2. 53)}$$

Where, df is difference in frequency of repetition rates, L is the distance between the transducers, θ is the angle between beam and direction of flow.

Transit time offered traverses

As shown in Figure 2- 32, the ultrasonic transit time clamp-on has the capability to offer number of traverses of its path as a result of the ultrasonic reflection (2 traverses = 1 reflection point, etc.). However, the reflections weaken the signal strength. In order to achieve the best possible signal quality, the lowest possible number of traverses should be implemented, Endress and Hauser.

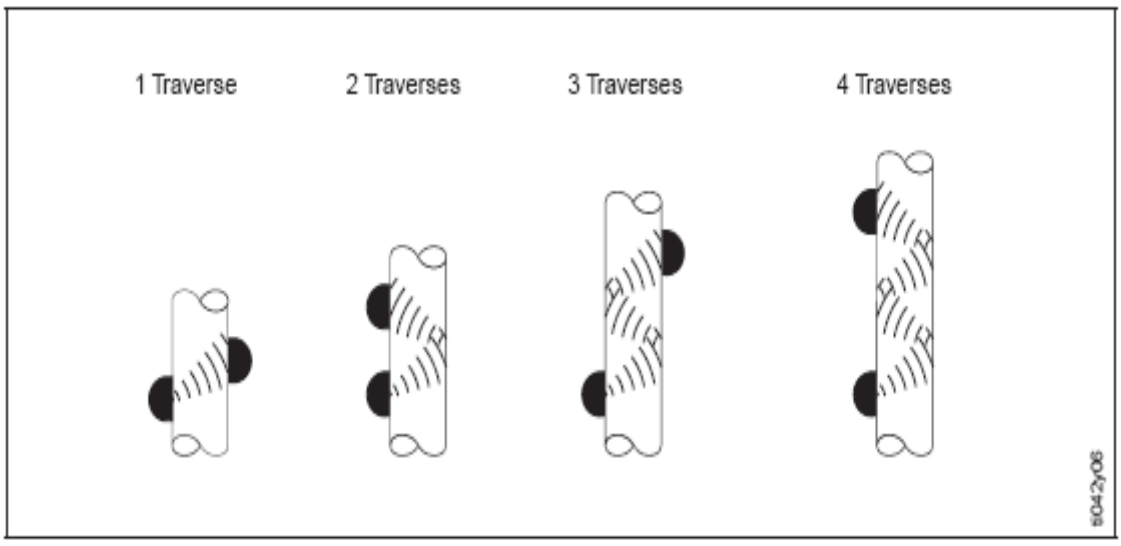

Figure 2- 32, Number of traverses, taken from (Endress and Hauser)

Advantages and disadvantages of ultrasonic transit time
The advantages

- No obstruction to flow
- Capability for retrofitting
- Available in clamp-on designs for liquid and gas
- Probably unaffected by pulsatile flow
- Suitable for most single-phase liquids
- Suitable for gas flows

The disadvantages

- Transducer cavities may collect air or debris
- Response time may be slow
- Unsuitable for most two-phase flow
- Piezo-electric crystals must be in contact with gas in most designs.

2.9.2.2 Doppler ultrasonic flowmeter

The Doppler ultrasonic flowmeter principle is based on the reflection of an acoustic wave from a moving element back to the source; the frequency shift is proportional to the velocity component of the object parallel to the acoustic beam - see Figure 2-33. However, the Doppler flowmeter's function is limited as a result of the character, size, spatial of the particles that differ from the attenuation of the ultrasonic stream. Since the sensed velocity is as a result of scatterers, scatterers might not correspond to fluid velocity (Sanderson and Yeung (2002). Normally, the near transducer wall section is the only section that is monitored. The zone of reflection is in a region of varying velocity (Benard, 1988).

If the transmitted frequency is ft, then the frequency shift of the reflected signal is given by:

$$\Delta f = 2\, ft(V / C_l)\cos\theta \qquad \textbf{(2. 54)}$$

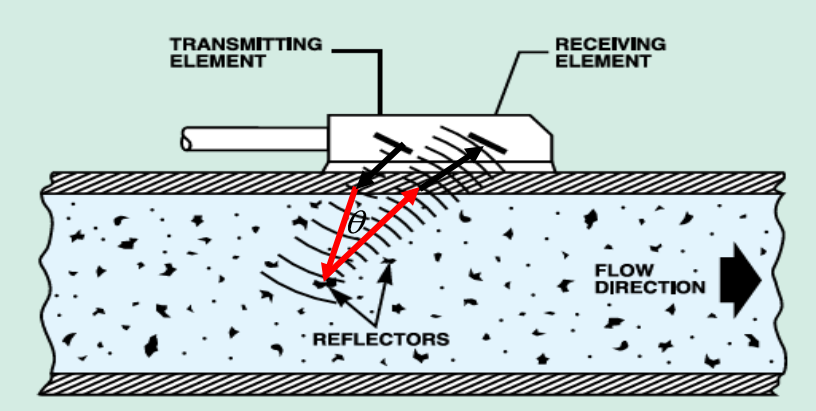

Figure 2-33, Doppler Ultrasonic flow meter

The main advantages of the ultrasonic Doppler flowmeter are that they are easy to install without disturbing the pipe-work and they are available as a clamp-on device which does not drop the pressure of the flowing fluid. However, their disadvantages are that they require second phase even in small quantities and dispersed or fluid variation, the reflecting interfaces, particles, or bubbles may not have the same velocity as the bulk flow, especially in upward and downward flows, and there may be a poor mounting combined with vibration which may cause spurious readings

(Baker, 2002). As a result, this flowmeter is used for liquid single phase flow measurement.

2.9.2.2.1 Ultrasonic Doppler configurations

The ultrasound Doppler flowmeters transducers (transmitter Tx and receiver Rx) have been changed enormously in terms of their size, angle, design and installations.

This section of the thesis is on ultrasonic Doppler transducer configurations which are widely implemented in the majority of Doppler versions and models. These Doppler transducers can be classified in different configurations: continuous wave (CW) and tone burst (Asher, 1997).

- Continuous wave (CW) Doppler flowmeters

Figure 2-34 illustrates the principles of ultrasonic Doppler transducers installation which can be clamped on as non-invasive and non-intrusive, as in figures A, B and C, or core-plug where the Doppler transducer touches the surface of the fluid, as in Figure 2-34 D and Figure 2-34 E.

Practically, ultrasonic Doppler transducers (Tx and Rx) are not installed diametrically (180^{o}) opposite each other; however, side by side are common configurations to create the frequency shift when scatterers are present. Tx and Rx can be in separate units as in Figure 2-34 A and Figure 2-34 B or combined as in Figure 2-34 C which allows them to work as a portable flowmeter for temporary application.

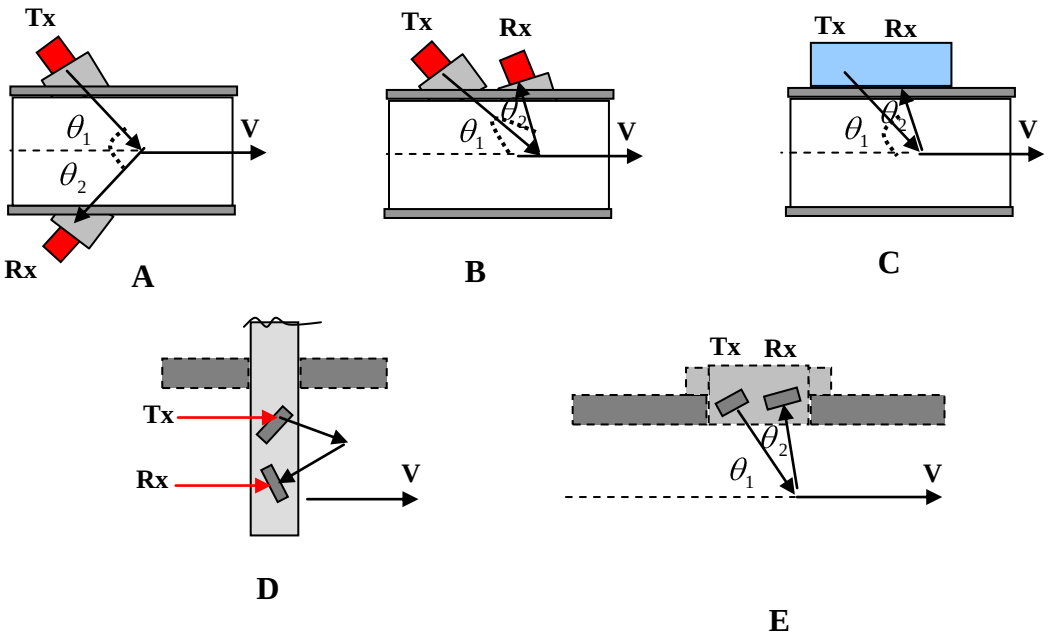

Figure 2-34, Continuous wave Doppler flowmeters

In a horizontal pipe the ultrasonic Doppler transducers can be positioned at specific locations around the pipe cross section. In single-phase liquid flow, they are not installed at the top or the bottom of the pipe (the 12 and 6 o'clock positions) where the higher concentration of bubbles is expected and they face the transducer and these bubbles may interrupt the signal. The most preferable Doppler positions are in the region 2 to 4 o'clock and 8 to 10 o'clock to avoid any bubbles concentration that may be travelling at the top of the pipe (Asher, 1997).

Transducers in Figure 2-34 A to Figure 2-34 C can be incorporated into a spool which gives better control in terms of the angle and coupling as well as the transmission through the wall. When the pipe is corroded or lined, the core-plug can offer a good solution as shown in Figure 2-34 D and Figure 2-34 E.

- Tone burst Doppler flowmeters (Range gating)

In the Continuous Wave (CW) ultrasonic Doppler transducer configurations, there are always two transducers which are installed – one as transmitter and other as receiver – and each transducer has to work as a transmitter or receiver, i.e. it cannot be working in both ways at the same time. However, in the tone burst Doppler flowmeter, there is a single transducer in use; this transducer takes on the role of receiver between bursts, Figure 2-35 illustrates a tone burst Doppler configuration

and its information window. It can be considered as a way of controlling the flow information window; it selects information from a desired position across the flow and thus facilitates averaging of the flow velocity.

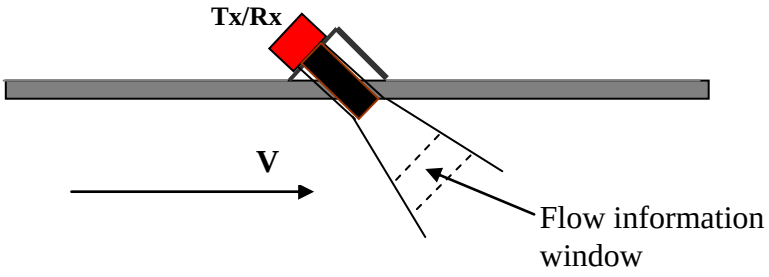

Figure 2-35, Range gating ultrasonic Doppler configuration, taken from Asher (1997)

The tone burst Doppler flowmeter transducer can be installed as clamp-on, clip-on, stuck-on or insertion probe configurations.

2.9.2.2.2 Ultrasonic Doppler signal travel

During the use of the ultrasonic Doppler, there are some processes involved between the signal and the signal receiver; these processes are as follows:

A. Propagation in the coupling media.

B. Refraction and reflection at the interface of the outside wall.

C. Propagation in the wall material.

D. Refraction and reflection at the interface of the inside wall.

E. Propagation in the fluid.

F. Backscattered by the bubbles.

G-J. Receiving the scattered ultrasound back via the same sensor via the same processes as A-F, as shown in Figure 2-36.

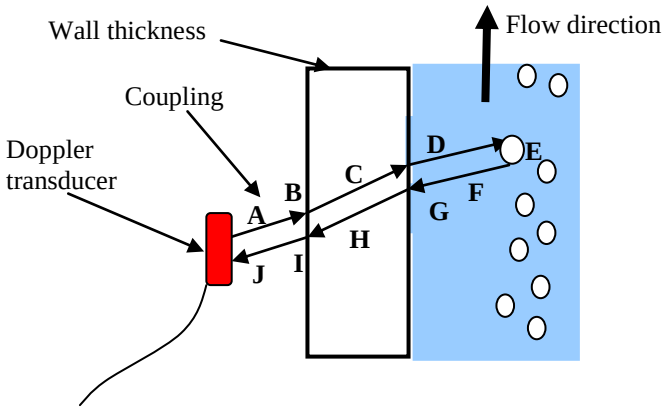

Figure 2-36, Ultrasonic signal travel during emission and receiving, adopted from Wang et al. (2003).

2.9.2.2.3 Ultrasonic Doppler angle

The precise determination of the ultrasonic Doppler angle is crucial. The Doppler angle is basically the angle θ between the bubble velocity and the ultrasonic beam as shown in Figure 2-37. However, the angle α is the wedge angle or the transducer angle in the case and it can vary in a fixed transducer case which is clamped on to the wall. When the transducer is used for laminar flow, where the bubbles velocity stays stable in both amplitude and in direction, it is easy to determine the Doppler angle; however, when the flow is turbulent this angle needs more consideration.

In fact, the ultrasonic refraction law can determine the relationship between α and θ where the change in the ultrasonic angle in pipe wall is neglected as it is too small. This law is very similar to the laws of light in terms of refraction and reflection.

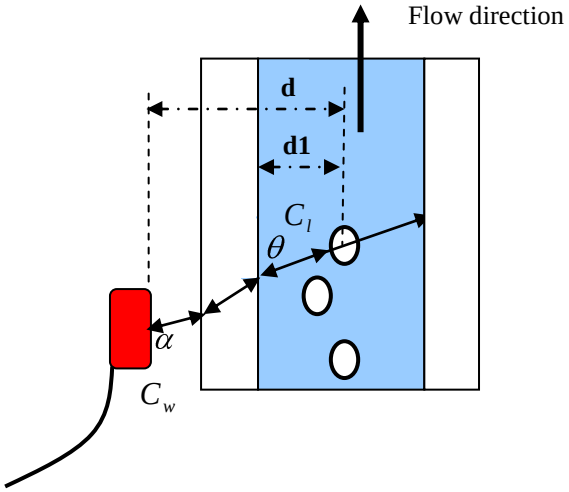

Figure 2-37, Ultrasonic Doppler angle in laminar flow

The following equations represent the refraction at the outside wall and the interface of the internal wall:

$$\frac{C_l}{C_w} = \frac{\cos\theta}{\cos\alpha} \qquad \textbf{(2. 55)}$$

$$\cos\theta = \frac{C_l}{C_w}\cos\alpha \qquad \textbf{(2. 56)}$$

As the Doppler shift frequency:

$$f_r = 2 f_t \frac{V}{C_l} \cos\theta \quad \textbf{(2. 57)}$$

$$f_r = 2 f_t \frac{V \cos\alpha}{C_w} \quad \textbf{(2. 58)}$$

Equation 2.58 shows that even if C_l changes, the Doppler shift does not, since the Doppler shift only depends on α the Doppler transducer angle in the case and C_w, and the angle θ is only dependent on α and C_l, where, C_l is the acoustic velocity in liquid, α the sensor placing angle, and C_w refers to the wall. Moreover, the coupling media that has been used is 'ultragel' which has acoustic about 1500m/s.

2.9.2.2.4 Ultrasonic Doppler flowmeter in multiphase applications

The ultrasonic Doppler flowmeter is used to measure a single liquid phase where its measurement is based on the micron scatterers contained within the flowing liquid; however, some researchers have introduced the Doppler flowmeter to be used with a multiphase flow with a low gas void fraction. Wang et al. (2003) have reported that a commercial ultrasonic Doppler DOP2000 Model 2030 can extend its application to multiphase systems. Their experiment was performed on very low void fraction in a vertical column; they reported that the complication of the ultrasonic reflection at the bubble interface leads to the signal being rather complex to deal with. Therefore, placing the sensor inside the pipe and with the flow direction is a better alternative which avoids the complexity of the Doppler angle determination. They added that in their case the gas void fraction was very low, and that if it increased, the flow became more complex and the attenuation coefficient of the received echo energy increased and became more difficult to interpret. Wang et al. (2003).

Murakawa et al. (2005) introduced a new technique for multiphase vertical bubbly flow measurements with a bubble diameter range of 2-4mm. Their technique was based on using an ultrasonic Doppler flowmeter with different dimensions of ultrasonic Doppler transducers and statistical methods. They added that with a rise in the amount of scatterers within the flowing liquid, it is difficult to gain the velocity

of the bubbles at the middle location in the pipe. They employed numerous kinds of scatterers dimensions; for each scatterers dimension, a multi wave transducer (TDX) was selected which emitted an ultrasonic beam independently for basic frequencies of 2 and 8 MHz. The considered velocity probability density function (PDF) initially consisted of a scatterers velocity appropriate for the diameter of the TDX. They recorded that the velocities of rising bubbles and liquid differ significantly in the vertical rising flow.

The experiments performed using an 8 MHz ultrasonic transducer with 0.00103m/s of superficial gas velocity established that a greater velocity of rising bubbles was captured close to the internal pipe wall. The velocity PDF suggested that approximately all the bubbles rise close to the internal pipe wall under this operational environment, and liquid velocity distribution becomes flattened as a result of the gas introduction. The ratio of higher velocity rises close to the pipe wall as the gas flow-rate enlarges. The experimental results from using the 2 MHz ultrasonic transducer under the same operating conditions are the same as the 8 MHz TDX which showed that the particles barely crossed the measuring line as the space from the pipe wall rose.

Chapelon et al (1990) used the Doppler signal generated by the moving bubble to measure bubble size, based on the double frequency technique of bubble sizing. The bubbles are insonified by two sound fields, a high frequency (imaging field) and low frequency (pumping field). The sum and different frequency signals generated from the oscillations of the pumped bubbles are used for size measurement. Their size measurement results obtained from this method agree with size measurements using Stoke's law.

2.9.1 Scattering in fluid

2.9.1.1 Introduction

Scattering occurs when the fluid restrains a second phase dispersion which can be suspensions, or bubbles in liquids, and it is caused by effects such as turbulence.

2.9.1.2 The effect of scatterers size

The relationship between the size of scatterers and the ultrasonic wavelength can determine the scattering type, a scatter size smaller than the ultrasonic wavelength is called Rayleigh. When the scatterer size is the same of this scale it is called Stochastic, and if the scatterer is larger, it is called Specular as shown in Figure 2-38. Asher (1997).

1. Scatterers much larger than the wavelength (Specular), $\frac{\pi D}{\lambda} >> 1$

This is located in region 1, also called the geometric region where each scatterer acts as a mirror with a diffraction occurrence. Scattering cross section (S) is independent of frequency in this region and it is equal to the geometry cross sectional area, and since the scatterer behaves as a mirror, the sound wave is considered to be scattered, with the exception of the sound rays which pass across the diameter and are deflected.

2. Scatterers similar in size to the wavelength (Stochastic), $\frac{\pi D}{\lambda} \cong 1$

Scatterers in this size are located in region 1, also known as the diffraction region. The scattered radiation has a geometric distraction which is crucially dependent upon the dimension, shape and acoustic properties of the scatterers. In this region the wiggles shown on the line on the diagram illustrate that there might be constructive or destructive interference, for example between the sound wave which reverberates inside the scatterer and the incident sound wave; creeping waves and surface waves on bubbles may contribute. So wiggles exist regardless of scattering.

3. Scattering much smaller than wavelength (Rayleigh) $\frac{\pi D}{\lambda}$<<1

This scattering size is familiar in light scattering and it extends to an upper limit of about $\frac{\pi D}{\lambda}$=1/2. In most dispersions, particles or bubbles are much less than 1 mm in diameter where the wavelength is considered as greater than 1 mm. The scattering cross section is independent of the particle or bubble shape and proportional to the fourth power of the frequency. Urick (1967).

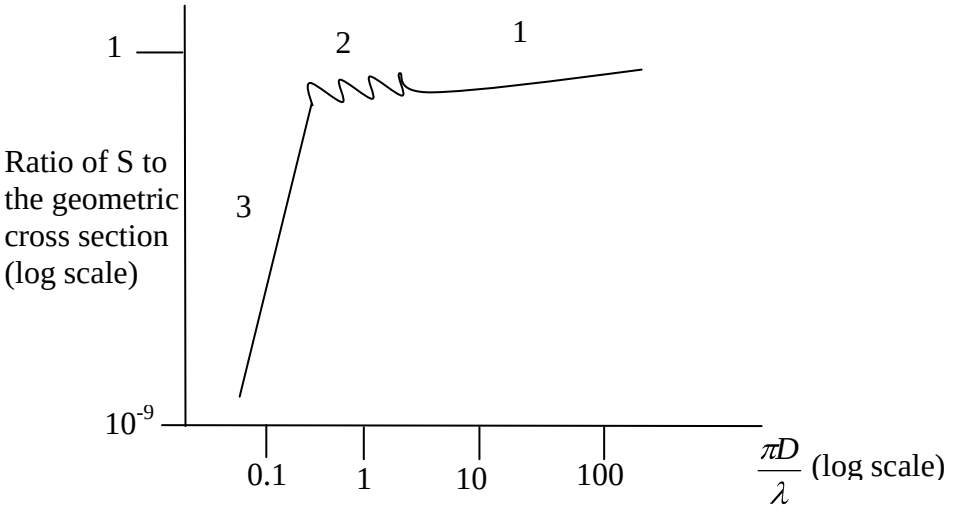

Figure 2-38, The dependence of (S) on $\frac{\pi D}{\lambda}$ for rigid sphere, taken from Asher (1997)

2.9.1.3 The behaviour of gas scatterers in liquid

A bubble and droplet scattering of the same diameter is very much similar in terms of scattering behaviour. However, at specific frequencies the bubble scattering can be significantly enhanced by resonance effects. These effects can be pictured as the interference between the incoming waves and the relatively powerful scattered waves generated by the resonating bubbles (Asher, 1997). The important mode of resonance is a simple expansion/contraction of the bubble sphere, for example monopole oscillation, and multipole oscillations, in which the shape of the bubble changes, are not of significant importance.

The monopole resonant frequency f_g is given by:

$$f_g = \frac{1}{\pi D}\sqrt{\frac{3\gamma P}{\rho}} \qquad \textbf{(2. 59)}$$

Where, P is the total hydrostatic pressure, ρ_l the density of liquid, D is the bubble diameter and γ is the isentropic index.

2.9.1.4 The scatterers concentration effect

In a given direction, the scattering intensity is proportional to the scatterer concentration. This is applied as long as the nature, size and shape of scatterers, nature of the continue phase, intensity and frequency of the ultrasonic are constant.

As a consequence, the scattered sound wave amplitude is proportional to the square root of the concentration of the scattering phase. This is because the intensity is proportional to the square of the amplitude. Practically speaking, this prospect is valid as long as the scatterer concentration is small. However, beyond a certain value an increase in the concentration leads to a drop of scatterers in the system. As a consequence, the intensity at high concentrations would reach the maximum when plotted against the concentration, as shown in Figure 2-39.

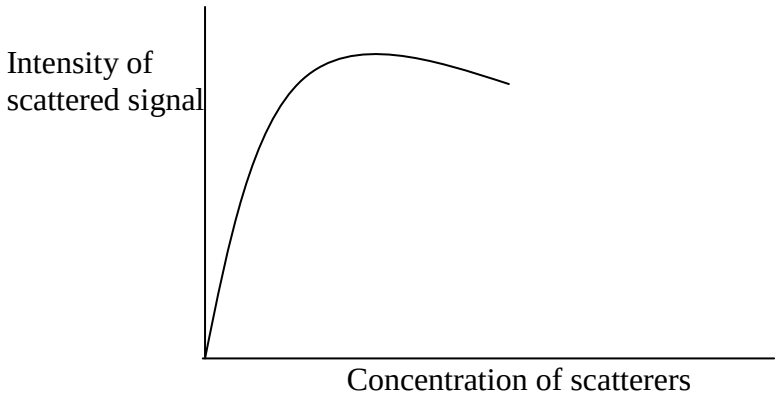

Figure 2-39, The dependence of scattering on concentration

2.9.2 Ultrasonic imaging

The ultrasonic imaging technique has been widely proposed to measure vorticity in a flow and to measure particle velocity in multiphase flow. Most of the ultrasonic tomography techniques originate from the area of medical ultrasound, and yet they are not fully implemented within the oil and gas industry multiphase flow (Carlson et al., 2002).

Ruzairi et al. (2005), say that the main purpose of using the tomography process in multiphase flow application is to visualise the internal flow, and that this can be obtained by using an electronic measurement system for liquid and gas flow.

As shown in Figure 2-40, generally the ultrasonic tomography techniques consist of sensors located around a pipe, such as a process pipe, electric measurement circuits, a data acquisition system and image processing.

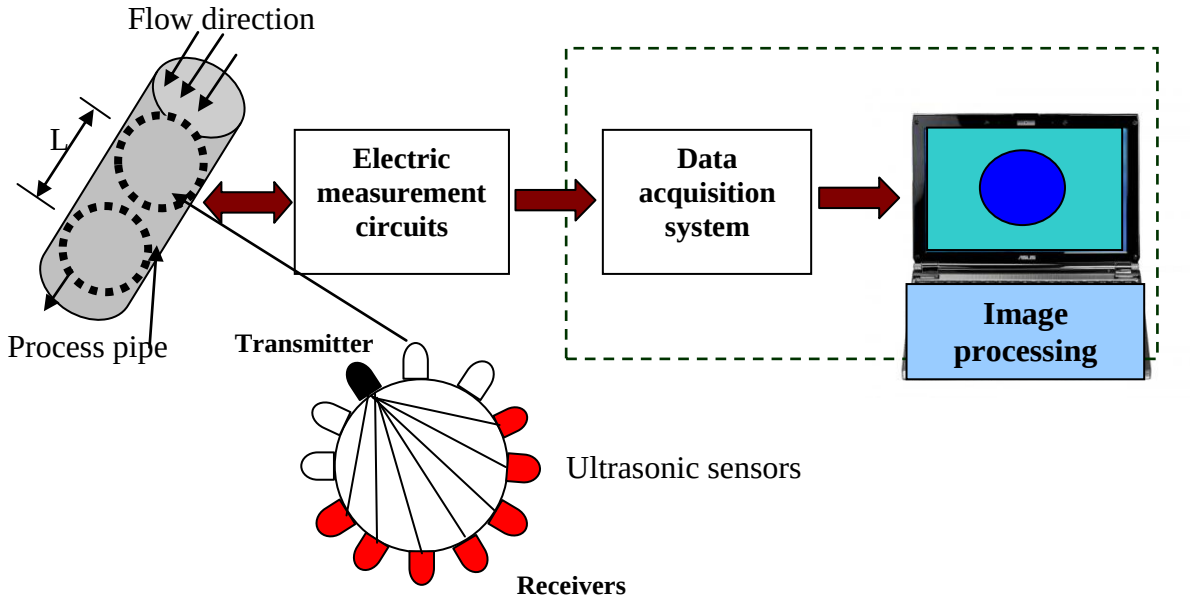

Figure 2-40, The ultrasonic imaging system block diagram, adapted from Ruzairi et al. (2005).

These ultrasonic sensors generate electric signals representing the flow inside the pipe cross section. These signals are then fed to the Data Acquisition System (DAS) and then to the computer to reconstruct the image of the internal pipe flow.

Ultrasonic tomography makes use of ultrasonic transmitting and receiving sensors that are axially spaced along the flow stream. The sensors are designed in the same pipe diameter to avoid any flow obstruction. (Ruzairi et al., 2005).

In order to track the particle movement in the multiphase flow, an array of ultrasonic transducers has been deployed. This array transducer is used in both ways; first to transmit a short pulse simultaneously on all elements and then the same array transducers are used as a receiver to record the backscattered signals. Two pairs of ultrasonic sensors are required with a known distance L between each other in order to obtain the velocity measurement using the cross-correlation method based on the scattered signals.

$$Rxy(\tau) = \frac{1}{T}\int_{0}^{T} x(t)\,y(t-\tau)dt \qquad \textbf{(2. 60)}$$

Assuming that there is no slip between the phases, the flow velocity can be obtained as follows:

$$V = L \diagup \tau_m \qquad \textbf{(2. 61)}$$

Ruzairi et al. (2005). The tomography images are derived using different software and algorithms to construct an image of flow concentration. As a result the gas and liquid fraction calculation by ultrasonic imaging can be obtained; it is as follows:

$$\text{Gas percentage} = \frac{\sum Average.value.in..each..pixel}{\sum Max..value.in..each..pixel}100 \qquad \textbf{(2. 62)}$$

The average value in each pixel depends on the attenuated voltage obtained by the receiver.

2.9.3 Ultrasonic void fraction measurement

A variety of techniques, including gamma ray, image analysis, capacitance and conductivity rings, and ultrasonic methods have been in use to measure flow void fraction.

Several attempts have been made towards void fraction measurement using the ultrasonic techniques. The reason behind using these techniques is that they have advantages over the other techniques in their applicability to large volume objects and they are safe to use and cost effective, since the majority of radiation methods (Gamma ray) require strict safety procedures.

2.9.3.1 Application of ultrasonic void fraction measurement

Diacon (2002). Void fraction measurement using ultrasonic transit time transducers has been deployed by Diacon in the laboratory. A set of identical Panametrics ultrasonic transducers were installed opposite each other on the pipe, as shown in Figure 2-41. An ultrasonic wave is then generated from an ultrasonic transducer working as a transmitter and is picked up by the same kind of ultrasonic transducer functioning as a receiver, which is located on the opposite side to the first transducer.

Large discrepancy in the instantaneous gas void fraction measurement resulted in bubbly flows. These deviations can be decreased via the oscilloscope by using a signals averaging method to record a great number of negotiated waves and then showing the average of these signals.

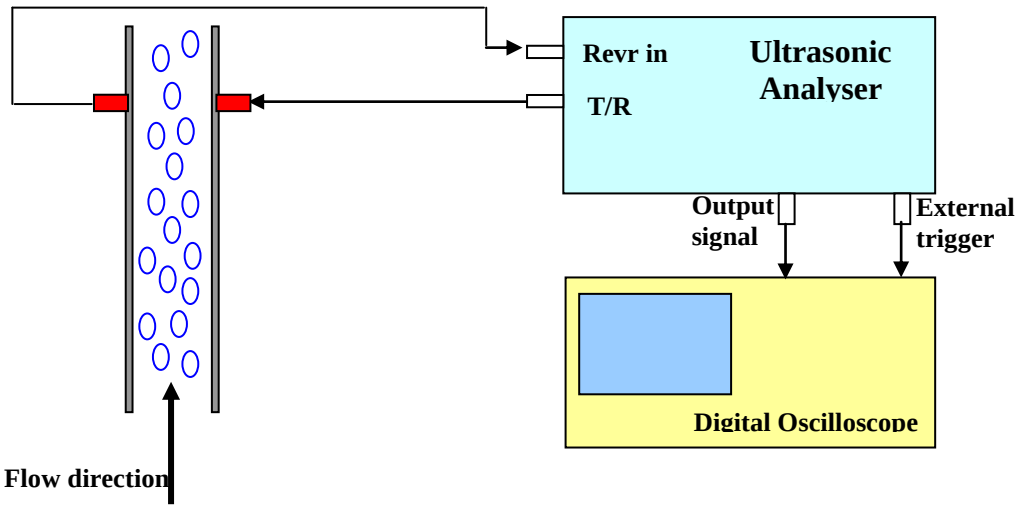

Figure 2-41, Ultrasonic Transmittance setup for measuring void fraction, adapted from Diacon (2002)

The relationship involving the transmitted ultrasonic wave signals can be theoretically obtained using the following model:

$$A_b/A_o = \exp(-k\alpha_g) \quad \text{or} \quad A_b = A_o e^{-k\alpha_g} \qquad \textbf{(22. 63)}$$

where A_b and A_o are the signal with scatterers and the signal with no scatterers, α_g is the void fraction, and k is a constant, depending on the average scatterer radius, R_B, the channel size, C_W, and the transducer radius, R_u, as shown in Table 2-3. In this testing the channel size was $C_W \approx 5cm$

R_B/R_u	C_W	k(R_B/R_u), C_W	Error
0.1	4.445	105.97	±2.2%
0.3	4.445	37.90	±6.7%
0.5	4.445	22.32	±6.8%
0.7	4.445	15.98	±4.4%
0.9	4.445	13.03	±4.5%
0.1	6.35	151.39	±2.2%
0.3	6.35	54.14	±6.7%
0.5	6.35	31.88	±6.8%
0.7	6.35	22.83	±4.4%
0.9	6.35	18.62	±4.5%

Table 2-3, Value of k(R_B/R_u), C_W in eq. for R_u = 0.3175cm for $A_b/A_o \geq 0.2$

Al-Lababidi and Sanderson (2006) have used a non-intrusive pulse-echo 2.25 MHz Panametrics ultrasonic transducer which they implemented in the slug flow as a liquid level measurement technique, referred to as a liquid hold-up measurement. Figure 2-42 illustrates the configuration and signal travel.

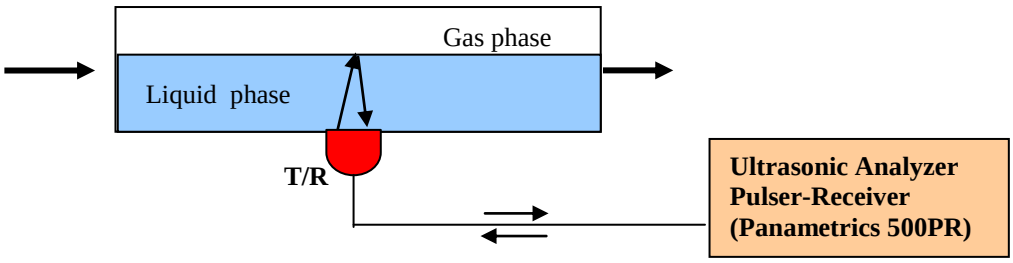

Figure 2-42, Ultrasonic liquid level measurement in a pipeline

The time required for an ultrasonic pulse echo to travel in the liquid and to be reflected back by the liquid surface to the transducer is proportional to the liquid level. This technique is flow regime dependent since the signal can easily be lost as a result of flow turbulence.

A static ultrasonic level measurement calibration using a ruler has been performed. The reason for performing this calibration is to derive a correlation between the measured liquid height $h_{L(U)}$ and the corresponding voltage output v_U from the Panametrics transducer.

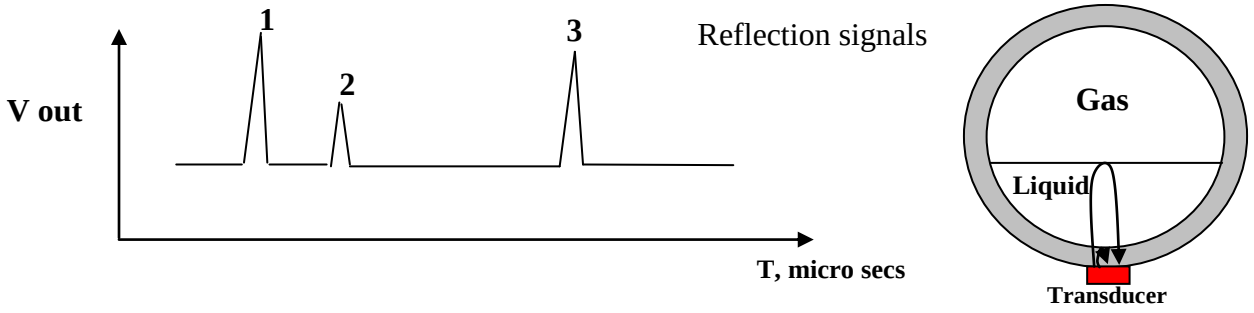

Figure 2-43, Schematic ultrasonic waveform signal reflected from liquid surface

Where the peak points 1, 2 and 3 represent the following: the transducer signal, signal reflections from the internal wall and the liquid surface, respectively. From this calibration, Al-Lababidi obtained a correction factor that he implemented to calculate the liquid height as follows:

$$h_{L(U)} = \frac{v_U - v_{U(\min)}}{v_{U(\max)} - v_{U(\min)}} d = v_U d \qquad \textbf{(2. 64)}$$

where $h_{L(U)}$ is the height of the liquid, v_U the normalised value for the voltage value, and d is the pipe diameter.

In order to calculate the liquid holdup using the ultrasonic technique, the following equation is suggested:

$$\alpha_l = \frac{1}{\pi}\left\langle \pi - \cos^{-1}\left[2\left(\frac{h_{LU}}{d}\right)-1\right] + \left[2\left(\frac{h_{LU}}{d}\right)-1\right]\sqrt{1-\left(2\left(\frac{h_{LU}}{d}\right)-1\right)^2}\right\rangle \qquad \textbf{(2. 65)}$$

2.10 SIGNAL PROCESSING

Signal processing involves the analysis and implementation of systems that extract information of most interest from existing data signals. The continued progress of digital technology and information theory has stimulated the development of very sophisticated signal processing techniques that are exploited in many different fields, including audio signal processing, digital communications, and analysis and control of industrial processes.

Most sensor outputs comprise a continuously varying analogue voltage waveform. In order to use the digital technology in further mathematical signal processing techniques on a computer system, it must be first digitised with an analogue-to-digital converter.

2.10.1 Sampling rate

The Nyquist-Shannon sampling theorem is a fundamental theorem in the field of information theory which stipulates the constraints for accurately constructing a signal from a sampled version of itself. It states that the sampling frequency f_s must be strictly greater than twice the signal's bandwidth B_s, the difference between the maximum and minimum frequencies of its sinusoidal components (Jackson, 1995).

$$f_s > 2\,B_s \qquad \textbf{(2. 66)}$$

Failure to satisfy the criterion set out in the Nyquist-Shannon theorem results in overlapping frequencies, whereby frequencies above half the sampling rate will appear as frequencies below half the sampling rate. This phenomenon is known as aliasing as the high frequencies are said to be under an alias.

2.10.2 Fast Fourier Transform (FFT) spectrum analyser

A Fast Fourier Transform is an efficient algorithm used to computationally calculate the Discrete Fourier Transfer (DFT).

The FFT decomposes the sets of transformed data into a sequence of minor data which are to be transformed. Then, it decomposes those minor sets into even more minor sets. At each stage of processing, the results of the previous stage are joined in a particular mode. Eventually, it calculates the DFT of each small set of data. For example, an FFT of size 32 is divided into 2 FFTs of size 16, which are broken into 4 FFTs of size 8, which are divided into 8 FFTs of size 4, which are divided into 16 FFTs of size 2. Calculating a DFT of size 2 is insignificant. Newland (1994).

The DFT obtains N^2 operations for N points. As at any stage the computation needed to join smaller DFTs into bigger DFTs is proportional to N, and there are $\log 2(N)$ stages (for radix 2), the total computation is proportional to $N * \log(N)$. Therefore, the ratio between a DFT computation and an FFT computation for the same N is proportional to $N / \log 2(N)$. This ratio is not very significant where N is small, but when N is large, this ratio becomes significantly large. (Every time you double N, the numerator doubles, but the denominator only increases by 1).

The FFT, therefore, offers an enormous reduction in computer processing time. Moreover, there is the added bonus of an increase in accuracy. Since fewer operations have to be undertaken by computers, round-off uncertainties due to the truncation of products by the limited word size (limited number of available digits) of the computer are reduced, and accuracy is accordingly increased.

If it is assumed that:

x_r , r = 0, 1, 2, ….., (N-1) is the sequence shown in Figure 2-44 a, when N is an even number, and that this is partitioned into two shorter sequences (y_r) and (z_r) as shown in Figure 2-44 b, then

$y_r = x_{2r}$

r = 0, 1, 2, …..(N/2-1).

$z_r = x_{2r}+1$

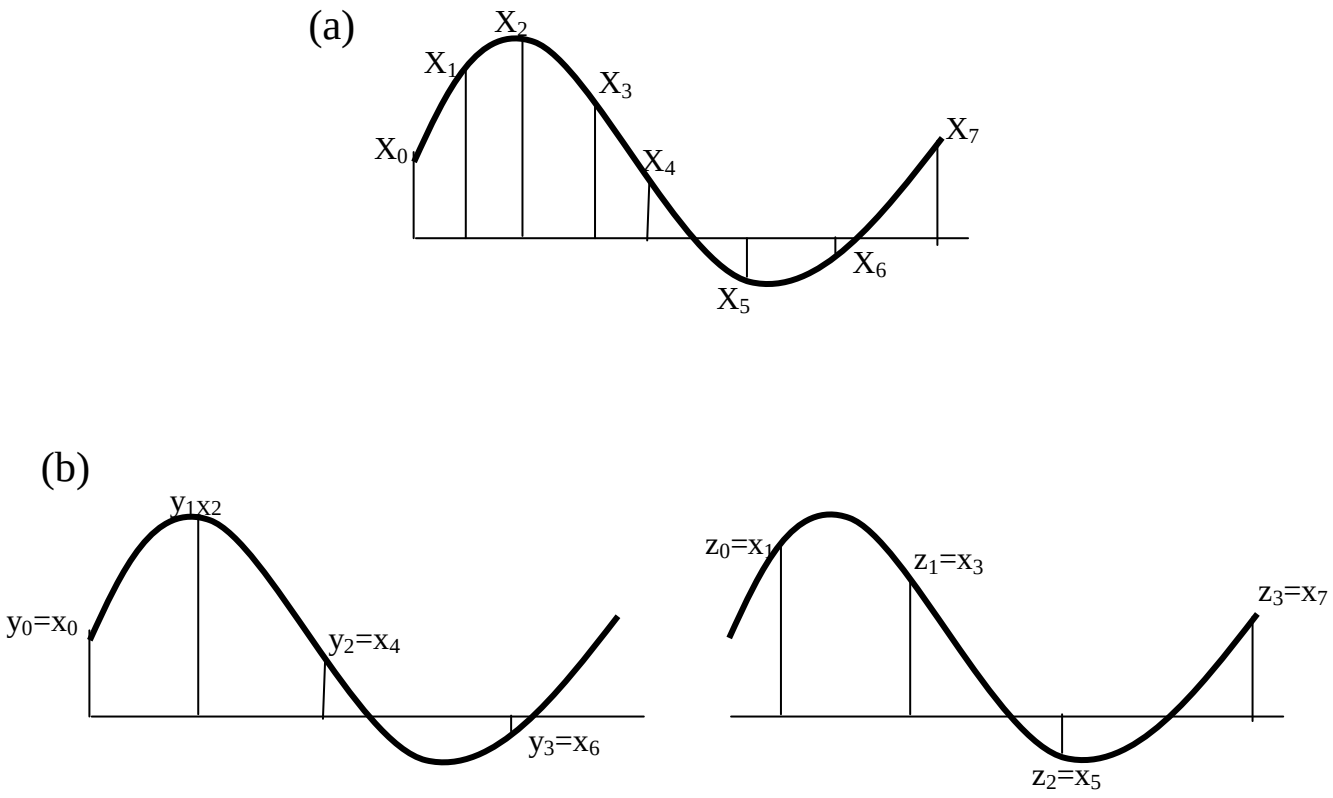

Figure 2-44, Partitioning the sequences x_r into two half sequences y_r and z_r

2.10.3 Short-Time Fourier Transform (STFT)

STFT is considered to be a significant tool for audio signal analysing. It describes a particularly useful class of time-frequency distributions that indicate complex amplitude versus time and frequency for any signal. STFT is a signal analysing method deployed for analysing non-stationary signals, whose statistic characteristics fluctuate with time. In essence, STFT extracts several frames of the signal to be analysed with a window that moves with time. In case the time window is adequately narrow, each frame gained can be presented as stationary so that Fourier transform can be deployed. As shown in Figure 2-45, with the window moving along the time axis, the relationship between the variation of frequency and time could be determined; Figure 2-46 shows different frequencies and time using STFT.

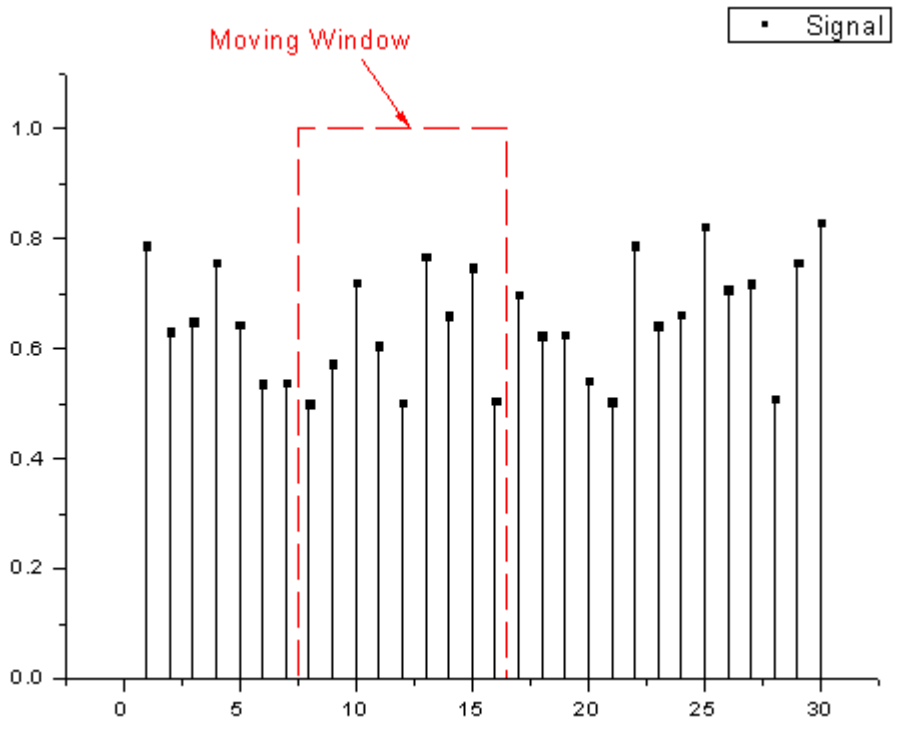

Figure 2-45, STFT moving window, taken from OriginLab software.

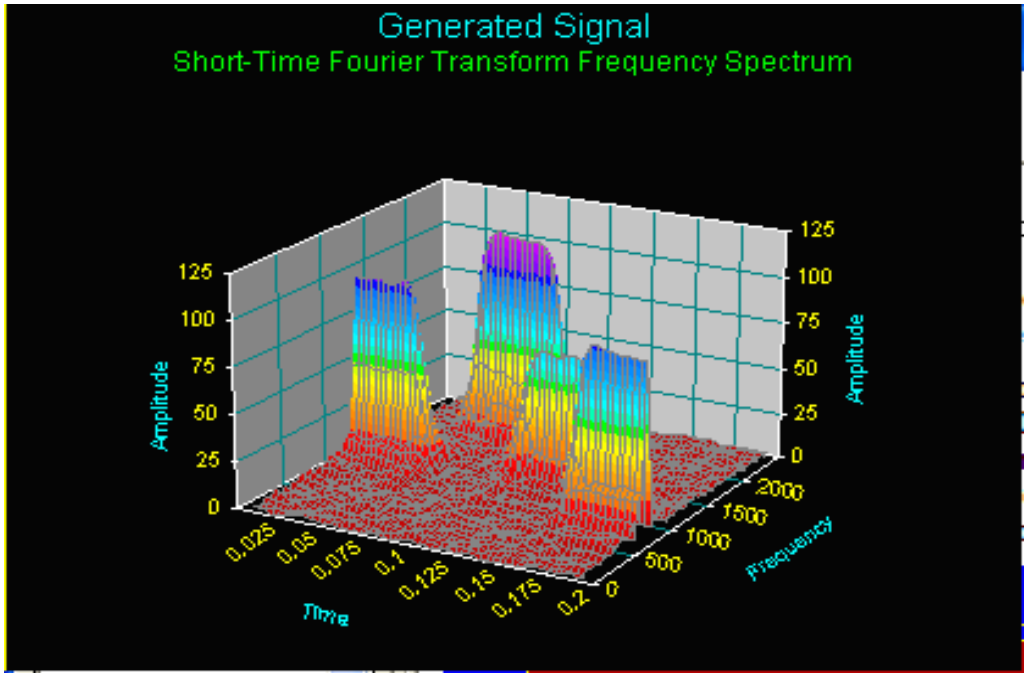

Figure 2-46, Variance frequencies and time using STFT, taken from Autosignal help page

Mathematical Definition of the STFT

When analyzing a non-stationary signal $x(t)$ it is assumed that it is approximately stationary in the span of a temporal window $w(t)$ w with finite support. The STFT of $x(t)$ is now represented by time frequency atoms $X(\tau, w)$ and it is given by:

The usual mathematical definition of the STFT as following:

$$X(\tau, w) = \int_{-\infty}^{\infty} x(t) w(t-\tau) e^{-jwt} dt \qquad \textbf{(2. 67)}$$

where,

$x(t)$ = input signal at time τ

$w(\tau)$ = length of window function (e.g., Hamming)

However, some real signals have large period small frequencies and small period big frequencies. Such a signal can be better explained by a transform that has high frequencies and short period resolution at low frequencies, and low frequencies and high period resolution at high frequencies. As a result the STFT is not the most useful tool and the wavelet transform could offer better information (Chikkerur et al., 2000).

2.10.3.1 Drawbacks of using Fourier Transform

Giurgiutiu V. and Yu L., 2003 reported that one of the most important drawbacks of Fourier Transform is that it cannot offer any description on the period at which a frequency happens. However, that is not a problem for motionless signals but can highlight room for development where motion signals are concerned.

Focus on a signal containing 2 frequencies, one frequency f1 occurring over time T and the second a frequency f2 occurring over another time T. The STFT plots a signal into a 2-D which is a function of period of time and frequencies. Nevertheless, the time and frequency information can only be acquired with restricted accuracy. This accuracy is verified by the dimension of the window which is deployed to analyse the signal. (Mathwork).

2.10.4 Wavelet transform

Lang. W. C. and Forinash K., 1998, reported that the wavelet transform can be used to produce spectrograms which show the frequency content of sounds, images or any other signals as a function of time. This technique is commonly used in the engineering community for signal analysis.

The wavelet transform (wavelet analysis) can be considered the main current remedy to overcome the weaknesses of the Fourier transform. In wavelet analysis the employment of a whole scalable modulated window offers a solution for the signal-cutting difficulty. It is a precise and dependable tool for understanding signals with rapid alterations of time and frequencies. It is a windowing tool, comparable to the STFT, with changeable sized windows. It offers the employment of long time periods, when more low frequency information is required, and shorter sections, when more high frequency information is captured.

Wavelet analysis has the capability to provide informative features of data that other signal analysing tools neglect, including features such as trends, collapse points, discontinuities, and self-match. It is often used to compress or de-noise a signal without any considerable degradation. It is also useful for audio/image/video analysing and processing, data compression, signal smoothing and de-noising, speech recognition and biomedical imaging.

2.10.4.1 Wavelet transform mathematical base

Wavelet transform computes the real continuous wavelet coefficient for each given scale presented in the Scale vector and each position b from 1 to n, where n is the size of the input signal.

Let *x(t)* be the input signal and b the chosen wavelet function, the continuous wavelet coefficient of *x(t)* at scale a and position b is:

$$C_{a,b} = \int_R x(t) \frac{1}{\sqrt{a}} \Psi(\frac{t-b}{a}) dt \quad \textbf{(2. 68)}$$

The result can be output to a range on a worksheet and, if the Coefficient Matrix checkbox is selected, a matrix. The output range on the worksheet is comprised of m columns, each of which has n rows, where m is the size of the scale vector. Each column corresponds to a scale and each row corresponds to a position. On the other hand, the resulting matrix, if one is generated, will have *n* columns and *m* rows. The value at a cell whose row number is M_0 and column number is N_0 is the coefficient of scale M_0 and position N_0.

There is more than one type of wavelet supported such as in this function, including the most common ones – Morlet, and the derivative of Gaussian wavelets – given as follows:

Firstly, the Morlet wavelet

It is the most commonly used continuous wavelet transform CWT which is defined as:

$$\Psi(x) = \pi^{-1/4} \cos(k_r x) e^{-x^2/2} \quad \textbf{(2. 69)}$$

where k_r is the wave number.

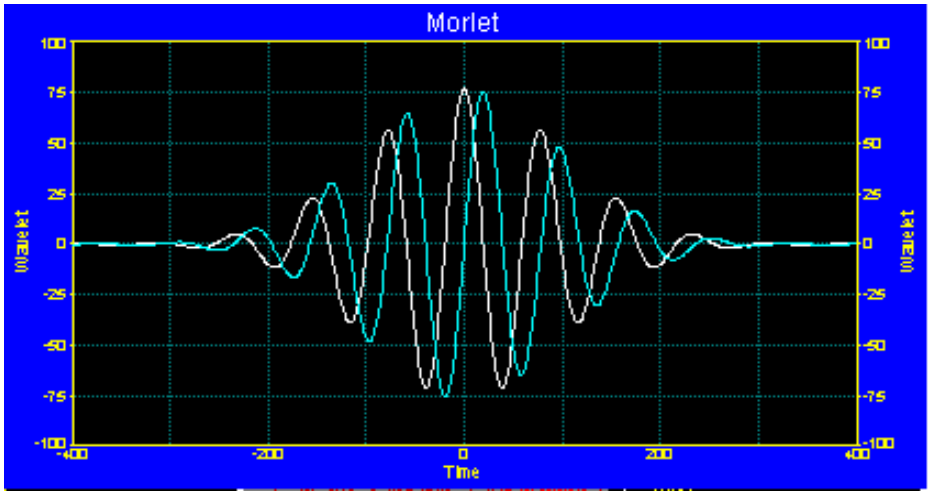

Figure 2-47, Morlet wavelet, taken from Autosignal help page

Secondly, the Gaussian wavelet

This is the derivative order *p*th derivative of the Gaussian function, which is defined as:

$$\Psi(x) = \left(\frac{2}{\pi}\right)^{-1/4} \times e^{-x^2} \qquad \textbf{(2. 70)}$$

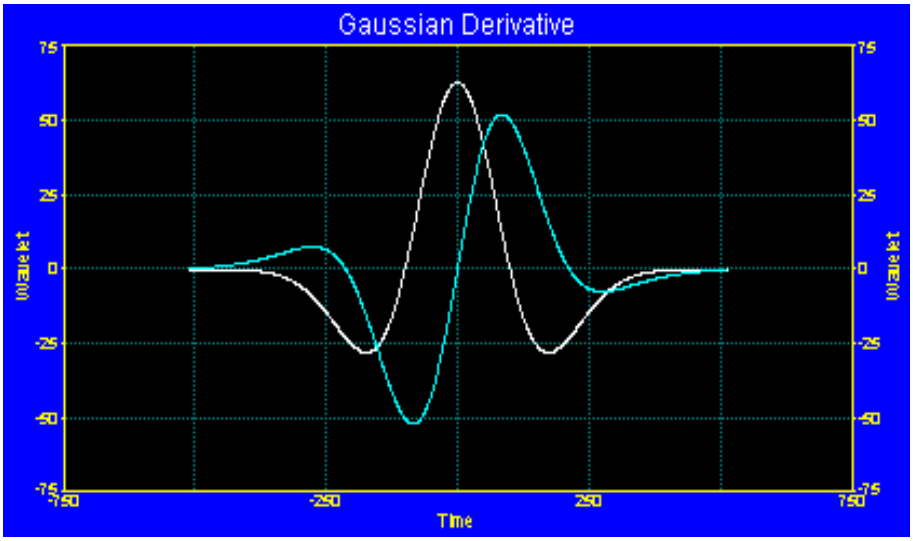

Figure 2-48, Gaussian wavelet, taken from Autosignal help page

2.10.5 Comparison between WT and STFT

The common characteristics of STFT and WT are that both give two dimensional spectra from time-frequency analysis. However, they are different in several aspects.

The basic different is that wavelet uses a size-adjustable window more advantageous than the fixed window used by STFT. When the local area has a low frequency, the window will be longer. The other advantage of WT over STFT is that it can extract the coefficients at a certain frequency of interest and WT is related to denoising when STFT can not do the denoising or filtering for signals. (Giurgiutiu V. and Yu L., 2003).

2.11 CHAPTER SUMMARY

In summary, in this chapter a literature review is presented which covers most of the available techniques implemented in the area of multiphase flow measurement in the area of multiphase flow measurement.

Ultrasonic multiphase flowmeters that are currently commercially available are described and explained in terms of installation, application and performances. They have also been considered in terms of their advantages and disadvantages.

This chapter has also focused on some signal processing techniques. The following chapter will therefore detail the metering concept proposed in the three measuring areas and general data acquisition systems performed for each area in the current research work.

Chapter 3

OVERALL METERING CONCEPT

3.1 INTRODUCTION

This chapter describes the experimental facility, equipment and sensors used to obtain the data for the measurement concept and schemes proposed (partially separated liquid dominated, homogeneous and raw slug) and described in this thesis.

The two-phase flow test rig in the department laboratory was used. This facility is capable of providing developed two-phase slug flows. The majority of the piping is in PVC with clear 50mm Perspex pipes for two-phase flow regime visual monitoring

The chapter starts with a brief description of the whole test rig, including the reference liquid and gas meters and their measurement ranges and working conditions. The T-Y junctions are clearly listed and defined. The locations for raw slug, partial separated and homogeneous measurements are highlighted. The respective sensors, their installation and data acquisition are described.

3.1.1 METERING CONCEPT OVERVIEW

Figure 3-1 illustrates the ultrasonic measurement concept under different flow regimes investigated in this thesis. The two-phase flow is partially separated using a T-junction and then these separated sections are combined using a Y-junction. Ultrasonic measurement techniques are implemented to measure the flow-rate of gas and liquid of the partially separated and combined flows. Ultrasonic cross-correlation method is used for the partially separated liquid dominated measurement, and an ultrasonic Doppler flowmeter for the homogeneous flow and in the raw slug flow.

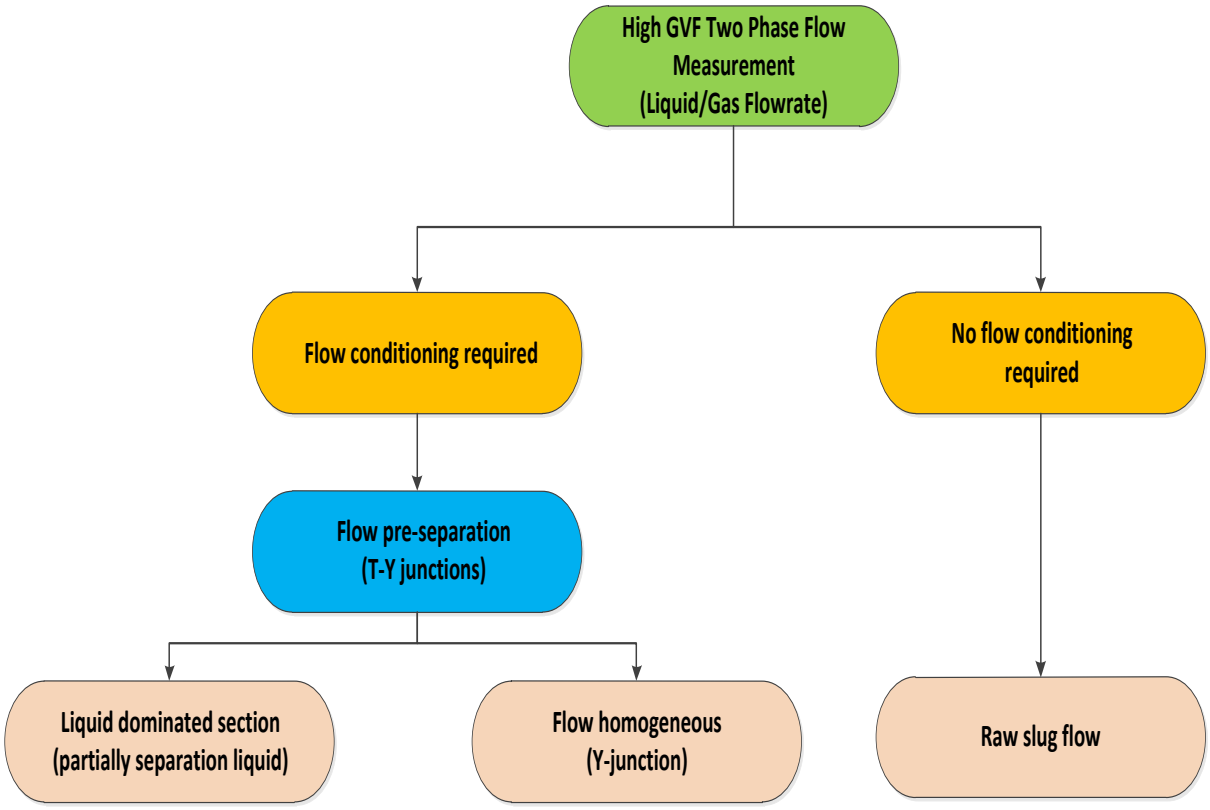

Figure 3-1, Flowchart for slug flow measurement

3.2 GENERAL SYSTEM DESCRIPTION

The test rig consists of a closed loop of two different internal pipe diameters as shown in Figure 3-2. The first pipe geometry has a 50mm internal diameter and 20 metre length, whereas the second pipe is 1.5 metre in length of the T-Y junctions system from 50mm to 150mm diameter, and then the separated flows are combined back to 50mm. The loop is approximately 1 metre high above the ground to allow ergonomic access, better visualisation of the fluid and easy access to control the liquid and gas valves. It is also required for the return mixture pipe to the water tank with the inlet above the water level in the tank which is at 90cm.

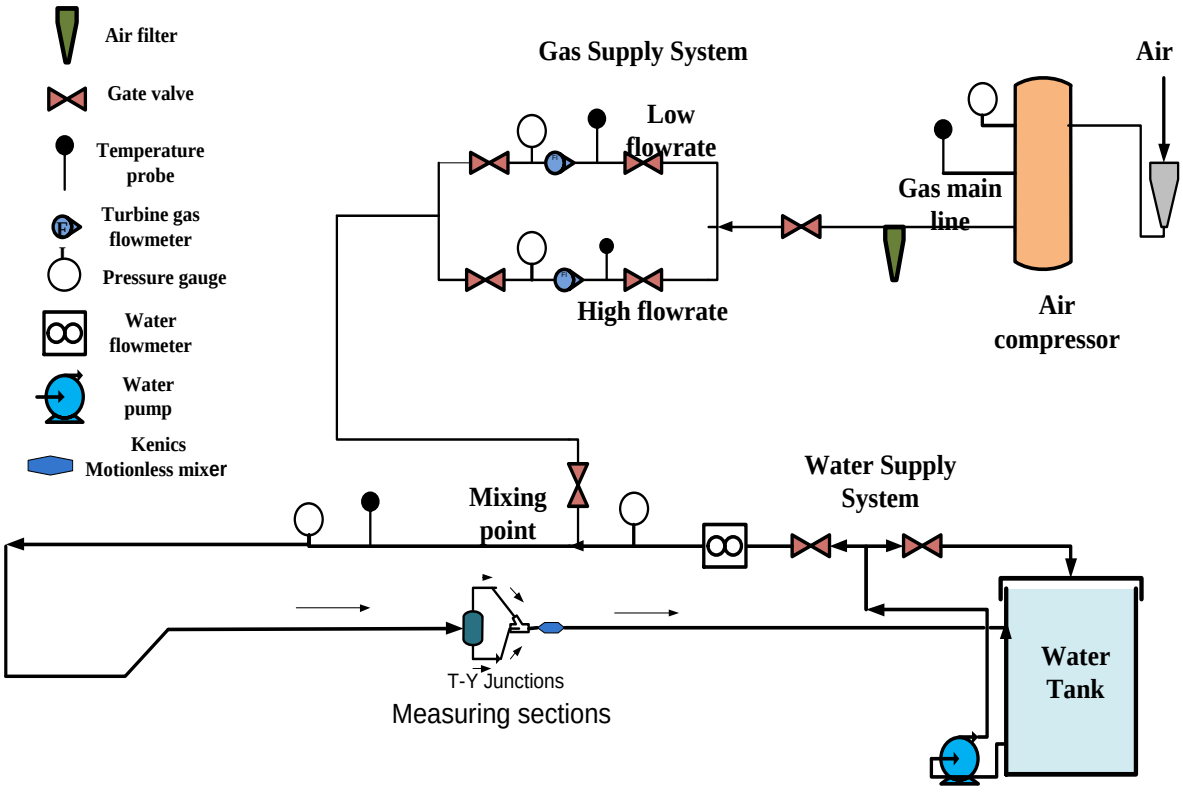

Figure 3- 2, Two-phase test rig facility

The main specifications of the two-phase test rig flow loop can be listed as:

- Location: Process and System Engineering laboratory
- Type: closed loop:
- Total length: 20 metres
- Fluids: Air, Water
- Pipe diameter: 50mm plastic pipe
- Temperature: 15 to 28^{o}C (no temperature control)

3.2.1 Liquid supply system

The liquid used in this test rig is tap water. It is supplied from a 2000 litres storage tank, at atmospheric pressure, and 1m high the same level as the experimental pipes and maintains the amount of water required for the experiments. The water is pumped into the 50mm diameter pipe to the test rig by a centrifugal pump with a maximum capacity of 40m^3/hr and a maximum discharge pressure of 500 kPa (gauge). This pump is installed at ground level. The pumped water passes through an electromagnetic flowmeter for volumetric flow measurement, as shown in

Figure 3-3, and then a pressure gauge before it mixes with air and flows to the test section.

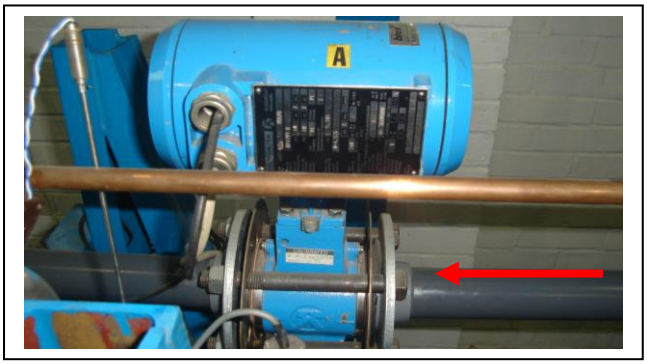

Figure 3-3, Water electromagnetic flowmeter

3.2.2 Air supply system

The laboratory compressor takes air from outside at atmospheric pressure. The compressed air is then stored in a high pressure vessel. The air then passes through a pressure regulator to minimise pressure fluctuation in the test rig. Air is divided into two branches, the high pressure line and low pressure line. In the high pressure line, the volumetric flow-rate is measured using a high air pressure turbine flowmeter installed on 18mm pipe diameter. Whereas, for the low pressure line, the volumetric flow-rate is also measured using another turbine meter installed on 12mm diameter pipe which can deliver different flow-rates required for the experiments. The compressed air temperature and pressure are measured upstream of the mixing point. Figure 3-4 shows the gas flow measurement technique which is used in the two-phase flow test rig.

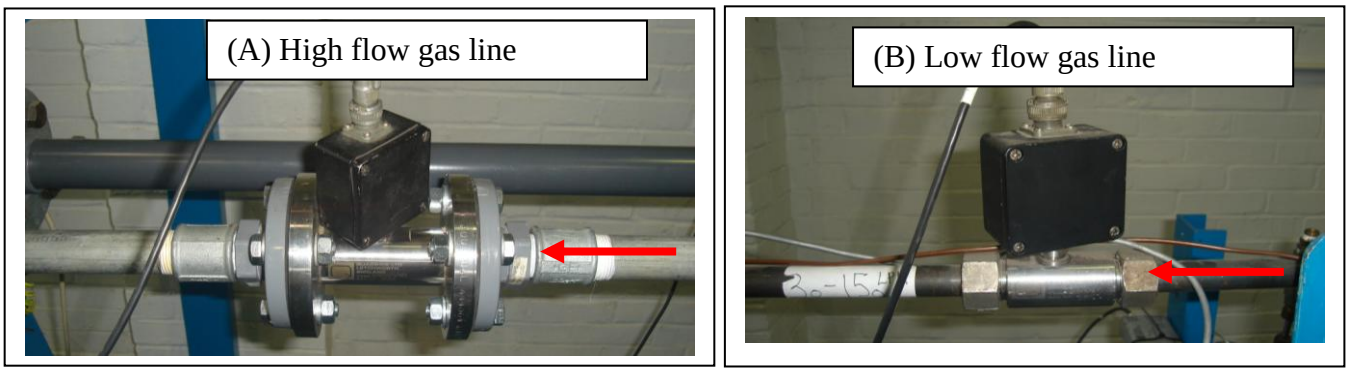

Figure 3-4, Turbine gas flowmeters

3.2.3 Reference measurement system

The two-phase flow rig has been provided with the following instrumentations, identified in Table 3- 1.

Designation	Description	Details	Range	Unit
Fw	Liquid Flowmeter	Krohne Altoflux Electromagnetic Flowmeter.	0-27.144	m^3/hr
FgH	Turbine Gas Flowmeter (High flow-rate)	Quadrina Turbine Meter	6-60	m^3/hr
FgL	Turbine Gas Flowmeter (Low flow-rate)	Quadrina Turbine Meter	1-8	m^3/hr
PgH	Pressure Sensor (High flow-rate)	Gauge Pressure Transducer	0-5	barg
PgL	Pressure Sensor (Low flow-rate)	Shape Instruments LTA	0-5	barg
Pm	In-line Pressure Sensor	Specification Not available in house.	0-5	barg
D.P	In-line Pressure Sensor	GE Druck LPX5480	4-20	mbar
TgH	Temperature Sensor	RS Thermocouple	0-100	^oC
TgL	Temperature Sensor	RS Thermocouple	0-100	^oC
Tm	Temperature Sensor	RS Thermocouple	0-100	^oC

Table 3- 1, Test rig instrumentations

3.2.4 T-Y JUNCTIONS AS A HYDRAULIC SYSTEM

3.2.4.1 General Descriptions of T-Y Junctions

In the measuring section, the test rig consists of a T-Y junction which is located 12m downstream of the reference metering points. The configuration includes a T-junction with horizontal input and vertical output arms and a horizontal Y-junction with a horizontal input, a 45^{o} input and a horizontal output.

The T-Y junction, acting firstly as a two-phase flow partial separator and then a flow homogeniser, has been tested in the Process System Engineering laboratory. Pre-separation of two-phase flow is a method to enable accurate measurements of each phase, see Chapter 2.3.2 for more details of partial separation flowmeter. In the present work this was achieved by the T-junction acting pre-separator.

The change in pipe geometry and direction allows the multiphase flow (slug flow) flowing in the 50mm (2inch) diameter pipe to be separated when it enters the vertical T-junction of the 150mm (6inch) diameter pipe. The flow was separated into a liquid dominant stream with gas carry under, and a gas dominant stream with liquid carry over.

The Y-junction with flat horizontal arm and 45^{o} arm inputs with a flat horizontal output has been installed downstream of the T-junction, connecting with the partially separated liquid and gas lines. The Y-junction in this configuration is working as the two-phase flow comingling device where the flow is homogenised. A 500 mm static mixer with 6 twisted elements inserted in the 50mm diameter pipe was installed after the junction to ensure that the flow mixture maintains its homogeneous state for a longer distance in the pipe.

As mentioned earlier, the proposed T-junction was not only to divide the flow in a high separation performance, it was assembled to maintain a continuous outlet flow with an amount of gas carry under. The partially separated liquid flow is measured using an ultrasonic cross-correlation method. Whereas, the Y-junction functions as (liquid and gas) flow homogeniser enforced by a static mixer to enhance the homogeneous mixture.

The ultrasonic cross-correlation method and ultrasonic Doppler flowmeters are deployed to measure the flow-rate within the liquid dominated section, the homogeneous section and raw slug flow. These measurements are made in combination with hold up measurement using conductivity rings.

In the experimental studies the flow regime in the 50mm pipe was adjusted to be slug flow by varying the liquid and gas superficial velocities. A conductivity ring was installed upstream of the T-Y junction together with the proposed ultrasonic measurement techniques used to monitor the flow regimes during the flow measurement.

As shown in Figure 3-5 a 1 metre riser upstream of the T–junction are installed, which has the effect of introducing intermittent flow regimes earlier than predicted by the Mandhane et al. (1977) flow regime map. The reason behind introducing this riser in the test rig is that the T-junction inlet and Y-junction outlet are not at the same level, so the inlet pipe needed to be lifted up to maintain the inlet level.

The final configuration of the T-Y junctions is presented in Figure 3-6, and it has been fitted and installed in the department laboratory.

Figure 3-5, The test rig 1m riser

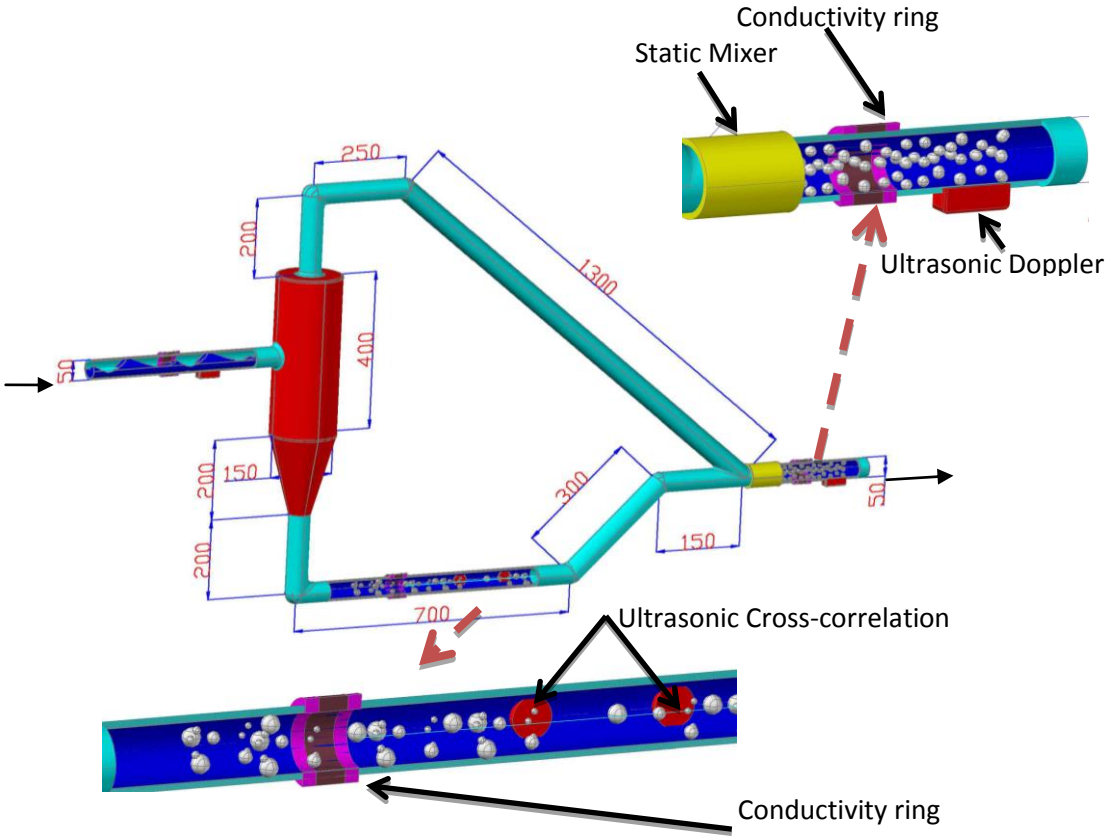

Figure 3-6, The proposed T-Y junctions' final configuration

At these measurement sections, multiphase flow parameters are measured and logged. The measurement devices and their installation are illustrated later in this thesis.

The measurement techniques and flow conditioners consist of the following:

- Two sets of invasive Olympus 1MHz ultrasonic transducers (TX/RX).
- Three pairs of flush mounted conductivity rings for measuring liquid fractions in the partially separated liquid, in the raw slug flow and in the homogeneous flow section.
- A 500 kHz ultrasonic Doppler flowmeter.
- A Kenics motionless flow mixer with six mixing stages and a flow straightener.

3.3 MEASURMENT METHODS AND TECHNIQUES

Table 3-2 shows the single and two-phase measurement techniques which are commercially available. The usage of some of these techniques depends upon the measured flow regimes and their properties.

Section of pipe / Techniques used	Raw slug	Partial separation liquid dominated	Homogenised
Conductivity rings	Slug velocity Slug frequency Slug length Flow regime identification Water/gas fraction	Water/ gas fraction in liquid side.	Water/gas fraction.
Ultrasonic cross-correlation technique	Flow regime identification Slug velocity Slug frequency Slug length Liquid hold-up	Bubble velocity Flow identification	Bubble velocity Flow identification
Ultrasonic Doppler	Slug and film velocity. Slug frequency. Slug length. Bubbles velocity within the slug.	Bubble velocity	Bubble velocity

Table 3-2, Some Multiphase flow measurement techniques

3.4 GENERAL DATA ACQUISITION SYSTEM

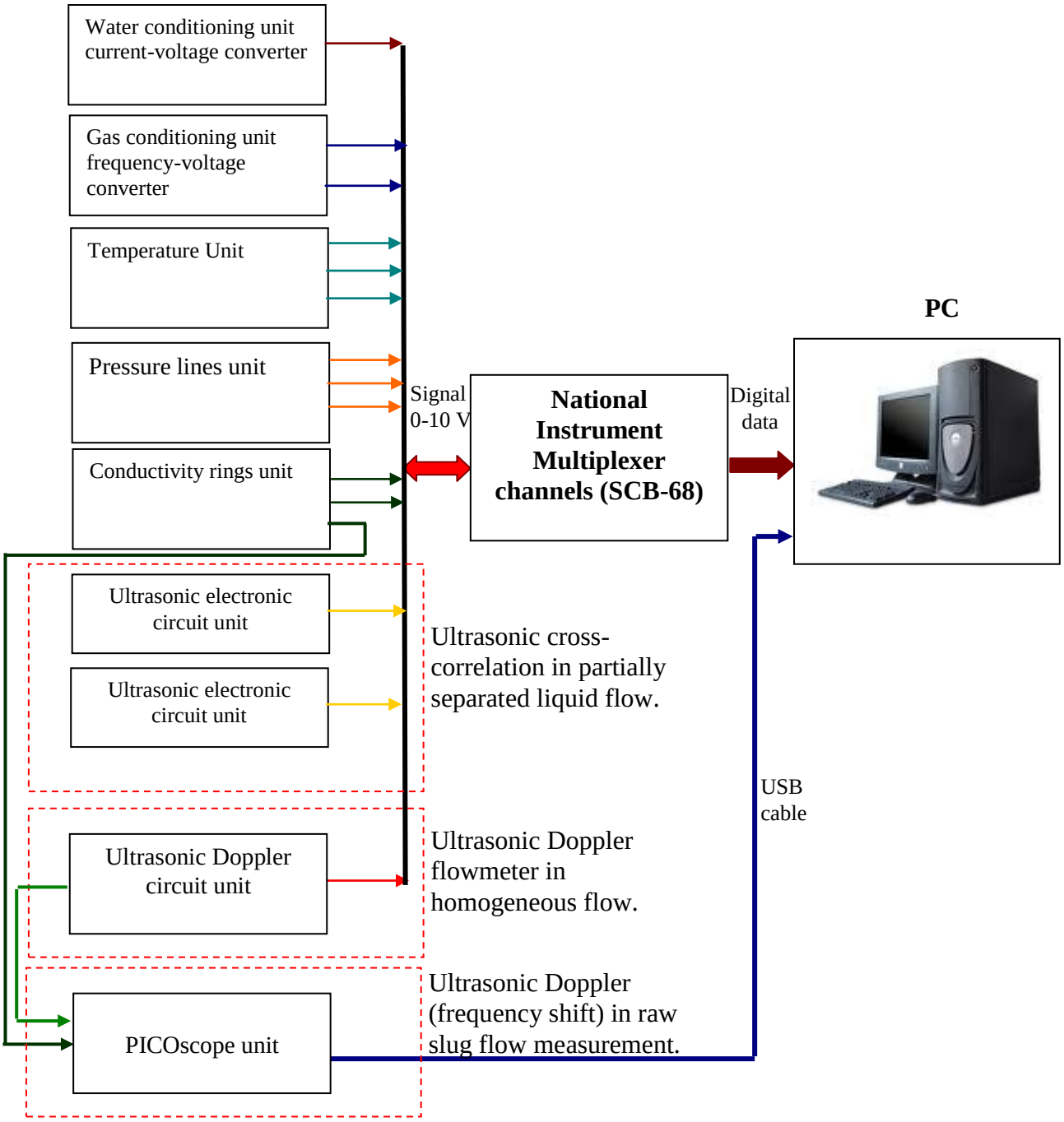

Figure 3-7, Schematic diagram of measurement signalling routes

The data acquisition system comprises an analogue-to-digital converter (ADC) card installed in a PC, together with a software program LABVIEW to drive the converter and carry out in-line processing of data.

The converter, manufactured by National Instruments, has 16 channels as shown in Figure 3-8. The ADC is a successive approximation type. The maximum sampling rate is 100 kHz and with a settling time of 50 micro seconds. Gain is software-selectable in steps between 100mV to 10V. The output signals of the transducers were conditioned to be between ± 5V. Signals were fed to the ADC via a specially made converter box (channels box) enabling the use of standard BNC connectors.

Signals from all transducers were scanned and displayed in panels appropriate to the type of signals being viewed. For example, parameters such as flow-rate (liquid) used to set up the test run were displayed in one panel while the readings of pressure transducers were displayed in another.

Some signals were processed online, e.g. the superficial gas and liquid velocities and GVF at the ultrasonic Doppler measuring section. This data, including ultrasonic Doppler display (m/s) measurement, are simultaneously saved to a text file format, whereas, the ultrasonic Doppler 'raw signal' is saved using PICOscope to a separate text file.

Figure 3-8, Data acquisition system (channels box)

The data analysis for the ultrasonic Doppler flowmeter was done using two methods. The first is based on the ultrasonic Doppler flowmeter data processing system where the data is displayed on the flowmeter display; this method is used when the flowmeter is deployed in a homogeneous flow regime, LABVIEW is used to record this data simultaneously together with the reference flow meters data. The second

data analysis method is processed using the ultrasonic flowmeter raw signal (frequency shift) and is processed using different software (Sigview and Autosignal); this method is associated with ultrasonic being deployed in slug flow.

Table 3-3 illustrates data acquisition channels that have been used in LABVIEW.

Instrument Name	TITLE (COL. HEADER)	ZERO	GAIN	UNITS	A/D Channel	On?
Fw	Water flow (Magflow)	0.5	6.27	l/s	0	y
FgL	Air flow (Low)	1	1.548	m/s	1	y
FgH	Air flow (High)	0	213.18	l/min	2	y
PgL	Air Pressure (Low)	-0.001	0.679	barg	3	y
PgH	Air Pressure (High)	0.012	1.332	barg	4	y
Pm	Mixture Pressure	0.003	0.863	barg	5	y
D.P	Differential Pressure	-5.396	0.1884	mb	6	y
Tg	Gas temperature	0	9.9	°C	7	y
Tm	Mixture temperature	0	10.1	°C	8	y
CA	Conductivity A	0	1	V	9	y
CB	Conductivity B	0	1	V	10	y
CC	Conductivity C	0	1	V	11	y
CD	Conductivity D	0	1	V	12	y
USA	Ultrasonic Head A	0	1	V	13	y
USB	Ultrasonic Head B	0	1	V	14	y
DOPPLER	Ultrasonic Doppler	-0.023	1.409	m/s	15	y

Table 3-3, Data acquisition system channels

3.4.1 LABVIEW software

The Department of Offshore, Process and Energy Engineering uses LABVIEW 7 (graphical programming for instrumentation) which has been installed and run in the departmental laboratory test rig computer. LABVIEW was used to measure and analyse the two-phase rig instrumentation data as well as monitoring the changes within the parameters during the experiments.

Figure 3-9, LABVIEW data display illustrates some rig test parameters such as superficial gas and liquid velocities, temperature and pressure of gas and liquid, or, for the mixture, flow-rate, conductivity rings and ultrasonic transducers signals, and some other essential parameters for the experiments.

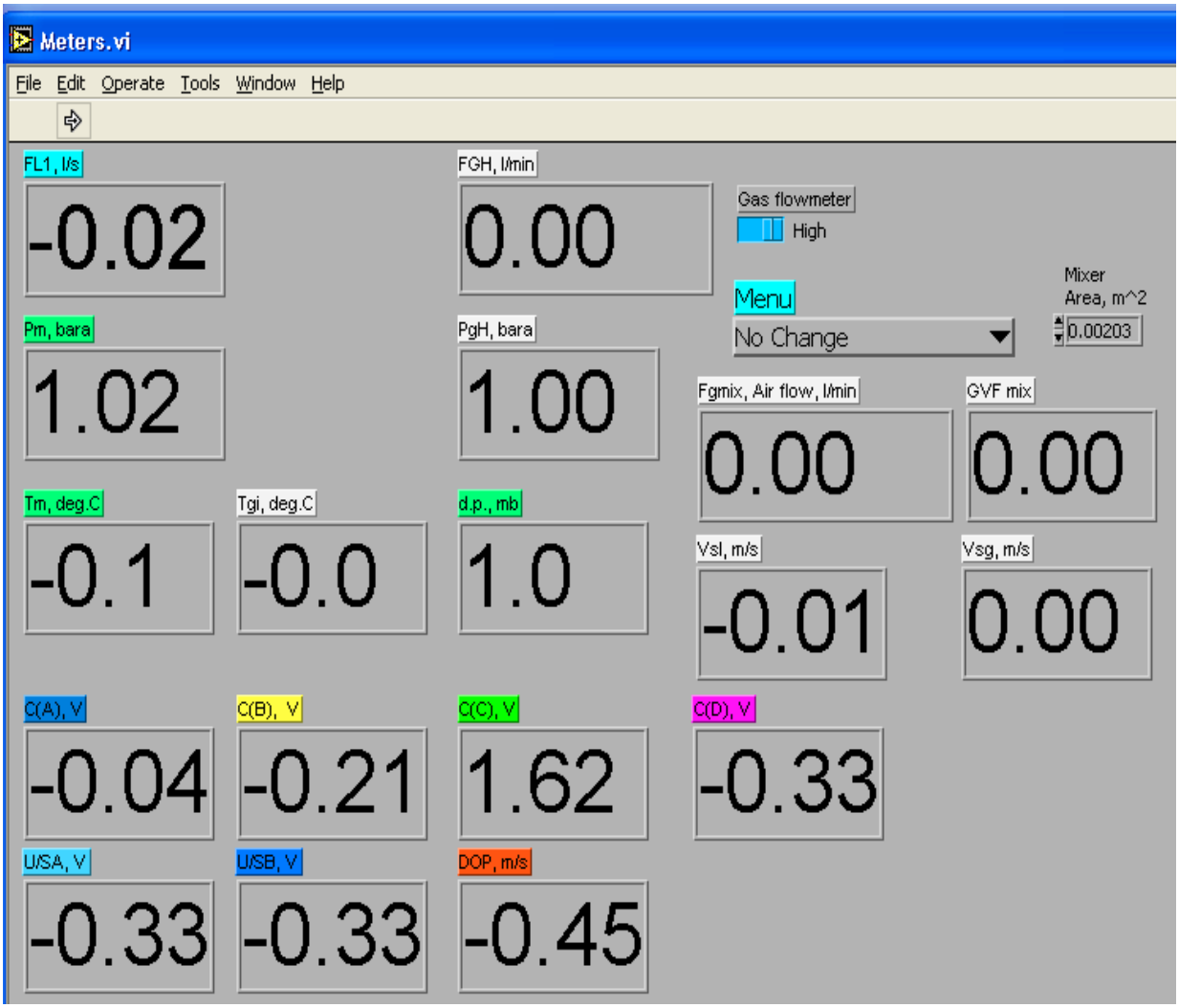

Figure 3-9, LABVIEW data display

3.5 CHAPTER SUMMARY

In this chapter, the experimental set up for the two-phase air-water facility was described in detail. The general metering concept overview was addressed in terms of T-Y junctions, measurement concepts and general data acquisition. This chapter also focuses on the measurement methods and techniques that have been proposed in measuring two-phase flow in different flow regimes.

Chapter 4

LIQUID DOMINATED FLOW MEASUREMENT AFTER PARTIAL SEPARATION

4.1 CHAPTER INTRODUCTION

This chapter documents the investigation of liquid flowrate measurement in the partial separated liquid flow using the ultrasonic cross correlation method to measure the flow velocity in a combination with a conductivity ring to measure phase fraction. T-junction works as a two-phase flow partial separated liquid dominated flow at the outlet. The chapter starts with a brief description of the experimental set-up for the partially separated liquid, including the T-junction dimensions, its installation and ultrasonic measurement techniques. Ultrasonic cross correlation signal processing as well as the signal conditioning circuit are clearly explained. Conductivity ring performance in liquid hold-up measurement is also addressed in this chapter. Finally, the volumetric liquid flowrate measurement in the partial separated liquid flow is obtained as a result of velocity measurement using ultrasonic cross correlation and liquid hold-up measured by the conductivity ring.

4.2 SECTION EXPERIMENTAL SET-UP

4.2.1 Liquid Dominated Flow Section Hydraulic Description

This T-junction is functioning as a partial separator of the two-phase flow. The vertical T junction was constructed using a vertical 150mm clear pipe with extending a 50mm pipes upward line for the separated gas line, and another 50mm downward line for the separated liquid as shown in Figure 3-6. The separation method is based on gravity without involving any complicated separation techniques.

The maximum flow-rate of liquid and gas upstream of the T-junction was based on recommendations from a specialist multiphase flow separation company. (CALTEC Ltd 2008). Figure 4-1 illustrates the recommended geometry of the T-junction functions as a partial separation device for two-phase slug flow.

The proposed T-junction body is assembled to accommodate the required liquid to maintain a continuous flow regardless of the upstream slug flow regime, so it is noticeable that the cross section area of the T-junction body is 150mm, this is three times the area of the outlet pipes making the T-junction a small feeding tank of the liquid, as shown in Figure 4-1. The liquid outlet is also provided with a 45^{o} upward riser. This rise ensures a back pressure to minimise gas entrainment and ensure liquid continuous flow.

The results obtained using a conductivity ring show good two-phase flow separation efficiency achieved by using the T-junction (maximum gas carried under <15%) under inlet two-phase slug flow from 0 to 60% GVF.

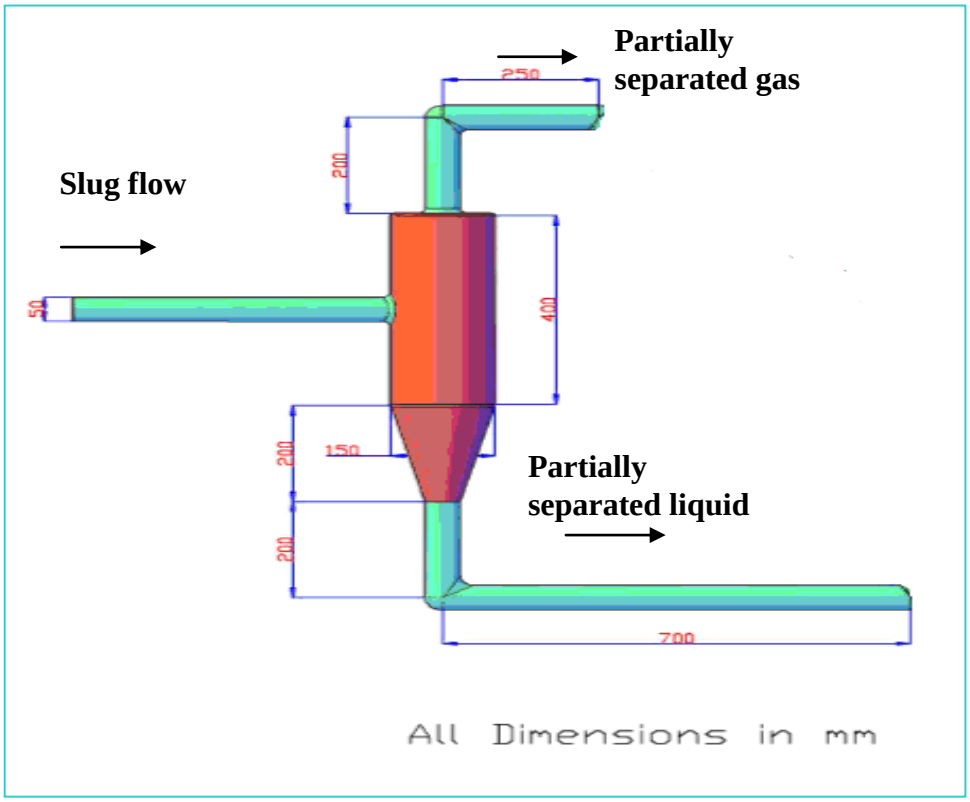

Figure 4-1, T-Junction assemble

Ultrasonic cross-correlation is used in this partially separated liquid stream as a velocity measurement technique and conductivity flush-mounted rings are utilised to measure the component fraction. These methods and techniques will be explained in more details in the section below.

4.2.2 Ultrasonic Cross Correlation measurement

The partially separated measurement section is located in the downward outlet arm of the T-junction where the fluid is a liquid dominated flow with gas carry-under (bubbly flow). The measurement section length is about 700mm to allow the measurement instruments to be installed, Figure 4-2 shows the liquid dominated section pipe configuration.

Two pairs of ultrasonic transducers are inserted within axial separation of 0.046 m. The aim of these transducers is to measure the bubble velocity, assuming that the liquid and gas bubbles are moving at the same velocity and no slip occurs between the two phases.

The ultrasonic transducers that have been used in this experimental work are 1MHz transducers, as shown in Figure 4-3. They are installed and fixed on the external pipe wall opposite to each other in a single path signal. Figure 4-2 illustrates the two pairs of ultrasonic transducers inserted into the 50mm plastic pipe. The ultrasonic transducers are fixed in a configuration that allows the transducers to partly touch the surface of the flow without causing any disturbance to the flow. These transducers are excited with 1MHz frequency from the frequency generator. The ultrasonic signal received by the transducers is correlated using a LABVIEW cross-correlation subroutine function to determine the time delay (τ). With the known distance between the two pairs of transducers, the velocity of the bubbles flowing within the fluids can then be calculated.

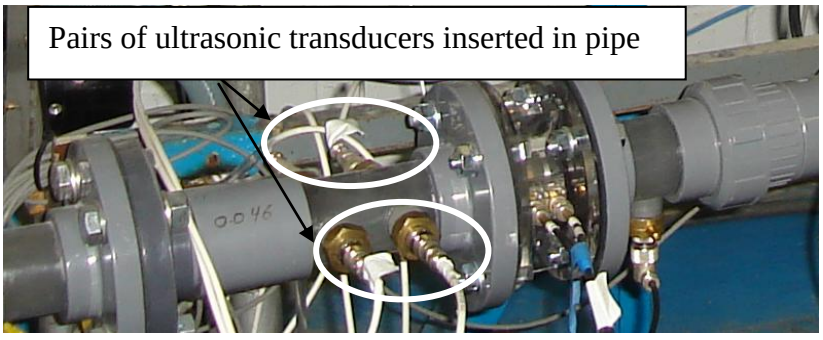

Figure 4-2, Set of ultrasonic cross-correlation transducers

Figure 4-3, 1MHz ultrasonic transducer

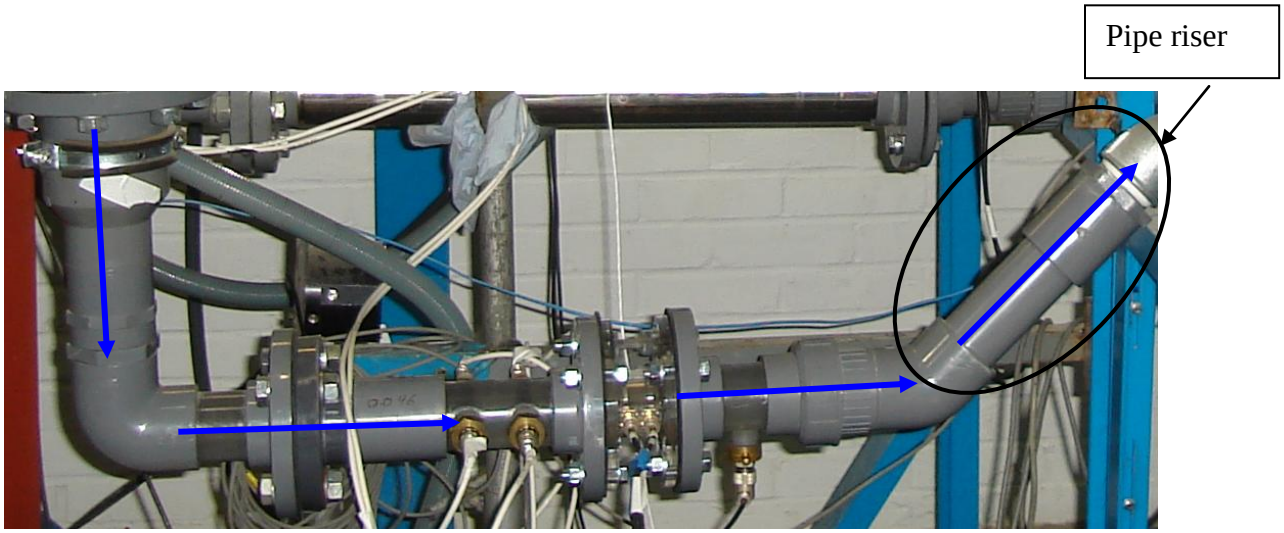

Figure 4-4, Partially separated liquid section

The ultrasonic cross-correlation measurement was obtained as the following:

$$Rxy(\tau) = \frac{1}{T}\int_{0}^{T} x(t)\,y(t-\tau)\,dt \qquad \textbf{(4. 1)}$$

$$V_{X.Corre} = L/\tau_{m} \qquad \textbf{(4. 2)}$$

There is more than one method to cross-correlate the time delay of the ultrasonic transducers. In this work, LABVIEW was used to gain the time delay and the flow velocity using equations 4.1 and 4.2. The liquid volumetric flow-rate can be determined by multiplying the velocity with liquid hold up as measured by conductivity ring.

$$Q_{l} = V_{X.Corre}\alpha_{l} A \qquad \textbf{(4. 3)}$$

4.2.3 Liquid flowrate measurement steps

The liquid and gas routes are explained in Figure 4-5. Intrusive sets of ultrasonic cross-correlation are installed at liquid dominated sections to measure the bubble velocity, assuming that the flow is a mixture and the two-phase (liquid and gas) is travelling at the same velocity (no slip). A flush-mounted conductivity ring was calibrated to measure the fraction, installed beside the ultrasonic cross-correlation flowmeter, as shown in Figure 4-6.

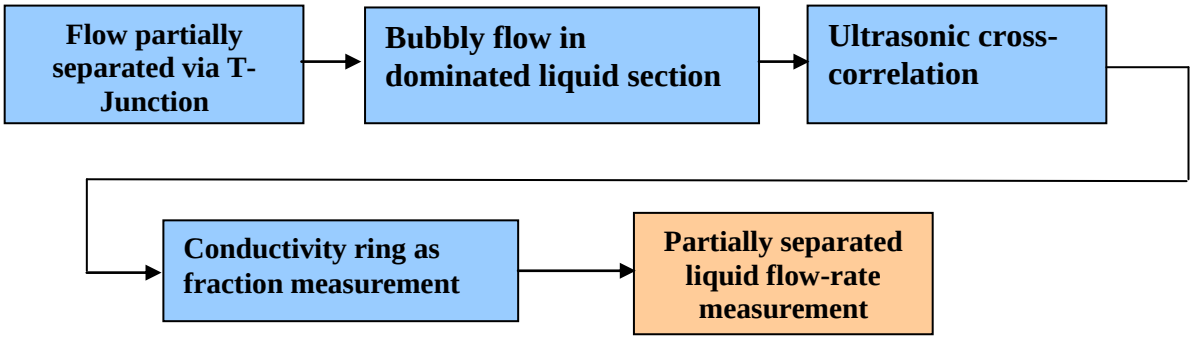

Figure 4-5, Partially separated liquid flow-rate measurement steps

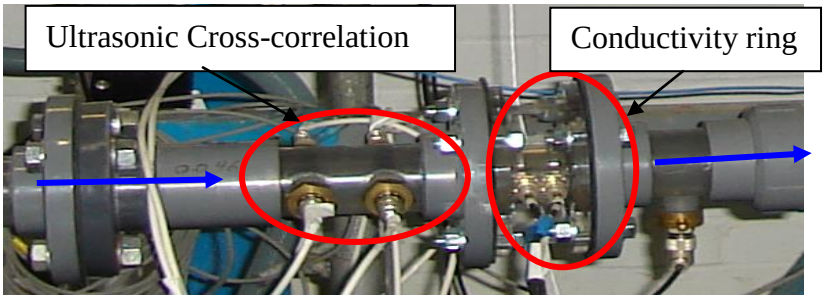

Figure 4-6, Liquid flow-rate measurement technique

4.3 ULTRASONIC CROSS CORRELATION SIGNALLING PROCESSING

4.3.1 Signal Conditioning Unit

To extract the envelope of the amplitude modulated ultrasonic signal, a signal conditioning unit was used with the ultrasonic transducers. (The signal conditioning unit consists of a non-inverting amplifier, an active full wave rectifier and a low pass filter, as shown in Figure 4-7. The raw ultrasonic sensors signals are filtered, amplified and positive full wave rectified in the signal conditioning unit, and then sent to the data acquisition system.

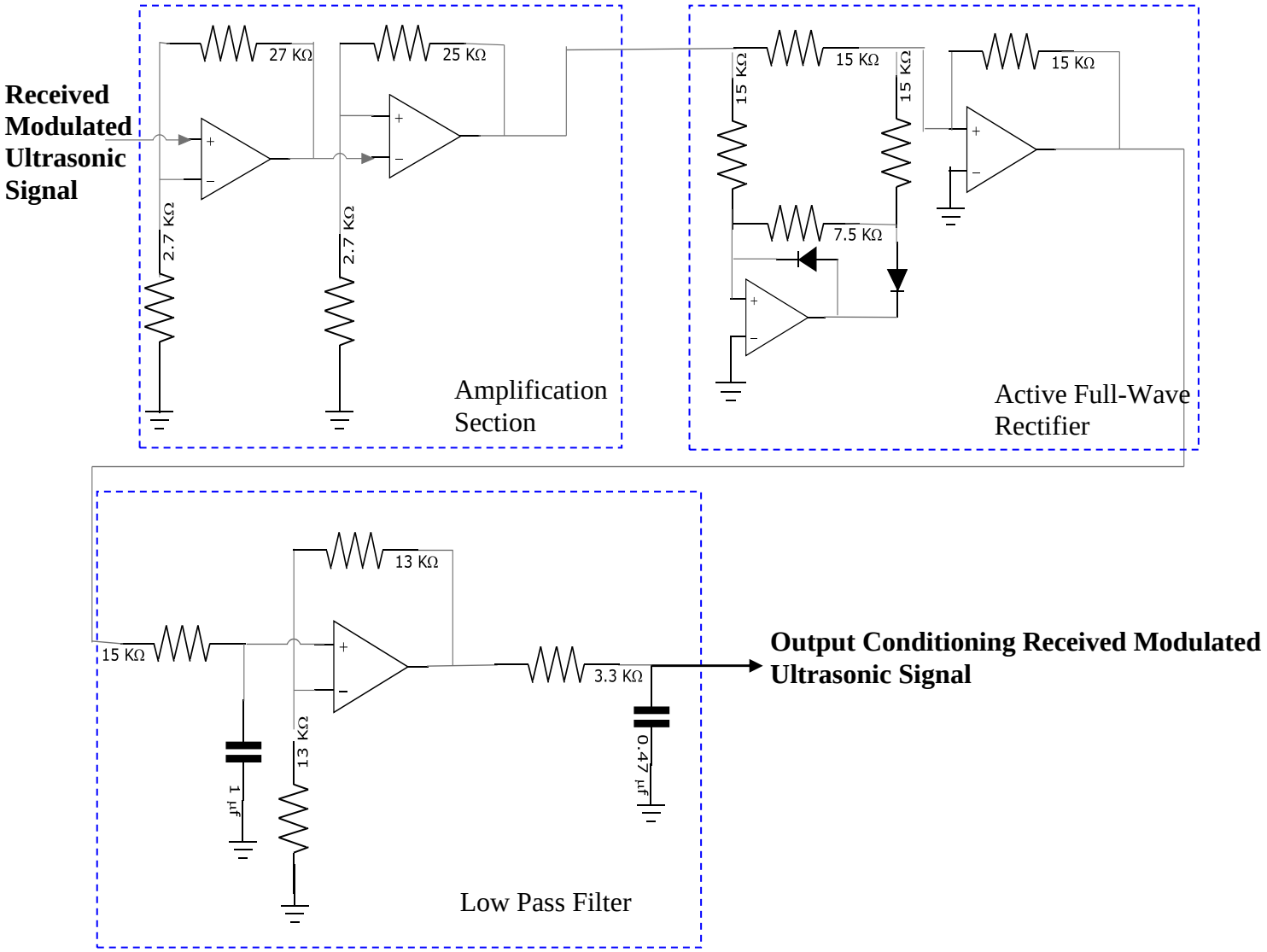

Figure 4-7, Electronic circuit of the signal conditioning unit

Conductivity ring outputs were also sent to the data acquisition system for recording and analysing.

The function generator excites the ultrasonic transducers which are installed opposite each other; the transmitters send an ultrasonic pulse through the flowing fluids, this signal is picked by the ultrasonic receivers which are located on the other side of the pipe. The signal which carries the flow information is then transmitted to the signal conditioning box and in turn to DAS and it is displayed on the LABVIEW. Figure 4-8 illustrates the ultrasonic cross-correlation signal processing route.

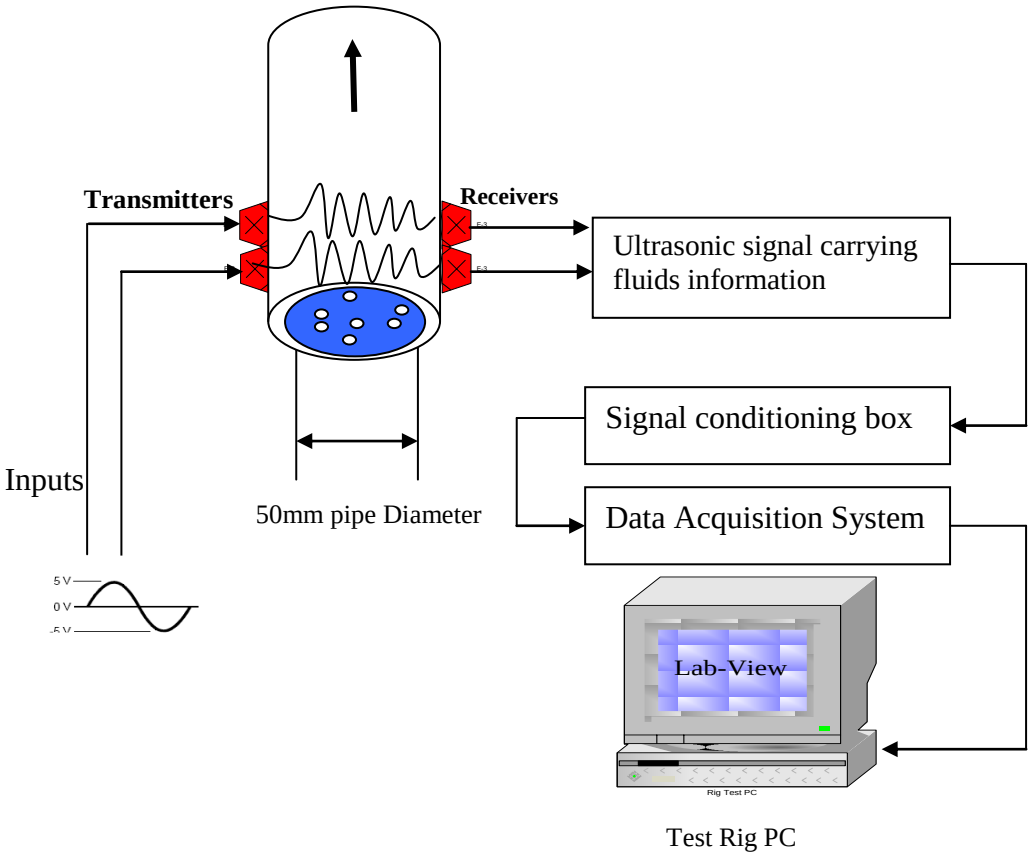

Figure 4-8, Cross-correlation data processing diagram

4.4 Liquid Hold-up at partially separated Liquid Flow

Liquid hold-up information is required to get the partially separated liquid flowrate and to demonstrate the effectiveness of the T-junction as partial separation device. Liquid hold-up is measured using a conductivity ring installed in the partially separated liquid flow at about 1.0m/s of liquid superficial velocity and at a wide range of superficial gas velocities from 0.5-7.8m/s. The conductivity ring void fraction measurement in this region was between 85-90% as the gas superficial velocity increases.

Figure 4-9 shows the liquid hold-up measured under the same operational conditions and the liquid hold-up is calculated from liquid flowrate divided by mixture flowrate. The correlated liquid hold-up decreases as the gas velocity increases, whereas the conductivity reading shows a reasonably good range regardless of the gas velocity change from the reference.

These results also show the capability of the T-junction as a partial separation device for the two-phase flow generating a high liquid dominated flow in this section.

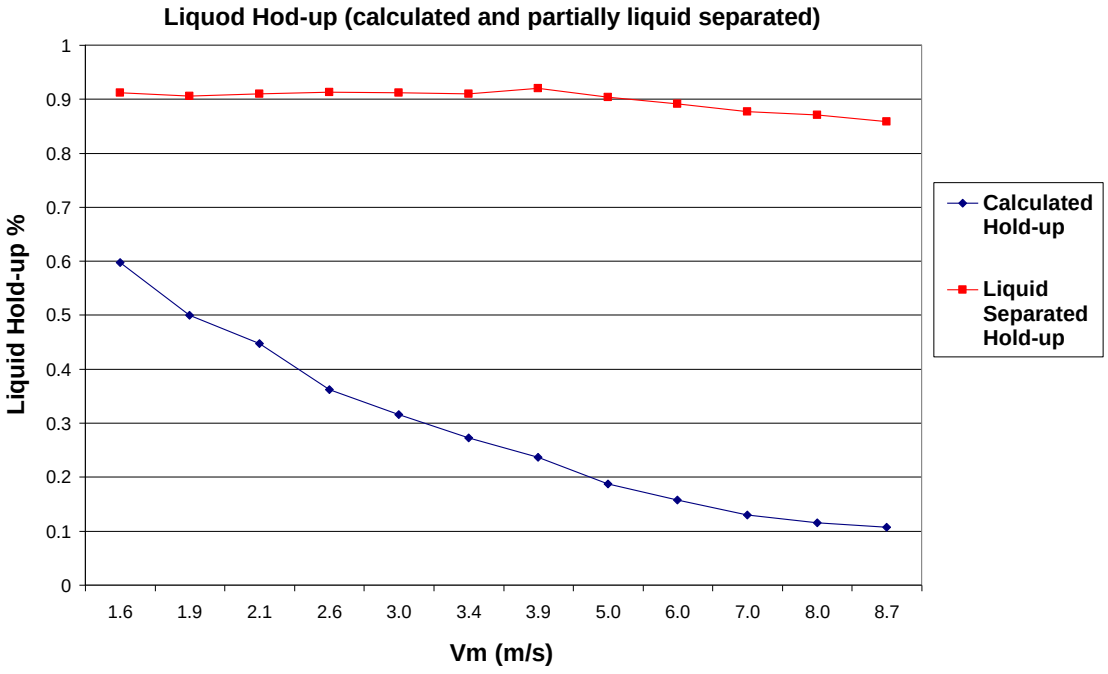

Figure 4-9, Liquid hold-up calculated and measured using conductivity ring

4.5 LIQUID FLOWRATE MEASUREMENT

The volumetric liquid flow-rate measurement was obtained and compared to the reference electromagnetic flowmeter for liquid flow-rate and reasonable accuracy was achieved, as shown in Figure 4-10.

The experimental test campaigns of liquid separated flow-rate measurement covered a wide range of superficial liquid and gas velocities, from 0.7-1.3m/s and from 0.5-7.8m/s, respectively, at atmospheric pressure and a room temperature of 20^{o}C.

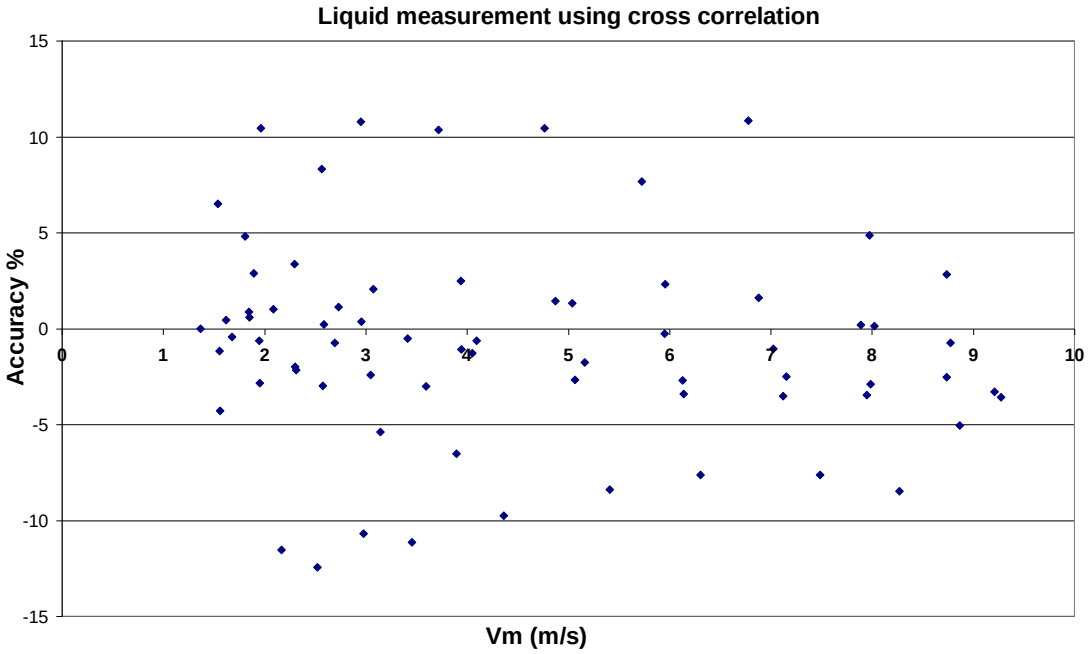

Figure 4-10, Liquid flow-rate measurement in partially separated liquid section

Figure 4-10 illustrates the liquid flowrate accuracy measured by ultrasonic cross-correlation. There are some points in the figure which exceeded $\pm 10\%$; these occurred as a result of the low liquid flow-rate which was observed to create a back-flow phenomenon inside the separated liquid section.

It is noticeable from this figure that the majority of the test points are located within $\pm 5\%$ which indicates the overall liquid flow measurement accuracy.

4.6 CHAPTER SUMMARY

This chapter has focused on the partially separation liquid flow section experiment set-up, starting with T junction as a two-phase flow conditioning device. Ultrasonic cross correlation for liquid velocity measurement and the conductivity ring for liquid hold-up measurement have been deployed. The main steps of how to implement this technique were illustrated and discussed. The ultrasonic signal processing route has been explained including full details of the electronic circuit. All the measurements were simultaneously recorded using LABVIEW.

Chapter 5

HOMOGENEOUS FLOW MEASUREMENT

5.1 CHAPTER INTRODUCTION

In the next pages, the limitations of the ultrasonic Doppler flowmeter with different gas liquid concentrations and the corrections that have been made to increase its performance are discussed. The homogeneous flow hydraulic section and the mixture flow enhancing device (mixer) and signal processing are illustrated in this chapter. Ultrasonic Doppler flowmeter combined with the conductivity ring and the static mixer are tested in controlled homogeneous flow downstream of the reference metering points (electromagnetic and turbine flowmeters). And then the flowmeter is installed downstream of T-Y junction and the liquid and gas flowrate are measured.

As the flow has been homogenised using the horizontal Y-junction and the Kenics static mixer. The mixed flow is then directed through a flush-mounted conductivity ring for a fraction measurement and it passes the ultrasonic Doppler for a mixture flow velocity measurement. The Doppler was installed further away from the static mixer to avoid problem caused in the flow mixture jetting region by the mixer and the flow straightener. There is a conductivity ring dynamically calibrated and installed beside the Doppler to measure the two-phase fraction, so the liquid and gas volumetric flow-rate can be identified.

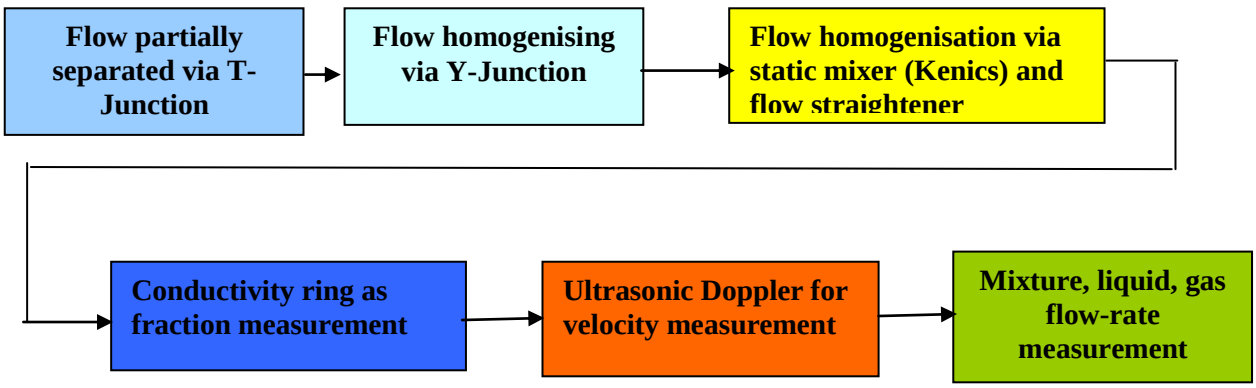

Figure 5-1, Flow-rate measurements steps

5.2 EXPERIMENTAL SET-UP

For the proposed T-Y junction measurement scheme, the two partially separated streams are combined using a Y junction, as shown in Figure 5-2. The partially separated gas line is a 45^{o} inclined pipe in order to allow any liquid carry over to run smoothly on the bottom of the internal pipe. For gas flow, there is not gas flow meter used in the current study. However, in the future gas flow measurement could be easily obtained by clamping-on or inserting-in ultrasonic transducers mounted on the side wall of the 50mm pipe. The inclined gas pipe also provides smoothing injection of the partially separated gas flow within the combined line (Y-junction).

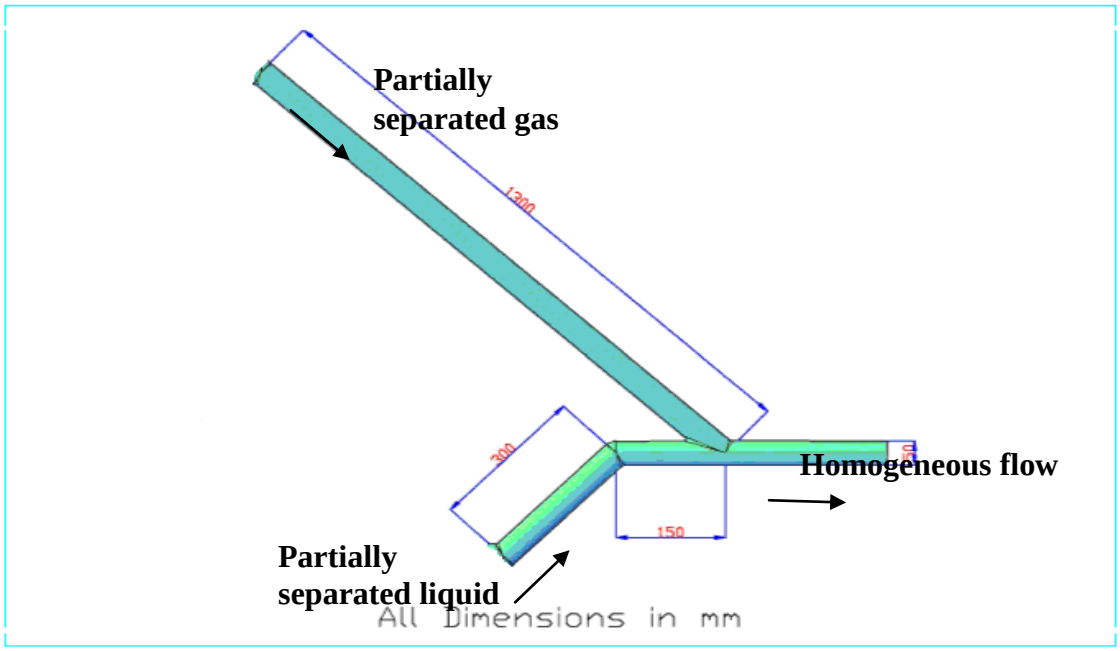

Figure 5-2, Y-junction for flow homogeniser

A static mixer used to homogenise the two-phase flow is illustrated in Figure 5-3. This mixer has six helical twisted elements at a 180^{o} standard element angle as shown These elements are housed in a flanged 50mm diameter pipe 450mm length. It is provided to enhance mixing of the two-phase flow (liquid and gas) downstream of Y-junction and reduce the slip between the two phases to the minimum.

Figure 5-3, The Kenics static mixer installed downstream of Y-junction

A flow straightener is installed downstream of the Kenics static mixer. This flow straightener is made up of 10 cm diameter of aligned tubes in parallel. The purpose of using the flow straightener is to remove the helical flow generated by the Kenics static mixer as shown in Figure 5-4. The ultrasonic Doppler is deployed to measure bubble velocity (homogeneous) of gas/liquid two-phase flows. This flowmeter is designed to be used with a single-phase liquid flow with a very tiny amount of scatters, implementing it in a well-homogenised flow can be a big challenge.

Before using the sensor in the T-Y junctions as described above the method was tested downstream of the reference flow meters on a straight length of 50mm pipe. Under this arrangement, the liquid and gas are both separately measured and flow-rate controlled before they are injected into the system. The ultrasonic Doppler flowmeter is located 12m away from the injection.

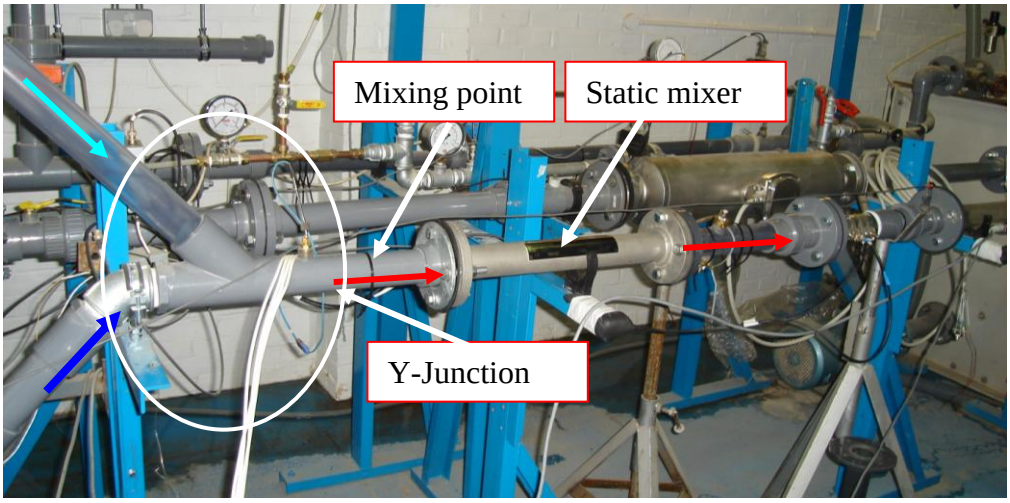

Figure 5-4, Y-junction as assembled in the Lab

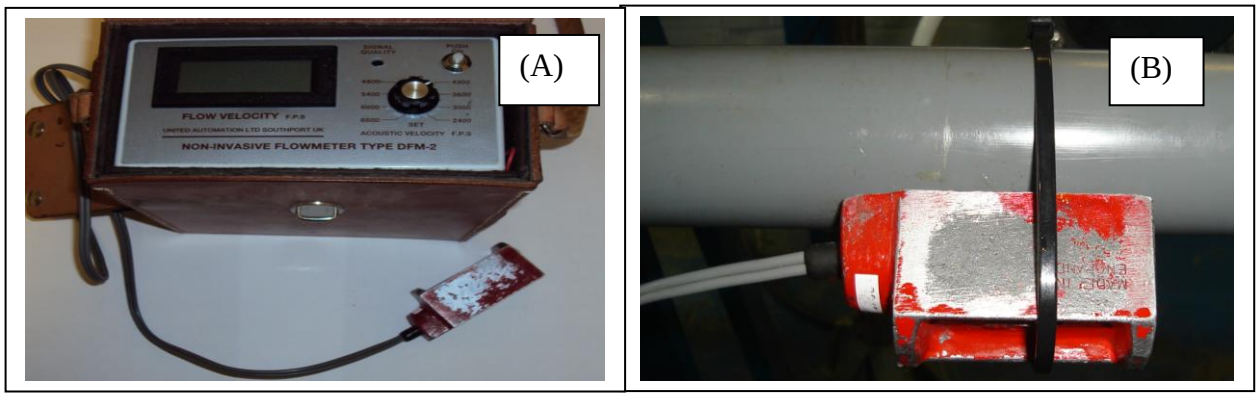

Figure 5-5, Ultrasonic Doppler flowmeter and its transducer

As shown in Figure 5-5 (A), the ultrasonic Doppler flowmeter is installed about 500mm downstream of the static mixer. This transducer is clamped on at the bottom of the pipe at the 6 o'clock position on the pipe, Figure 5-5 (B), where liquid flow always exists with a lower gas concentration compared with that at the top of the pipe. The ultrasonic Doppler flowmeter is connected to the PC to record the change in the signal according to the change in the flow-rate of liquid and gas via a channels box and LABVIEW software. The ultrasonic Doppler flowmeter operation principle is illustrated in more detail in the next section.

5.3 ULTRASONIC DOPPLER FLOWMETER SIGNALLING ROUTES

The ultrasonic Doppler flowmeter was installed downstream of the T-junction where the flows (gas and water) are combined into a 50mm pipe where the Doppler is performing, to measure the mixture velocity. These measurement results are illustrated later on in this chapter.

The reason for using the ultrasonic Doppler is because it is simple in terms of its signal processing, and the approximate frequency attenuation of the scattering material (bubbles of gas) is taken into account; these scatterers have an approximate frequency of 100 kHz.

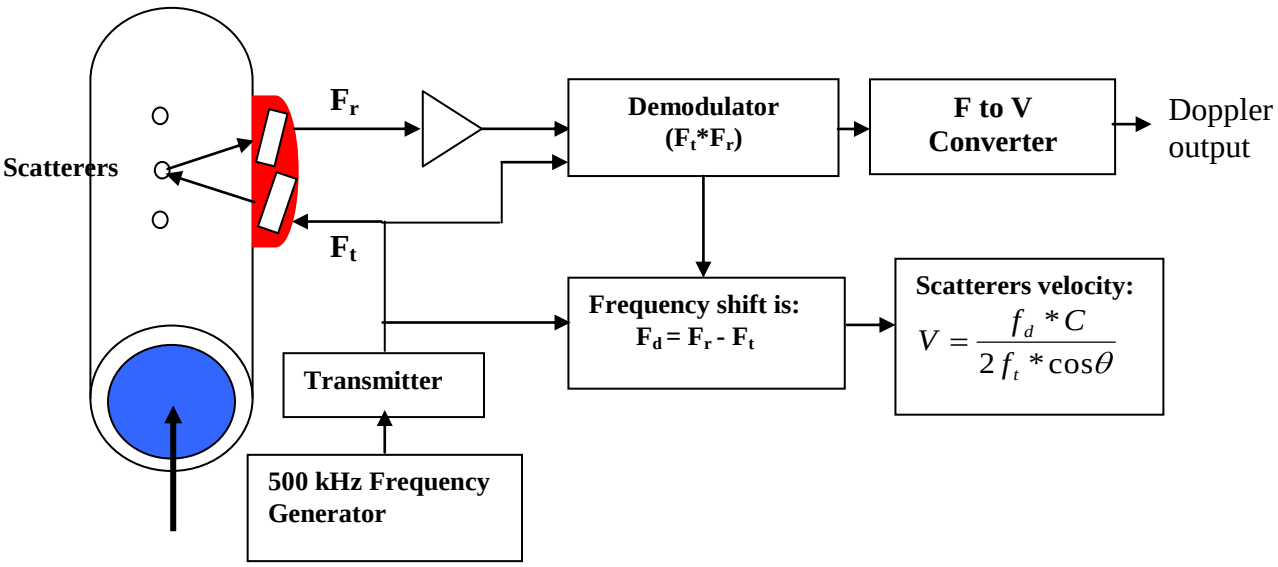

Figure 5-6, Ultrasonic Doppler signal processing schematic diagram

The ultrasonic Doppler diagram in Figure 5-6 shows that the ultrasonic processing starts from the frequency generator to the ultrasonic Doppler transducer where the signal is sent to the transmitter transducer and there is an ultrasonic Doppler transducer receiver. The received and transmitted frequencies are multiplied and the average scatterers velocities are obtained from the velocity equation.

Figure 5-7 illustrates the steps taken to obtain better accuracy of liquid and gas measurement.

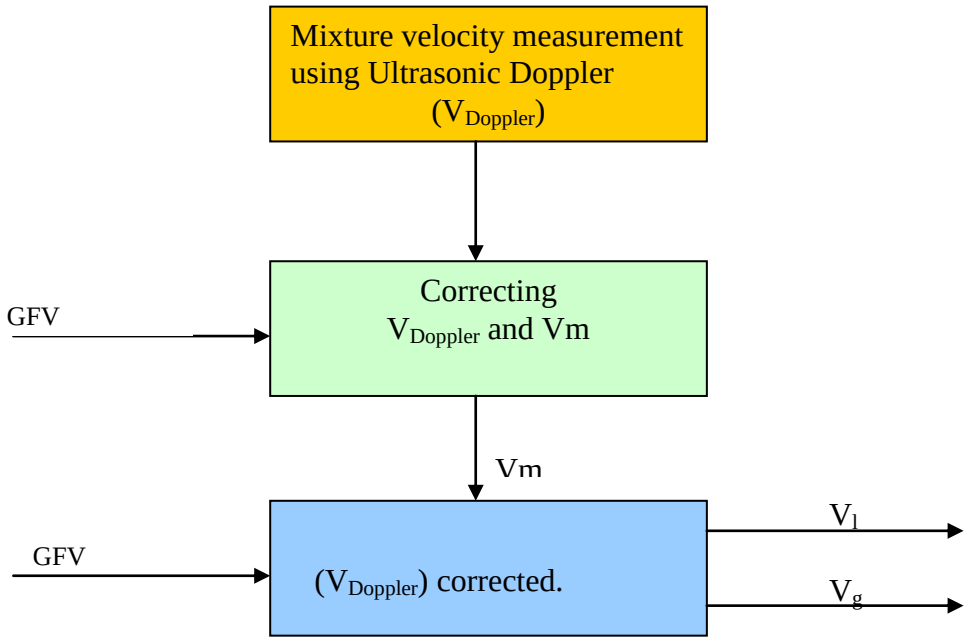

Figure 5-7, Homogeneous measurement flowchart

5.4 LIQUID AND GAS FLOWRATE MEASUREMENTS IN THE STRAIGHT SECTION DOWNSTREAM OF REFERENCE METERS

The ultrasonic Doppler transducer, the Kenics static mixer and the conductivity ring were placed downstream of the reference points (electromagnetic and turbine gas flowmeters) where liquid and gas are introduced to the system. A series of experiments have been conducted with the configuration, as shown in Figure 5-8. The liquid flow-rate was fixed, whereas the gas flow-rate was gradually changed to increase the gas void fraction and the Doppler behaviour and reference points data were recorded.

For photo clarity, the ultrasonic Doppler transducer is shown as being installed in Figure 5-8 on the top of the pipe as the transducer in the picture cannot be demonstrated clearly when the transducer is installed in the bottom of the pipe.

Figure 5-8, Ultrasonic Doppler and static mixer in front of the reference

A total of 120 different test points which were collected, spanning the full operating range of the Cranfield University two-flow test facility.

- Superficial liquid velocity: 1 to 2.2m/sec.
- Superficial gas velocity: 0.1 to 4m/sec.
- Mixture velocity: 1.0 to 5m/sec.
- Gas volume fraction: 0 to 60 %.
- Static pressure: 1-2 bar abs.
- Temperature: room temperature (18 to 24^{o}C).

Figure 5-9 illustrates the effect of increasing the gas superficial velocity at each fixed superficial liquid velocity. As the gas velocity increases, the bubble concentration on the top of the pipe increases and then a cloud of bubbles spread downwards and layers of bubbles block the ultrasonic signal path, eliminating the opportunity to detect any fluid behaviour at the top of the pipe. As a result the Doppler signal declines.

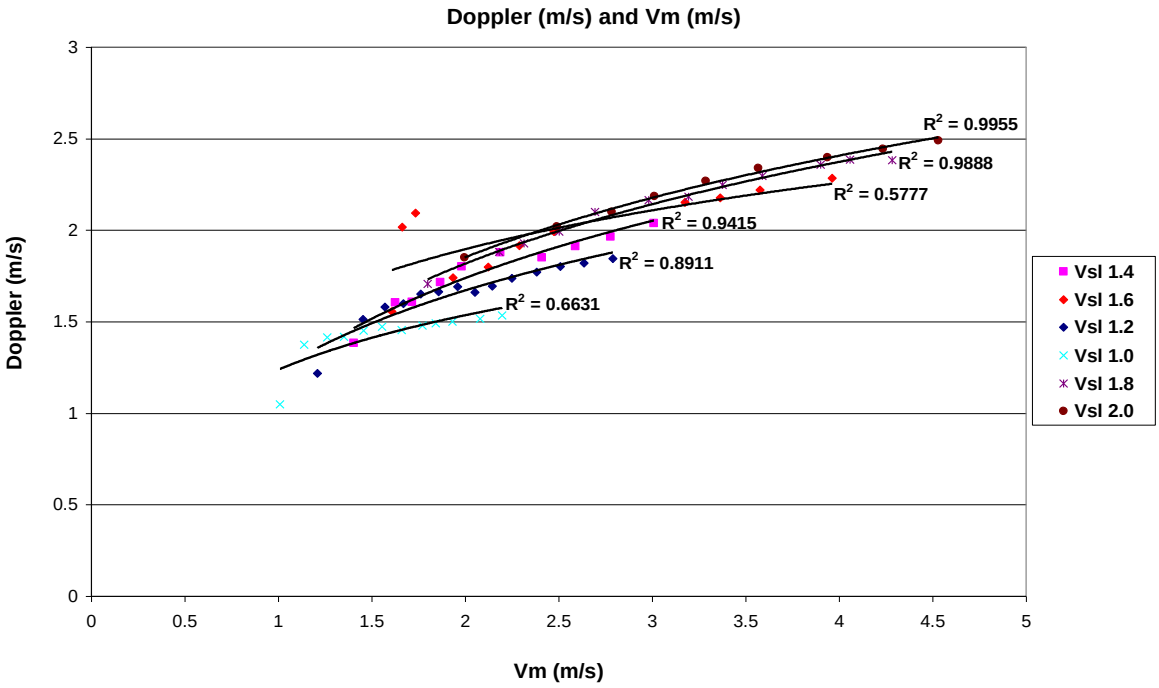

Figure 5-9, Doppler behaviour clamped on front of the reference points

The Doppler data (m/s) obtained from each experiment campaign was plotted against the mixture reference velocity (m/s) and the results can be seen in Figure 5-9. Liquid flow-rate covered a wide range of flow, starting from 1.0 to 2.0m/s whereas the gas void fraction (GVF) increased from about 0% to 60%. In this configuration, the ultrasonic Doppler behaved unsteadily for all of the liquid/gas test ranges; 1.0m/s liquid seems to flatten early compared to the T-Y junction downstream configuration (described in the chapter 3) and this is clearly noticeable in 1.6m/s of liquid where the Doppler was reading significantly higher than it should have been.

The Doppler flowmeter limitation has been assessed by comparing the mixture velocity reading measured by the ultrasonic Doppler flowmeter to the superficial mixture velocity. Figure 5-10 illustrates this performance.

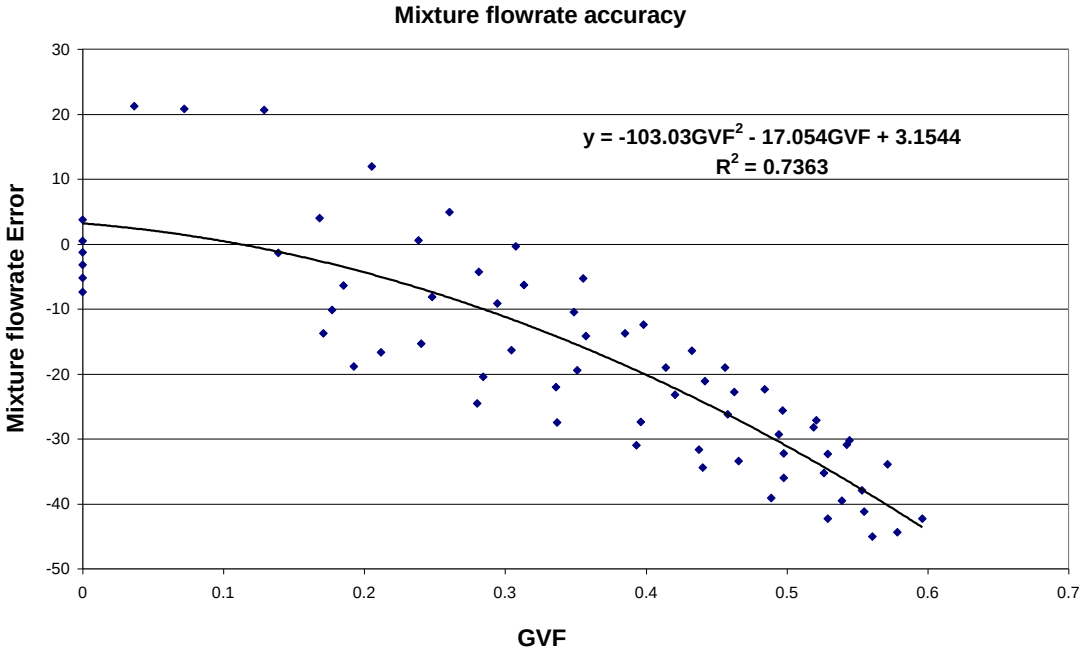

Figure 5-10, Doppler flowmeter in mixture flow-rate accuracy measurement

It is worth mentioning that the Doppler flowmeter is designed to be deployed to measure the velocity of the tiny particles scattered in the single-phase (liquid) assuming that both (liquid/gas) are flowing with the same velocity. In this experimental work, the particles are air bubbles introduced into the system at gradually increasing flow-rates of gas to reach a high gas void fraction.

As shown in Figure 5-10 that by increasing GVF within the mixture, the ultrasonic Doppler flowmeter error increases for all flow-rates.

5.4.1 Ultrasonic Doppler flowmeter correction in controlled homogeneous flow

The Doppler obtained results in Figure 5-10 were corrected as a function of GVF identified by the conductivity ring. The assumption is based on the error in the ultrasonic Doppler as only an effect of GVF. The Doppler correction is performed as follows:

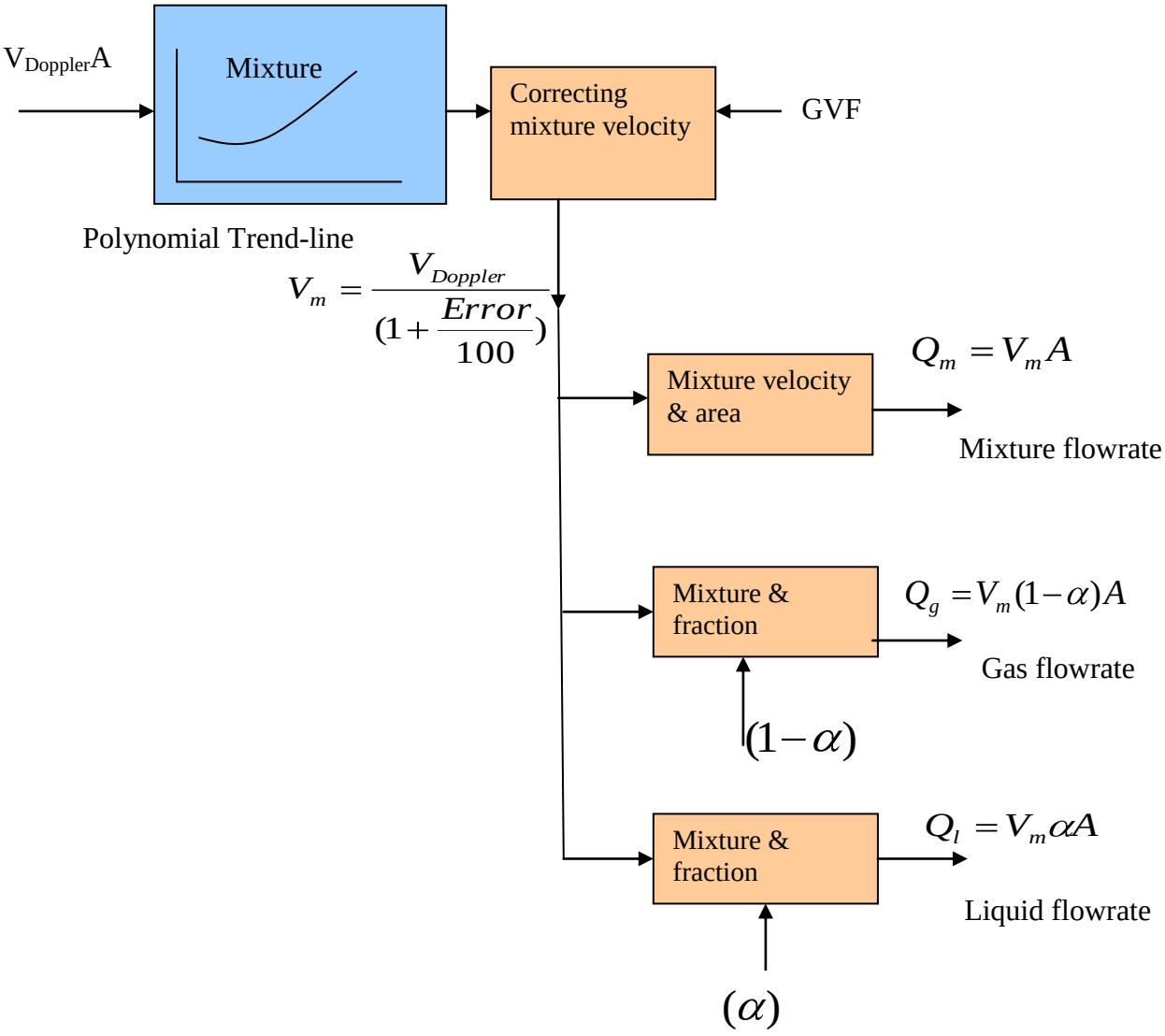

Figure 5-11, Flowchart of ultrasonic Doppler in homogeneous flow

The ultrasonic Doppler correction is performed as a result of the GVF; basically, the Vm is corrected in the GVF function to obtain a better accuracy of the ultrasonic Doppler as follows:

As;

$$V_m = V_{sl} + V_{sg} \tag{5. 1}$$

and:

$$Error = \left(\frac{V_{Doppler} - V_m}{V_m} \right) \times 100 \tag{5. 2}$$

and then,

$$\frac{Error}{100} = \frac{V_{Doppler} - V_m}{V_m} \tag{5. 3}$$

So,

Error = $-103.03GVF^2 - 17.054GVF + 3.1544$

$$V_m = \frac{V_{Doppler}}{\left(1 + \frac{Error}{100}\right)} \tag{5. 4}$$

The error in equation 5.4 is a function of GVF measured by the conductivity ring which was calibrated in the homogeneous flow and installed in the homogeneous section.

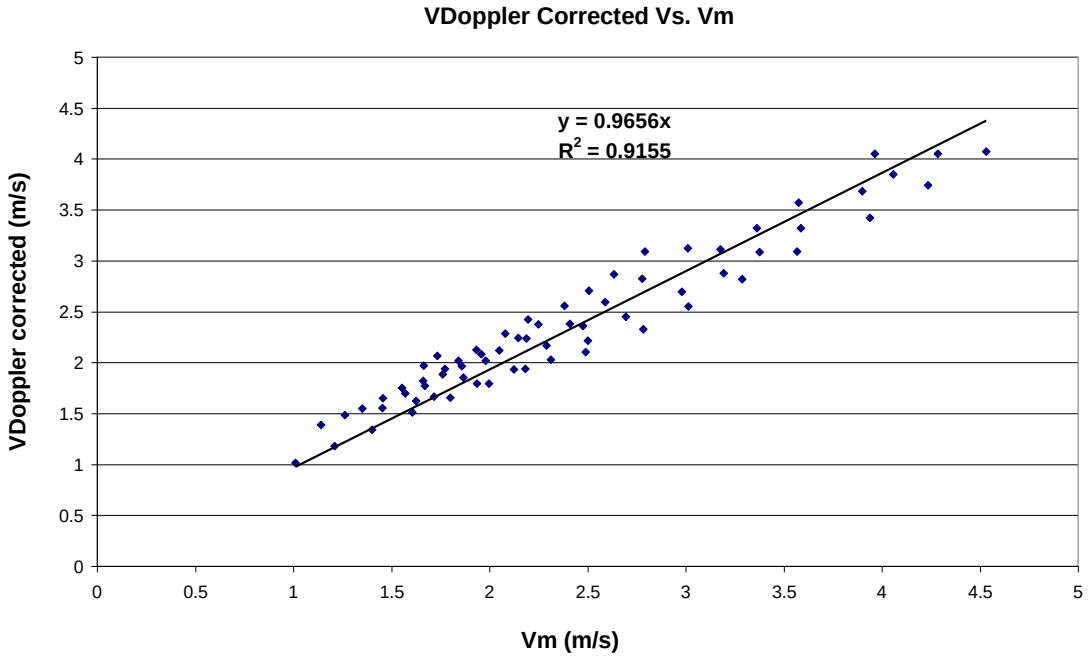

Figure 5-12, Ultrasonic Doppler after correction

5.4.2 Conductivity rings homogeneous calibration

The conductivity ring was calibrated against the references GVF via electromagnetic flowmeter for a liquid flow-rate measurement and a turbine gas flowmeter for gas flow-rate measurement. Figure 5-13 illustrates the result of the performed calibration.

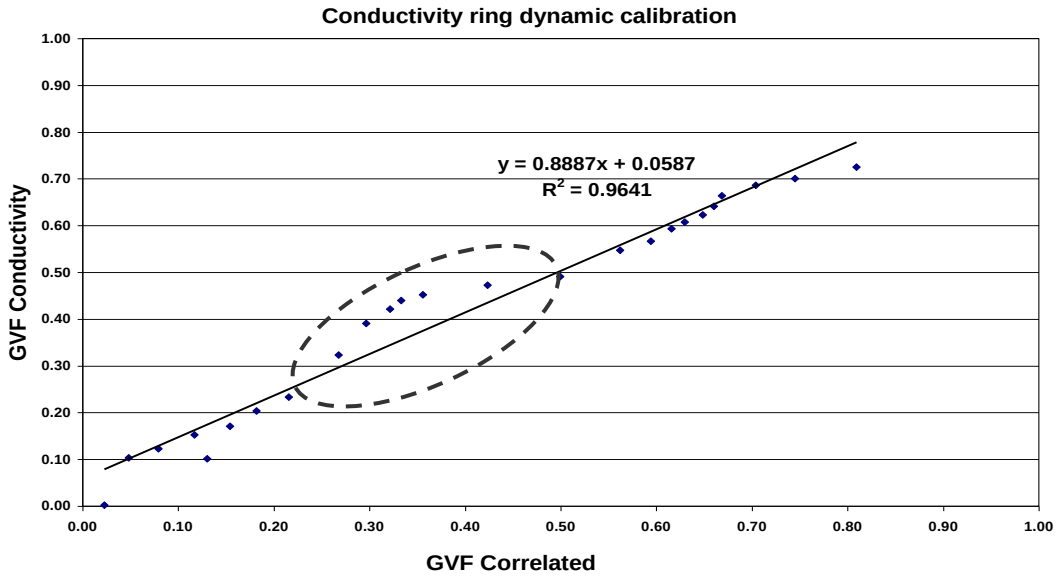

Figure 5-13, Conductivity ring dynamic calibration

The reason behind the gas flowmeter behaviour at about 40% GVF, is that there are two turbine flowmeters working in this test rig; the low gas flow-rate is not reliable in the high gas flow-rate measurement range, and the high gas flow-rate is not reliable in the low gas flow-rate measurement range, and as a result the calibration shows a clear error at 40% GVF.

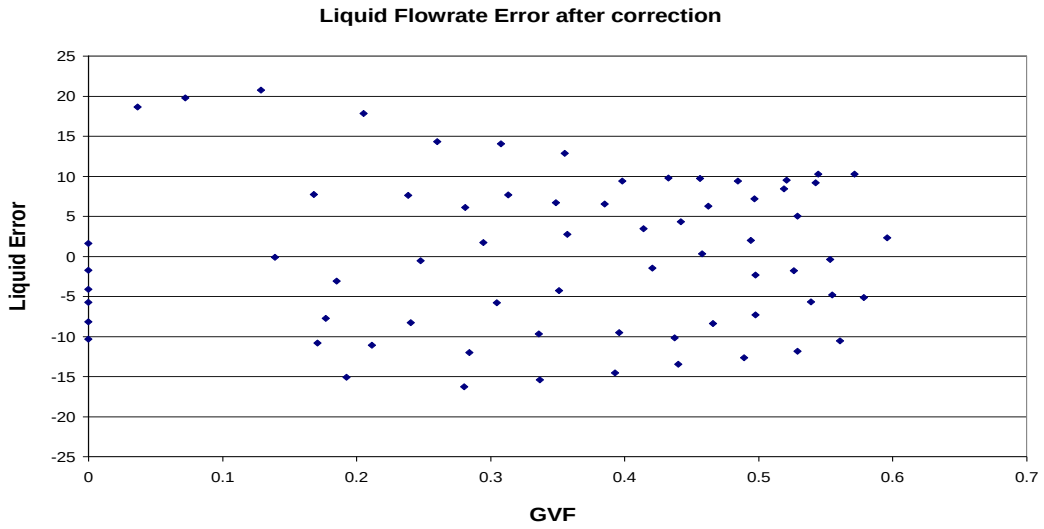

Figure 5-14, Ultrasonic Doppler flowmeter performance after the correction

The ultrasonic Doppler correction was performed for the Doppler configuration where it is installed in front of the reference points; however, the overall Doppler accuracy performance did not show a good agreement when compared with the reference point. This is as a result of the unsteadiness of the flow which occurred directly downstream of the injecting points.

5.5 LIQUID AND GAS FLOWRATE MEASUREMENTS DOWNSTREAM OF T-Y JUNCTIONS

The response of the ultrasonic Doppler flowmeter signal as a function of mixture velocities for the homogenised flow after the static mixer and flow straightener was examined. In this experiment campaign, the Doppler was clamped on within the homogeneous section where the liquid flow-rate is fixed in certain velocities V_{sl} (1.0, 1.2, 1.4, 1.6, 1.8, and 2m/s) and the gas flow-rate is changed to obtain the required GVF.

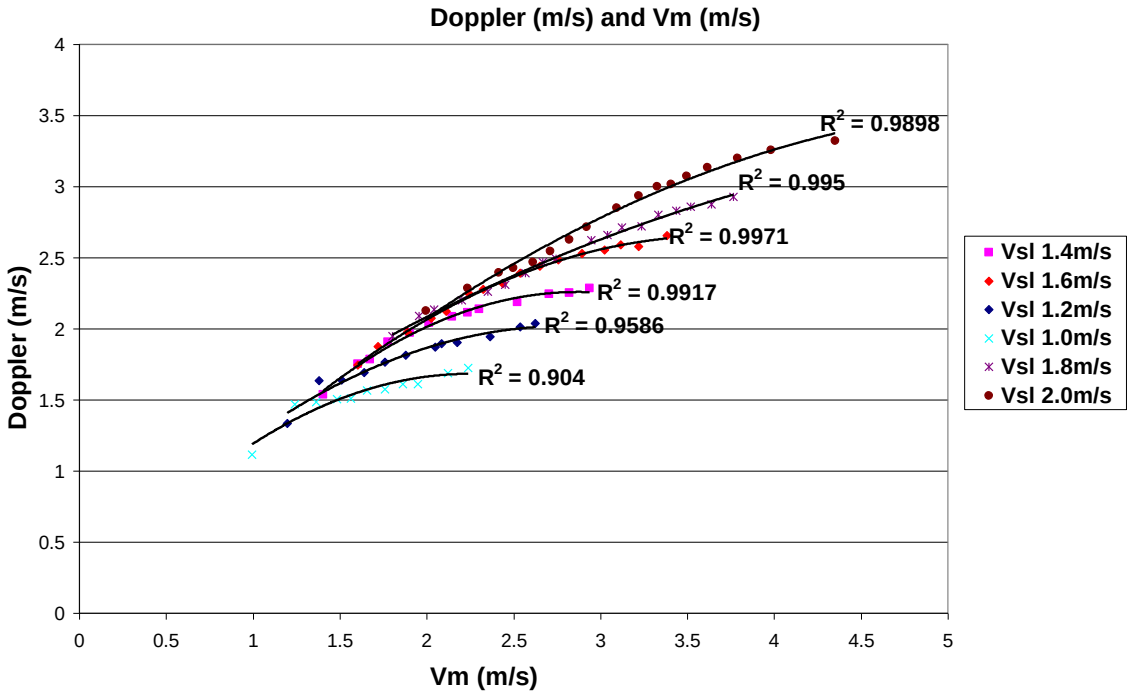

Figure 5-15, Doppler mixture flow-rate measurement

The recorded ultrasonic Doppler flowmeter signal has been plotted against the mixture velocity correlated by the reference measurement. Figure 5-15 shows the homogeneous velocity measurement using an ultrasonic Doppler and comparing the reference points from 0 to 0.6 GVF.

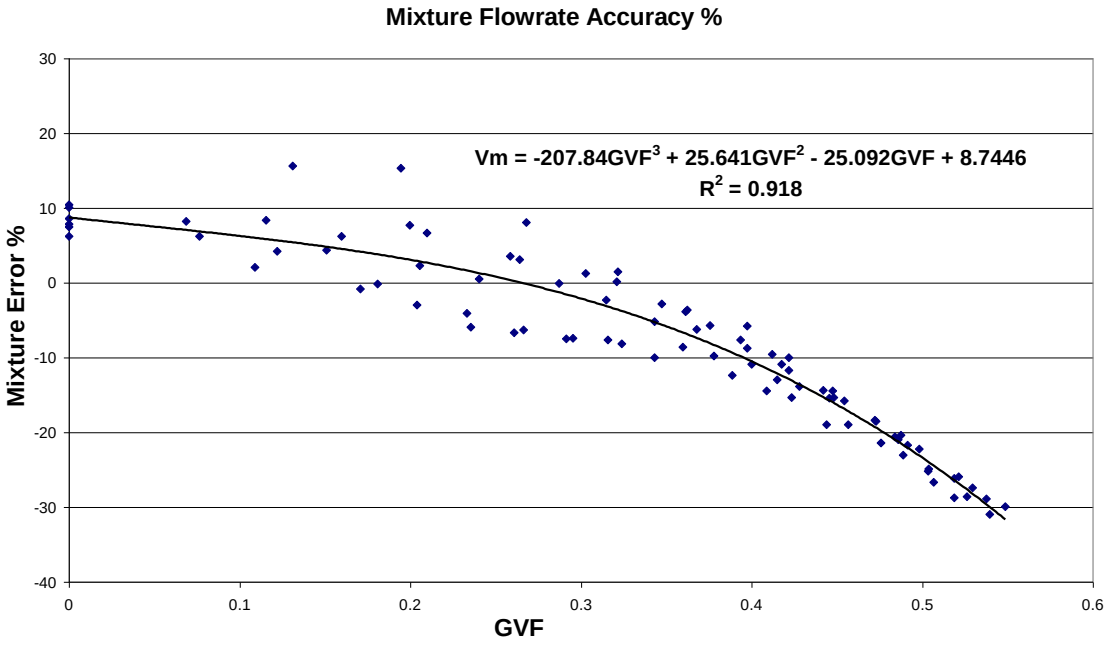

Figure 5-16, Mixture flow-rate measurement accuracy

Figure 5-16 illustrates the mixture of accuracy measurements using an ultrasonic Doppler as a homogeneous velocity measurement technique and GVF correlated from the reference.

As shown in Figure 5-16, Doppler shows over-reading at low GVF and then at high GVF the Doppler reading seems to be declining as bubble concentration increases and generates a cloud of thick layers of bubbles which deepen towards the bottom of the pipe. Additionally, at high GVF, the gas is dominant in the mixture and the homogeneous mixture starts to become separated and slip between gas and liquid has occurred.

As the superficial gas velocities are gradually increased, the Doppler performance shows a clear inclination in the homogenised flow measurement; this is as a result of the separation of gas and liquid in the pipe. This effect will be explained in more detail in the next few sections.

There were some visual observations made during the test measurement, which are also discussed in the following sections.

The ultrasonic Doppler correction is performed as a result of the GVF. The V_m is corrected in the GVF function to obtain a better accuracy of the ultrasonic Doppler.

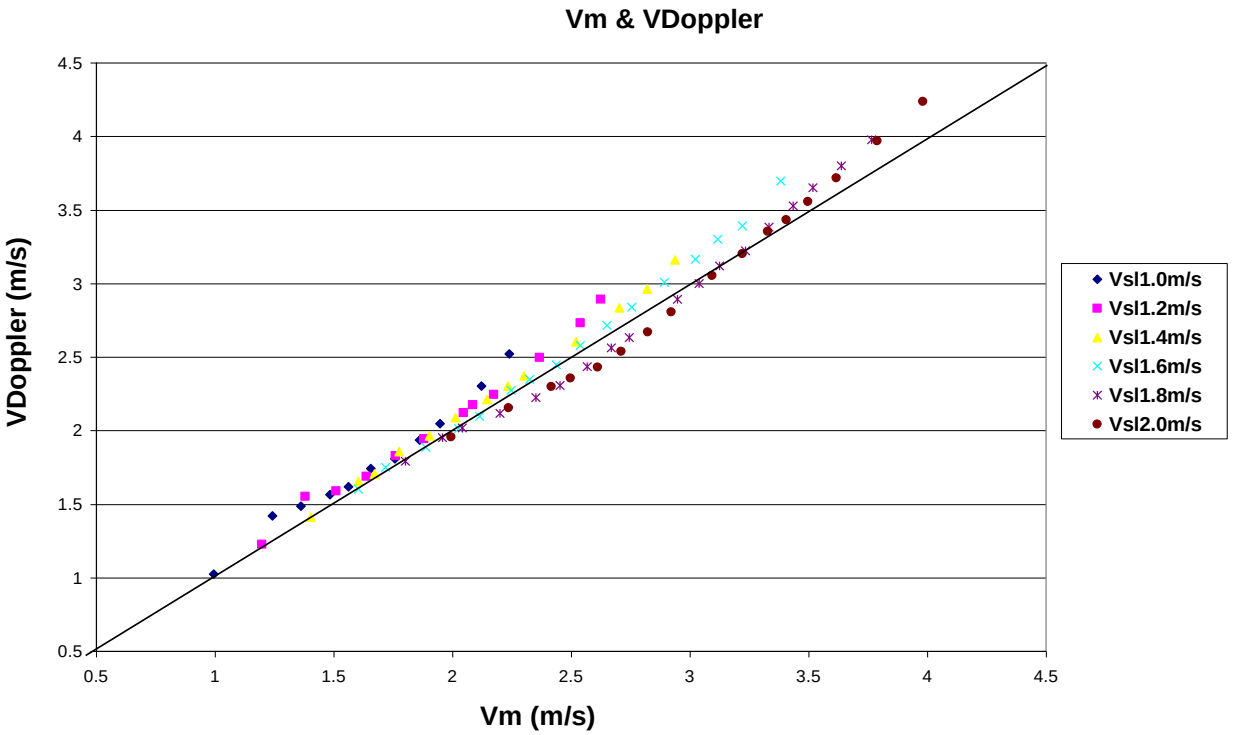

Figure 5-17, Corrected ultrasonic Doppler mixture flow-rate

Figure 5-17 shows good agreement between mixture measurement using corrected ultrasonic Doppler and the correlated mixture flow from the reference points. It is believed that by having the ultrasonic Doppler mixture measurement accurately, the whole gas and liquid flow-rate measurements are very likely to be accurate too.

5.5.1 Liquid Hold-up measurement in the homogeneous flow

Using the conductivity ring dynamically calibrated to measure the liquid hold-up in the homogeneous flow. Figure 5-18 shows the liquid hold-up measured by the conductivity ring at 1.2 m/s of fixed superficial liquid velocity with various superficial gas velocity ranges (0-0.6 of GVF). The conductivity ring reading in the homogeneous flow was corrected by the correction factor generated in the dynamic calibration and shown in Figure 5-18.

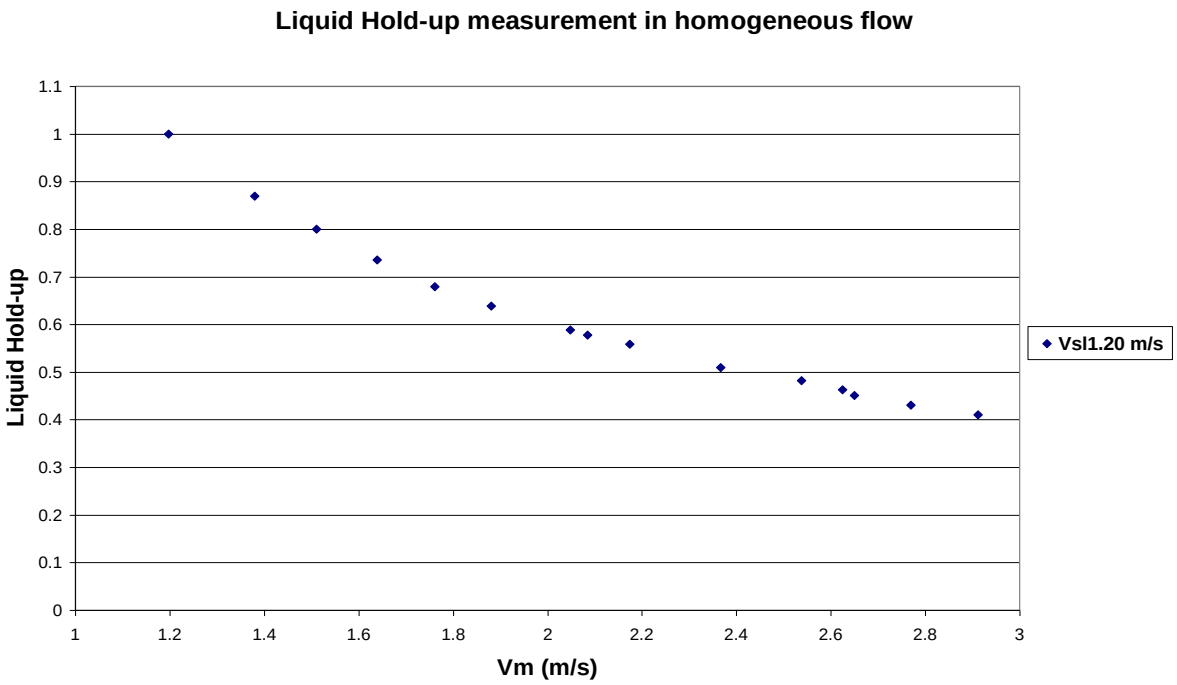

Figure 5-18, Liquid hold-up measurement in homogeneous flow

As illustrated earlier, the Doppler correction has been implemented as a function of GVF. Figure 5-19 shows the liquid accuracy results after the correction has been applied. The liquid error seems to be decreased as the gas flow increases, and a big error clearly exists at some gas flow-rates. As a result of the previous calculation for correcting the Doppler performance and the conductivity ring for fraction measurement, the liquid flow-rates accuracy is shown in Figure 5-19.

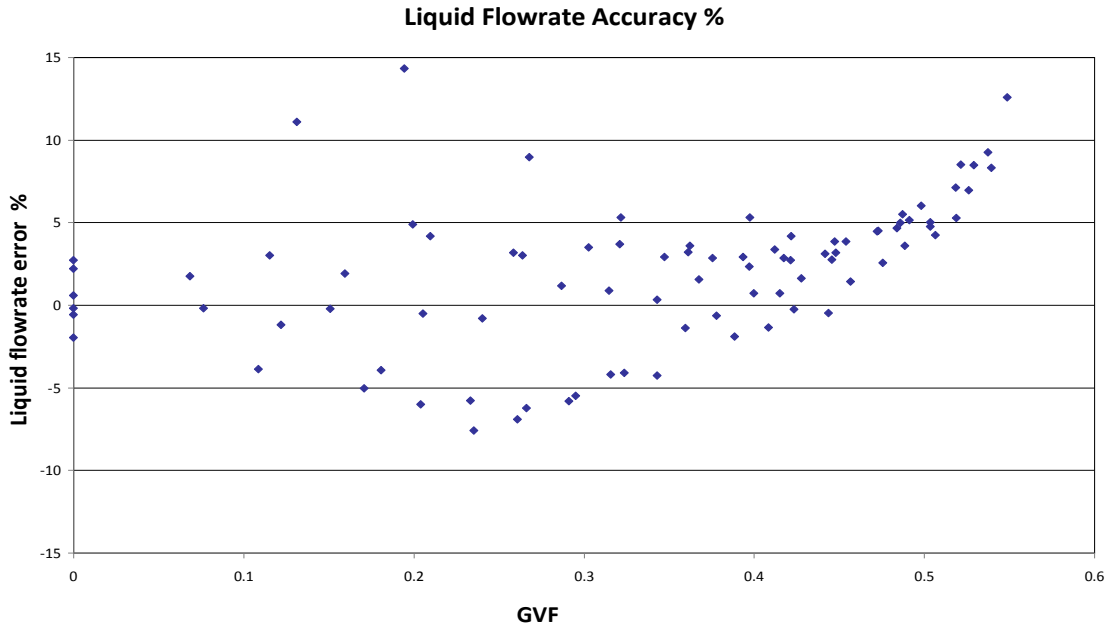

Figure 5-19, Liquid flow-rate accuracy after performing the correction

In Figure 5-19 the overall accuracy obtained is less than ±10 in the majority of measurement points; however, there are some big error points (above 10%) which are as a result of the separation (gas/liquid) which occurs in the pipe at a low liquid flow-rate.

Finally, the gas flow-rate can be easily calculated by extracting the liquid flow-rate measured as a result of the Doppler reading and gas fraction of the mixture flow-rate, as can be seen from Figure 5-20.

As the mixture flowrate is equal to the sum of liquid flowrate and gas flowrate, so the gas flowrate can be extracted using equation 5.5.

$$Q_g = Q_m - Q_l \qquad \textbf{(5. 5)}$$

$$\text{Where, } Q_m = V_{Doppler} A \qquad \textbf{(5. 6)}$$

The gas flow-rate calculated is then corrected to its working pressure and temperature into the measuring section.

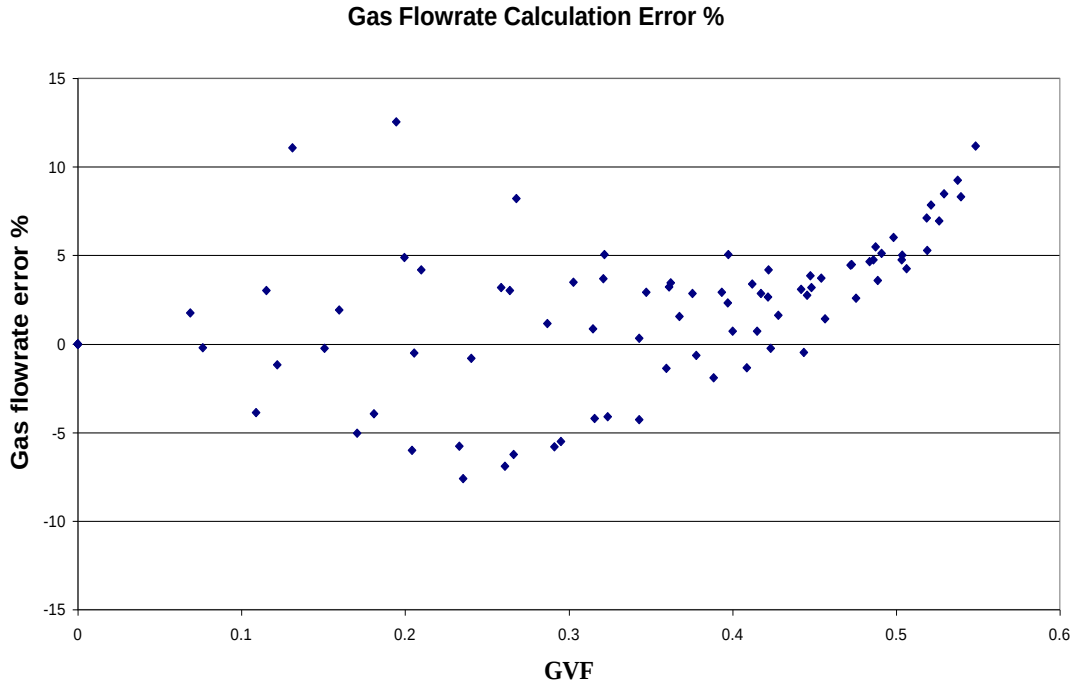

Figure 5-20, Gas flow-rate calculation

5.6 CHAPTER SUMMARY

Chapter 5 has documented the investigation of ultrasonic Doppler flowmeter in homogeneous flow. This investigation was done over a wide range of gas flow-rates, and at a constant liquid flow-rate, where these flow-rates were accurately controlled and recorded. The behaviour of the ultrasonic Doppler flowmeter was determined by its measured flow-rate, relative to that measured by the reference points (electromagnetic and turbine flowmeters). However, the performance of the clamp-on ultrasonic Doppler flowmeter in a homogeneous two-phase flow was tested in different test rig locations (downstream of the references points and downstream of T-Y junctions) and different operational environments to investigate the behaviour and its limitation.

In order to measure the liquid and gas flowrate in homogeneous flow, the conductivity ring was calibrated against the references GVF via electromagnetic flowmeter for a liquid flow-rate measurement and a turbine gas flowmeter for gas flow-rate measurement. Liquid and gas flowrate in homogeneous flow were obtained as a result of ultrasonic Doppler measuring the flow velocity and conductivity for fraction measurement.

Chapter 6

RAW SLUG FLOW MEASURMENT

6.1 CHAPTER INTRODUCTION

In this chapter the ultrasonic Doppler transducer was investigated in two-phase raw slug flow in a horizontal pipe to measure slug and film velocities. It focuses on the experimental set-up used in the slug flow measurement, including ultrasonic Doppler transducer installations at different pipe locations. The ultrasonic Doppler data analysis using different software is illustrated. The slug and film velocities in the raw slug flow are explained. Liquid and gas flowrate is obtained using Doppler for slug velocity and a conductivity ring for fraction measurement.

In the slug flow measurement, the signal used is based on a frequency shift signal. This signal is extracted from the Doppler transducer before the flowmeter own physical signal processing. The data analysis of the slug measurement was processed off-line for different liquid and gas flow-rates with a wide range of GVF ranges, from 0% to 90%.

6.2 SECTION EXPERIMENTAL SET-UP

The experiment rig for the slug flow in a horizontal 50mm diameter pipe measurement contains some in-house measurement techniques and components which are as follows:

- Ultrasonic Doppler flowmeter with extracted frequency shift signal
- Conductivity ring
- PICOscope 2 channels box

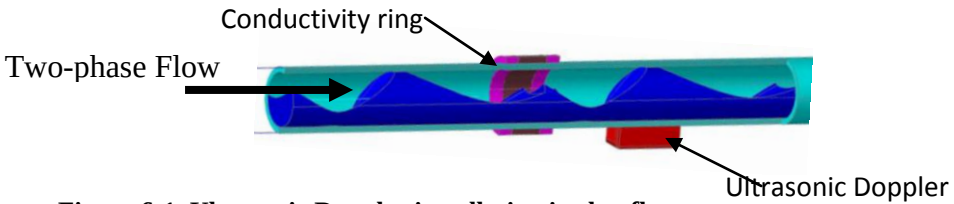

Figure 6-1, Ultrasonic Doppler installation in slug flow

Figure 6-1 illustrates ultrasonic Doppler transducer and a conductivity ring installation in raw slug flow in horizontal pipe.

The PICOscope used in this section captures the ultrasonic Doppler transducer frequency shift signal and the working conductivity ring reading and saves the signals in a TEXT file in order to be analysed using different software. The two channels of PICOscope have a sampling rate of up to 10MHz with sensitivity from 5V to 10mV.

The PICOscope has a software application enabling the use of a PC to display and record voltage waveforms. It has been used when the ultrasonic Doppler raw signal is recorded in order for further signal processing to be undertaken. The software provides four types of display: oscilloscope, spectrum analyser, meter and XY oscilloscope; however, in this work it is used as oscilloscope and spectrum analyser windows, as shown in Figure 6-2 and Figure 6-3.

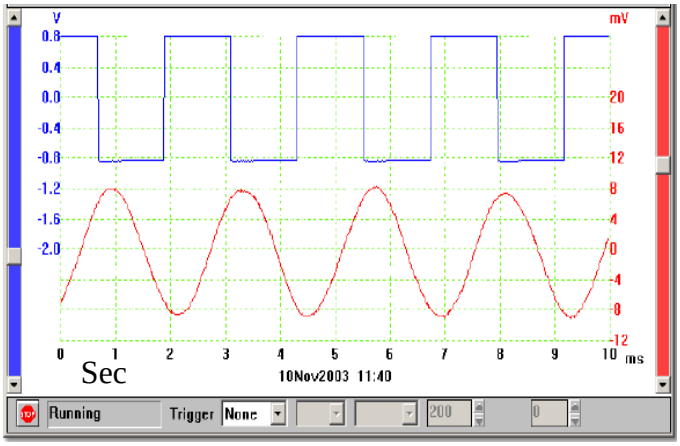

Figure 6-2, Oscilloscope window, taken from PICOscope operation manual

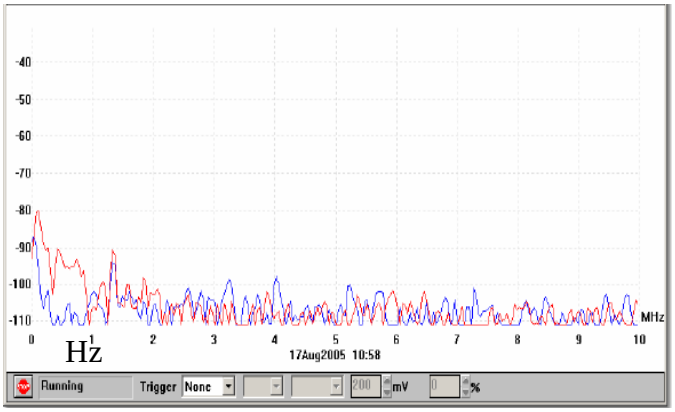

Figure 6-3, Spectrum analyser window, taken from PICOscope operation manual

The ultrasonic Doppler transducer was clamped on next to a conductivity ring, in two locations around the pipe (3 and 6 o'clock), initially it was installed at the 3 o'clock position in order to identify the slug flow regime flowing in the 50mm horizontal pipe, as can be seen in Figure 6-4. Figure 6-5 illustrates the Doppler slug flow identification, and because the transducer position, it is limited use for detecting the film movement. When the film level is lower than the middle of the pipe, it considers this as zero and above the middle it considers it as a slug flow. This position can miss significant information about the film liquid when its level is less than the middle of the pipe cross section.

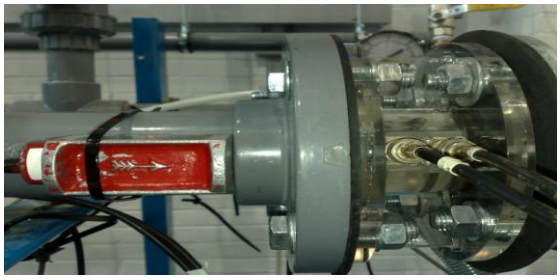

Figure 6-4, Ultrasonic Doppler clamped on at 3 o'clock position

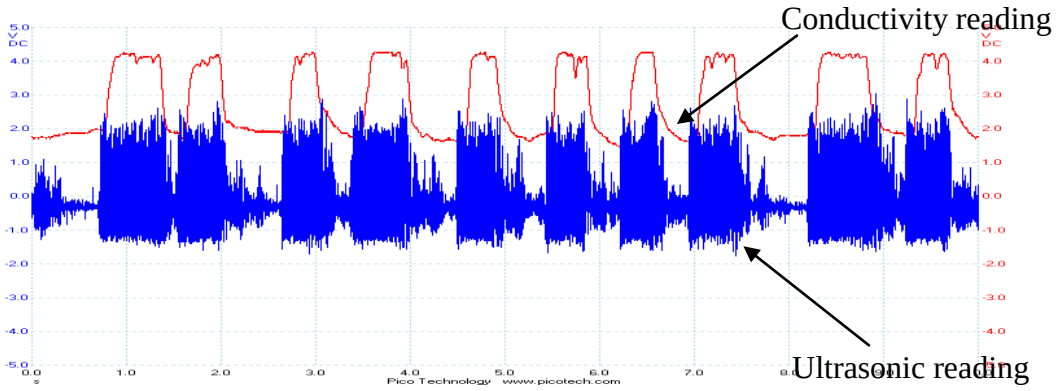

Figure 6-5, Ultrasonic Doppler at 3 o'clock position

The transducer was then moved to be clamped on at the 6 o'clock position (at the bottom) of the pipe where liquid is always present. However, the challenge at this position is how slug liquid and film liquid velocities can be identified by the transducer. Figure 6-6 illustrates the ultrasonic Doppler transducer clamped on at the bottom of the pipe.

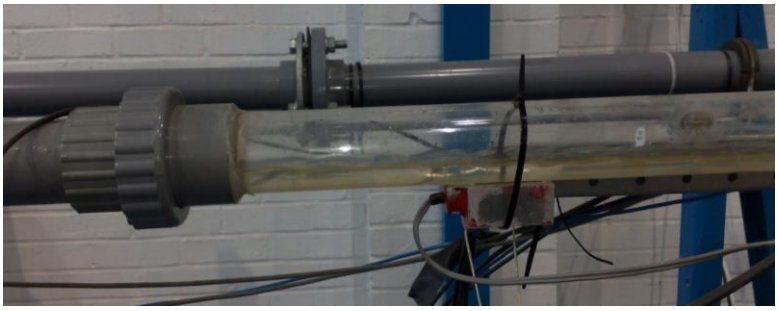

Figure 6-6, Ultrasonic Doppler clamped on at 6 o'clock position

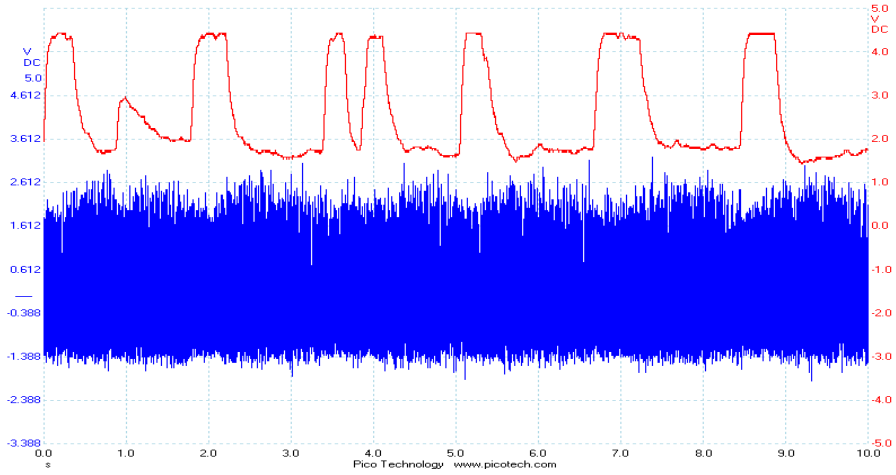

Figure 6-7, Ultrasonic Doppler at 6 o'clock position

Using PICOscope two channels box instantly captured and recorded signals from the conductivity ring and ultrasonic Doppler frequency raw signal at a fixed sampling rate (750 kHz) as shown in Figure 6-7. This data was then analysed using different commercial software such as SigView and Autosignal.

6.3 ULTRASONIC DOPPLER TRANSDUCER (FREQUENCY SHIFT) SIGNAL ANALYSIS

This section shows the ability of the using the raw signal of the ultrasonic Doppler flowmeter which is clamped on at the bottom of a horizontal pipe. The Doppler meter is combined with a conductivity ring to measure liquid and gas flow-rate within a raw slug flow where the slug flow requires no pre-conditioning.

The reason that the ultrasonic Doppler transducer is clamped on at the bottom of the pipe (6 o'clock position) is because liquid always exists at the bottom of the pipe regardless of the slug or film flow.

The ultrasonic Doppler flowmeter frequency shift signal (raw signal) was identified in slug flow and the signal was recorded via a PICOscope.

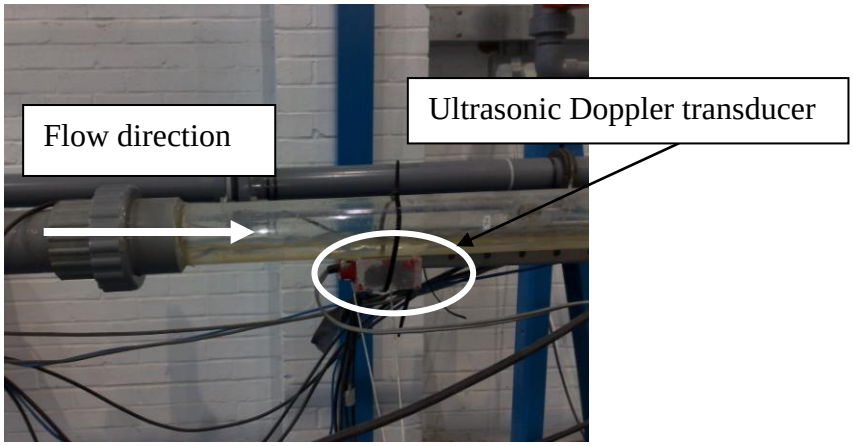

Figure 6-8, Ultrasonic Doppler transducer clamped on at 6 o'clock

Through the local liquid tank and in-house compressor, a two-phase flow is introduced to the test rig and the slug flow is maintained by seeing the flow through a clear two inch pipe, as illustrated in Figure 6-8.

6.3.1 Signal gathering and method of analysis

The Sigview software is used carry out Fast Fourier Transform (FFT) of the slug and film frequency shift. The Autosignal software is used carry out wavelet analysis of the Doppler signal to identify the frequency shifts change from slug to film according to the time. Therefore, the ultrasonic Doppler frequency signals are analysed where observably the relatively low frequency (low signal intensity) shift is representing the film velocity and the high frequency (high signal intensity) shift represents the slug velocity using the following equations:

$$V_s = \frac{f_{ds} C_w}{2 f_t \cos\alpha} \text{ and } V_f = \frac{f_{df} C_w}{2 f_t \cos\alpha} \quad \textbf{(6.1)}$$

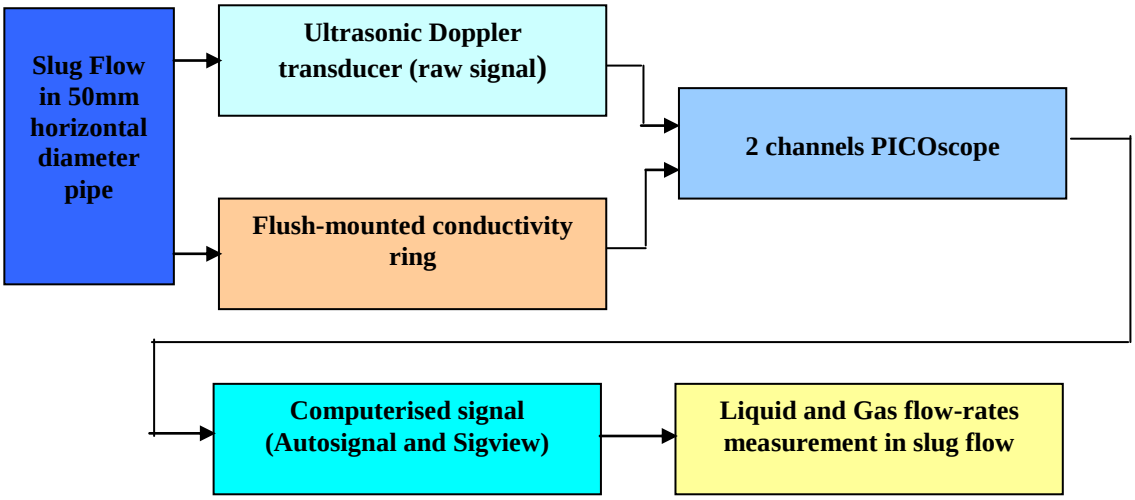

Figure 6-9, Ultrasonic Doppler on raw slug box scheme

The second part in measuring slug flow is to measure the slug/film liquid fraction using a flush-mounted conductivity ring and then finally the liquid/gas flow-rates. So the flow-rate of liquid and gas can be identified using the following equations:

$$Q_l = \frac{(t_s \alpha_s V_s + t_f \alpha_f V_f) A}{(t_f + t_s)} \tag{6.2}$$

$$Q_g = V_C (1 - \alpha_f) A \text{ and } Q_g = Q_m - Q_l \tag{6.3}$$

Where Q_m is as a result of $V_s . A$, V_C is translational velocity correlated.

Figure 6-10 and illustrate the slug parameters that have been used to calculate liquid and gas flow-rate within the slug flow.

Liquid hold-up within the slug body and film region were measured using conductivity ring. These measurements are based on taking the average over each recording time period. However, as the GVF increases the slug length decreases and the film region increases. And as the PICOscope recording time is fixed, the number of the recorded slug is reduced in this time and the liquid flowrate in the slug body may not be represented accurately.

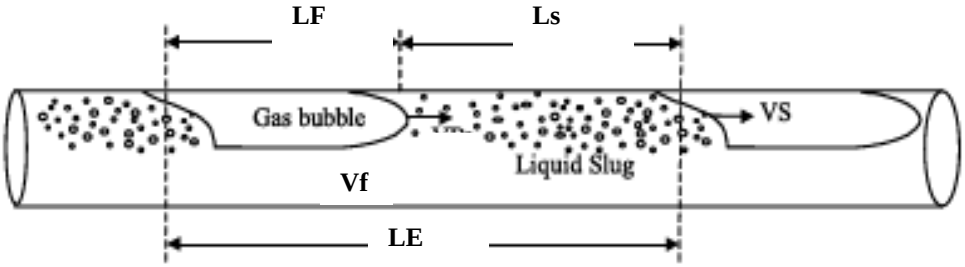

Figure 6-10, Simplified slug flow model construction

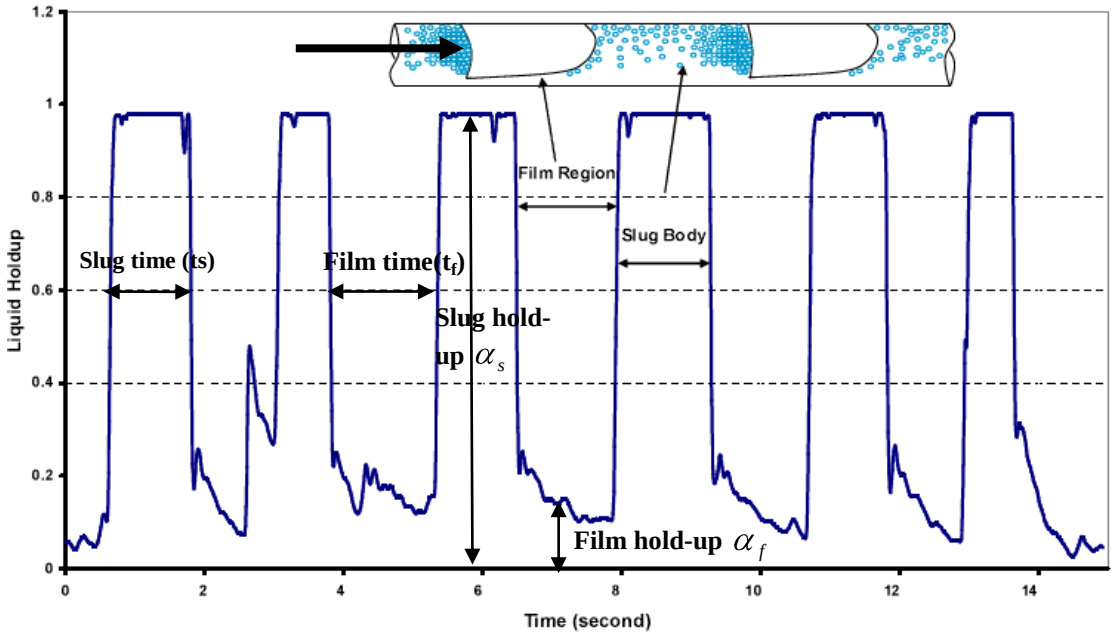

Figure 6-11, Slug flow signal captured by a conductivity ring

6.4 DATA ACQUISITION SYSTEM

The transducer was moved and clamped on at the 6 o'clock position (at the bottom) of the pipe where liquid is always present whether liquid in film or in slug; however, the challenge at this position is how slug liquid and film liquid velocities can be identified by the transducer. Figure 6-12 illustrates typical signal from the ultrasonic Doppler transducer clamped on at the bottom of the pipe.

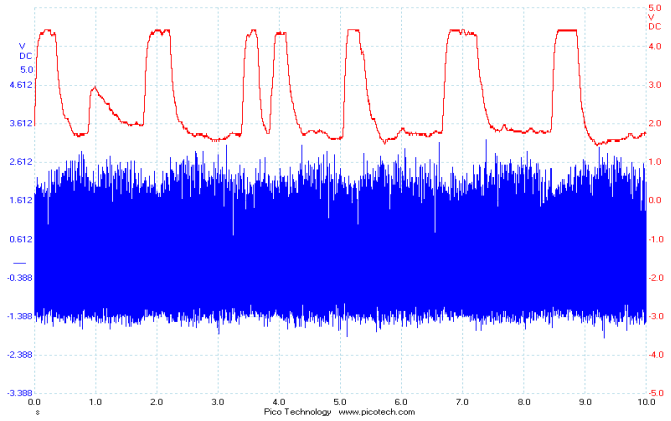

Figure 6-12, Ultrasonic Doppler signal

A PICOscope two channels box was used to instantly record signals from the conductivity ring and ultrasonic Doppler at a fixed sampling rate. This data was then analysed using different commercial software such as Sigview and Autosignal.

By focusing on a shorter recording time of Doppler, a clear change in signal intensity can be visually identified in Figure 6-13.

6.4.1 Signal analysis using Sigview and Autosignal

As illustrated in Figure 6-13, have two clear intensities in recorded signals from Doppler which can represent frequency shifts from slug body and film which is referred to as slug velocity and film velocity in the pipe. Sigview was used to identify the frequency shift from high and low intensity signals.

6.4.1.1 Analysing high and low intensity signal (slug body and film)

The slug body and film are illustrated in Figure 6-13, this shows their frequency shifts can be extracted using Sigview and Autosignal software.

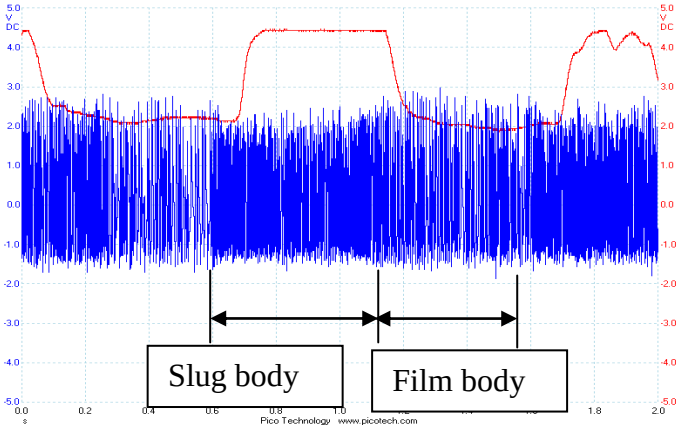

Figure 6-13, High and low intensity of slug flow

The slug body has a clear frequency shift which represents its velocity.

The Autosignal wavelet spectrum shows the frequency change when slug liquid and film liquid pass, see Figure 6-14.

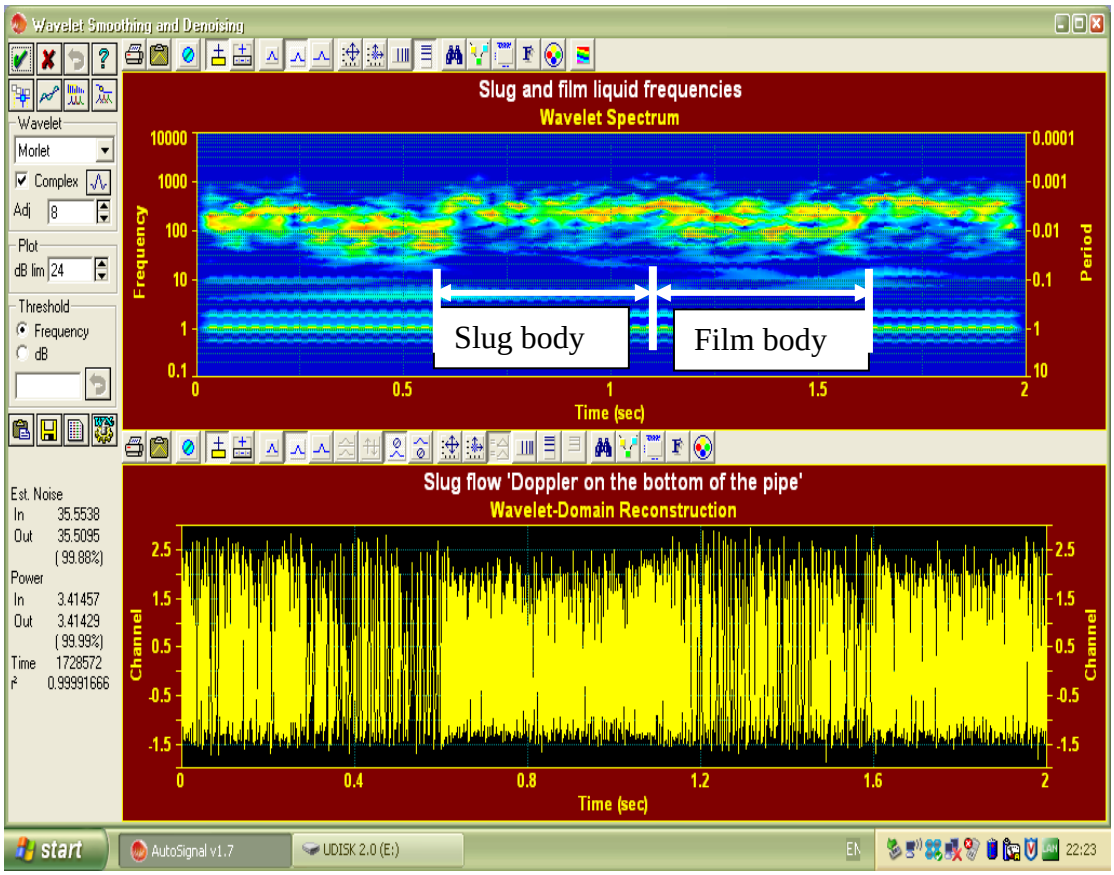

Figure 6-14, Slug liquid and film liquid frequency

To be able to represent an ultrasonic Doppler raw signal in the time and frequency domain at the same time, a wavelet spectrum function in Autosignal software has been deployed. In order to identify slug body and film region in slug flow, an ultrasonic Doppler signal can be analysed using a wavelet spectrum. A high frequency region represents slug body and lower frequency region represents film body. Figure 6-15 illustrates the wavelet spectrum as a slug and film body frequencies identifier. Additionally, Sigview software was used to average the slug body and film body frequencies throughout a long time span.

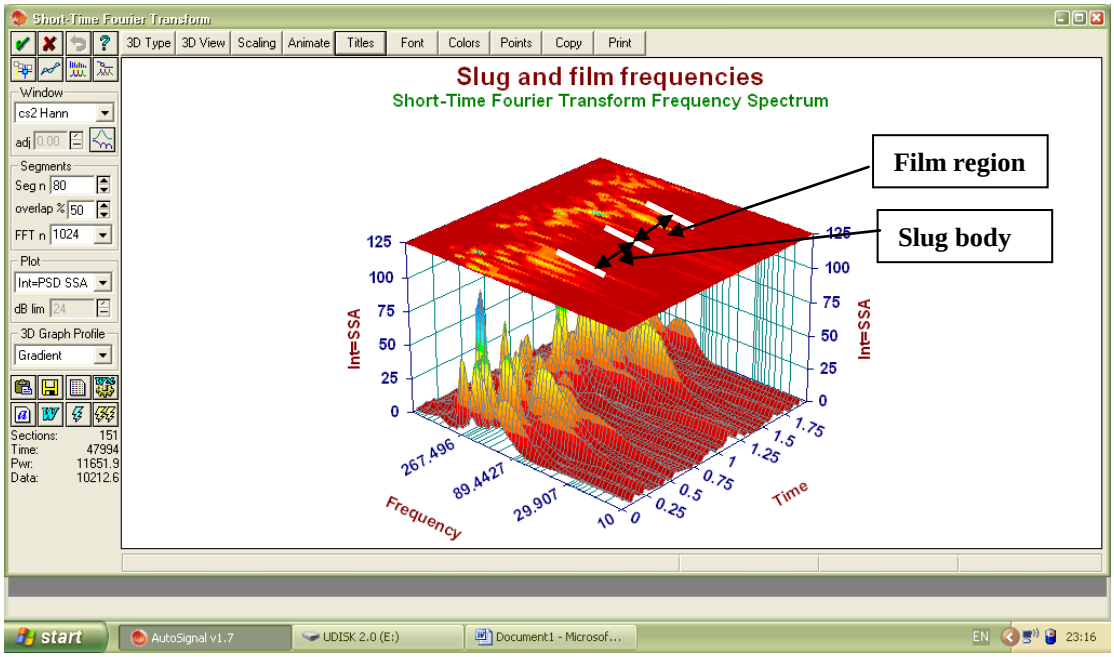

Figure 6-15, Short-Time Fourier Transform frequency spectrum

There are two frequencies generated as a result of deploying ultrasonic Doppler in the slug flow regime, low frequency represents the film velocity and high frequency represents slug body velocity. Where one frequency exists over a period of time and the second frequency exists over another time, the best information can be given by using Short-Time Fourier Transform with the contour on the top, as shown in Figure 6-15, which illustrates the slug and film flow represented by the change in frequency value.

6.4.2 Slug and film liquid velocity measurements

A set of experiments have been performed to investigate the behaviour and the performance of a clamp-on ultrasonic Doppler flowmeter under two-phase air/water slug flow in a horizontal pipeline, and to measure the instantaneous velocity of slug liquid and film liquid ultrasonically.

Firstly, the high intensity (slug body) signal is analysed using Sigview to extract its frequency shift at the peak which directly represents its velocity, as can be seen from Figure 6-16.

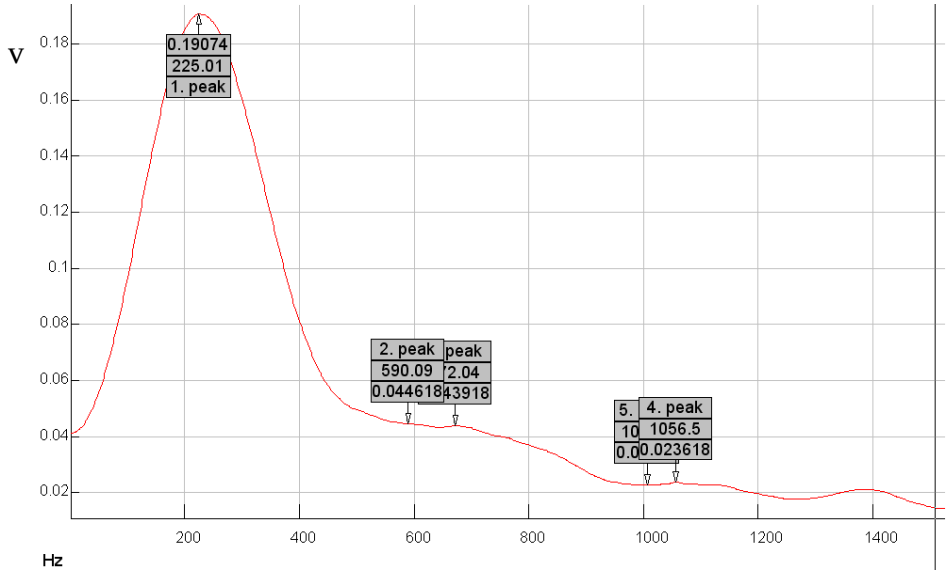

Figure 6-16, Slug body frequency peak shift

Secondly, the low intensity (film body) signal is extracted and by using the same procedure for the high intensity signal, the frequency shift can be determined. Figure 6-17 illustrates the frequency shift of the film liquid.

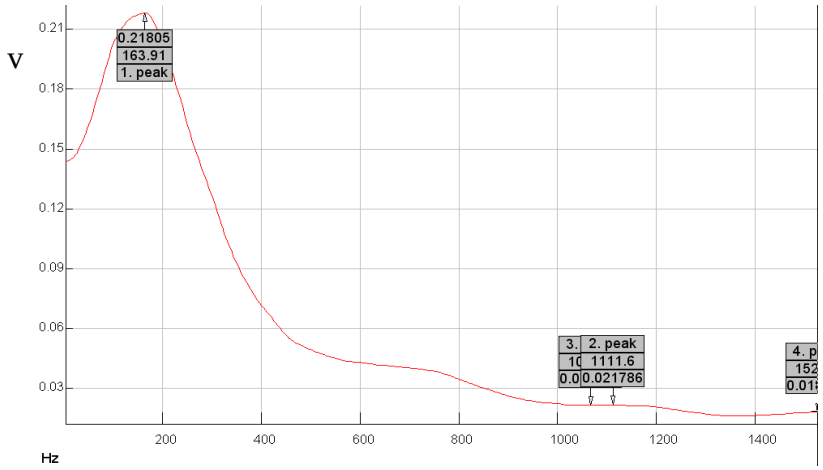

Figure 6-17, Film body frequency peak shift

It can be seen that the height of the frequency peak in the Figure 6-17 figure which represents the ultrasonic Doppler frequency shift which refers to the film region flow velocity. Velocity measurements can be determined from the Doppler equation which is as follows:

$$V_s = \frac{f_{ds} C_w}{2 f_t \cos\alpha} \quad \textbf{or} \quad V_f = \frac{f_{df} C_w}{2 f_t \cos\alpha} \qquad \textbf{(6. 4)}$$

where, V_s, V_f , represent average slug liquid and film liquid velocities respectively, and f_{ds}, f_{df} represents slug liquid and film liquid frequencies , respectively.

C_w is the acoustic velocity in wedge.

f_t and $\cos\alpha$ are the transmitted Doppler frequency and its angle respectively.

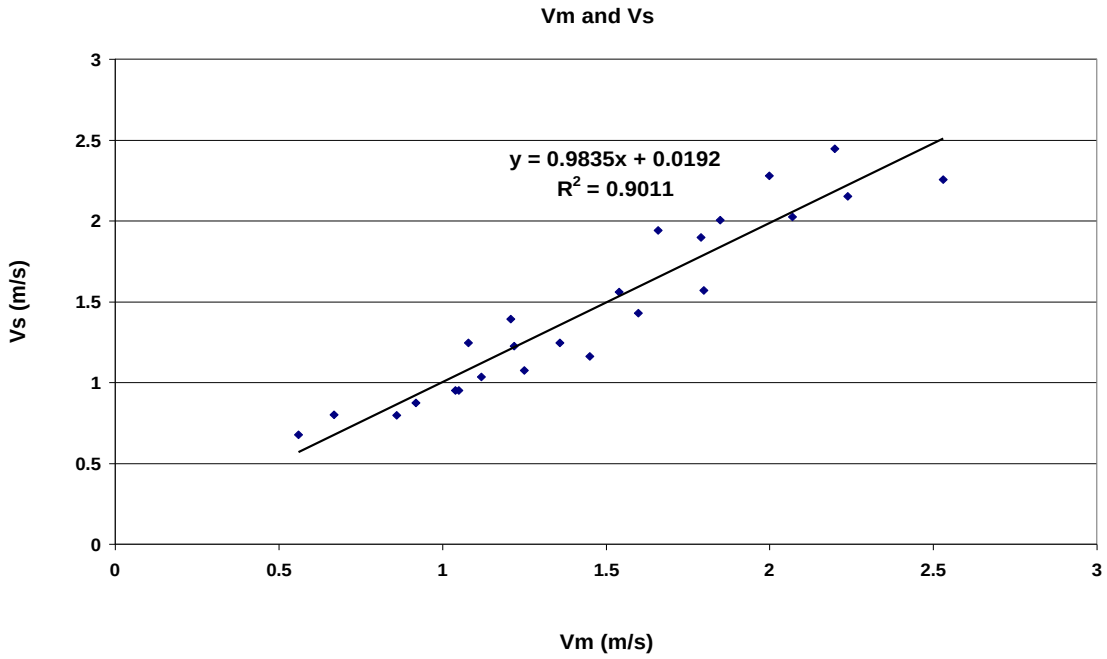

Figure 6-18, Slug velocity (Doppler) and mixture velocity (reference)

Currently, the frequency shift and velocities are determined manually by identifying the film and slug body regions from the time series. The signals from each region are then analysed to give the film and slug velocity. The averaged values are then calculated. The linear relationship between the Doppler slug velocity and mixture velocity at the reference can be seen from Figure 6-18.

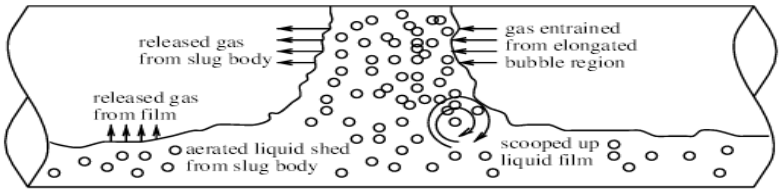

Figure 6-19, Slug flow unit, adapted from Bonizzi and Issa 2003

Nydal and Banerjee (1996), shows aeration in the slug body which increases with slug velocity, and can only be neglected if the slug velocity is significantly low. Fernandes et al., (1983) stated that this is as a result of the direct effect of the strong turbulent action induced by the large vortex movement set up by the entrance of the

liquid film at the slug head. This can have a significant impact on ultrasonic Doppler slug velocity measurement behaviour, since Doppler shift depends on the scatterers within the slug and film body and because there is a vortex movement for these scatterers, so the Doppler reading can be lower compared to the correlated slug velocity which assumes there is no bubble elongated within the slug and film body as shown in Figure 6-19.

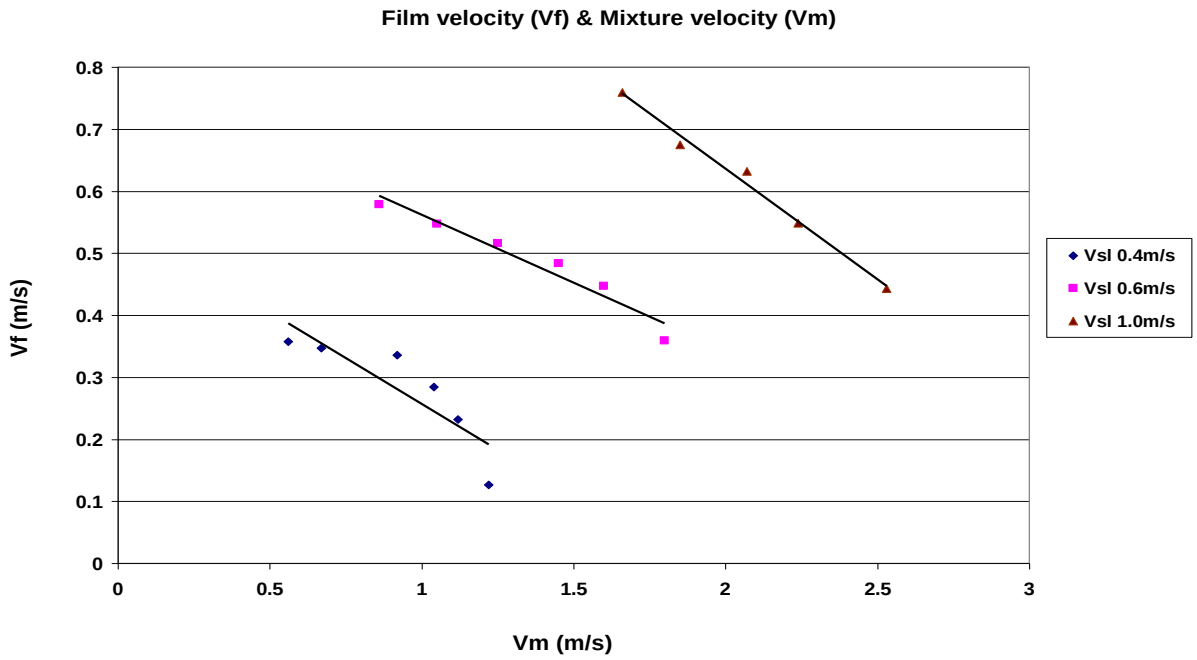

Figure 6-20, Film liquid velocity (Doppler) and mixture velocity

Relatively low frequency shifts, which represent film velocity, have been recorded. The averaged film velocities are plotted against mixture velocity. Figure 6-20 illustrates the relationship between increasing the gas flow-rate and decreasing the film velocity.

Noticeably, as the GVF increases, the liquid hold-up within the film region decreases and the velocity decreases as well, The opposite occurs when the gas flow-rate within slug flow decreases, i.e. the liquid hold-up within the film region decreases and its velocity increases until the film hold-up and slug hold-up are equalised to flow at the same velocity. Figure 6-21 illustrates the decrease in the liquid holdup in the film region as the GVF in the mixture increases. The experiment condition is at 0.6 m/s of superficial liquid velocity and a wide range of superficial gas velocity (0.2 to 1.2 m/s). Appendix C illustrates this change in more details.

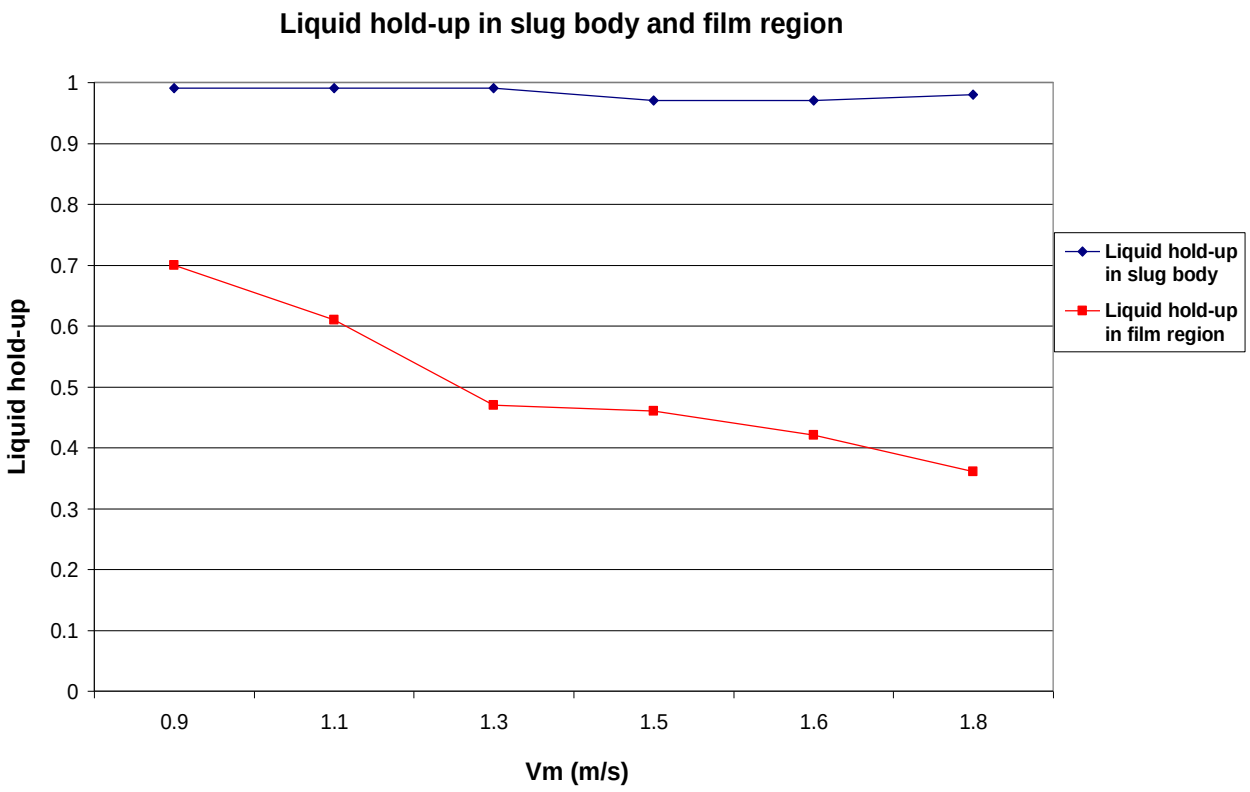

Figure 6-21, Liquid hold-up in slug body and film region

Vermeulen and Ryan (1976) reported that the liquid film velocity is small. In the Duckler and Hubbard (1976) model, they mentioned that the liquid film thickness varies along the film, starting with liquid hold-up in the film being equal to the liquid hold-up in the slug body and the film velocity decreases while the gas velocity increases.

6.5 LIQUID AND GAS FLOWRATE MEASUREMENT WITHIN SLUG FLOW

In this work, experiments were conducted on the two-phase liquid/air facility at atmospheric pressure. An ultrasonic Doppler transducer was installed on the bottom of the horizontal pipe beside a flush-mounted conductivity ring and self-calibrated pressure transducer and temperature probe. The experiments were based on the slug flow measurement by using a clamp-on ultrasonic Doppler system to measure slug body velocity and film region velocity. The conductivity ring was used to measure the liquid hold-up in the slug body and film region, slug body passage time and film region passage time.

Table 6- 1Table 6- 1 shows the slug flow measurement parameters and the methods of obtaining each parameter.

Fluid condition	**Measurement techniques**	**Results obtained methods**
Mixture flow Q_m	Ultrasonic Doppler	$Q_m = V_s A$
Slug flow Q_l	Ultrasonic Doppler and Conductivity ring	$Q_l = \frac{(t_s \alpha_s * V_s + t_f \alpha_f V_f) A}{(t_f + t_s)}$
Slug flow Q_g	Ultrasonic Doppler and Conductivity ring.	$Q_g = \frac{V_C * (1-\alpha_f) A t_f}{(t_f + t_s)}$ or $Q_g = Q_m - Q_l$
Slug time t_s	Conductivity ring	Time when the slug occurs
Film time t_f	Conductivity ring	Time when the film occurs
Liquid hold-up in the slug α_s	Conductivity ring	Liquid hold-up in slug body
Liquid hold-up in film α_f	Conductivity ring	Liquid hold-up in film region

Table 6- 1, Two-phase slug flow measurement methods

Since the velocities of the slug and the film are determined, the liquid and gas flow-rate measurement can be obtained in combination with a conductivity ring which is installed to measure the fraction within the average slug body and film zone

α_s and α_f, respectively. The flow-rate of liquid and gas with the slug and film can be calculated using adopted equations.

A series of experimental campaigns were performed. The experimental campaigns cover a wide range of GVF from 0.1-0.65% with superficial gas and liquid velocities as shown in Table 6-2.

The experimental campaigns strategy was based on the fixing of the value of the superficial liquid velocity and increasing the gas superficial velocity gradually. All the campaigns were conducted at atmospheric pressure. These experimental points are plotted on the flow regime map in Figure 6-22.

Experimental Campaigns	Vsl (m/s)	Vsg (m/s)	GVF
Campaign 1	0.4	0.16, 0.27, 0.52, 0.64, 0.72, 0.82	0.28, 0.40, 0.56, 0.61, 0.64, 0.67
Campaign 2	0.6	0.26, 0.45, 0.65, 0.85, 1, 1.2	0.30, 0.42, 0.52, 0.58, 0.62, 0.66
Campaign 3	0.8	0.28, 0.41, 0.99, 1.2, 1.4	0.259, 0.33, 0.55, 0.60, 0.63
Campaign 4	1.0	0.36, 0.54, 0.66, 1.07, 1.24, 1.53	0.26, 0.35, 0.39, 0.46, 0.51, 0.55, 0.60

Table 6-2, Two-phase slug flow measurements campaigns

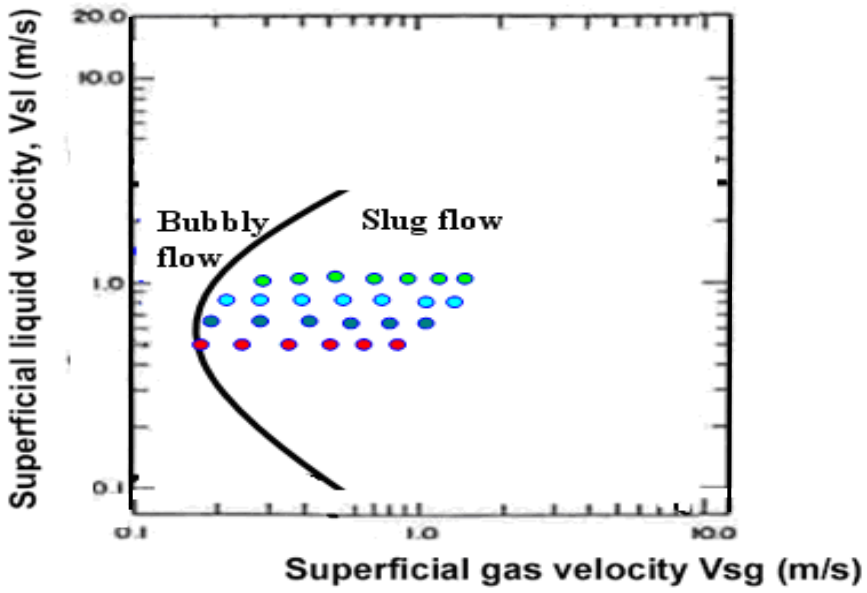

Figure 6-22, Two-phase liquid/gas experimental campaigns' flow map regimes

6.5.1 Slug velocity and transitional velocity correlations

To increase the gas flow-rate accuracy measurement, it is important to implement a V_T correction factor based on the slug flow V_s measurement by the ultrasonic Doppler and V_T obtained by $V_m C$ Based on Froude number Fr<2 and 2<Fr<4, V_T was correlated and plotted against V_s measured by the ultrasonic Doppler.

Based on the literature, Al-lababidi (2006) reported the translational velocity can be obtained as the following:

$$V_T = V_m 1.141+0.2017 \qquad \text{Fr}<2 \qquad \textbf{(6. 5)}$$

$$V_T = V_m 1.1891+0.0285 \qquad 2<\text{Fr}<4 \qquad \textbf{(6. 6)}$$

Figure 6-23 and Figure 6-24 illustrate the two correlations between V_T (equation 6.5 and 6.6) and V_s measured by the Doppler as slug body velocity. These correlations are used later to measure the volumetric gas flowrate Q_g .

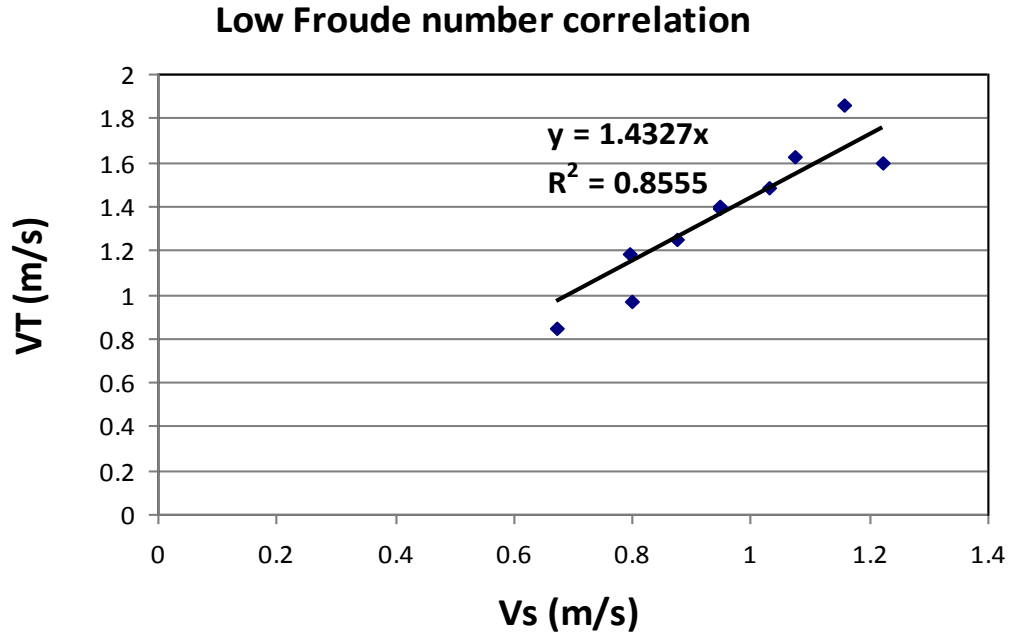

Figure 6-23, Low Froude number correlation

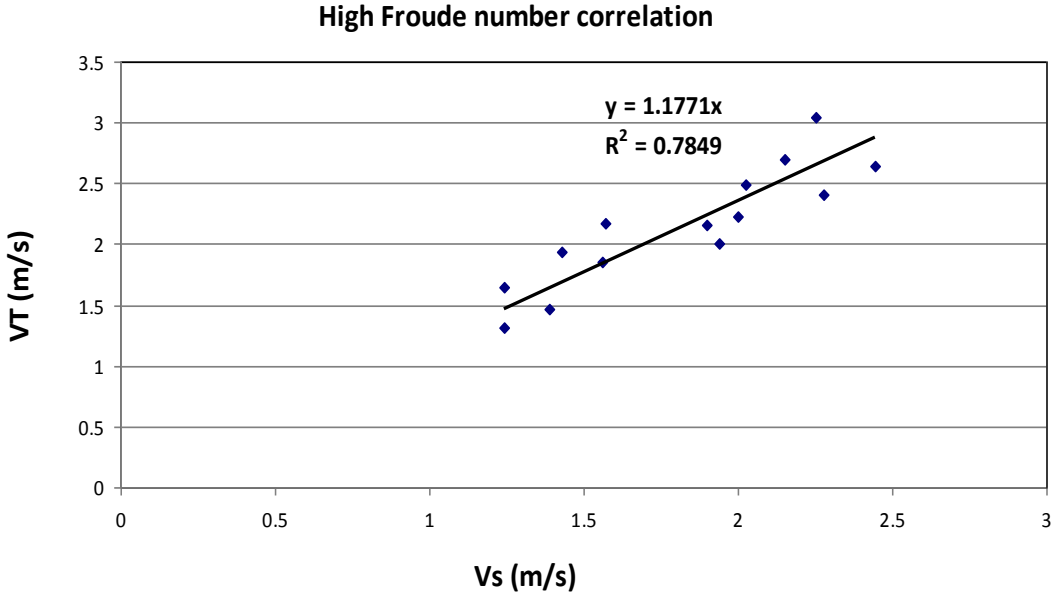

Figure 6-24, High Froude number correlation

6.5.2 Liquid flow-rate measurement

Based on slug body and film region frequency shifts, slug velocity and film velocity can be calculated using the following equations:

$$V_s = \frac{f_{ds} C_w}{2 f_t \cos\alpha} \quad \textbf{or} \quad V_f = \frac{f_{df} C_w}{2 f_t \cos\alpha} \qquad \textbf{(6. 7)}$$

where C_w is acoustic velocity in the wedge, f_t, f_{ds}, f_{df} are Doppler transmitted frequency, slug frequency shift and film frequency shift, respectively, $\cos\alpha$ is Doppler angle in the transducer case 45°.

t_s is passage time slug body, identified using a conductivity ring, the data is analysed using Microsoft Excel and extracted from the slug start peak to end peak. t_f is passage time film region, identified using a conductivity ring, the data is analysed using Microsoft Excel.

α_s is the average liquid hold-up in the slug body which is measured using a static calibrated conductivity ring. The data is analysed using Microsoft Excel.

α_f is the average liquid hold-up within the film region, measured using a static calibrated conductivity ring. The data is analysed using Microsoft Excel.

Liquid flow-rate measurement in the two-phase slug flow can be obtained using the scheme illustrated in Figure 6-25.

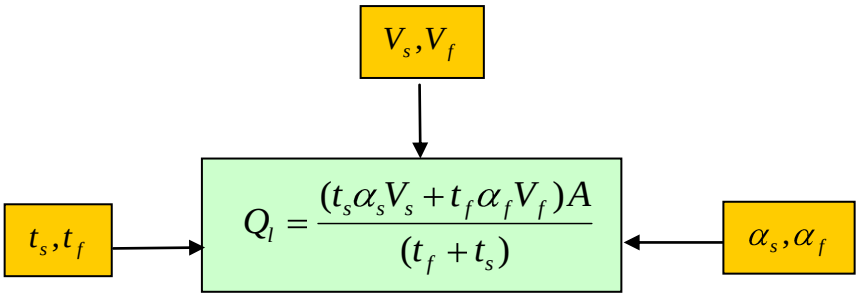

Figure 6-25, Liquid flow-rate measurement scheme

The film and slug time was obtained from the average of multiple of slug and film time.

$$Q_l = \frac{(t_s \alpha_s V_s + t_f \alpha_f V_f) A}{(t_f + t_s)} \quad \textbf{(6. 8)}$$

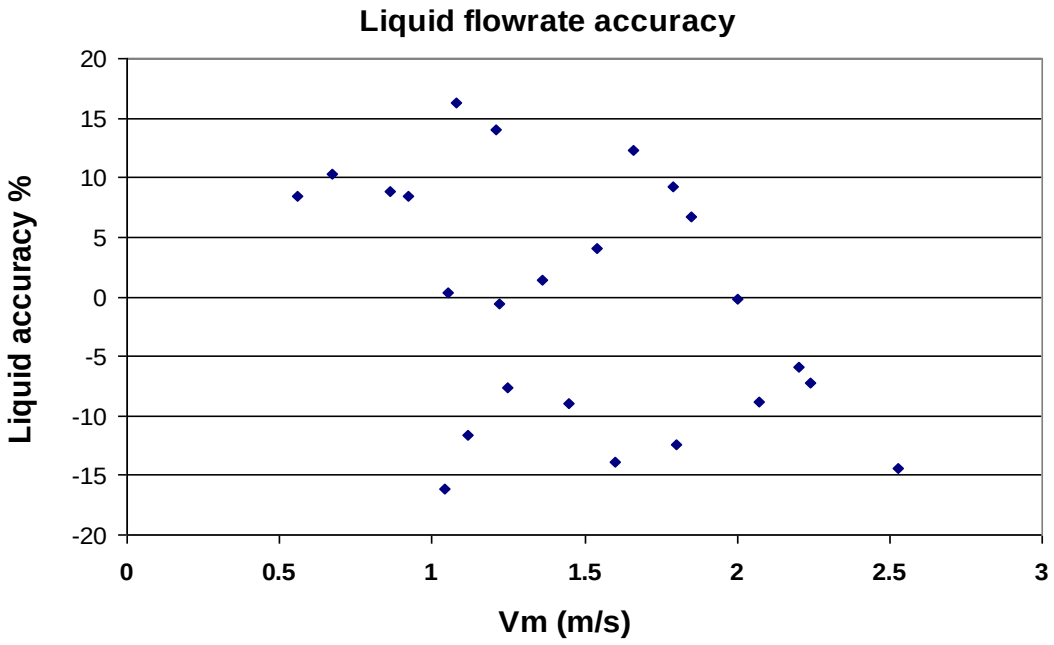

Figure 6-26, Volumetric liquid flow-rate (Doppler) accuracy

Figure 6-26 illustrates liquid ultrasonic Doppler flow-rate performance in different superficial liquid velocities.

Doppler shows a good agreement with the reference when it is implemented to measure liquid flow-rate in two-phase slug flow.

Due to the unstable behaviour of the slug flow, the velocity measurements used by the results obtained from ultrasonic Doppler flowmeter, are characteristic for "an average slug unit". For a given gas and liquid flow data "an average slug unit" is defined to have an average length of the liquid slugs, an average length of the gas pockets between the liquid slugs and an average translational speed of the slugs.

6.5.3 Gas flow-rate measurement

Gas flow-rate in two-phase slug flow can be measured using an ultrasonic Doppler, a flush-mounted conductivity ring and self-calibrated pressure transducer.

There are two methods to obtain gas flow-rate within the slug flow:

6.5.3.1 Gas flow-rate measurement using V_C

The first method is measuring the gas flow-rate in slug flow using correlated transitional velocity (V_C) from the slug body velocity Doppler measurement V_s. V_T is literature based correlation which is using two region equations; one equation is for a Froude number less than 2 and the other is for a Froude number bigger than 2 but less than 4.

$V_C = V_s$ 1.4327 Fr<2 **(6.9)**

$V_C = V_s$ 1.1771 2<Fr<4 **(6.10)**

These two correlations are extracted from the relationship between V_T extracted by CV_m and V_s measured by the Doppler, as shown in Figure 6-23 and Figure 6-24.

$$Q_g = \frac{V_C(1-\alpha_f)At_f}{(t_f + t_s)} \quad \textbf{(6. 11)}$$

where, $V_C = V_s$ 1.4327 and $V_C = V_s$ 1.1771

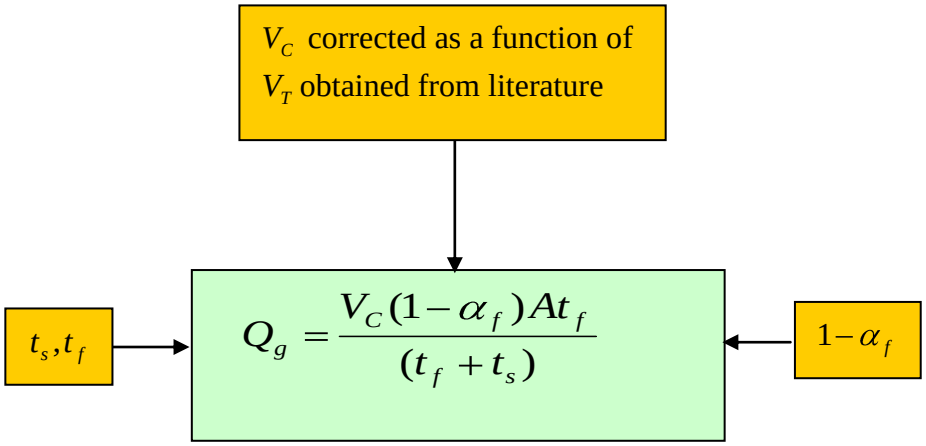

Figure 6- 27, Gas flow-rate measurement scheme

Figure 6-28 and Figure 6-29 show the comparison between the gas flow-rate measured by Doppler and corrected by V_C.

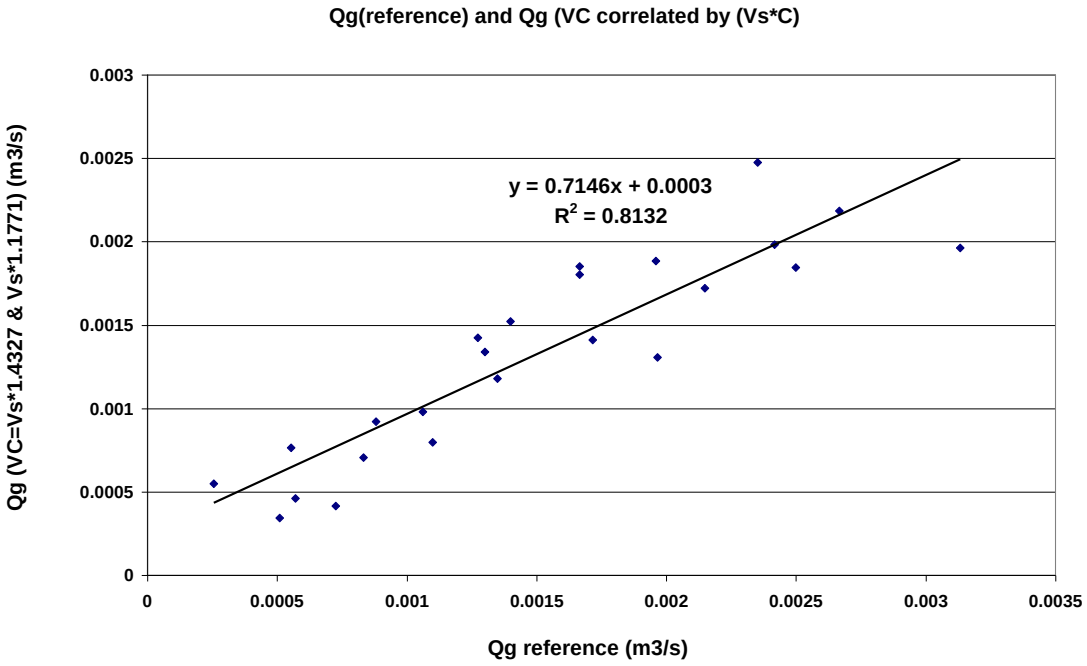

Figure 6-28, Gas flow-rate measured and reference comparison

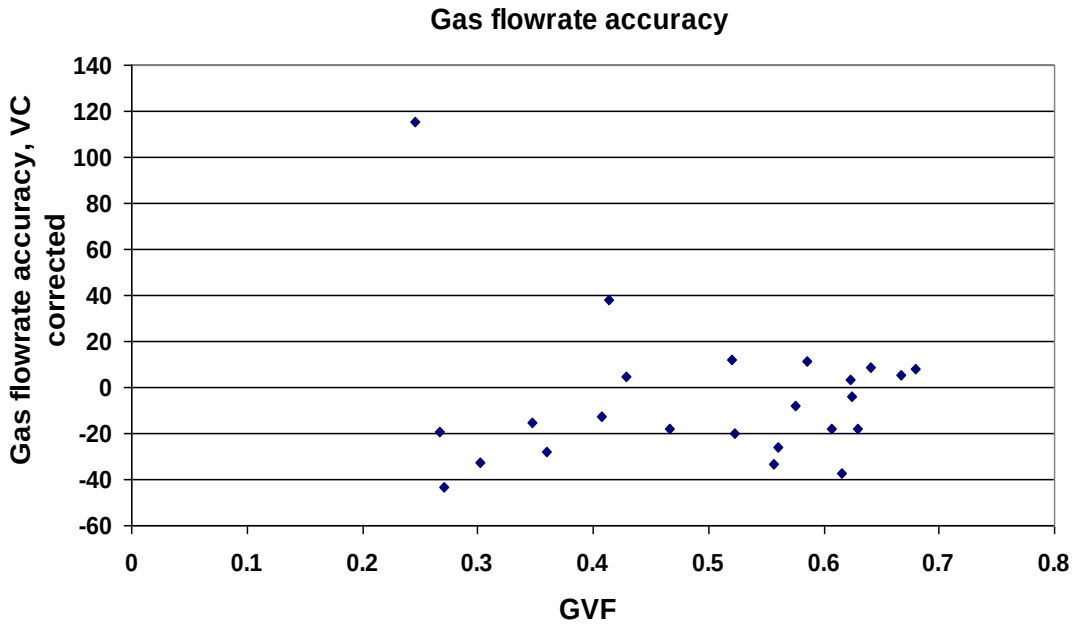

Figure 6-29, Gas flow-rate accuracy

6.5.3.2 Gas flow-rate measurement using Qm

The second method for gas flow-rate measurement in slug flow is using the liquid flow-rate measured previously by Doppler subtracted from mixture flow-rate which is a result of Vs measured by Doppler and multiplied by cross section area A.

Assuming $V_m \cong V_s$ figure 6-19

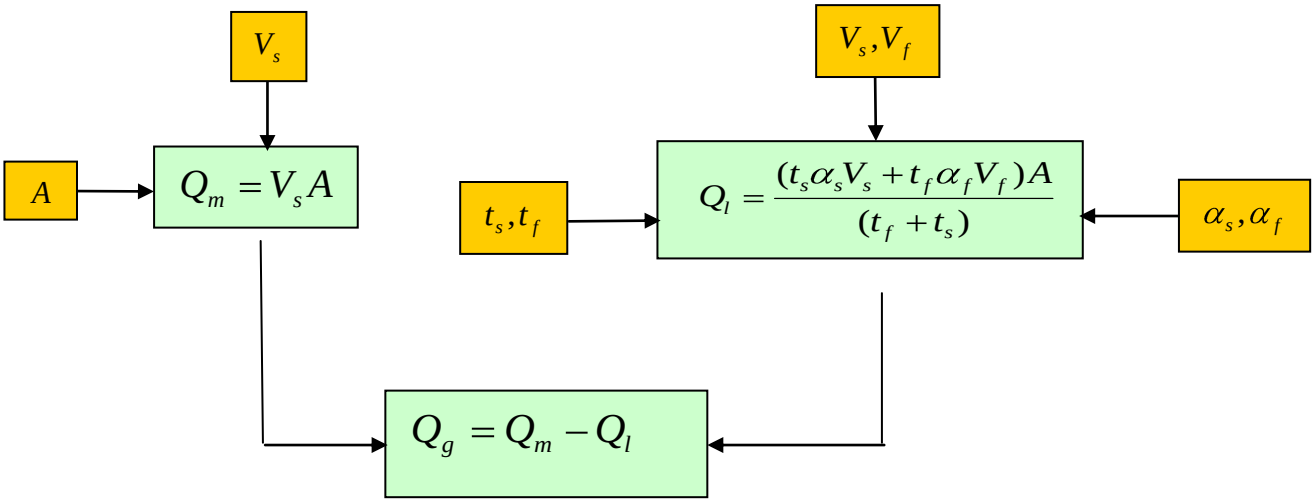

Figure 6-30, Gas flow-rate measurement using measured liquid and mixture flow-rate

$$Q_m = V_s A \tag{6. 12}$$

$$Q_l = \frac{(t_s \alpha_s V_s + t_f \alpha_f V_f) A}{(t_f + t_s)} \tag{6. 13}$$

$$Q_g = Q_m - Q_l \tag{6. 14}$$

The gas flow-rate measurement using liquid flow-rate is subtracted from mixture flow-rate; this measurement shows a good accuracy agreement when the results are compared with the reference points (gas turbine flowmeter). Figure 6-31 and Figure 6-32 illustrate this agreement.

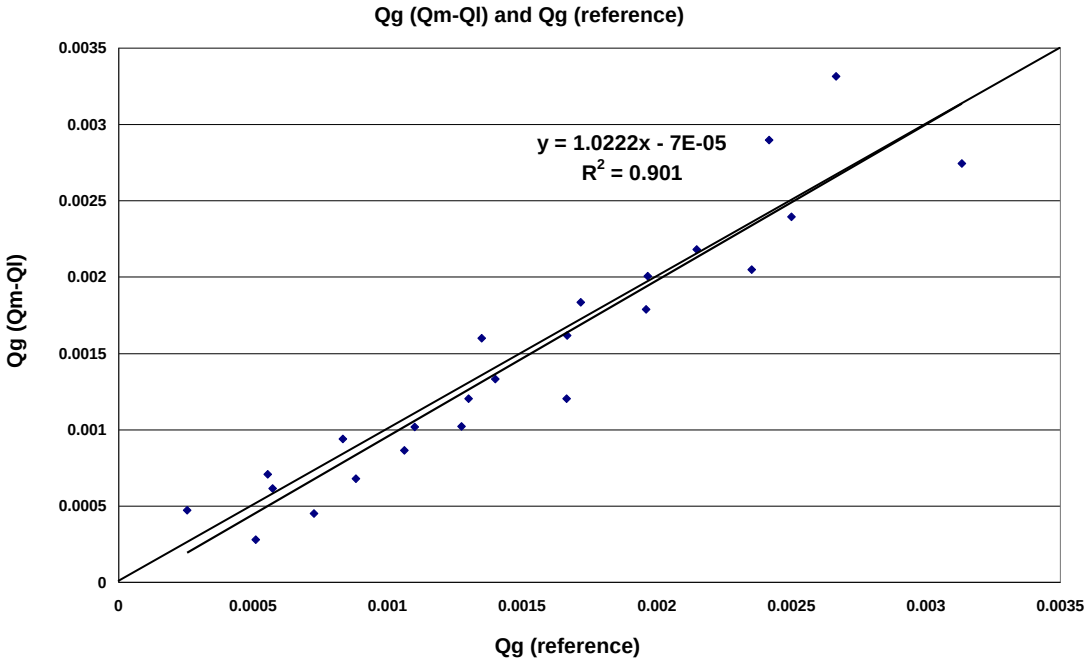

Figure 6-31, Gas flow-rate comparison between measured by the Qm-Ql and reference

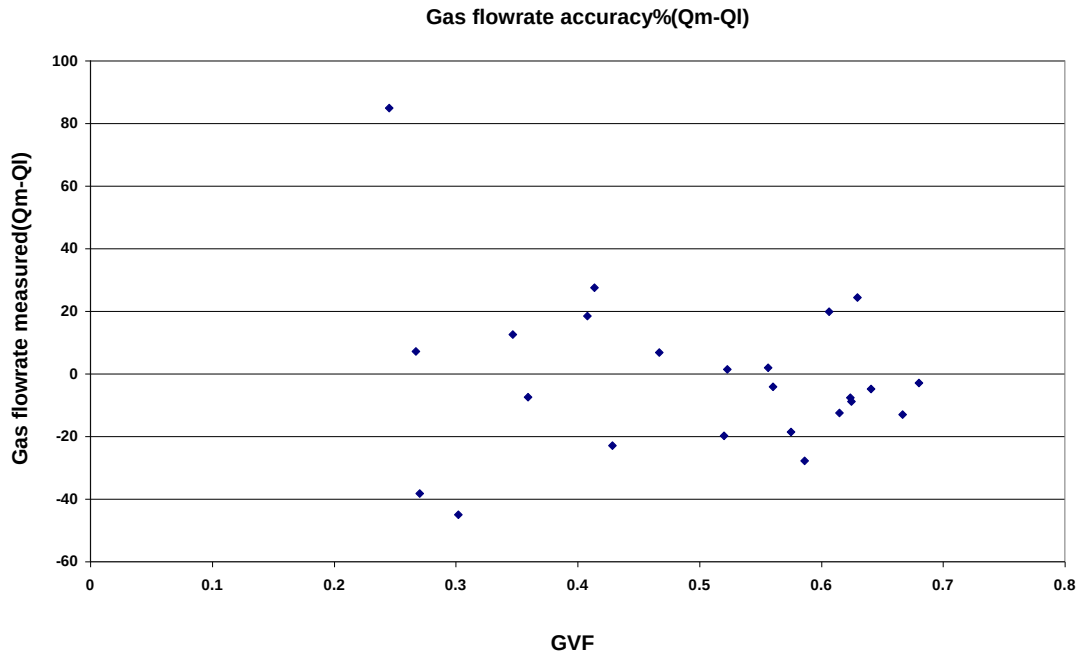

Figure 6-32, Gas flow-rate accuracy using Qm and Ql

Figure 6-33 shows the gas flow-rate measured by correlated V_C and by $Q_m - Q_l$ which are plotted together to show the accuracy and limitation of each method.

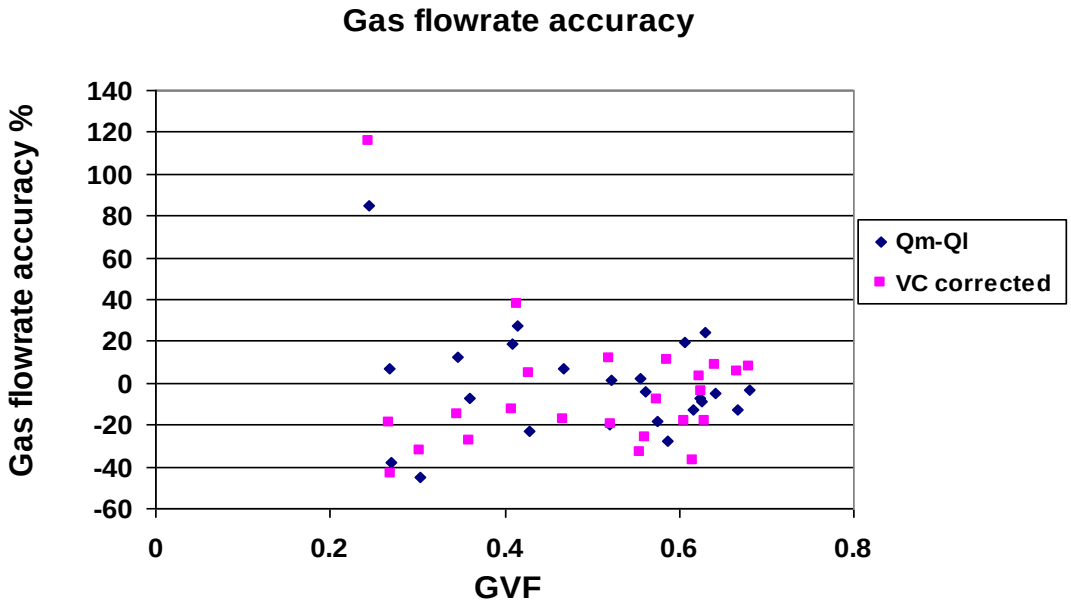

Figure 6-33, Gas flow-rate measurement plot using both measurement methods

The gas flow-rate, measured by V_C and $(Q_m - Q_l)$ comparison, shows similar performance when plotted against GVF; however, the $(Q_m - Q_l)$ gas flow-rate shows

a slightly better accuracy measurement than the V_C gas measurement. Figure 6-34 illustrates this comparison.

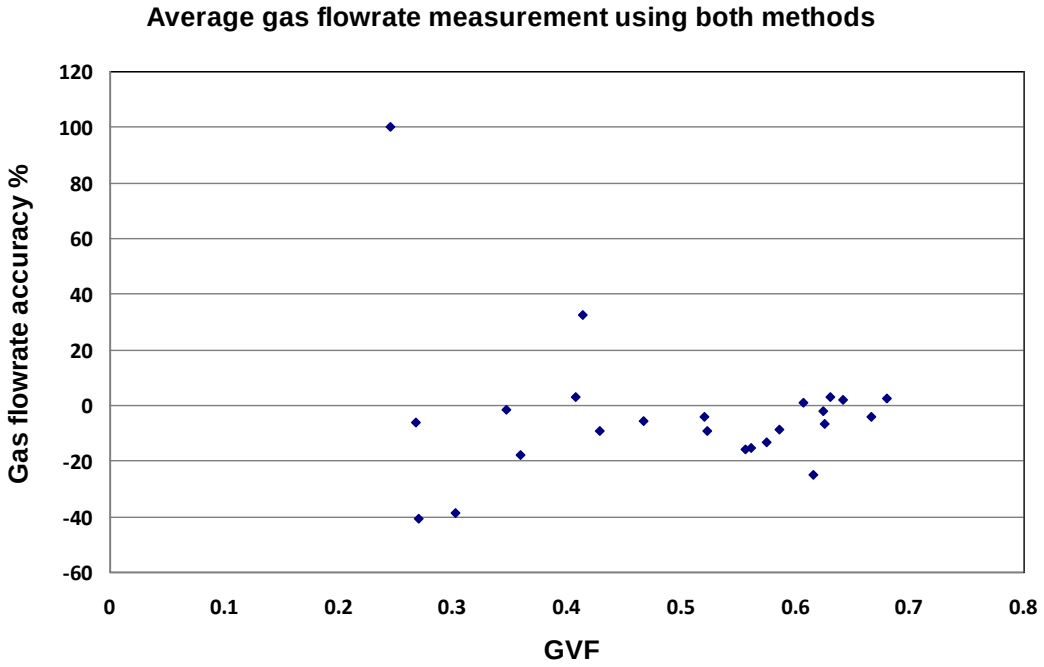

Figure 6-34, Average gas flow-rate measurement for both methods

6.6 CHAPTER SUMMARY

This chapter has focused on the raw slug flow measurement using ultrasonic Doppler transducer to measure slug and film velocities. It started with a brief description of the raw slug measurement experimental set-up. Ultrasonic Doppler transducer location around the pipe was illustrated. Ultrasonic Doppler and conductivity ring signal gathering, methods of analysis and data acquisition system were explained. Slug and film velocity measurements using Doppler were demonstrated.

As liquid hold-up was obtained using conductivity ring, and the liquid velocity in the slug and film were measured using ultrasonic Doppler, so the liquid flowrate was obtained. Gas flowrate within the slug flow was obtained by correlated slug velocity and conductivity ring for fraction measurement.

Chapter 7

CONCLUSION AND FUTURE WORK

7.1 CONCLUSION

In this work, ultrasonic measurement techniques in combination with the T-Y junctions have been presented. The reason behind using the T-Y junctions is to eliminate the slug flow which occurs upstream of T-Y junctions and modify it into partially separated liquid dominated and a homogeneous flow.

This approach has been tested on water/air flows in a 50mm diameter pipe facility in the Department of Offshore, Process and Energy Engineering at Cranfield University. The water flow-rate measurements using the proposed technique were compared with a reference measurement and a good agreement between these two measurements was obtained. Such performance offers good potential for the proposed in-line multiphase flowmeter with improved performance.

Different ultrasonic techniques have been deployed to measure the flow velocity. An ultrasonic cross-correlation method was deployed in the liquid dominated flow, an ultrasonic Doppler flowmeter was used in the homogeneous flow for velocity measurement, and in the raw slug section frequency shifts from the ultrasonic Doppler transducer were used to measure the slug and film velocities. These measurement techniques have been also tested for a wide range of superficial velocities on a horizontal pipe. Flush-mounted conductivity rings have been installed and tested to measure a phase fraction in all measuring sections. As a result, the liquid flow-rates in partially separated liquid dominated flow, homogeneous flow, and raw slug flow were successfully obtained. Gas flow-rates were also measured in the homogeneous flow and in the raw slug flow.

The experimental test condition ranges were performed as follows:

- Superficial liquid velocity 1 - 2m/sec.

- Superficial gas velocity range 0.2 - 3.5m/sec.
- Mixture velocity range 1.2 - 5.5m/sec.
- Gas volume fraction range 10% - 60%.
- Static pressure range 1.02 bar abs.
- Room temperature 18 - 35C^{o}.

The flow-rate measurement results can be summarised as below:

7.1.1 Liquid Flowrate Measurement after Partially Separated

Liquid flow-rate in the partially separated liquid dominated section down arm of the T-junction was measured using ultrasonic cross-correlation in combination with a flush-mounted conductivity ring. Several experiments were run and a good agreement average error of $\pm 10\%$ was obtained when the measured liquid was compared with the reference point.

7.1.2 Homogeneous Flowrate Measurement

7.1.2.1 Homogenised mixture flow-rate

The mixture flow-rate measurement was made using the ultrasonic Doppler flowmeter and it was corrected for its working pressure and temperature. The overall error was within ± 10 % of the reference mixture flow-rate of gas and liquid.

7.1.2.2 Homogenised liquid flow-rate measurement

The liquid flow-rate measurement within the homogeneous flow was performed using an ultrasonic Doppler and a conductivity ring. The results were within an averaged error of $\pm 10\%$ of the reference liquid flow-rate.

7.1.2.3 Gas flow-rate within the homogeneous section

The gas flow-rate measurement within the homogeneous section was obtained using ultrasonic Doppler flowmeter as mixture velocity measurement and the flush-mounted conductivity ring as GVF measurement. About 99% of the calculated gas flow-rate results were within $\pm 10\%$ of the reference. However, some further investigation needs to be made since this reference is not very reliable as it required very frequent calibrations for the low gas flow-rate. Additionally, the gas flow-rate can also be calculated by subtracting the liquid flow-rate from the mixture flow-rate measured within the homogeneous section.

7.1.3 Raw Slug Flow Measurement

7.1.3.1 Slug and film velocity measurement

The ultrasonic Doppler transducer was clamped on to the bottom of the pipe, as liquid exists there all the time. The difference in frequency shift illustrated by the wavelet spectrum can be clearly referred to slug body and film velocities.

7.1.3.2 Liquid flow-rate in slug flow

Liquid flow-rate measurement in a horizontal slug flow regime was undertaken using a raw signal ultrasonic Doppler and a flush-mounted conductivity ring. The Doppler was clamped on to the bottom of the pipe where liquid (slug/film) always exists. Slug and film velocities were ultrasonically measured. The measured flow-rate was compared with the reference and the accuracy obtained was within ± 15 %.

7.1.3.3 Gas flow-rate within slug flow

A series of experiments were performed to accurately measure the gas flow-rate within slug flow using the ultrasonic Doppler and the conductivity ring. More than one method was used to determine the gas flow-rate within slug flow. The first was based on the slug body velocity corrected by slug velocity correlation V_T. The gas flow-rate accuracy obtained using this measurement method was within ± 20 % with the majority of the data showing under valued (in negative). The second was based on liquid flow-rate subtracted from the mixture flow-rate and the accuracy obtained using this method of measurement was ± 20 % but showing over valued (in positive). In both methods a conductivity ring was used to measure GVF within the film zone and in liquid hold-up in the slug body. The combined gas flow-rate accuracy from the two gas flow-rate measurement methods suggested the accuracy of the majority of the measurement points was within ± 10 %.

It can be concluded that T-Y junctions have shown promising and successful results as the slug flow is eliminated, and it was partially separated and well-homogenised. When the proposed metering techniques have been compared to the reference points, they have provided a very good overall accuracy of measuring the slug flow liquid and gas measurement, and liquid and calculated gas flow-rate within the homogenised section.

7.2 Recommendations and Future Work

A considerable amount of time and effort have been devoted in the laboratory towards achieving ultrasonic flow-rate measurement in combination with in-house built T-Y junctions. In order to build upon the research work described in this thesis, it is recommended that a number of elements should be further investigated.

7.2.1 Liquid flowrate calculation in raw slug

Currently, the liquid and gas flowrates separately measured in three flow regimes (partially separated, homogeneous and raw slug).

Combining the gas flowrate in raw slug regime has led to improvement in the overall accuracy and reduces the uncertainty at individual measurement.
The equipment has not allowed the measurement to be instantaneously in all the three sections and be combined together.

It could be argued that combining these measurement would be further improve the accuracy and reduce the uncertainty.
An experimental programme which is undertaken this should be consistent.

In the raw slug regime the use of Short Time Fourier Transfer (STFT) should be considered in conjunction with instantaneous fraction, this may allow an improved calculation of liquid flowrate when liquid flowrate is calculated as the following:

$$Q_l = \frac{\int_0^{t_s} \alpha_s(t) V_s(t) A.dt + \int_{t_s}^{t_s+t_f} \alpha_f(t) V_f(t) A.dt}{t_s + t_f} \quad \textbf{(7.1)}$$

Or

$$Q_l = \frac{\int_0^{t_s+t_f} \alpha(t).V(t).Adt}{t_s + t_f} \quad \textbf{(7.2)}$$

7.2.2 Experimental Facility

- Further experiments should be conducted on a larger pipe diameter test rig to establish the diameter effect on T-Y junction performance in different operational environments, and to evaluate T-Y junction design in order to extend their ability to cover a wider range of flow regimes that occur in horizontal pipes.

- Further study of a higher liquid flow-rate should be conducted.

- Investigate ultrasonic Doppler performance on different viscosity liquids which could be more relevant to the oil and gas industry.

- Investigate the ultrasonic Doppler technique on slug flow oil/gas measurement on different pipe diameters.

7.2.3 Instrumentation

Replace the flush-mounted conductivity ring with a capacitance ring or Gamma-ray involves assessing the ultrasonic Doppler technique for oil flow-rate measurement.

REFERENCES

Addali A. (2010), Monitoring Gas Void Fraction in Two-Phase Flow with Acoustic Emission, PhD Thesis Cranfield University, School of Engineering.

Aggarwal, R. and Yonghua, S., June 1997, Artificial Neural Networks in Power Systems, Part 2 General Introduction To Neural Computing, Power Engineering Journal.

Akinyemi, O.A. 2008, Multiphase Flow Measurements Using an in-Line Separator and Ultrasonic Sensors, MSc thesis, Cranfield University, UK.

Aldridge, E.E. and Tattersal, H.G. 1971, Ultrasonic Conference, London, Pp 49-51.

Al-lababidi, S. 2006, Multiphase Flow Measurement in the Slug Regime Using Ultrasonic Measurement Techniques and Slug Closure Model, PhD Thesis, Cranfield University, UK.

Asher, R.C., Ultrasonic Sensors, Institute of Physics, London, 1997.

Babelli, I.M.M., October 2002, In Search of an Ideal MultiPhase Meter For The Oil Industry, The Arabian Journal for Science And Engineering, Volume 27, Number 2b.

Baggi, AGAR Multiphase Flow-meters-400 Series Operation Manual.

Baker, R.C. 2000, Flow Measurement Handbook, Industrial Designs, Operating Principles, Performance, and Applications 1st, Cambridge University Press.

Baker, R.C., 2002 An Introduction Guide to Flow Measurement, 2nd, Professional Engineering Publishing Limited, 2002 UK.

Barnea, D. and Taitel, Y. 1993, A Model for Slug Length Distribution in Gas-Liquid Slug Flow, Int. J. Multiphase Flow Vol. 19, No. 5, Pp. 829-838, 1993.

Belegrantis, V. and Azzopardi, B., March 2007, Gas/Liquid Two Phase Flow at A Combining T-Junction, University Of Nottingham, School of Chemical Engineering,.

Benard, C.J., (1988), Handbook of Fluid Flow-Metering, The Trade & Technical Press Limited, Surrey, England.

Blaney S. and Yeung H., 2007, Investigation of the Exploitation of a Fast-Sampling Single Gamma Densitometer and Pattern Recognition to Resolve the Superficial Phase Velocities and Liquid Phase Water cut of Vertically Upward Multiphase Flows, Flow Measurement and Instrumentation 19 (2008) 57–66.

Bonizzi, M. and Issa, R.I., 2003, A Model for Simulating Gas Bubble Entrainment in Two-Phase Horizontal Slug Flow, International Journal of Multiphase Flow 29 (2003) 1685–1717.

Carlson J., Delsong J. and Grennberg A. 2002, Ultrasonic Characterization of Materials and Multiphase Flows, Department of Computer Science and Electrical Engineering, Lulea University of Technology.

Chapelon V., Cathignol J.Y. Newhouse, Bubble Sizing with High Spatial Resolution, IEEE Transactions on Ultrasonics 37 (1990) 30–37

Chikkerur, S., Cartwright, N. and Govindaraju, V., 2000, Fingerprint Image Enhancement Using STFT Analysis, Center For Unified Biometrics and Sensors, University at Buffalo, NY, USA, UB Commons, Suite 202,520 Lee Entrance Amherst, NY 14226, USA.

Diacon B. 2002 Film Thickness and Void Fraction Measurement using Ultrasonic Techniques, Engineering Physics, Mcmaster University.

Dong F., Liu X., Deng X., Xu L. and Xu, L-A., 2001 Identification of Two-Phase Flow Regimes In Horizontal, Inclined and Vertical Pipes, Institute of Physics Publishing, Science and Technology. 12 (2001) 1069-1075.

Duckler, A.E, and Hubbard, M.G., 1976, A Model for Gas-Liquid Slug Flow in Horizontal and Near Horizontal Tubes, Ind. Eng. Chem. Found., 14, 337-347.

Ekambara K., Sanders R.S., Nandakumar K. and Masliyah, J.H. 2008, CFD Simulation of Bubbly Two-Phase Flow in Horizontal Pipes, Chemical Engineering Journal 144 (2008) 277–288.

Endress and Hauser, Ultrasonic Flow Measuring System Prosodic Flow DMU 93, Technical Information TI 042D/06/en No. 50091532.

Fabre J. and Line A., 1992 Modeling of Two-Phase Slug Flow, Annual Review of Fluid Mechanics, January 1992, Vol. 24, Pages 21-46.

Fernandes, R.C., Semiat, R. and Dukler, A.E., 1983. Hydrodynamic Model for Gas–Liquid Slug Flow in Vertical Tubes., J. Aiche 29, 981–989.

Fossa M. and Guglielmini G., 1998, Dynamic Void Fraction Measurements in Horizontal Ducts with Sudden Area Contraction, International Journal of Heat and Mass Transfer 41.

Giurgiutiu V. and Yu L., 2003, Comparison of Short-time Fourier Transform and Wavelet Transform of Transient and Tone Burst Wave Propagation Signals for Structural Health Monitoring, 4th International Workshop on Structural Health Monitoring, Stanford University, Stanford, CA, USA.

Goudinakis G., Dickson S. and Hanich L., 1999, Application of Artificial Neural Networks (Anns) to the Modelling of Multiphase Flow from Oil Wells, Cranfield University, UK.

Gregory G., Scott A., Correlation of Liquid Slug Velocity and Frequency in Horizontal Co-current Gas–liquid Slug Flow, AIChE J. 15 (1969) 933–935.

Guanghui, S., Fukuda, K., Morita, K., Pidduck, M., Dounan, J., Matsumoto, T. and Akasaka, R., 2002 Application of Artificial Neural Network for The Prediction of Flow Boiling Curves, Journal of Nuclear SCIENCE and Technology, Vol. 39, No, P. 1190-1198 (2002).

Handbook of Multiphase Flow Metering, March 2005 Norwegian Society for Oil and Gas Measurement.

Haoues, L., Olekhnovitch A. and Teyssedou, a. 2007 Influence of The Void Fraction Profile on The Distribution Parameter C_o for Bubbly Gas-Liquid Flow in Horizontal Round Pipe, Nuclear Engineering and Design, 24 September 2007.Institute De Genie Nuclear Department.

Hauptmann P., Hoppe N. And Puttmer A., 2002 Review Article Application of Ultrasonic Sensors in The Process Industry, Institute Of Physics Publishing, Meas. Sci.13 2002 R73-R83.

Iskandrani, A. and Kojasoy, G. Local Void Fraction And Velocity Field Description in Horizontal Bubbly Flow, Department of Mechanical Engineering, University of Wisconsin-Milwaukee, 18 July 2000.

Ismail, I., Gamio, J.C., Bukhari, S.F.A., and Yang, W.Q., 2005, Tomography for Multiphase Flow Measurement in The Oil Industry, Flow Measurement and Inst. 16145-155.

Jackson, L.B., Digital Filters and Signal Processing, 3rd Edition, Kluwer Academic Publisher, 1995, P. 156.

Jama, A.A. 2004. Wet Gas Flow Metering with Pattern Recognition Techniques, Ph.D. Thesis, University of Cranfield, UK.

Jiang, J. and Rezkallah, K.S. 1993, An Experimental Study of the Suitability of Using a Gamma Densitometer for Void Fraction Measurements in Gas-Liquid Flow in a Small Diameter Tube, Meas. Sci. Technol. 4 (1993) 496-505.

Kavosh, M. 2005, Multiphase Slug Flow Measurement, MSc Thesis, Cranfield University.

Kocamustafaogullari, G., Wang, Z. and Huang, W.D. 1994, Internal Structure and Interfacial Velocity Development for Bubbly Two-Phase Flow, University of Wisconsin-Milwaukee Report, DOE/NE/151 - 79-101.

Lang P., Sarishvili A., Wirsen A., 2003 Blocked Neural Networks for Knowledge Extraction in The Software Development Process, Berichte Des Fraunhofer Itwm, Nr. 56 (2003).

Lang. W. C. and Forinash K., 1998, Time-frequency analysis with the continuous wavelet transform, Natural Sciences Division, Indiana University Southeast, New Albany, Indiana 47150.

Liu S., Chen, Q., Wang, H.G., Jiang, F., Ismail, I. and Yang, W.Q., 2005, Electrical Capacitance Tomography for Gas–Solids Flow Measurement for Circulating Fluidized Beds, Flow Measurement and Instrumentation 16 (2005) 135–144.

Mandhane J.M., Gregory G.A. and Aziz K., A Flow Pattern Map for Gas-Liquid Flow in Horizontal Pipes, Int. J. Multiphase Flow, Vol. 1, pp. 537-553. Pergamon Press, 1974.

Moissis, R. and Griffith, P., 1962 Entrance Effects in a Two-Phase Slug Flow. J. Heat Transfer 84, 29-39.

Murakawa, H., Kikura, H., and Aritomi, M., 2005 Application of Ultrasonic Doppler Method for Bubbly Flow Measurement Using Two Ultrasonic Frequencies, Tokyo Institute of Technology, Experimental Thermal and Fluid Science 29 (2005) 843-850.

Newland, D.E. 1994, An Introduction to Random Vibrations, Spectral and Wavelet Analysis, Third Edition, Longman Scientific and Technical, UK.

Nydal O.J. and Banerjee S., 1996, Dynamic Slug Tracking Simulations for Gas–Liquid Flow in Pipelines. Chemical Engineering Comm., 141–142, 13–39.

Olsvik K, Marshall M and Whitaker T, 1995, Fluenta Multiphase Flow Meter, Tested and Marinised, Proc. 13th North Sea Flow Measurement Workshop (Lillehammer, Norway)

O'sullivan, I.J. and Wright, W.M.D., 2002, Ultrasonic Measurement of Gas Flow Using Electrostatic Transducers, Department of Electrical and Electronic Engineering, Cork, Ireland, Ultrasonic 40407-411.

Phase Dynamics, Technology for Precision Measurements, Compact Cyclone Multiphase Meter (CCM).
http://www.asgmt.com/default/papers/asgmt2002/docs/44.pdf
(Accessed 10/6/2009)

Piwoda L., July 2003, Metering of Two-Phase Geothermal Wells Using Pressure Pulse Technology, Diploma Thesis, Norwegian University of Science and Technology, Department of Petroleum Engineering and Applied Geophysics.

Private communication with Cyclone Separation Company CALTE Ltd 2008.

Qiu, C., Hoyle, B.S. and Podd, F.J.W., 2007, Engineering and Application of a Dual-Modality Process Tomography System, Flow Measurement and Instrumentation 18 (2007) 247–254.

Roxar MPFM 1900VI, Manufacture Manual Operation, Repsol Oil Operating Company Archive (2007).

Ruzairi A.R., Nayan, M., Rahiman, N. and F., and Hafiz, M., 2006, Ultrasonic Tomography System for Liquid/Gas Flow: Frame Rate Comparison between Visual Basic and Visual C++ Programming, Jurnal Teknologi, 44(D) Jun 2006: 131–150, Universiti Teknologi Malaysia.

Sanderson M.L., 1999, Industrial Flow Measurement by Ultrasonic, Insight 41 (1) 16-19.

Sanderson, M. L., 2009 Multiphase Flow and Multiphase Flow Measurement Techniques, Msc Process and Systems Engineering, Cranfield University, Course Notes.

Sanderson M.L. and Yeung, H. 2002 Guidelines for the Use of Ultrasonic Non-Invasive Metering Techniques, Flow Measurement and Instrumentation 13 (2002) 125-142.

Shaikh A. and Al-Dahhan M., 2003, Development of an Artificial Neural Network Correlation for Prediction of Overall Gas Holdup In Bubble Column Reactors, Chemical Engineering And Processing 42 (2003) 599_/610, USA.

Taitel, Y. and Barnea, D. 1990, Two Phase Slug Flow. In Advances in Heat Transfer (Edited By Hartnett, J. P. Irvine, T. F. Jr), Vol. 20, Pp. 83-132. Academic Press, New York.

Taitel Y. and Dukler E. A., A Model for Predicting Flow Regime Transitions in Horizontal and Near-Horizontal Flow, AIChE, Vol. 22, pp. 47-55, 1976.

Tea Sistemi S.P.A., Piazza Mazzini 1 - 56126 Pisa – Italy
www.tea-group.com/pdf_03/Models_HSE.pdf
(Accessed 10/6/2009)

TGA group, VEGA Multiphase Flowmeter
www.pi.ac.ae/doc/PI_AR_2009Online.pdf
(Accessed 10/6/2009)

The Mathworks Help Page, Inc.
https://tagteamdbserver.**mathworks**.com/.../452_9797v00_Boeing_SMV_ROI.pdf
(Accessed 180/4/2010)

The Petroleum Science and Technology Institute for the European Commission Offshore Technology Park Market Prospects For Multiphase Technology, Aberdeen, UK.

Thorn R., Johansen G.A. and Hammer, E.A., 1997, Recent Developments in Three-Phase Flow Measurement, Meas. Sci. Technol., Vol 8, No. 7, Pp. 691-701.

Thorn, R., Johansen, G.A., And Hammer, E.A., 1999, Three-Phase Flow Measurement in the Offshore Oil Industry is there a Place for Process Tomography?, 1st World Congress on Industrial Process Tomography, Buxton, Great Manchester, April 14-17.

Ujang P.M., Lawrence, C.J., Hale C.P. and Hewitt, G.F., 2006, Slug Initiation and Evolution in Two-Phase Horizontal Flow, International Journal of Multiphase Flow 32 (2006) 527–552.

Urick R.J. 1967, Principles of Underwater Sound for Engineers, Mcgraw-hill.

Vermeulen, L.R., and Ryan, J.T., 1976, Two-Phase Slug Flow in Horizontal and Inclined Tubes, Canadian Journal of Chemical Engineering, 49, 195-201.

Wang T., Wang J., Ren, F. and Jin Y., 2003 Application of Doppler Ultrasonic Velocimetry In Multiphase Flow, Department of Chemical Engineering, Tsinghua University, Beijing, Chemical Engineering Journal 92 (2003)111-122.

Wren, E. and Azzopardi, B., September 2001, Geometric Effect on Phase Split at A Large Diameter T-Junction, University of Nottingham, School of Chemical Engineering.

Xu, L-A., Green, R.G., Plaskowski, A. and Beck, M.S., The Pulsed Ultrasonic Cross-Correlation, J. Phys. E: Sci. Instrum. 21 (1988) 406- Flowmeter for Two-Phase Flow Measurement.

Yan, Y., Review Article Mass Flow Measurement of Bulk Solids In Pneumatic Pipelines, Meas. Sci. Technol. 7 (1996) 1687–1706, Printed In The UK.

Geng Y., Zheng J., Shi T., and Shi G., 2007, Wet Gas Meter Development Based on Slotted Orifice Couple and Neural Network Techniques, Chinese Journal of Chemical Engineering, 15(2) 281-285 (2007).

Appendices:

Abbon AS, AFM Product Specification Sheets:
http://www.abbon.com/images/stories/abbon/pdf/afm_prodsheet.pdf
http://www.abbon.com/images/stories/abbon/pdf/oc400_prodsheet.pdf
(accessed 04/08/2010)

Accuflow AMMS Product Technology Information:
http://accuflow.com/images/brochure_sr.pdf
(accessed 20/07/2010)

AGAR MPFM 300 and 400 Summary of Field Experience, Series Meters, 1995-2001, AGAR Corporation 5150 Tacoma Drive, Houston, Texas 77041, USA

ESMER Multiphase Flow Meter for the Oil & Gas Industry Expert System for Multiphase and Wet Gas Metering Applications, ESMER, Petroleum Software Limited.
http://www.petroleumsoftware.co.uk/rome04sfjt.pdf
(accessed 27/09/2010)

eProduction Solution Corporate Website:
http://www.epweatherford.com/Solutions/EP/Red_Eye_Multiphase_Metering_Systems.htm
(accessed 20/07/2010)

FlowSys TopFlow Official Website:
http://info.smithmeter.com/literature/docs/ssmp001.pdf
(accessed 04/08/2010)

Jiskoot official website:
www.**jiskoot**.com/download.php?id=38
(accessed 20/07/2010)

Haimo Technologies Inc. Website
www.Haimotech.Com
(accessed 04/08/2010)

Neftemer Official Website:
http://www.neftemer.com/downloads/neftemer-presentation-mmr07.pdf
http://www.neftemer.com/scope-of-supply.html
(accessed 04/08/2010)

Appendix A-Review of Commercial MPFMs

Multiphase flowmeters are alternative measurement methods compared to those of bulky fully separating single-phase measurement methods. For reservoir monitoring, allocation purposes or appraisal wells, these meters offer considerable economic advantages. However, problems of multiphase metering start from the complex nature and messy behaviour of the fluid as it travels through pipe lines.

A1. Multiphase flowmeters requiring pre-conditioning

As a primary conditioning for some multiphase flowmeters is required, in the next pages, multiphase flowmeters are categorised on pre-conditioning requirement.

A1.1. AGAR MPFM-400

The Agar MPFM-400 series is an example of pre-conditioning flowmeters. The flowing mixture of gas/oil/water enters the T-junction where the flow is separated into wet gas and liquid. As shown in Figure A- 1, the wet gas goes up the side of the T-junction to be measured using conventional single-phase flowmeters, whereas, the liquid goes down through positive displacement which measures the liquid volumetric flow-rate. Microwave technology is used to determine the fraction of oil and water. The gas and the liquid are reunited as they leave the Agar meter to the pipeline (AGAR MPFM 300 AND 400).

Agar flowmeter performance is described as shown in **Error! Reference source not found.**.

Instantaneous Void Fraction	0 to 99.6%
Water-cut	0 to 100%
Flow Patterns	All: (e.g. Bubbly, Wavy, Slug, Annular flows, etc.)
Pressure	Up to 10,000PSI / 680 bars
Ambient Temperature	-40ºC to 70ºC (-40ºF to 160ºF)
Process Temperature	15ºC to 93ºC (60ºF to 200ºF)
Optional High-Temp	(15ºC to 232ºC / 60ºF to 450ºF)
Viscosity	0.5 to 100 Centipoise (Higher viscosity optional)
Salinity	0 to 20% by weight
Sand/Particulate	Up to 5% by volume
Max. Pressure Drop	Less than 15 PSI (1 bar)

Table A- 1, Agar flowmeter performance

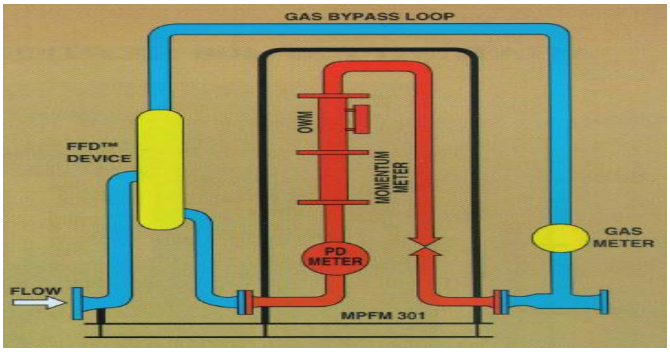

Figure A- 1, Agar flowmeter taken from BAGGI AGAR MPFM 400 serious

A.1.2. Framo MPFM

The Framo flowmeter is an example of MPFM which is used in a homogeneous flow system. The multiphase flow enters into a tank mixer where the phases flow is well mixed to ensure that the entire measurements are obtained with a homogeneous flow. The mixture leaves the mixer tank axially to pass through a Venturi meter which measures the homogeneous flow velocity. Gamma ray attenuation is implemented to identify the liquid (gas and water) and gas fraction. When the gas fractions are less than 70%, the Framo multiphase flowmeter provides gas fractions measurements to better than $\pm 5\%$, and oil and water flow measurements with an accuracy of $\pm 5\%$, (Thorn et al., 1999). Since this flowmeter works with a premixed flow, and the actual measuring flow is in homogeneous flow, so this flowmeter does not have the problem of flow dependency. Figure A- 2 shows MPFM used within a homogeneous flow which is commercially available.

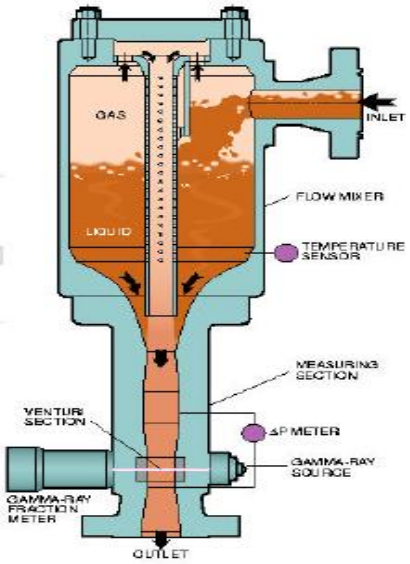

Figure A- 2, MPFM homogenises the flow, taken from a three-phase flow measurement in off-shore.

A1.3. Jiskoot Mixmeter Multiphase Meter

This multiphase flow flowmeter is based on homogeneous flow in the Mixmeter which is designed to generate a characteristic differential pressure (DP) for bulk measurement, a technique well established for its stability in multiphase flow. The DP provides reliable measurement and has been proven in laboratory and field applications over a wide range of fluids.

As shown in Figure A- 3, phase fractions are measured by a dual energy gamma absorption instrument. Mixmeter uses a single Caesium137 source which is already used extensively for density measurement in oil production. This technology provides high resolution and low uncertainty giving Mixmeter accurate measurement and differentiation between the three phases throughout the full operating envelope.

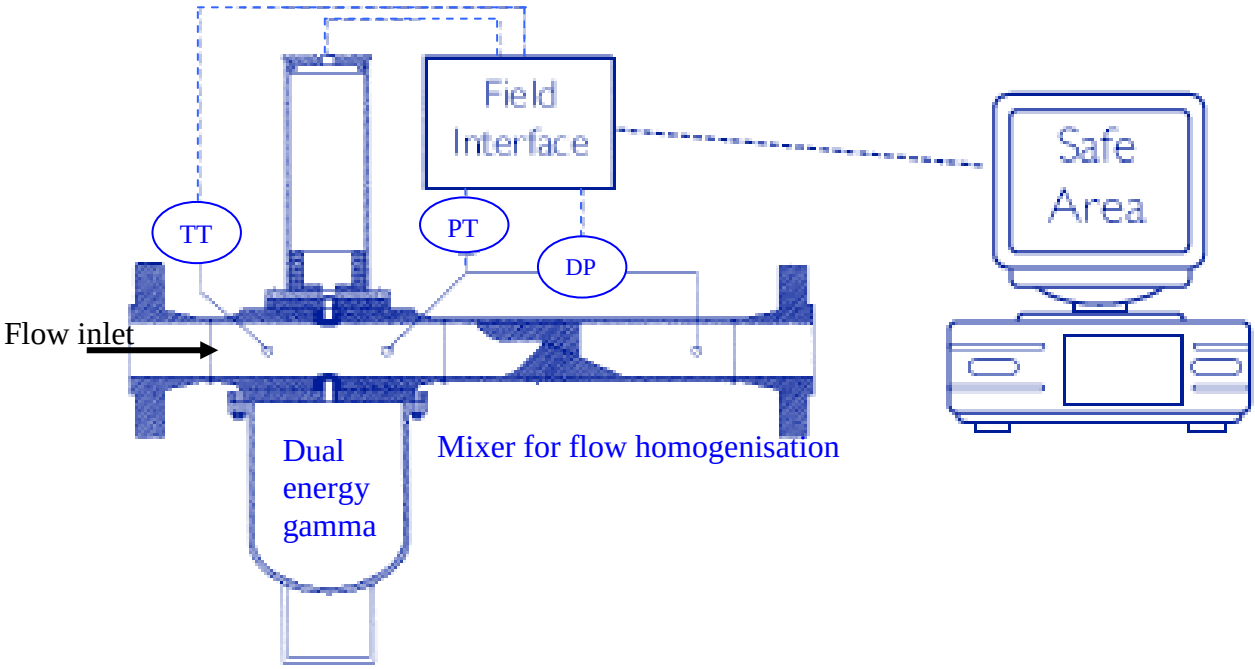

Figure A- 3, Mixmeter MPFM

Operating envelope:

- Watercut: 0 - 100%
- GVF: 0 - 90%
- Velocity 1 - 30m/s multiphase mixture velocity

Accuracy:

- 0 - 65% GVF, Watercut ±4% (of full range), Liquid error ±2.5% (of reading), Gas error ±9% (of reading)

- 65 - 90% GVF, Watercut ±5% (of full range), Liquid error ±5% (of reading), Gas error ±10% (of reading)

A1.4. ISA MPFM

This flowmeter contains two counter-rotating shafts (positive displacement). The constant volume cavity and the rotation imparted to the shafts are proportional to the total volume flow-rate. A single energy gamma ray is mounted to measure the phase fraction.

A1.5. Kongsberg MCF-351

Capacitance sensors are used in this flowmeter. Two of these parallel plates with an array of capacitance sensors on the surface of each plate are fixed on the pipe cross section area. The capacitance sensors measure the gas/liquid interface and calculate the gas fraction. The capacitance between the lower sensor pairs below the gas/liquid interface derives the average water cut of the liquid. The velocity of the mixture is obtained by cross-correlation between sensor signals. So the phase fraction is shared with the mixture velocity to measure the phase flow-rate.

A1.6. TEA Sistemi Spa LYRA

The LYRA MPFM has been originally developed for in-line measurements of wet gas flow, it is based on the isokinetic sampling of the gas-liquid mixture, followed by phase separation and metering of the individual phases. It can be employed as light oil meter, with Gas Volume Fractions in the range 0-100%, water-cute 0-100%, at liquid and gas flow-rate accuracy of 2.5%. The meter measures the individual gas and liquid flow-rates and the water-cut. Additionally, it measures directly the water flow-rate (TEA Simtemi SPA).

Figure A- 4 shows the Sistemi Spa LYRA multiphase flowmeter.

Operative principles

The flowmeter operation is based on the sampling of the gas/liquid mixture, followed by phase separation and metering of the individual phases. Sampling is performed at a position of the meter where the velocity profiles of the gas and the liquid streams are uniform. The sample is typically less than 10% of the total flow (TGA Group).

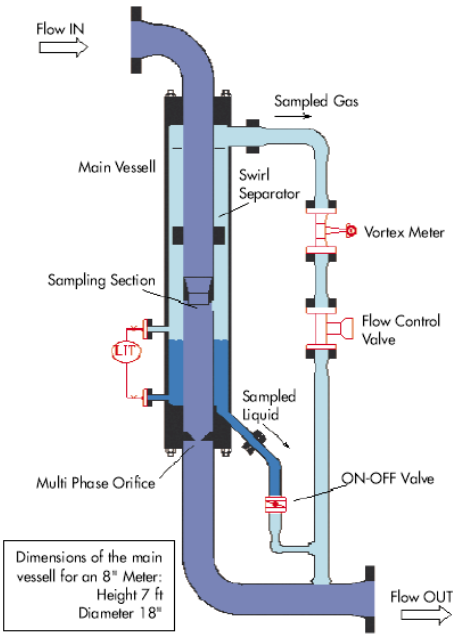

Figure A- 4, TEA Sistemi Spa LYRA

A1.7. Haimo MPFM

The Haimo MPFM shown in Figure A- 5 is reported to be an arrangement of a gas and liquid two-phase (in-line) flowmeter and a full range of three phase flowmeter where the gas/liquid flow-rate measurement and water cut are undertaken independent of each other.

It contains a Venturi flowmeter and two equal signal (59.5 KeV) gamma sensors to measure the gas/liquid two-phase flow mixture velocity and the fraction, respectively. Additionally, a dual energy (22 and 59.5 KeV) gamma densitometer is provided to identify the phase fraction of the three phase, and a flow conditioning device is located upstream of the meter. Both the gas and liquid flow-rates are measured upstream of the flow conditioning device in the two-phase flowmeter, which is in-line without the need for any flow pre-conditioning. The Dual gamma meter is deployed to measure the water cut. The Haimo accuracy under a broad operating series with water cut 0-100% and GVF 0-99.8% is ±1.5% abs (Haimo Technologies).

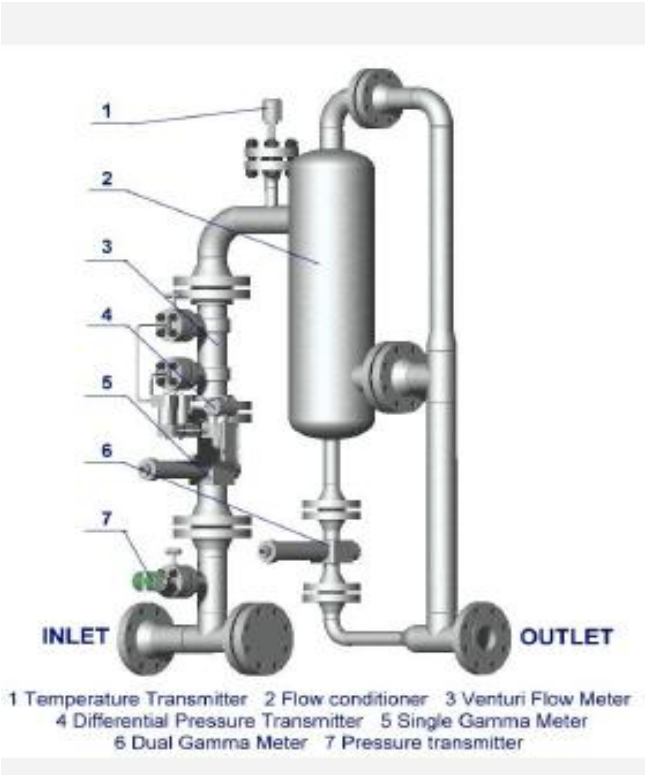

Figure A- 5, Haimo MPFM, taken from Haimo Technologies Inc.

A.1.8. Compact Cyclone Multiphase meter (CCM)

This multiphase metering system is based on flow pre-conditioning, it is to separate the liquid and gas phases upstream of the measuring section. The flow-rate measurements of the separated liquid and gas have been undertaken by Coriolis meters; the separated liquid is directed through a full-range microwave water cut analyser forming an integral part of the CCM (Compact Cyclone MPFM). Figure A-6 shows CCM.

The following tables are general descriptions of the CCM specifications:

- Measuring range

Water Cut	0 to 100%
GVF at operation conditions	0 to 100% Gas Void fraction.
Liquid and gas flow-rates	The configuration of flowmeters and instruments to be designed according to the actual flow-rates and specifications.
Flow regimes	All with some reservation on severe slugging flow.

- Individual flowmeter

Gas flow meter	Coriolis
Liquid flow meter	Coriolis
Water cut analyser	Phase Dynamics Inc. microwave.

- Overall uncertainties

Liquid flow-rate	Relative uncertainty of $\pm 5\%$
Gas flow-rate	Relative uncertainty of $\pm 5\%$
Water cut	Absolute uncertainty of ± 3 to 5%

Figure A- 6, Compact Cyclone Multiphase meter CCM

A.1.9. Accuflow Multiphase Metering System (AMMS)

Accuflow Multiphase Metering System (AMMS) is a patented technology comprising a vertical pipe section and a horizontal pipe section connected together Figure A- 7. Multiphase fluid (oil, water, gas) enters the vertical pipe tangentially, creating a cyclonic action in the pipe where a majority of the gas is separated and flows upward.

The remaining gas is carried under with the liquid stream (oil and water) and enters the horizontal pipe where the gas is completely separated. Liquid level in the horizontal pipe is controlled at the centre of the pipe using a control valve located in the gas flow line. A Coriolis-type flow meter is typically used to measure liquid flow rate. Water cut in the liquid stream is measured by one of two methods, density differential or conventional water cut meter. The conventional water cut meter is based on microwave frequency shift principle. A net oil transmitter or PLC receives liquid flow rate signal from the Coriolis flow meter to perform net oil calculations and display net oil and water rates and volumes.

Anticipated Accuracy:

- Liquid flow rate: $\pm 1\%$ of reading
- Gas flow rate: $\pm 5\%$ of reading
- Water cut in liquid: $\pm 2\%$ absolute (light oils)

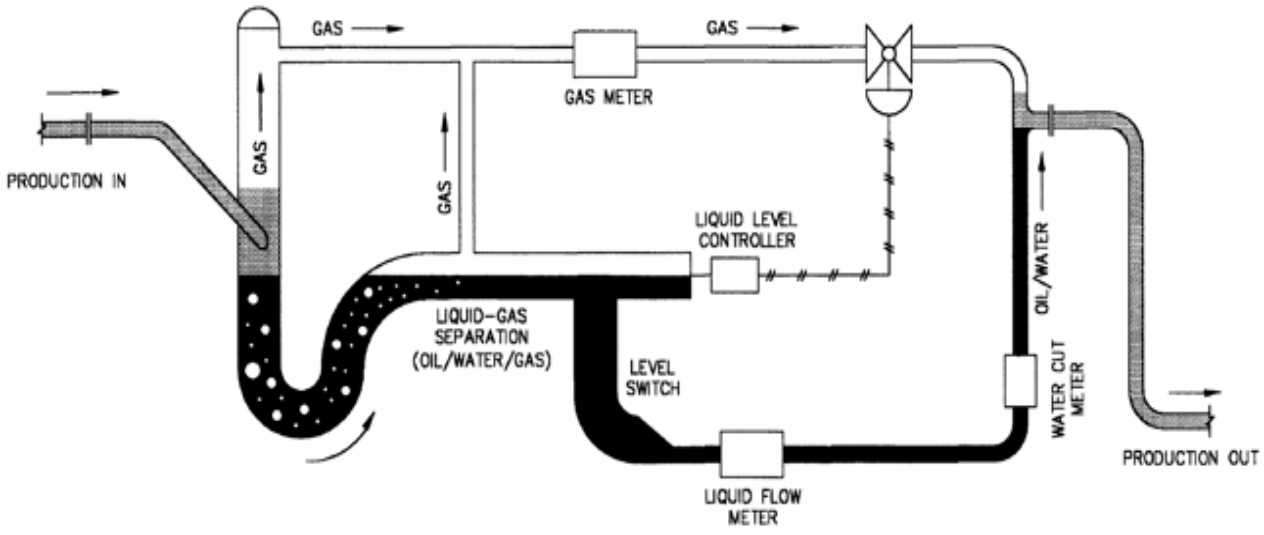

Figure A- 7, Operation Principle of AMMS

A.1.10. eProdution Solutions Inc. REMMS

The Red Eye multiphase metering system (REMMS), combines partial separation technology with conventional liquid and gas metering to provide a multiphase measurement. The main components of these multiphase metering systems are a gas-liquid cylindrical cyclone (GLCC) separator, flow metering instruments, and level control valves, as shown in Figure A- 8. An advanced controller governs the operation of the system as well as interpreting and recording data and providing communications with external host systems.

The principle of operation is based on inducing bulk separation of the liquid and gas phases by creating a cyclonic flow pattern. Once separated, individual streams are measured with conventional liquid and gas meters. The separated phases are then recombined or transported in separate flow lines.

- Operating range:

0 to +95% GVF

- High accuracy:
    - ±2% volumetric gas measurement
    - ±2% volumetric liquid measurement
    - ±2% water cut over full measurement range

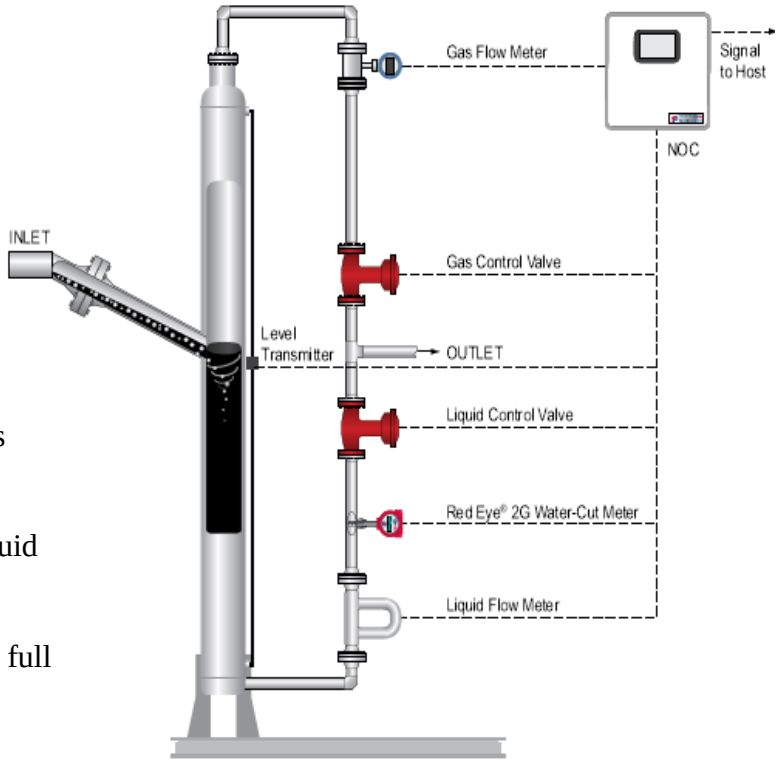

Figure A- 8, REMMS MPFM

A2. Multiphase flowmeters requiring no flow conditioning

In these methods pre-conditioning of the flow is not needed. The instrument has been divided in several stages of measuring the flow-rate of each phase; it generally uses a single gamma energy method in combination with an electrical capacitance sensor which is used for oil/gas mixtures, whereas a conductivity sensor is used for water/gas mixtures to determine the fraction of each flowing phase.

Venturi meter and cross-correlation techniques are used to measure the flow velocity. A gamma ray "densitometer" is also used to determine the phase fraction, (The Petroleum Science and Technology).

A2.1. Roxar MPFM 1900

The ROXAR MPFM 1900 is an example of the multiphase flowmeters that are commercially available and require no pre-conditioning of the fluid. The instruments used for ROXAR flowmeters are: temperature and pressure transmitters to calculate the flow density; a single-energy attenuation ray in combination with an electrical capacitance sensor for oil/gas mixtures and conductivity sensor for water/gas mixture to determine the fraction of the flowing phases; a differential pressure transmitters are installed on a Venturi tube to measure the mixture velocity and cross-correlation, to determine the velocity of small and large bubbles that refer to liquid and gas velocities, respectively (ROXAR MPFM).

Moreover, the ROXAR flowmeter is required to be installed in a vertical position. Because of this requirement, it may be claimed to have pre-conditioning for the flow meter. Figure A- 9 illustrates ROXAR MPFM.

ROXAR MPFM, as mentioned in the operation manual of the meter, has gained accuracy as follows:

- Gas +/- 8%,
- Liquid, +/- 6%, and
- Water-cut +/- 2%.

Figure A- 9, ROXAR MPFM installed in the El-Sharara oil field in Libya.

A2.2. CSIRO MPFM

This MPFM uses gamma rays attenuation at two different energies to derive the multiphase flow components (oil/water/gas) fraction. Velocity measurement is by the cross-correlation of multiphase features. Hence the velocity and fraction are measured, and the oil, water and gas flow-rates are identified.

A2.3. Multiphase meter AS MPM

The AS MPM metering system has been claimed to be a high performance multiphase flowmeter based on patented 3DBroadband technology which measures the dielectric constant in 3-D to calculate the water density, salinity and conductivity. A densitometer is implemented to measure the fraction while a Venturi system is employed to measure the mixture velocity and flow pre-conditioning, as shown in Figure A- 10.

It has been reported that this meter has been operational since 2006 without any malfunction of hardware or software failure. It has also performed accurate measurements with good repeatability for a wide range of flow-rates, GVF (5-95%), and WLR (0-95%) compared to the conventional test separator measurements.

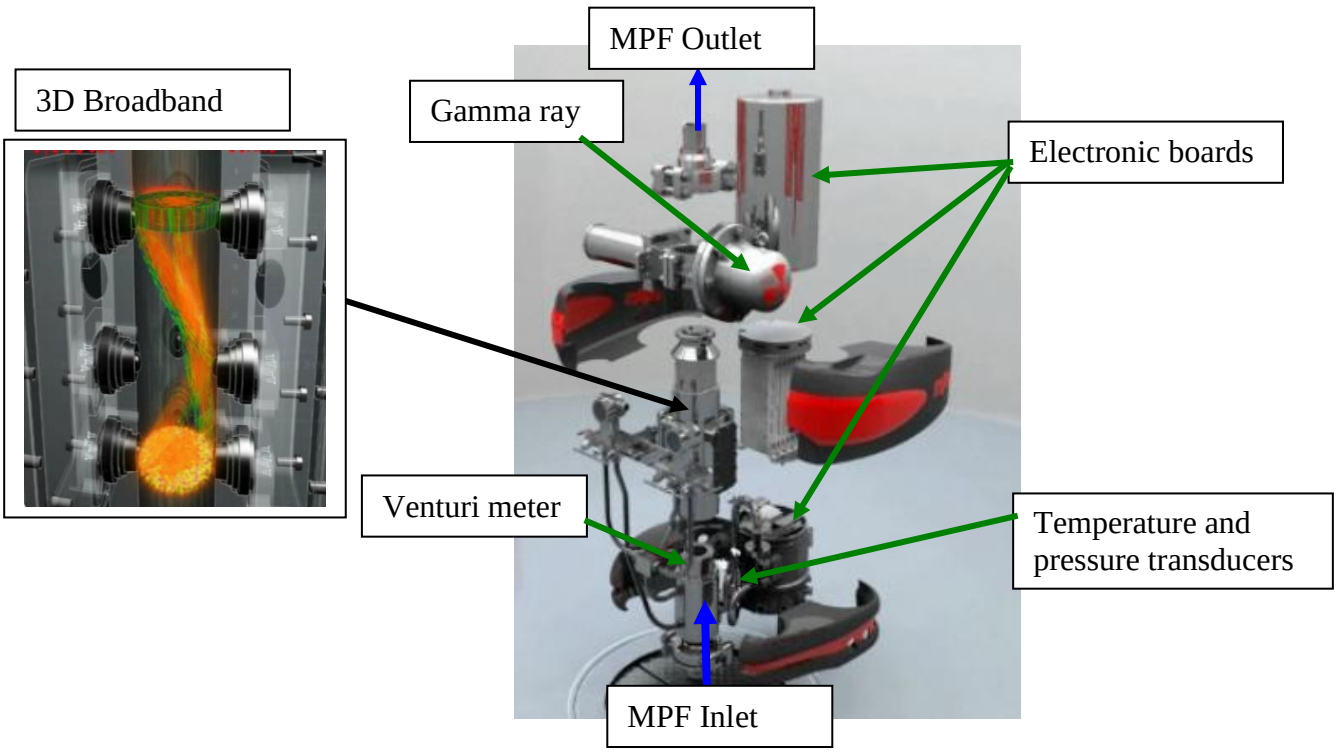

Figure A- 10, Multiphase meter AS MPM, adapted from MPM official site

A2.4. Multiphase solution (Virtual Metering System) VMS

The VMS system is software based; it utilises fuzzy-logic algorithms to achieve a wide-ranging data integrity inspecting and sorting. It is employed to calculate flow-rates based on different arrangements of the fed data sets; it retrieves real-time data from existing sensors around the well for the follow points via a SCADA/DCS boundary:

- Manifold Pressure
- Bottom-hole Pressure
- Bottom-hole Temperature
- Pressure Before and After Choke
- Temperature Before & After Choke
- Wing Valve Position
- Master Valve Position
- Manifold Temperature
- Choke Position

The VMS Real-Time forecast offers an online flow-rate measurement of the multiphase flow gas and liquids with typical accuracies in the 2 to 5% range for instrumented systems. PIMS VMS produces a measurement of uncertainty for each approximate and concerns a precise methodology for weighting the ambiguity in each rate to yield accurate outputs (MSI Multiphase Solutions Inc).

A2.5. PSL ESMER

This multiphase and wet gas flowmeter measures the flow-rates of each phase in light and heavy oil, condensate and wet-gas production pipes without requiring flow conditioning or complicated sensoring techniques. Its technology is based on a combination of signal analysing techniques and conventional hydro/thermodynamic flow models; these signals are emitted by well-known standard sensors (orifice/Venturi/V-cone) with absolute pressure gauges and a temperature sensor. The signals are processed in-line and flow-rates are calculated.

Figure A- 11, PSL ESMER

The accuracy measurement depends on particular operational conditions in the processing line and the extent of the "tune up" that could be practised against references. The ESMER has a level of uncertainty in the range $\pm 5\%$ for liquid and gas flow-rates in relative terms and $\pm 3\%$ water cut in an absolute term. (ESMER Multiphase Flow Meter). Figure A- 11 illustrates an ESMER installation.

A2.6. Neftemer Multiphase Meter

This MPFM is using a single energy Gamma densitometer and it is reported to identify the fractions of oil, water and gas as well as offering a method to measure two-phase velocities. The systems are characterised by their use of simple sensors combined with complex signal processing.

This technique comprises two elements as shown in Figure 2 below: a Cs 137 661 kev gamma source housed in a holder unit (left) and a fast (250 Hz) gamma detection unit (right). These units are mounted diametrically opposite each other on a vertical pipe section containing a vertically upward multiphase flow.

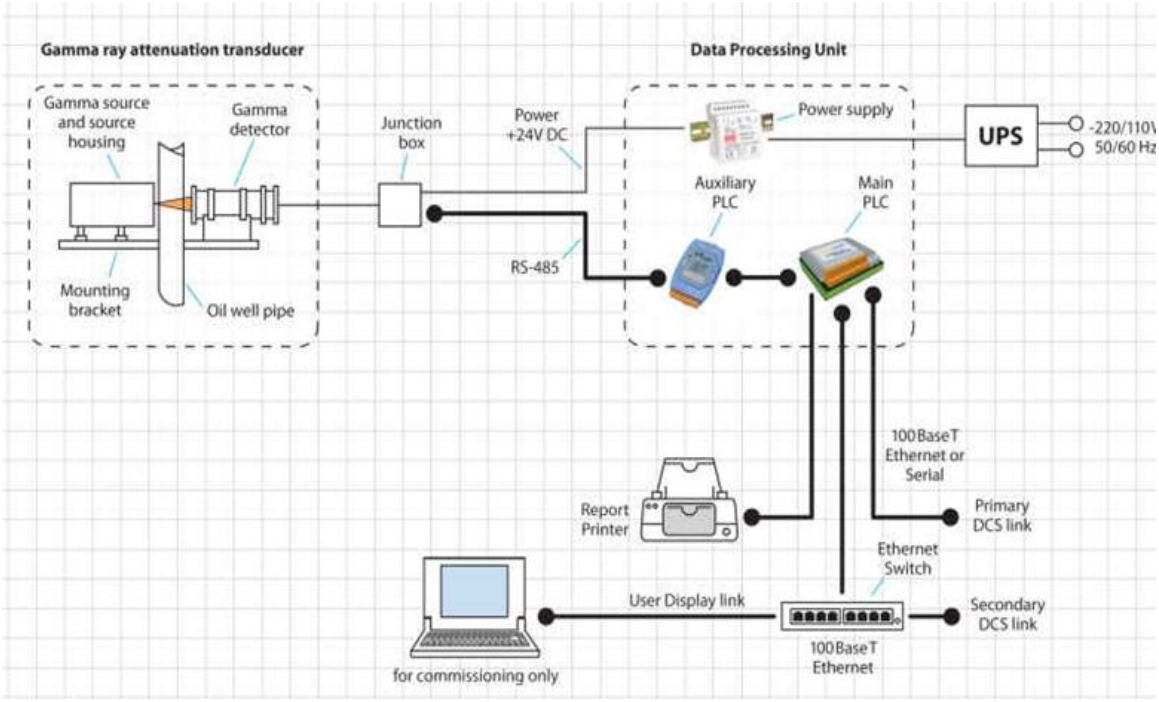

Figure A- 12, Neftemer MPFM, taken from Neftemer Official Website, (2010)

Neftemer is used one measuring method to measure several parameters such as the phase fraction, velocity measurement and pattern recognition. The key to the operation of Neftemer is the determination of the velocities of the different sized gas bubbles in no conditioning flow. Small gas bubbles size refers to liquid velocity and larger gas bubbles size refers to gas velocity. Analysis of the pattern of gamma absorption fluctuations gives these velocities. (Neftemer Official Website, 2010).

Analysis of the direct 661 kev photons and the lower energy photons scattered by the pipe wall and the multiphase fluid gives the oil and water fractions of the liquid. The average relative error of gas and liquid measurement using this technique is $\pm 5\%$ as shown in Figure A- 13

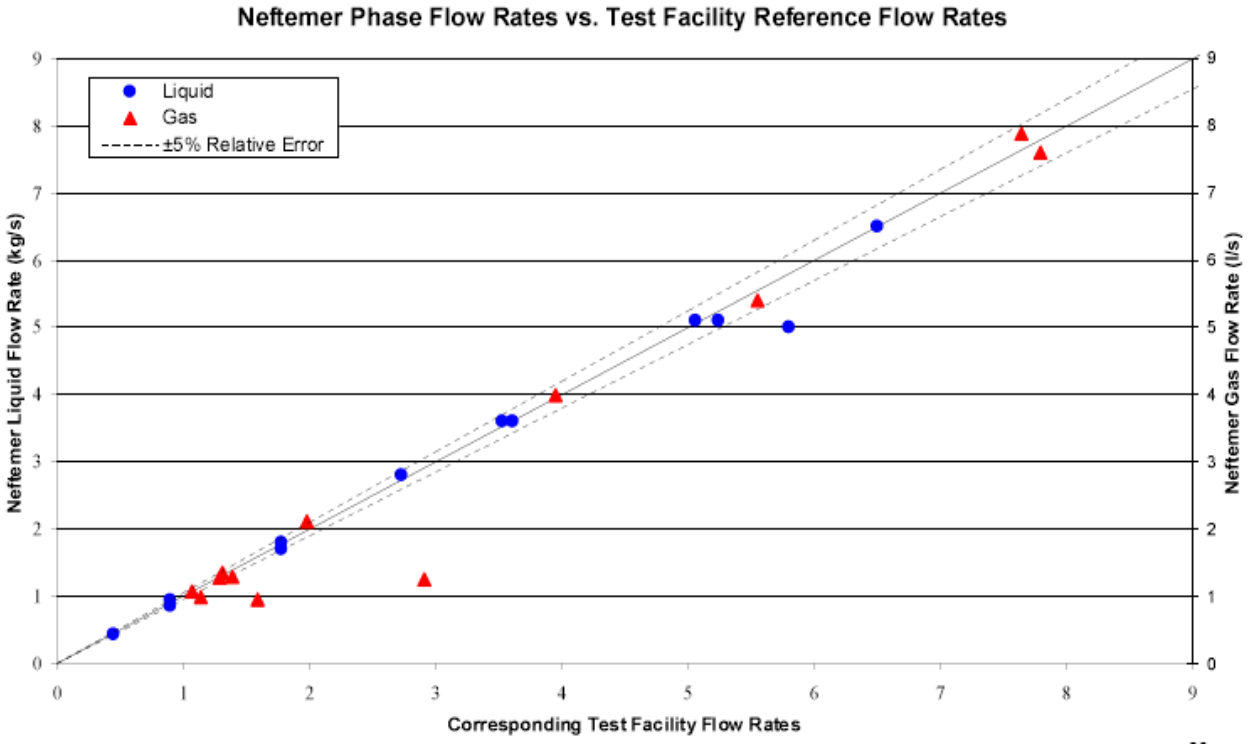

Figure A- 13, Neftemer MPFM Accuracy, taken from Neftemer website

A.2.7. Abbon Flow Master (Optimum C400)

Abbon's Acoustic Flow Meter (AFM) comes in different meter versions. It provides real-time MPF measurements of oil, gas and water flow rates for use in well testing, production allocation, reservoir management and well diagnostics applications.

As illustrated in Figure A- 14 The AFM is used for both multiphase and wet gas applications. Acoustic sensors feed the analog and digital signal processing electronics which combined with a Venturi is used to predict flow rates and fractions through a proprietary modelling technique. An optional capacitance sensor can be used to improve the water cut accuracy at low water cuts.

The electrical characteristics of the oil, gas and water mixture is measured through an advanced electrical impedance sensor system. The sensor signal is sampled more than 1 million times per second and advanced signal processing algorithms are used to extract velocity information as well as the phase fractions of the flow. (Abbon AS, AFM Product Specification Sheets)

Figure A- 14, Abbon flow Master Optimum C400, taken from Abbon product specification sheet

Abbon flow master operating range:

- 0-99.8% Gas Void Fraction
- 0-100% Water Liquid Ratio
- No flow rate limitations
- Max operating temperature: 125 °C
- Max Operating Pressure: According to pipe specification
- Pipe size: Any pipe size
- Pressure drop: < 1 bar

A2.8. FlowSys TopFlow

The FlowSys TopFlow meter is based on well-established measurement principles like Venturi, capacitance/conductance and cross-correlation as shown in figure Figure A- 15. The major parts of the FlowSys TopFlow meter are the Venturi insert and the electrodes incorporated inside the throat of the Venturi. The flow rates of oil, water and gas are calculated based on the measurement obtained by the electrodes and the measurement of the differential pressure across the Venturi inlet. No flow conditioning is required in this metering system.

Liquid phase and oil flow rate measurements obtained were within a relative uncertainty band of ±5% to ±15, whereas, the gas flow rate measurements were found to be within ±5% across a large proportion of the operating range. (FlowSys TopFlow Official Website).

Flow range:

- Gas volume fraction (GVF): 0-97%
- Water cut/WLR: 0 – 100%
- Flow regime: all

The accuracy for the FlowSys TopFlow meter is shown in the table A1-5. It shows the expected deviation from the true value at a 90%. The meter specification has been spilt into several GVF.

GVF range (%)	0-25%	25-60%	60-70%	70-85%	85-92%	92-97%	97-100%
Liquid Flow Rate	5%		7%		10%	15%	-
Gas Flow Rate	-	10%					
Water Cut	2%			3%		5%	-

Table A-2, FlowSys TopFlow accuracy

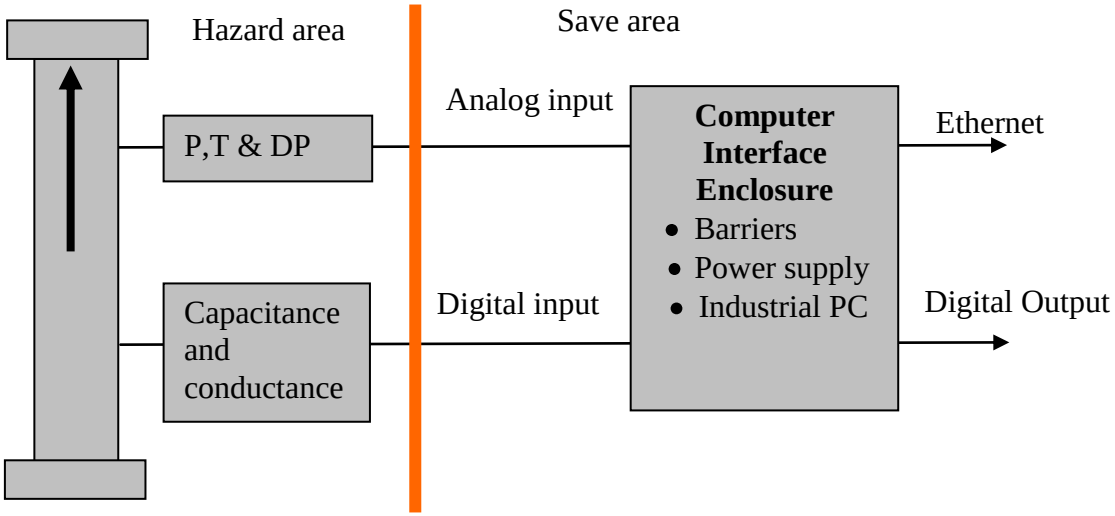

Figure A- 15, FlowSys TopFlow Meter

A3. Commercial multiphase flowmeter classification

Table A1-3 illustrates some well-known multiphase flow measurement techniques and their classifications. Different gas fraction and water-cut measurement techniques have been shown for each multiphase flowmeter.

Meter Developer	Flow condition	Flow measurement	Gas fraction measurement	Water cut measurement	Classification
AGAR	Partial separation	Positive displacement	Venturi	Microwave	In-line
Fluenta	Homogeneous	Venturi and cross-correlation	Densitometer	Capacitance	In-line
Framo	Homogeneous	Venturi	Dual gamma	Dual gamma	In-line full stream mixer
Kongsberg	Homogeneous	Cross-correlation	Cross section mapping	Dielectric Constant	In-line
MFI	Homogeneous	Cross-correlation	Densitometer	Microwave	In-line
Scrolflow		Progressive cavity meter	Densitometer	Sample WC monitor	Intrusive
Texaco	Separation	Mass meters densitometer	Separator	Microwave	Sample separation
Wellcomp	Separation	Coriolis meter	Sample analysis	Capacitance	Sample separation

Table A-3, Multiphase flow metering techniques and classifications, adapted from Babelli (2002)

A3.1. Flow conditioning and water-cut handling range

The main requirement for some multiphase flowmeters to function properly is to condition the flow at the flowmeters' inlet. Conditioning the flow is achieved by making special configurations forcing the flow to establish a particular flow pattern (e.g. partial separation or homogeneous). The success of any dielectric method used to determine the properties of a multiphase system is limited by the physical properties of the continuous phase. Capacitive methods function as long as the continuous phase is oil (low water-cuts), otherwise they short-circuit; on the other hand conductivity methods are deployed when the continuous phase is water.

Appendix B- General Instrument calibrations

B1. Low flowrate turbine gas flow-meter calibration

Calibration of the low flowrate turbine gas flowmeter was performed. It was based on measuring gas flowrate m^3/s using a clamp on the ultrasonic gas flowmeter (GF 868) that was available in the laboratory with a flow accuracy of $\pm 2\%$ to 5% of readings.

Extra care had been taken when the calibration was performed since the ultrasonic gas flowmeter was installed on a 50mm diameter pipe, whereas the turbine flowmeter was installed on 25mm diameter pipe. So it is preferable for the measurement to be based on flow-rate rather than on velocity.

The readings of the turbine gas flowmeter were recorded and then given enough time for the ultrasonic flowmeter to stabilise to obtain its readings.

Moreover, there is another reliable calibration method that can be obtained which is by sending the flowmeter to the manufacturing company to be accurately calibrated according to its original manufacturing standard.

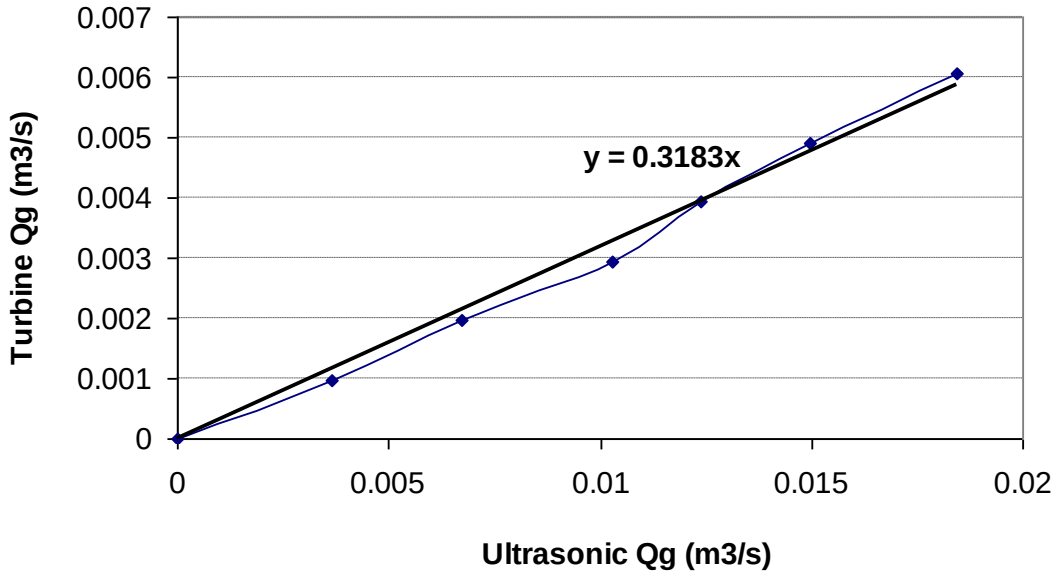

Figure A- 16, Turbine gas flowmeter calibration

Error! Reference source not found. illustrates the same ultrasonic gas flowmeter that was used to calibrate the turbine gas flowmeter.

B2. Gas pressure transducers calibration

The two-phase gas/water facility test rig has several pressure transducers used for measuring gas, water and mixture pressure in both sections (inlet and measuring sections). These transducers have been calibrated and installed in the T-Y junctions test rig.

This pressure transducer calibration was performed in the process and systems engineering laboratory. A Multi-channel Pressure Indicator (MPI) was used to supply the transducer with the working pressure which is between 0 to 2 bar. Then the transducer was connected to a power supply device around 10Vdc, and a voltmeter was used to measure the change in sensor voltage output mV according to pressure changes from the MPI. **Error! Reference source not found.** shows the steps that have been taken to calibrate the pressure transducer. As a result the calibration curve can be obtained by plotting the change in pressure mbar against change in mV.

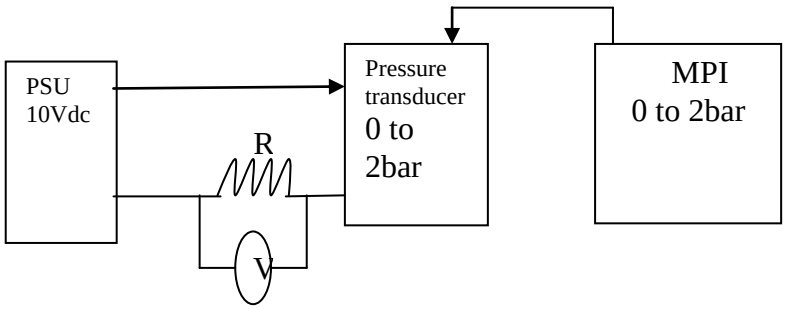

Figure A- 17, Pressure transducer calibration diagram

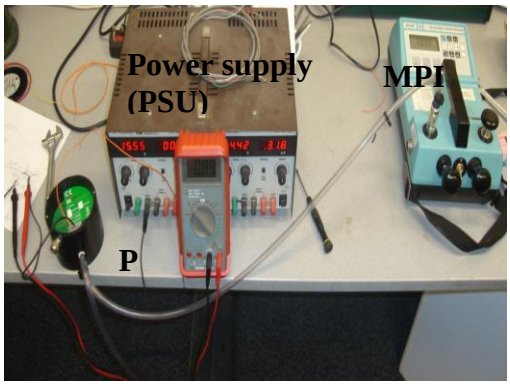

Figure A- 18, Pressure transducer calibration scheme

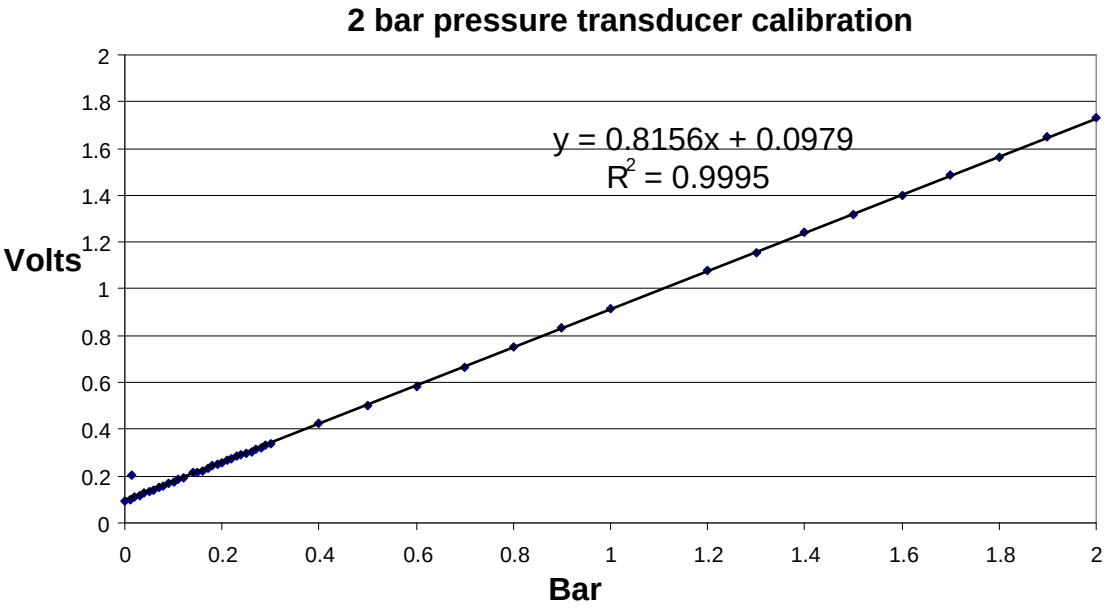

Figure A- 19, Pressure transducer calibration

B3. Conductivity rings

As it can be seen from **Error! Reference source not found.**, there are four conductivity rings installed upstream, downstream of the T-junction and downstream of Y-junction. The conductivity rings A identify the flow regime and liquid fraction in the 50mm diameter pipe which occurs upstream of the T- junction, whereas the conductivity rings C and D are installed on the partially separated liquid section and on the homogeneous section which occur downstream of the Y-junction.

These rings were calibrated by introducing known masses of water into their measuring volume. At each measurement point, the weight of water introduced, the cumulative weight of water added and the corresponding voltage reading (response) from the rings were recorded. The liquid hold up (α_l) at each point was calculated as a ratio of the weights of the cumulative water added up till that point and the weight of the measurement volume when full of water.

The corresponding voltage reading proportional to the conductivity of the liquid air mixture being measured was normalised by taking the ratio of this voltage reading with the voltage reading obtained when the measurement volume was full of water. This was taken as the dimensionless conductivity reading (G*) having a value of 1 when the measurement volume is full of liquid and 0 when it is empty. The temperature at which the calibration was done was also recorded.

A correlation relating the dimensionless conductivity with the measured liquid hold-up was obtained and this correlation was used to normalise all the conductivity readings in all subsequent experiments.

Conductivity rings upstream and downstream of the T-Y junctions

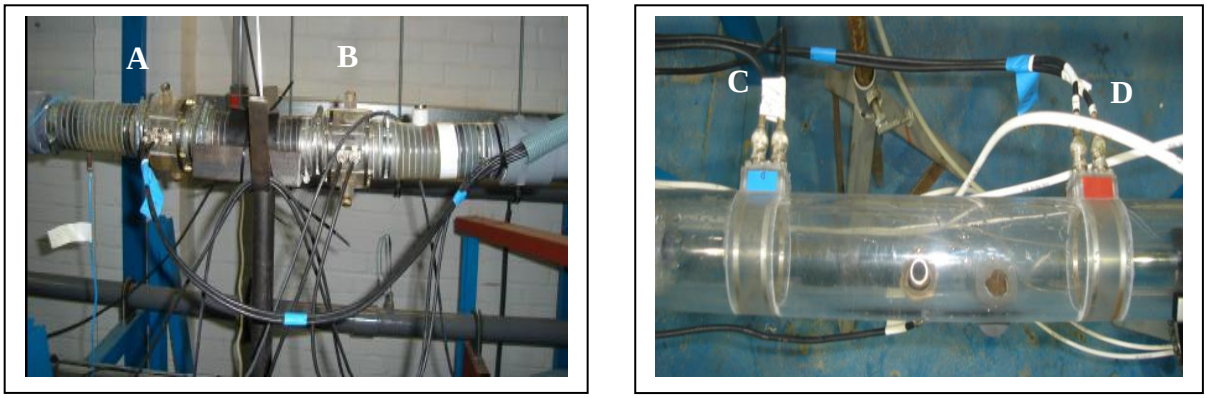

Figure A- 20, Conductivity rings installed in the two phase flow test rig

Error! Reference source not found. shows the conductivity rings calibration curve.

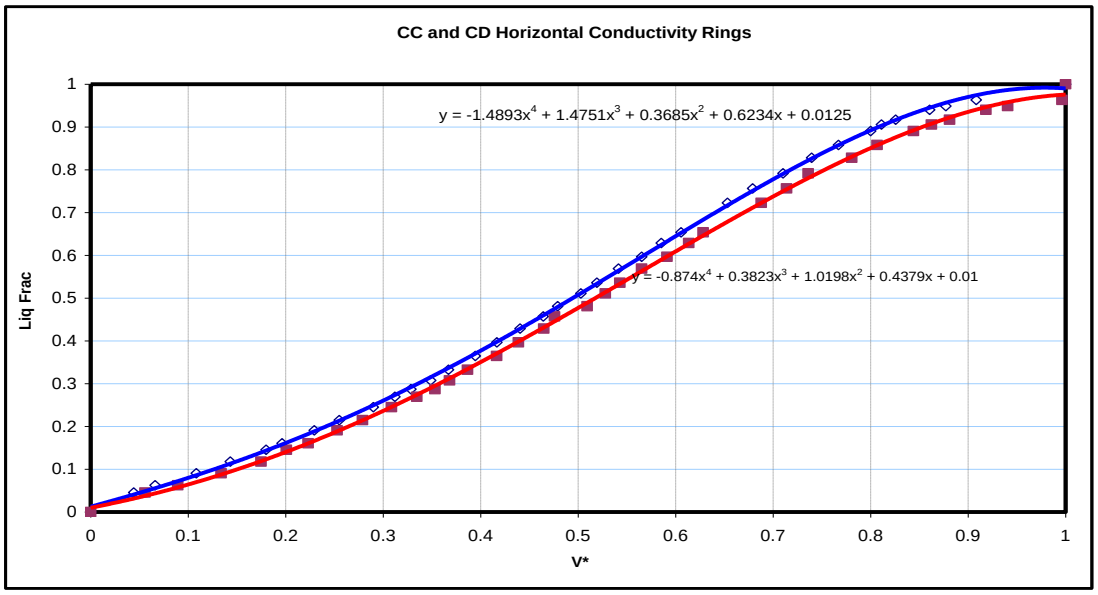

Figure A- 21, Conductivity rings calibration curve

B4. Conductivity ring temperature effect

In terms of the conductivity ring temperature effect, some experiments have been conducted on two conductivity rings. The introduced liquid temperature was monitored and recorded via (C and D) electrodes, and the changes in both conductivity rings outputs (v) also recorded. The test rig liquid temperature increased because of the friction that occurred as a result of the pump working for a long time, and as the liquid flows in a closed loop from and back to the local water tank, the temperature keeps increasing as long as the test rig pump is working. The conductivity rings show a clear increase in their readings as the temperature increases. The temperature curve is illustrated in **Error! Reference source not found.**. The incremental changes in conductivity sensed by these rings were used as a correcting basis for the increases in conductivity measurements in the two-phase flow.

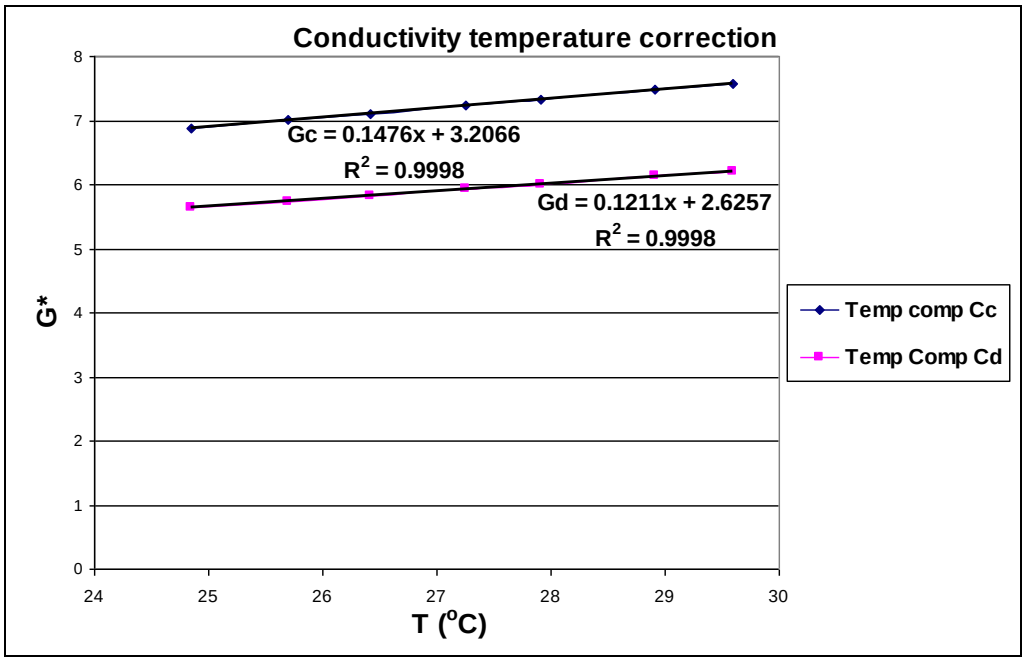

Figure A- 22, Conductivity ring temperature correction

In these instances, the temperature variation curve was obtained by measuring the conductivity responses of the two rings to the high temperature liquid. These values were used to understand the conductivity ring reading behaviour at different single flow temperature changes.

Appendix C, Slug flow measurement using ultrasonic Doppler closure measurement technique

Test no.	Vsl	Vsg	Vm	GVF	α_s	α_f	f_{ds}	f_{df}	V_s	V_f	t_s	t_f	Q_l Ref	Q_l	Error	Q_g Ref	Q_g	Error	Re_s	C	V_{gdrift}	Froudds number
1	0.4	0.16	0.56	0.285714	0.98	0.57	190.73	101	0.674332	0.357	0.934	0.92	0.000784	0.000838	6.827589	0.000255	0.000772	202.8793	23691.13	0.23353	0.266	0.799592149
2	0.4	0.27	0.67	0.402985	0.96	0.61	226.5	98	0.800798	0.346	0.65	0.927	0.000784	0.000849	8.239698	0.000553	0.000906	63.65892	28321.04	0.237279	0.353	0.956654892
3	0.4	0.52	0.92	0.565217	0.95	0.48	247.36	95	0.87455	0.336	0.755	1.1	0.000784	0.000776	-1.04649	0.001062	0.001152	8.529481	38967.46	0.24398	0.336	1.313615673
4	0.4	0.64	1.04	0.615385	0.95	0.44	268.22	80.46	0.948301	0.284	0.446	1.2	0.000784	0.000657	-16.1612	0.0013	0.001283	-1.31428	44079.1	0.246569	0.327	1.484956848
5	0.4	0.72	1.12	0.642857	0.96	0.4	292.06	65.56	1.032588	0.232	0.531	1.3	0.000784	0.000692	-11.6736	0.0014	0.001497	6.908882	47504.24	0.24814	0.292	1.599184298
6	0.4	0.82	1.22	0.672131	0.94	0.36	345.75	35.76	1.222411	0.126	0.643	1.372	0.000784	0.000779	-9.5836	0.001667	0.001847	10.82243	51772.92	0.249947	0.262	1.74196861
7	0.6	0.26	0.86	0.302326	0.99	0.7	225.01	163.91	0.79553	0.579	1	0.545	0.001176	0.00128	8.808846	0.00051	0.000679	33.23309	36541.3	0.24263	0.541	1.227945086
8	0.6	0.45	1.05	0.428571	0.99	0.61	268.22	154.97	0.948301	0.547	0.69	0.87	0.001176	0.001179	0.273053	0.000892	0.001154	30.83911	44551.03	0.246792	0.542	1.499235279
9	0.6	0.65	1.25	0.52	0.99	0.47	303.98	146.03	1.074732	0.516	0.61	1	0.001176	0.001117	-5.02036	0.001274	0.001601	25.66303	52920.1	0.250407	0.648	1.784803904
10	0.6	0.85	1.45	0.586207	0.97	0.46	327.83	137.09	1.159054	0.484	0.76	1.36	0.001176	0.00107	-8.98786	0.001666	0.002013	20.82252	61366.91	0.253517	0.479	2.070372528
11	0.6	1	1.6	0.625	0.97	0.42	403.82	165.8	1.427719	0.447	0.633	1.53	0.001176	0.001012	-13.9309	0.00196	0.002262	15.38595	67845.92	0.255625	0.374	2.284548997
12	0.6	1.2	1.8	0.666667	0.98	0.36	444.05	101.33	1.569954	0.359	0.47	1.2	0.001176	0.00103	-12.3865	0.002352	0.002926	24.40563	76404.93	0.25812	0.358	2.570117621
13	0.8	0.28	1.08	0.259259	0.98	0.65	351.67	184	1.243341	0.651	0.6	0.34	0.001568	0.001824	16.33691	0.000572	0.001084	89.57297	45632.07	0.247296	0.614	1.542070573
14	0.8	0.41	1.21	0.338843	0.955	0.59	393.39	171	1.390844	0.605	0.48	0.359	0.001568	0.001789	14.06705	0.000833	0.0014	68.03771	51160.96	0.249697	0.604	1.727690179
15	0.8	0.99	1.79	0.553073	0.95	0.57	536.44	157	1.896602	0.555	0.6	1	0.001568	0.001712	9.176403	0.001967	0.001776	-9.69175	75705.36	0.257927	0.467	2.55583919
16	0.8	1.2	2	0.6	0.95	0.5	643.73	143	2.275929	0.506	0.44	1.1	0.001568	0.001565	-9.21038	0.002417	0.002358	-2.43327	84684.08	0.26028	0.459	2.855686246
17	0.8	1.4	2.2	0.636364	0.93	0.44	691.41	131	2.444503	0.463	0.44	1.218	0.001568	0.001476	-5.87268	0.002667	0.002527	-5.25349	93229.76	0.262299	0.436	3.14125487
18	1	0.36	1.36	26	0.98	0.75	351.67	298.02	1.243341	1.054	0.446	0.406	0.00196	0.001988	1.441196	0.000727	0.000736	1.345031	57371.64	0.252103	0.941	1.941866647
19	1	0.54	1.54	0.350649	0.97	0.65	441.07	274.18	1.559418	0.969	0.365	0.42	0.00196	0.002039	4.044671	0.0011	0.001263	14.83892	65061.03	0.254745	0.875	2.198878409
20	1	0.66	1.66	0.39759	0.96	0.55	548.36	214.58	1.938745	0.759	0.365	0.382	0.00196	0.002201	12.27975	0.00135	0.001957	44.9462	70236.8	0.256352	0.739	2.370219584
21	1	0.85	1.85	0.459459	0.96	0.48	566.24	190.73	2.001961	0.674	0.4	0.46	0.00196	0.002091	6.702966	0.001717	0.00224	30.51092	78364.9	0.258652	0.658	2.641509777
22	1	1.07	2.07	0.516908	0.95	0.43	572.2	178.81	2.023033	0.632	0.325	0.514	0.00196	0.001786	-8.89897	0.002148	0.002387	11.10326	87748.76	0.261027	0.609	2.955635264
23	1	1.24	2.24	0.553571	0.95	0.39	607.97	154.97	2.149499	0.548	0.365	0.57	0.00196	0.001818	-7.25806	0.0025	0.00257	2.797619	95017.59	0.262698	0.544	3.198368595
24	1	1.53	2.53	0.604743	0.93	0.33	637.77	125.17	2.254857	0.443	0.4	0.7	0.00196	0.001677	-14.4514	0.003133	0.002619	-16.4016	107412.4	0.265273	0.432	3.612443101

Table A- 2, Slug closure measurement